INFORMATION TO USERS

This manuscript has been reproduced from the microfilm master. UMI films the text directly from the original or copy submitted. Thus, some thesis and dissertation copies are in typewriter face, while others may be from any type of computer printer.

The quality of this reproduction is dependent upon the quality of the copy submitted. Broken or indistinct print, colored or poor quality illustrations and photographs, print bleedthrough, substandard margins, and improper alignment can adversely affect reproduction.

In the unlikely event that the author did not send UMI a complete manuscript and there are missing pages, these will be noted. Also, if unauthorized copyright material had to be removed, a note will indicate the deletion.

Oversize materials (e.g., maps, drawings, charts) are reproduced by sectioning the original, beginning at the upper left-hand corner and continuing from left to right in equal sections with small overlaps.

Photographs included in the original manuscript have been reproduced xerographically in this copy. Higher quality 6" x 9" black and white photographic prints are available for any photographs or illustrations appearing in this copy for an additional charge. Contact UMI directly to order.

Bell & Howell Information and Learning
300 North Zeeb Road, Ann Arbor, MI 48106-1346 USA
800-521-0600

Université d'Ottawa · University of Ottawa

Title/Titre

Mechanosusceptibility of a Voltage-Dependent Ion Channel

Cicely Xi Gu

Thesis submitted to the
School of Graduate Studies and Research
University of Ottawa
in partial fulfilment of the requirements for the
Ph.D. degree in the

Ottawa-Carleton Institute of Biology

Thèse soumise à
l'École des études supérieures et de la recherche
Université d'Ottawa
en vue de l'obtention de la maîtrise ès sciences à

L'Institut de biologie d'Ottawa-Carleton

This thesis is dedicated to my dear parents, my husband

and my lovely daughter

Acknowledgements

I would like to express my gratitude for the support I have received from numerous sources in getting to this stage.

First of all, I would like extend my sincere thanks and appreciation to my supervisor, Dr. Cathy Morris, for affording me the opportunity of joining her laboratory, the tremendous amounts of time devoted to my project and for providing unfailing inspiration for "biophysics". I would also like to express my thanks for her enthusiasm and excellent guidance and, above all, her willingness to act as an advisor for a student whose native language is not English and the complicated undertaking this involved.

I am deeply grateful for the valuable suggestions and critiques from my advisory committee members, Dr. Jim Cheetham, Dr. Vance Trudeau, Dr. Donal Hickey and Dr. Balwant Tuana. My thanks also go out to Dr. Johne Liu for his generosity in letting me share the microinjector in his laboratory, to Doctors Daniel Small, Christine Murray and all the professors and teachers who instructed, guided and inspired me over the course of my graduate studies.

I am particularly grateful to all the scientists who helped me in my research project at the Loeb Health Research Institute, in particular, Doctors Petro Doroshenko, Bin Hu, Andrea Sisneros, Andrew Ridsdale, Luning Cui and Kolaj Miloslav for their helpful discussions, their valuable time in facilitating this work. Thanks also go out to my colleagues and friends, Shuxin Li, Jie Zheng, Tammy Herring, Lorin Gaertner, Barbara Calabrese and Iustin Tabarean, for helping me with data analysis and for proofreading my manuscripts. Most of all, I am indebted to Dr. Peter Juranka for his generosity in sharing his time and expertise with me on this project. Without his help and support on molecular biology techniques, my thesis project would never have been started.

My deepest gratitude goes to my parents, my brother and my sister, for their continued emotional support and encouragement, but most of all, for always believing in me. This often became my

reason for continuing the pursuit of my Ph.D. when wrestling with the many days and nights of frustration. Above all, I would like to thank my husband and my daughter for enduring many hours of overtime worked and my pursuit of an uninterrupted experiment on too many occasions. Their love and support provided the inspiration for completing my thesis.

Finally, I would also like to thank MRC and NSERC, Canada for the financial support which enabled me to pursue my graduate studies.

Ottawa, Canada

Abstract

Mechanosensitive (MS) channels are those whose open probability (P_{open}) changes in response to mechanical stimulation. Principally, there are two types of mechanical effects on the channel activity, stretch-activation and stretch-inactivation. Mechano-responses can be detected with patch-clamp recordings in cells from bacteria to human, indicating the ubiquitous distribution of MS channels. Mechanosensitivity has recently been shown to be associated with a variety of unrelated channel types, suggesting that susceptibility to membrane tension could be an inherent property of many integral membrane proteins. In this thesis, I tested the hypothesis that an arbitrarily chosen channel with no known mechanotransducer function could be mechanosusceptible under conditions when (1) studied by patch-clamp recordings and (2) heterologously expressed where the protective machinery of its native environment is absent.

In order to test this hypothesis, a simple well characterized voltage-dependent K^+ channel, Shaker-Inactivation-Removed (Shaker-IR) was expressed in *Xenopus* oocytes in which the endogenous MS channels were blocked by Gd^{3+} (100 μM $GdCl_3$) to facilitate the observation of mechano-response of Shaker-IR. Characteristic conductance-voltage (G-V) curves were obtained for Shaker-IR by two-electrode voltage clamp recordings, although Gd^{3+} shifted the voltage gating by 23 mV. Shaker-IR currents (I_{Sh}) were studied in cell-attached and inside-out excised patches with or without mechanical stimulations. In macropatches, various mechanical effects on I_{Sh} were recorded at different activation levels (i.e. at different membrane potentials). At the foot of the G-V curves where P_{open} was low, stretch-activation dominated the MS Shaker-IR channel activity. At the intermediate range of the curves, only minor stretch effects were detectable. At the top of the curves where P_{open} was high, sustained stretch frequently caused stretch-inactivation. In small patches, stretch-activation and -inactivation were evident as single channel events. Single channel recordings revealed that at a given membrane potential, P_{open} changed steeply with the applied pressure, in a dose-dependent manner. As in macro-patch recordings, both stretch-activation and stretch-inactivation were induced in the same patch, depending on the pre-stretch P_{open}.

Before reaching a conclusion that the observed mechanical effects were indicative of the mechanosusceptibility of a voltage-dependent channel, it was necessary to rule out the possibility that these effects might be caused by stretch-induced changes in membrane area or by "breakthrough

currents" from the oocytes' endogenous MS channels. These possibilities were excluded by the following arguments: (1) Mechanical stimuli produced no apparent increase in capacitance of the patched-membrane, while the increase of the channel activity upon stretch was often one to two orders of magnitude. (2) Stretch-inactivation (not expected from increased area of the recording patch) occurred and could be observed in the same patch that showed stretch-activation. (3) Both the activation and inactivation could be elicited by either suction or blowing. (4) None of these responses were observed in no-Shaker-IR control oocytes. (5) The effects of mechanical stretch depended on the membrane potential, i.e. on the pre-stretch P_{open} of the Shaker-IR channel. In conclusion, membrane stretch can interfere with the voltage gating of Shaker-IR, consistent with the assumption that mechanosusceptibility may be an inherent property of many integral membrane proteins. Since mechanosusceptibility is easy to demonstrate, it might play a role in the physiology of cells by a) modifying the activity of ion channels and b) creating a need for mechanoprotection for channels when they are not used to monitor bilayer tension.

Table of Contents

ACKNOWLEDGEMENTS i

ABSTRACT iii

TABLE OF CONTENTS v

LIST OF FIGURES xii

LIST OF TABLES xv

ABBREVIATIONS xvi

CHAPTER 1. General Introduction **1**

ION CHANNEL CLASSES 1

CHANNELS RESPONSIVE TO MECHANICAL STIMULATION 2
- I. MS channels and MT channels
- II. Criteria for MT channels
- III. Evidence for mechanotransduction by MT channels
  - A. Overview
  - B. Biophysical evidence that vertebrate hair-cells have MT ion channels
  - C. Genetic and cell biology evidence from *C. elegans*
  - D. Problems with the study of MT channels

OVERVIEW OF MS CHANNELS 14
- I. MS channels are ubiquitous and diverse
  - A. Distribution
  - B. Classification
  - C. Diversity of MS channels
- II. Typical SA channel behaviour
  - A. Channel characterization
  - B. Kinetics of the SA channels
  - C. Other properties of SA channels
- III. Membrane tension and pipette pressure
  - A. Laplace's law
  - B. Membrane tension controls gating
  - C. Mirror images of pressure activation curve for SA and SI channels
- IV. How much tension is required to change channel P_{open}?
- V. Mechanisms of mechanosensitivity
  - A. Overview
  - B. Gating energy transmitted via spectrin-like network
  - C. Integrity of the cortical cytoskeleton and mechanosensitivity
  - D. Evidence supporting the lipid bilayer model
- VI. Problems in studying MS channels
  - A. Lack of specific blockers
  - B. Discrepancy between patch and whole cell study
  - C. X-ray crystallography of a bacterial MS channel

OUR APPROACH 40

OVERVIEW OF VOLTAGE-DEPENDENT CHANNELS 41
- I. Voltage-dependent activation
- II. The voltage sensing S4 segments move outward during channel activation
  - A. Overview
  - B. Site-directed mutagenesis
  - C. Cysteine-substitution mutagenesis

D. Site-specific fluorescence labelling

RATIONAL FOR TESTING MECHANOSENSITIVITY OF A VOLTAGE-GATED CHANNEL 51
I. Attachment of a voltage-dependent channel to the membrane cytoskeleton
II. MS channels are ubiquitous and diverse
III. An unifying explanation for MS gating
IV. Hypothesis
A. Global hypothesis
B. Specific hypothesis
C. General approach

CHAPTER 2. General Methods **54**

PREPARATION OF OOCYTES 54
I. Overview
II. Maintenance of *Xenopus laevis*
III. Isolation of single oocytes
A. Surgery
B. Defolliculation of oocytes
C. Selection of "good" oocytes

PREPARATION OF SHAKER-IR cRNAs 60
I. Subcloning of Shaker-IR into pcDNAI/Amp
A. Overview
B. Subcloning
II. Subcloning of Shaker-IR into pSP64TM vectors
A. Overview
B. Subcloning
C. *In vitro* transcription cRNA

MICROINJECTION 63
I. Preparation of transferring and injection pipettes
II. Sample preparation and pipette calibration
III. Microinjection of Shaker-IR cRNA into the cytoplasm
IV. Microinjection of Shaker-IR cDNA into the nucleus

ELECTROPHYSIOLOGY 67
I. Patch clamp overview
II. Manufacturing of recording pipettes
III. Preparation of the surface of the oocytes
IV. Seal formation
V. Two patch clamp configurations
A. Cell-attached patch configuration

B. Excised inside-out patch configuration

MECHANICAL STIMULATION OF THE CELL MEMBRANE 74

DATA ACQUISITION AND DATA ANALYSIS 75
I. Data acquisition
II. Conductance-voltage (G-V) curve
III. Open probability (P_{open}) and pressure activation curves
A. Calculation of P_{open}
B. All-point amplitude histograms

SOLUTIONS 79

CHAPTER 3. Shaker-IR K^+ Channel Expression and Characterization **80**

INTRODUCTION 80
I. Shaker-a voltage-dependent K^+ channel
A. Overview
B. Structural basis of Shaker channel function
C. General properties of Shaker-IR
D. Reasons for using Shaker-IR
II. Gadolinium (Gd^{3+})
III. Objectives

MATERIALS AND METHODS 93
I. Oocytes preparation and microinjection
II. Biochemical analysis of Shaker-IR protein made in oocytes
III. Electrophysiological testing of Shaker-IR expression
A. Overview
B. Electrode pipette preparation
C. Recording chamber
D. Current recording
E. Perfusion of oocytes with 100 μM Gd^{3+}

RESULTS 97
I. Electrophysiological evidence for expression of Shaker-IR in *Xenopus* oocytes
II. Biochemical evidence of expressed Shaker-IR protein in *Xenopus* oocytes
III. Characterization of Shaker-IR in the presence of 100 μM Gd^{3+}
A. Overview
B. Effect of Gd^{3+} on V_{50} and slope of the G-V curve
C. Partial inhibition of G_{max} by Gd^{3+}
D. Reversal potential (V_{rev})

DISCUSSION 105

I. Shaker-IR expression
II. Mechanisms of surface charge on the voltage-dependent gating
III. Effects of divalent or trivalent ions on voltage-dependent channels
A. Overview
B. Effect of La^{3+} on Shaker-like K^+ channel
C. Effect of Gd^{3+} on the voltage-dependent channels in *Xenopus laevis* axons

CHAPTER 4. Stretch-activation of Shaker-IR **112**

INTRODUCTION 112

RESULTS 112
I. Shaker-IR has mechanosensitive (MS) channel properties
A. Endogenous SA cation channels in *Xenopus* oocyte
B. Expression of Shaker-IR channels in *Xenopus* oocytes
C. Selecting a voltage range for recording single I_{Sh}
D. Mechanical effects on Shaker-IR channels
II. Stretch-activation of Shaker-IR at the foot of the G-V curve
A. Establishing a step pair protocol
B. Applying step pairs to non-injected and Shaker-IR-injected oocyte patches
C. Disproportionate increase of I_{Sh} at different step pair voltages
III. Stretch-activation of Shaker-IR at the single channel level
IV. P_{open} of Shaker-IR channel is a sigmoidal function of applied pressure
V. Shaker-IR is activated by membrane tension

DISCUSSION 134
I. Stretch-activation of Shaker-IR
II. Modulation of Shaker-IR P_{open} by mechanical stimulation
III. Stretch-activation of Shaker-IR is not due to an increased membrane area
IV. Half-maximum activation curve depends on how a curve is fitted
V. Gd^{3+} shifted the G-V curves of Shaker-IR
A. General considerations
B. Variations of V_{50} from patch to patch
C. Discrepancy in V_{50} measurements

CHAPTER 5. Stretch-activation and stretch-inactivation of Shaker-IR **144**

INTRODUCTION 144
I. Overview
II. SI channel coexist with SA channels
III. SI channels in dystrophic muscles
IV. SI cation channels in osmosensory neurons may be mechanotransducer (MT) channels
V. Molecularly identified SI channels

RATIONALE 149

METHODS 149

RESULTS 150
I. Stretch-activation and -inactivation of Shaker-IR at the macroscopic level
  A. Voltage-dependent mechanical effects on Shaker-IR
  B. Comparison of mechanical effects between Shaker-IR and endogenous MS channels
  C. Tension-induced mechanical effects
  D. Pressure-dependence of stretch-activation and -inactivation
II. Stretch-inactivation in a multichannel patch
III. Stretch-inactivation of Shaker-IR at the single-channel level
  A. Stretch-inactivation coexist with stretch-activation in the same patch
  B. P_{open} decreases with increasing suction

DISCUSSION 168
I. Summary
II. Is mechanical effect on Shaker-IR a truly gating interference?
  A. Contamination of endogenous MS currents
  B. Gating interference versus drawing in more membrane
III. Why does Shaker-IR exhibit both stretch-activation and -inactivation?
  A. Channel microenvironments are "granular", so microstresses may differ among channels
  B. Shaker-IR occupies multiple states at any voltages
  C. Pre-stretch P_{open} and mechanical effects on Shaker-IR
IV. Pre-stretch P_{open} and other channels

CHAPTER 6. General Discussion **182**

WHAT MAKES SHAKER-IR AN MS CHANNEL 182
I. Tension favours larger area conformation state(s)
II. Tension leads to destabilization of S4 segments
III. Tension thins the lipid bilayer, altering the electric field sensed by S4
IV. Tension changes multimeric state of the channel

COUPLING OF MECHANICAL ENERGY TO THE GATING OF SHAKER-IR 186
I. Direct or indirect gating
II. Bilayer pathway vs cytoskeleton pathway

BROADER IMPLICATIONS 188
I. Channels are intrinsically mechanosusceptible
  A. Widespread occurrence of mechanosusceptibility
  B. MS channels have no common structural motif

C. Conformational flexibility of channel proteins
II. Native channels may be protected from mechanical perturbation
A. Through tethering to the membrane cytoskeleton
B. Mechanoprotection
III. Evolution of Channels

FUTURE PERSPECTIVE 195
I. Are gating currents affected by membrane tension?
II. Does the native *Drosophila* cell environment provide mechanoprotection for Shaker?

APPENDIX Tethering a Voltage-gated Channel to the Membrane Skeleton: a Model for Studying the Mechanical Effects on Gating 202

INTRODUCTION 202

COMPONENTS OF CHIMERIC FUSION CHANNEL 205
I. Overview
II. Spectrin: the filament
III. Ankyrin: the linker
IV. Shaker-IR: the channel

RATIONALE 211
I. A possible rigid and high affinity linkage
II. Contribution of adjacent transmembrane segments to the S4 gating

HYPOTHESIS 214

METHODS 214
I. Preparation of Shaker-IR and ShanX cRNA
II. Heterologous expression in *Xenopus* oocyte
III. Two-electrode voltage clamp and cell-attached patch-clamp

RESULTS 215
I. Functional expression of Shaker-IR and ShanX in *Xenopus* oocytes
II. Confirmation of expression by analysis of biophysical properties
A. Voltage-dependent activation
B. Ion-selectivity
III. Mechanical stimulation on Shaker-IR and ShanX currents
IV. Mechanical effects on Shaker-IR and ShanX co-injected oocytes
V. Mechanical stimulation during voltage-dependent gating of Shaker-IR

DISCUSSION 230

REFERENCES 233

List of Figures

Figure 1-1 Mechanotransduction in vertebrate hair cells 6

Figure 1-2 Model of touch transducing complex in *C. elegans* touch receptor neurons .. 11

Figure 1-3 Characteristics of MS channels 18

Figure 1-4 Idealized symmetrical dose-responses of SA and SI channels 24

Figure 1-5 Cartoon of a tethered channel model for MS channels 29

Figure 1-6 Model of a MS gating transition in an alamethicin channel 34

Figure 1-7 Amphipaths changing the bilayer curvature and the MS channel behaviour .. 36

Figure 1-8 The structures of voltage-dependent channels 42

Figure 1-9 S4 segment serves as voltage sensor for the voltage-dependent channels 43

Figure 2-1 *Xenopus laevis* and oocyte 56

Figure 2-2 Six developmental stages of *Xenopus* oocytes 59

Figure 2-3 Microinjection set up 65

Figure 2-4 Various patch clamp configurations 69

Figure 3-1 A model for the membrane topology of a Shaker K^+ channel subunit 82

Figure 3-2 A representation illustrating a crystallized bacterial K^+ channel 84

Figure 3-3 Expression of Shaker-IR in *Xenopus* oocytes 99

Figure 3-4 Detection of Shaker-IR protein in *Xenopus* oocytes by anti-1D4 antibody .. 101

Figure 3-5 Effects of Gd^{3+} on I_{Sh} expressed in *Xenopus* oocyte 103

Figure 4-1 Mechanical effects of endogenous SA cation channels 114

Figure 4-2 Expression of Shaker-IR and mechanical effects on I_{Sh} 116

Figure 4-3 Stretch-activation of Shaker-IR by paired-step protocol 120

Figure 4-4 Stretch-activation at one pressure in one or all patches 123

Figure 4-5 Disproportional increase of I_{Sh} over one or a range of pressures 125

Figure 4-6 Effect of increasing suction on single I_{Sh} 128

Figure 4-7 All points histogram of I_{Sh} events over a range of pressures 129

Figure 4-8 Effect of suction on the P_{open} of Shaker-IR 131

Figure 4-9 U-shaped P_{open} / pressure activation curve 133

Figure 5-1 Suction effects on I_{Sh} at various V_m by excised patch clamp 151

Figure 5-2 Suction effects on I_{Sh} and endogenous SA currents 155

Figure 5-3 Suction and blowing produce the same effects at given voltages 158

Figure 5-4 Pressure dose-responses by extreme step pairs 160

Figure 5-5 Reversible macroscopic to single I_{Sh} by suction 163

Figure 5-6 Suction effects on single I_{Sh} at two different V_m 165

Figure 5-7 Pressure dose-response of stretch-inactivation 167

Figure 5-8 Schematic diagram of hypothetical changes in membrane area 173

Figure 6-1 Three hypothetical stretch-effects on gating currents 197

Figure A-1 Schematic diagram of primary structure of Shaker-IR & ShanX monomers 204

Figure A-2 Tension effects on erythrocyte membrane cytoskeleton 207

Figure A-3 Model of channel / ankyrin linkage via ankyrin-spectrin network 213

Figure A-4 Expression of Shaker-IR and ShanX in *Xenopus* oocytes 216

Figure A-5 G-V curves of Shaker-IR, ShanX and control 218

Figure A-6 ShanX has the same V_{rev} as that of Shaker-IR 221

Figure A-7 Macropatch currents of Shaker-IR and ShanX with mechanical stimulation . 224

Figure A-8 Susceptibility to mechanical interference of Shaker-IR and ShanX 225

Figure A-9 Mechanical effects on steady-state voltage-dependent currents 228

Figure A-10 Mechanical effects on Shaker-IR current (I_{Sh}) and their G-V curves 231

List of Tables

Table 1-1 Mechanotransducer (MT) versus mechanosensitive (MS) channels 4

Table 1-2 Membrane stimuli relevant for MS channels 25

Table 3-1 Effects of Gd^{3+} on Shaker-IR gating parameters 109

Table 5-1 Complex composition of the cell membrane 176

Table 5-2 Kinetic complexity of Shaker and Shaker-IR 179

Table 6-1 The structural differences of MS channels 189

Table A-1 Voltage-dependent gating parameters with & without suction 229

Abbreviations

1D-4	8 amino acid epitope from bovine rhodopsin
ABP	actin-binding protein
C. elegans	*Caenorhabditis elegans*
CTX	charybdotoxin
degenerins	a family of genes involved in mechanotransduction
E. coli	*Escherichia coli*
$\mathbf{E_K}$	equilibrium potential for Shaker-IR
ENaC	epithelial Na^+ channel
G-V	conductance-voltage relation
GABA	γ-amino-butyric acid
$\mathbf{Gd^{3+}}$	gadolinium
GIRK	G-protein gated inward rectifying K^+ channel
$\mathbf{G_{max}}$	maximum conductance
GPI	glycosol-phosphatidyl-inositol
HEK	human embryonic kidney cell line
I-V	current-voltage relation
$\mathbf{I_{control}}$	ionic current before stretch
$\mathbf{I_{leak}}$	leak current
$\mathbf{I_{Sh}}$	Shaker-IR current
$\mathbf{I_{stretch}}$	ionic current elicited by stretch
$\mathbf{K_{ACh}}$	muscarinic K^+ channel regulated by acetylcholine via G-proteins
mec	mechanosensory phenotype-related gene
min	minute
ms	millisecond
MS	mechanosensitive

MscA	a bacterial MS channel analog from an Archiea species
MscL	*E. coli* mechanosensitive channel of large conductance
MT	mechanotransducer
MTS	methanethiosulfonate
NMDA	N-methyl-D-aspartate (glutamate channel agonist)
NP_{open}	number of channels times the open probability
OR2	Ca^{2+}-free frog medium
P_{open}	open probability
PSD	post-synaptic density
S-like K^+ channel	MS channel resembling the *Aplysia* serotonin-regulated K^+ channel
S4	voltage sensor (fourth transmembrane segment)
SA	stretch-activated
Shaker-IR	Shaker-Inactivation-Removed
SI	stretch-inactivated
STX	saxitoxin
TEA	tetraethylammonium
TEVC	two-electrode voltage clamp
TMRM	tetramethylrhodamine-maleimide, a membrane-impermeant fluorescent dye
TMS	transmembrane segments
TREK	a mammalian MS S-like K^+ channel
V_{50}	midpoint potential of the G-V curve
V_{hold}	holding membrane potential
V_m	net electrical potential across the membrane
V_P	pipette potential
V_{rest}	resting membrane potential of the cell
V_{rev}	reversal potential

CHAPTER 1

General Introduction

ION CHANNEL CLASSES

Ion channels are specialized transmembrane proteins that form water-filled pores in the membrane to allow the selective passage of ions. Based on the effective stimuli for their gating mechanism, ion channels are generally classified into three basic types: voltage-gated, ligand-gated and mechanotransducer (MT) channels (Jan and Jan, 1989). Originally, each channel type was thought to belong to a specialized channel superfamily and to have acquired distinct structural motifs for their corresponding gating. Just as their names imply, voltage-gated channels open preferentially when the membrane is depolarized whereas ligand-gated channels activate when specific agonists (neurotransmitters such as acetylcholine, N-methyl-D-aspartate (NMDA), glycine, or γ-amino-butyric acid (GABA)) bind to the channels. MT channels, on the other hand, respond primarily to various physiologically relevant mechanical signals, such as light or heavy pressures (i.e. touch or pain sensation), vibrations (i.e., pressure waves), gravity, body movements, changes in cell volume and shape, and shear forces (García-Añoveros and Corey, 1997).

Despite these distinct physiological properties, the gating mechanism of each channel type may not be sharply demarcated from one another. It has been shown that a given channel is often susceptible to more than one type of stimulus. For example, the neurotransmitter modulated "S-like" K^+ channels (TREK) are susceptible to stretch (Vandorpe and Morris, 1992; Vandorpe et al., 1994).

Likewise, the NMDA channel, a ligand-gated channel whose major physiological ligand is glutamate shows responsiveness to both voltage and mechanical stimuli (Paoletti and Ascher, 1994; Casado and Ascher, 1998). Up to now, we still do not understand the basis for these overlapping sensitivities, either at the biological or the biophysical level. The aim of this thesis has been to explore the susceptibility of a voltage-gated channel to stretch.

CHANNELS RESPONSIVE TO MECHANICAL STIMULATION

I. MS channels and MT channels

Mechanosensitive (MS) channels are defined operationally as those channels whose open probability (P_{open}), studied under patch clamp conditions, changes in response to mechanical stimulation (Morris, 1990). Since the first discovery of MS channels responding to mechanical stimuli at patch clamp single channel recordings (Guharay and Sachs, 1984), MS channels have been found in various cells types, including both sensory cells and non-sensory cells (Morris, 1990; Martinac, 1993). However, since Morris and Horn (1991) reported that they could not record whole-cell currents anticipated by single channel currents, it has been suspected that MS channel behaviour might be due to some artificial effects of patch clamping. Although there is no doubt about the existence of MS channels as channels, the finding of Morris and Horn (1991) put the physiological role of many MS channels into question, particularly those in non-sensory cells. After another eight years' study on MS channels, there is still a resounding lack of success in recording MS whole cell currents that correspond to the single channel data. To date, the only MS channel, whose whole cell

channel activity has been reported to correlate with the single channel recordings and with a physiological role, is a channel type in hypothalamic supraoptic osmosensory neurons (Oliet and Bourque, 1993; Bourque and Oliet, 1997).

Due to the serious discrepancy between single channel and whole cell activities, most MS channels have not been confirmed to be MT channels. We reserve the name MT channels only for those channels with defined physiological roles in mechanotransduction such as detection of touch, sound, osmotic gradients, cell swelling, position of body parts, movements, acceleration, gravity and fluid pressure. To illustrate the distinction between MT channels and MS channels, several examples are listed in **Table 1-1** along with some background descriptions for each.

II. Criteria for MT channels

To claim that MS channels are physiological MT channels, several criteria have to be met (Morris, 1992). 1) Being able to demonstrate mechanosensitivity at the single-channel level. 2) The MS channel must be specifically blocked or alternatively, the difference between a mutant organism (or a cell deficient in the MS channel) and a normal (or wild type) must be demonstrated. 3) Show that some physiological aspect of the cell's behaviour or development is mechanosensitive. 4) Show that the physiological function is impaired with a selective MS channel blocker or by mutation. 5) Finally, characteristics obtained from macroscopic whole-cell recordings should correspond to single channel recordings in selectivity, pharmacology, and stretch sensitivity. In other words, the MS macroscopic current data should be consistent with single channel kinetics and amplitude. Clearly, only one of the MS channels listed in **Table 1-1** meets this set of criteria.

Table 1-1 Mechanotransducer (MT) versus mechanosensitive (MS) channels *

MT channels	Original location	Name	Molecular identity	Transduction physiology		
1	*C. elegans* touch cell	MT cation channel [A]	degenerins & auxiliary proteins	putative channel subunits have been cloned and shown to interact with intra/extracellular proteins		
2	vertebrate hair cell	MT cation channel [B]	*unknown*	whole cell electrophysiology and cell biology indicate that channels are present and functionally dependent on extracellular tip links		
3	mammalian osmosensory neuron in CNS	SI cation channel [C]	*unknown*	the osmosensitivity expected from whole organism physiology is evident in both single channel and whole cell currents		
MS channels	**Original location**	**Name**	**Molecular identity**	**Biophysical mechanosensation**	**Proven physiological function**	**Putative mechanical function**
1	snail neuron mouse brain	SA K^{D}	TREK[E] two pore four TMS K^{+} channel	patch clamp on cell line, oocytes amphipaths are stimulating	modulation of excitability in response to neurotransmitters	*none*
2	bacterial inner membrane	MscL [F]	MscL, 15 kD multimer	patch clamp of liposome amphipaths are stimulating	adaptation to osmotic stress[G]	osmo-regulation
3	mammalian CNS neuron	NMDA[H]	NMDA type glutamate channels	patch clamp on HEK, oocytes amphipaths are stimulating	synaptic transmission	*none*
4	rabbit atrial myocyte	K_{ACh}[I]	GIRK[H] G-protein gated two TMS one pore	inflating under whole cell clamp of myocytes	modulate cardiac rhythm	atrial volume regulation

TMS: transmembrane segments; *rest of the abbreviations as defined in abbreviation list

A. Tavernarakis and Driscoll, 1997
B. Garcia-Añoveros and Corey, 1997
C. Oliet and Bourque et al., 1993
D. Vandorpe and Morris, 1992
E. Patel et al., 1998
F. Sukharev et al., 1997
G. Levina et al., 1999
H. Paoletti and Ascher, 1994; Casado and Ascher, 1998
I. Krapivinsky et al., 1995; Ji et al., 1998

III. Evidence for mechanotransduction by MT channels

A. Overview

Mechanosensation, the ability to detect mechanical force, is a form of sensory transduction that may be useful for all living cells and is highly developed in the specialized mechanoreceptors (see **Table 1-1**). The cellular response to these stimuli has been assumed to be mediated directly by ion channels (Guharay and Sachs, 1984) because the rapidity of mechanosensory responses (in the scale of milliseconds, ms) can not be explained by multiple steps of a biochemical signalling pathway. Currently, two major areas of studies have provided evidence that some ion channels may be MT channels which are responsible for either MT currents or MT behaviour. First, using combined biophysical and cell biological techniques, evidence suggests that vertebrate hair cells contain channels and are responsible for the mechanotransduction (Hudspeth, 1989). Second, genetic and cell biological studies suggest that putative MT channels in a subset of *Caenorhabditis elegans* (*C. elegans*) neurons are responsible for touch sensation in this organism (see review by Tavernarakis and Driscoll, 1997).

B. Biophysical evidence that vertebrate hair-cells have MT ion channels

1. Structure of hair cells

Hair cells are found in the auditory and vestibular organs of all vertebrates, as well as in the lateral line system of fishes and amphibians (Marcus, 1998). In structure, each hair cell has a projected tuft (or hair bundle) of 20 to 300 stereocilia which are tapered at their bases and inserted into the apical surface of the cell (**Fig. 1-1A**). Stereocilia are aligned in a constant increment in height and the two adjacent stereocilia are interconnected by a single-strand filament called a tip link, which joins the tip of one stereocilium to the side of the next taller stereocilium (**Fig. 1-1B**).

Figure 1-1. Mechanotransduction in vertebrate hair cells

(A) Two hair cells in the sensory epithelium of a bullfrog vestibular organ are shown as electron micrograph pictures. Each bears on its apical surface a tuft of stereocilia, in a staircase arrangement of increasing height up to 8 μm high. **(B)** A tip link, shown in an electron micrograph of two adjacent stereocilia, is a thin filament (arrow) that contacts the end of shorter stereocilium to the side of the taller one. **(C)** Because stereocilia stick together at their tips, the tip links between stereocilia are stretched when the stereocilia are deflected towards the longer stereocilium. **(D)** Such a "spring-like" tip link has been proposed to be attached to the MT channels at both ends, one at the tip and the other along the side of a stereocilium. Evenly spaced actin filaments form the cytoskeleton of the stereocilia. MT channels are thought to be tethered (via unknown linker proteins, but probably involving myosin) to the actin filaments (from Corey and García-Añoveros, 1996).

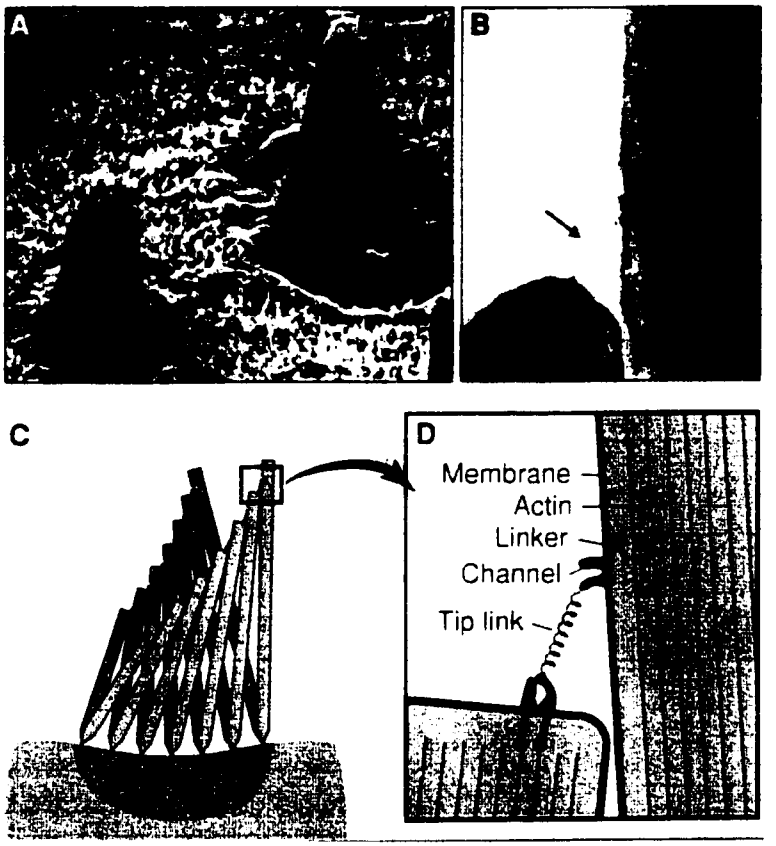
A
B
C
D
Membrane
Actin
Linker
Channel
Tip link

Evidence summarized below suggests that the tufts of stereocilia contain channels responsible for the mechanoelectrical transduction (i.e., MT channels).

2. Evidence for location of the MT channels

Early studies done by Corey and Hudspeth (1979) suggests that MT channels are located at the tips of the stereocilia. A mechanical stimulation probe was attached to the tip of the hair bundle and made to oscillate at a certain frequency. Simultaneously, a recording microelectrode "tuned" to detect extracellular current density at the same frequency, was placed at various sites around the hair bundle. The finding that mechanical stimuli elicited the highest current density near the tip of the hair bundle indicates that mechanoelectrical transduction occurs near the stereocilia tips and therefore, that the location of the MT channels might be in this region (Hudspeth, 1982). Recently, calcium (Ca^{2+}) indicators have been used to assess the presence and location of MT channels in individual stereocilia, the new evidence suggests that MT channels may be situated not only at the tip of the lower stereocilium but at both ends of each tip link (Denk et al., 1995; Lumpkin and Hudspeth, 1995).

Later studies also support the idea that tip links might be attached to the MT channels in the tip of each stereocilium. These studies include the observation with transmission electron microscope of the fine filaments between the tips of adjacent stereocilia (Pickles et al., 1984), the observation that BAPTA, a Ca^{2+} chelator, disrupts these tip links (as shown by scanning electron microscope) and induces a loss of mechanosensitivity (Assad et al., 1991). Therefore, the tip link protein could act as a gating spring which controls the opening and closing of transduction MT channels (Hudspeth, 1989).

3. *Proposed mechanotransduction model for hair cells*

From studies of the electrophysiological response to bundle deflection, a direct mechanical gating was proposed for the following reasons. 1) The transduction process is extremely rapid, with channels opening within tens of ms in response to mechanical stimuli (Corey and Hudspeth, 1983). 2) The latency of channel opening decreases as the bundle deflection increases (Corey and Hudspeth, 1983; Crawford et al., 1989), suggesting that the mechanical input acts directly on the channel itself. 3) MT currents were recorded only when the bundle of a vertebrate hair cell was displaced in the positive direction (toward the taller stereocilia), suggesting that the gating springs act more like rubber bands, i.e., capable of exerting force when stretched but not when compressed (Corey and Hudspeth, 1983).

This direct gating model (Corey and Garcia-Añoveros, 1996) implies that the P_{open} of the MT channel is a direct function of tension, while tension is conveyed by an elastic "gating spring"(**Fig. 1-1C and 1-1D**). Hypothetically, in response to a mechanical stimulation, if the stereocilia are displaced toward the bundle's taller edge, which would increase the tension of the tip links, the MT channels near the tips of the stereocilia tend to be open. Under these conditions, the cells are depolarized. If the stereocilia are displaced in the opposite direction, the tip link shortens and tension releases, the MT channels then tend to be closed. As shown (**Fig. 1-1D**), two MT channels (one at the tip of the lower stereocilium and the other at the side of the taller stereocilium) are connected through an elastic tip link. MT channels are not only attached to the extracellular filamentous component, such as tip links, but also to the intracellular cytoskeleton via an intracellular linker.

4. *Molecular identification of transduction elements*

Using biochemical and molecular biology techniques, additional information about protein

components of the hair cells have been provided.

The cross-linked filaments within each stereocilium have been identified as actin (Pickles, 1993), and the adjacent actin filaments are extensively cross-linked to form a rigid network for transmitting forces. Evidence suggests that MT channels attach intracellularly to actin via a tension-regulating myosin, located in a cluster in the cell bodies of the hair cells. In response to changes in the gating spring tension, myosin move up and down along the polarized actin cytoskeleton, returning tension to near its resting level (Gillespie and Corey, 1997).

Biochemically, the tip link is most likely a glycoprotein, because it is unaffected by detergent treatment (Assad et al., 1991), and may in some way be linked to the underlying cytoskeleton. It has also been proposed that the tip links may be polymers of smaller subunits, like actin or tubulin (Garcìa-Añoveros and Corey, 1997). Calculation of the molecular weight based on the diameter of the tip link of 5 nm estimated to be in excess of 100 kD if the tip link is a single protein. This is similar to an elastin filament; physiological experiments suggest that elastin can stretch to three times its resting length without breaking (Shepherd and Corey, 1994), as would be required if tip links were the gating springs. Other than what is outlined above, little is known about the nature of the tip link.

C. Genetic and cell biology evidence from *C. elegans*

Since hair cell MT channels have not been cloned, their molecular identity is unknown. A genetic approach has, however, been used to study the molecular nature of mechanotransduction in the nematode *C. elegans* (Huang and Chalfie, 1994; see review Garcìa-Añoveros and Corey, 1997). This study has identified a group of mechanosensory (*mec*) genes and the gene products which are required for the function of touch-neurons. Molecularly, the *mec* genes are members of a "degenerin"

gene family, they are so named because mutation of these genes will cause neurodegeneration (Huang and Chalfie, 1994).

1. Proposed MT channel apparatus

Two of these genes, *mec*-4 and *mec*-10, were expressed specifically in touch sensitive cells. The sequence and topology of the gene products, MEC-4 and MEC-10 are similar to the amiloride sensitive epithelial sodium channel (ENaC) subunits, i.e., a two-membrane-spanning-domain protein assembled as a multimer of unidentified size (Canessa et al., 1994). This finding suggests that MEC-4 and MEC-10 may function as channel proteins. Since degeneration caused by a *mec*-10 mutation can be fully suppressed by mutations in *mec*-4 but not *vice versa* (Huang and Chalfie, 1994), MEC-4 may be able to form a channel in the absence of MEC-10, playing a similar role as the α subunit for ENaC, while MEC-10 may require MEC-4 to be functional. In addition, point mutations in the second membrane spanning domain of MEC-4 could abolish mechanotransduction and cause lethal cell swelling (Hong and Driscoll, 1994), indicating that MEC-4 forms a critical part of an ion pore. Moreover, mutations in *mec*-6 can suppress either *mec*-4- or *mec*-10-induced degenerations (Huang and Chalfie, 1994), showing that *mec*-6 might encode a third channel subunit required for channel assembly or signalling. Based on this assumption, a multimeric channel model of three subunits (MEC-4, MEC-10 and MEC-6) has been proposed for touch sensitive MT channels (Huang and Chalfie, 1994. **Fig. 1-2**). Unfortunately, this very plausible scenario has not yet been confirmed by electrophysiological data.

2. A supramolecular structure underlying mechanical gating in C. elegans

(i) MEC-2, a putative linkage protein

In addition to the structure of MT channels, gene interaction studies involving the

Figure 1-2. Model of touch transducing complex in *C. elegans* touch receptor neurons

"MEC-number" labels refer to a variety of proteins which, when mutated, can yield touch insensitivity. Proposed MT channel subunits are MEC-4, MEC-10 and probably MEC-6. In the absence of mechanical stimulation, the channel is closed (left). Application of a mechanical pressure (right) results in displacement of the channel complex between the intra- and extra-cellular attachments, which in turn promotes the channel opening. The MT channel subunits interact with MEC-5, 9 and/or 1 in the extracellular matrix mantle as well as MEC-7 and 12 in intracellular microtubules via a linkage protein MEC-2 (from Tavernarakis and Driscoll, 1997).

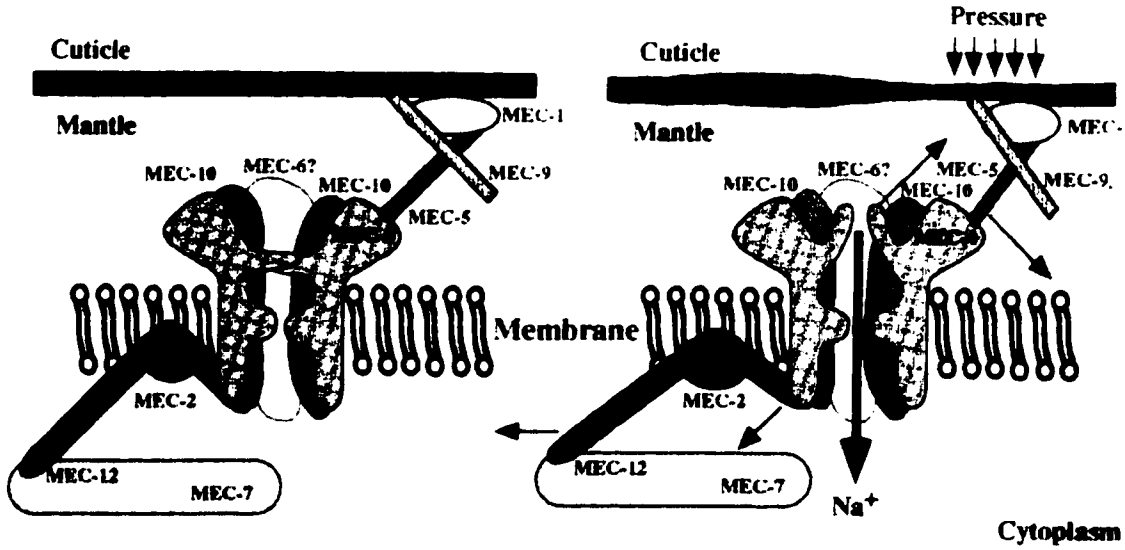
Cuticle
Mantle
MEC-1
MEC-10
MEC-6?
MEC-10
MEC-9
MEC-5
Membrane
MEC-2
MEC-12
MEC-7
Pressure
Cuticle
Mantle
MEC-1
MEC-10
MEC-6?
MEC-5
MEC-10
MEC-9
MEC-2
MEC-12
MEC-7
Na+
Cytoplasm

identification of suppression and enhancing mutations suggest that the interaction between an MT channel and intra- and/or extracellular proteins is also needed for touch cell functions (Liu et al., 1996).

This interaction might involve MEC-2, a stomatin-homologue protein (Huang et al., 1995; Mannsfeldt et al., 1999). Stomatin is an integral membrane protein in erythrocytes. Stomatin deficiencies are associated with an apparent increase in passive membrane permeability to the univalent cations, such as Na^+ and K^+ and lead to erythrocyte swelling and lysis(Stewart et al., 1993). In *C. elegan* touch neurons, MEC-2 may function as a linker between the MT channels and the intracellular microtubules (Huang et al., 1995). Like stomatin in erythrocytes, MEC-2 may interact with the cytoskeleton; a proline-rich region at the C-terminus of MEC-2 may bind to a SH3-binding site of spectrin, in a manner similar to the ENaC proteins (Huang et al., 1995; Rotin et al., 1994). Additionally, genetic interaction studies indicate that the N-terminus of MEC-2 also interacts with specialized microtubules (Huang et al., 1995). Touch cell microtubules are composed of MEC-7 ß-tubulin and MEC-12 α-tubulin (Huang and Chalfie, 1994). Since genetic disruption of these microtubules lead to touch insensitivity, MEC-2 is thought to link the proposed multimeric channel, an MEC-4-MEC-10-MEC-6 complex, and the intracellular microtubules via interactions with MEC-7 and MEC-12 (see **Fig. 1-2**).

(ii) Extracellular matrix and mechanosensitivity

The *C. elegan* touch cells are attached to the epidermis by an extracellular matrix called the mantle (**Fig. 1-2**) (Du et al., 1996). While the protein product of *mec*-1 has yet to be determined, *mec*-5 encodes a collagen which is synthesized and secreted by the neighbouring hypodermal cells (Du et al., 1996). Mutations of *mec*-1 and *mec*-5 disrupted the formation of mantle and cause touch

insensitivity, suggesting that the MT channels might also be linked to the mantle (Du et al., 1996). Another extracellular protein MEC-9 is apparently not required for mantle formation. Mutations in *mec*-9 abolished touch sensitivity but are not lethal for touch cells, suggesting that MEC-9 does not directly contribute to the gating of the proposed MT channels. MEC-5 and MEC-9 may jointly form an extracellular linkage between the mantle and the MT channel that is required for mechanosensitivity (Du et al., 1996).

3. Proposed model for mechanotransduction in C. elegans

Genetic and molecular studies in *C. elegans* have resulted in a mechanotransduction model first proposed by Huang et al. (1995) then modified by Tavernarakis and Driscoll (1997) (**Fig. 1-2**). The model's central component is an MT channel composed of three subunits, MEC-4, MEC-10 and MEC-6, regulated by interactions with extracellular matrix and intracellular cytoskeleton proteins. The MT channel subunits may interact with MEC-5 and/or MEC-9 in the extracellular matrix mantle as well as MEC-12 in intracellular microtubules via a linkage protein named MEC-2. Thus, the delivery of tension hypothetically requires that the channel is tethered to both the extracellular matrix and intracellular microtubules. In response to mechanical stimulation, the movements of a MT channel between the intracellular and the extracellular attachment points would readily produce a displacement of the stiff microtubule.

4. Common features of MT channel models in hair cells and C. elegans

The above proposed mechanotransduction model from *C. elegans* shares some common features with the proposed gating mechanism of the hair cell. In hair cells, mechanotransduction may involve rigid movement between extracellular tip links and rigid-cross linked intracellular actin network. Similarly, the mantle attachment together with the microtubules might provide rigidity for

the MT channels in *C. elegans* (Huang et al., 1995). In summary, these two models suggest that mechanotransduction involves mechanical forces impinging on a channel tethered between rigid extracellular components and a rigid intracellular cytoskeleton.

D. Problems with the study of MT channels

Unlike the voltage-dependent or ligand-gated channels, MT channels are the only major class of channels with little structural/functional information; the molecular nature of the hair cell MT channels are completely unknown. Because of the limitations in the accessibility and availability of mechanosensory organs, characterization of the corresponding gene products has been difficult (Garcìa-Añoveros and Corey, 1997). A further difficulty arises from the structural complexity of MT channels in both hair cells and *C. elegans*. Many mechanosensory organs usually operate in a complex of accessory structures. It is possible that not only the multimeric MT channel subunits, but also essential interacting proteins, will have to be assembled to gate the channel. Thus, *in vitro* assays for isolated components may not be very meaningful (Du et al., 1996).

OVERVIEW OF MS CHANNELS

I. MS channels are ubiquitous and diverse

A. Distribution

MS channels have been reported in all cell types across the five kingdoms (see **Table 1-1**), almost every cell tested with patch clamp recording has revealed one or two types of MS channels (Morris, 1992). Under patch clamp studies, MS channels are generally at a low density of about one

channel per μm^2 of membrane (Morris, 1997). The MS channels have been found in sensory cells including auditory cells (Iwasa et al., 1991), stretch receptors (Erxleben, 1989), muscle cells (Hisada et al., 1991; Dopico et al., 1994) and supraoptic neurons (Oliet and Bourque, 1993). They also exist in non-sensory cells, such as blood and epithelial cells in which the necessity of mechanical sensing is less obvious (Hamill and McBride, 1992). Although MS channels are widely distributed, their physiological roles remain unclear (Sachs and Morris, 1998).

B. Classification

1. Ion selectivity and stretch-sensitivity

MS channels can be operationally classified according to differences in their ionic selectivity or stretch sensitivity. The MS channels display a variety of permeation properties. Some are non-selective; some are cation-selective (K^+ or Na^+ selective) and some are anion selective or solely Cl^- selective. That these MS channels with different ion selectivities are molecularly related is unlikely. Based on the response to increased membrane tension, two kinds of MS channels have been reported: those that show increased activity with membrane tension and those that show decreased activity with membrane tension (Morris and Sigurdson, 1989). The channels that have an increased P_{open} during tension are called SA (stretch-activated) channels while those that have reduced P_{open} with tension are called SI (stretch-inactivated) channels. The former type is more abundant (Morris, 1997). The gating of such channels is a function of membrane tension and can be related to the transmembrane pressure by Laplaces's law (discussed later).

MS channels are named collectively based on their stretch-sensitivity and ionic-selectivity. For example, SA cation channels or SI K^+ channels. The majority of MS channels are SA cation selective. This type of channel has been most extensively studied in *Xenopus* oocytes and chick

skeletal muscle (Methfessel et al., 1986; Yang and Sachs, 1987). These SA cation channels are poorly selective among mono- and divalent-ions such as Na^+, K^+ and Ca^{2+}. Another type of MS channel is the SA K^+ channel (Vandorpe and Morris, 1992; Vandorpe et al., 1994) which shows classical K^+ channel selectivity (Small and Morris, 1995).

2. Curvature sensitivity

While most MS channels are equally activated by either negative (suction) or positive (blowing) pressures (Morris, 1990), a third channel type (other than SA and SI channels), termed curvature-sensitive, is gated by changing the direction of the membrane curvature. Using both cell-attached and inside-out excised patches, Marchenko and Sage (1997) reported that suction and blowing yielded opposite effects on an MS cation channel from an endothelium of rat aorta. Blowing increased channel activity whereas suction decreased it. These MS cation channels are activated by protrusion of the membrane towards the cell interior (concave curvature) and inhibited when the patch is pushed out, towards the extracellular space (convex curvature), suggesting that MS channels are activated only when the patch membrane is in a specific, permissive curvature. In this way, the bending of the membrane lipids by positive pressures would generate sufficient energy to open the channels, independent of membrane tension (Marchenko and Sage, 1997). A similar curvature-sensitive channel has also been found in astrocyte cells in which combined patch clamp recording with light microscopy showed that the channels can only be activated when the patch dome is curved toward the cytoplasm by positive pressures (Bowman et al., 1992).

C. Diversity of MS channels

Although MS channels are gated by mechanical force, many are activated by a variety of other stimuli (see **Table 1-1**). This diversity of channel types indicates that MS channels may belong

to several different channel families. In addition to direct mechanical stimulation, the mechanosensitivity of several cloned channels including a large conductance MS channel (MscL) in *Escherichia coli* (*E. coli*), TREK and NMDA, is mimicked by amphipathic compounds (Martinac et al., 1990; Casado and Ascher, 1998; Patel et al., 1998).

Despite the differences in ion selectivity, stretch sensitivity, and a variety of activators, there are several properties common to the different MS channels. Since SA channels are a major class of channels in MS channel family, the following section is focused on SA channel behaviour, unless otherwise indicated. The SI channel behaviour will be discussed in detail in **Chapter 5**.

II. Typical SA channel behaviour

A. Channel characterization

In response to applied mechanical stimuli, most SA channels are activated in bursts of flickery openings (Yang and Sachs, 1990). For example, SA cation channels in *Xenopus* oocytes are characterized in cell-attached mode by its non-selectivity among cations and long-lasting openings with a single-channel conductance of 28 pS (Methfessel et al., 1986; Yang and Sachs, 1990). A sustained increase in P_{open} is observed when either negative or positive pressure is applied to the patch pipette (Methfessel et al., 1986; Yang and Sachs, 1990).

A typical SA channel responding to suction is shown in **Fig. 1-3a** (Morris and Sigurdson, 1989). With increasing membrane tension, the P_{open} and the number of activated channels increased (up to three channels in this case). Upon release, the channel activity returns to the pre-stretch level. Taken from work on the crayfish stretch receptor neuron, **Fig. 1-3b** further illustrates the general effect of a SA cation channel to the increasing levels of suction at a single channel level. The

Figure 1-3. Characteristics of MS channels

(a) Typical SA K^+ channel activity recorded from a snail neuron. At V_m = +70 mV, the outward K^+ currents appear as upward spikes. A suction of -40 mmHg (bar) produces simultaneous activation of up to 3 channels. Scales: 4 pA, 2 s (from Morris and Sigurdson, 1989). **(b)** SA cation channel recordings from a single channel in crayfish stretch receptor membrane patch. At resting membrane potential of -50 mV, the currents are inward, shown as downward deflections. With increasing suction from 0 to -26 mmHg, the frequency of channel openings increases and remains constant during sustained suction levels. Another way to describe this is that a long closed state gets progressively shorter with increasing membrane tension. Dotted line indicates the zero current of closed state. Scales: 10 pA, 100 ms (from Erxleben, 1989).

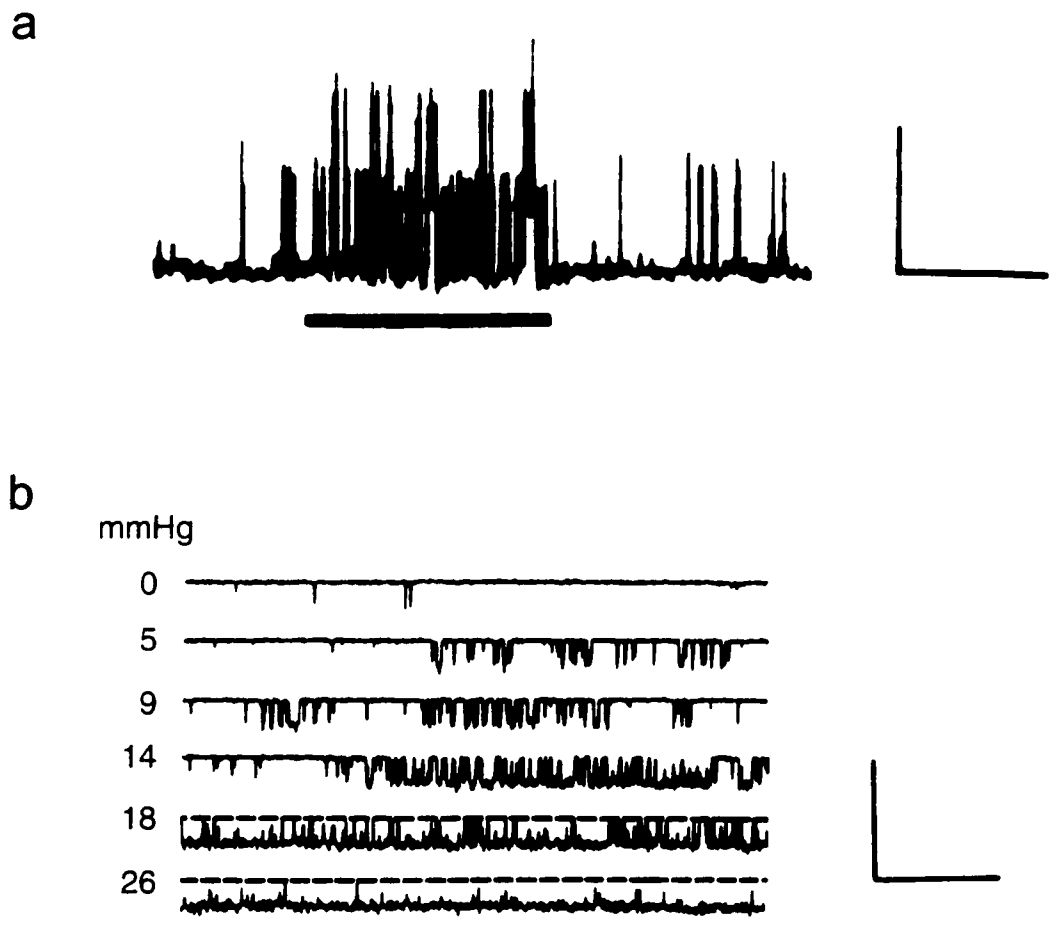
a
b
mmHg
0
5
9
14
18
26

channel's P_{open} increased with increasing pipette pressures and remained constant at sustained suction (Erxleben, 1989). In fact, at -26 mmHg (**Fig. 1-3b**), the P_{open} of this channel approaches 1.

The value of P_{open} as a function of the applied pressures can be fitted to Boltzmann functions and exhibit a sigmoidal activation curve (Erxleben, 1989; Yang and Sachs, 1990; Morris and Sigurdson, 1989). From the sigmoidal P_{open} vs pressure activation curve, the slope of the curve is extracted, representing the pressure sensitivity of the channel. The average sensitivity for SA channels in crayfish receptor is 5.6 mmHg for an e-fold change in P_{open} (Erxleben, 1989), compared to 8 mmHg for MS channels in *E. coli* (Martinac et al., 1987).

B. Kinetics of the SA channels

The mechanical response of most SA channels is rapid, occurring almost immediately when the membrane patch is stretched. For example, MS cation channels in oocytes can be turned on with a latency of less than 2 ms and with a rise time of less than 1 ms (McBride and Hamill, 1993). Suction steps applied to the gently sealed cell-attached patches on *Xenopus* oocytes typically produced a rapid (<1 ms) activation of MS channel currents (Hamill and McBride, 1997).

The open time distribution of SA channels can be described by a single exponential function whereas the closed time distribution required at least three exponentials, indicating that the SA channel has at least one open and three closed states (Guharay and Sachs, 1984). It has been shown that these open and closed components are not equally affected by suction, only the last (longest) component of the close time distribution is sensitive to suction. For example, for SA cation channels in *Xenopus* oocytes before suction, the open time distribution has a time constant of 0.8 ms while the time constants for the three closed time distributions are: 0.1, 0.5 and 325 ms. With a -50 mmHg suction, these components are: 1 ms for open time constant and 0.2, 0.6, 31 ms for the three closed

time constants. Thus, it is evident that -50 mm Hg shortened the last closed time duration by 10-fold, whereas other components seem to be relatively insensitive to suction (Guharay and Sachs, 1984). A common feature shared by all SA channels is that as the pipette pressures increased, the closed intervals between openings were shortened (Yang and Sachs, 1990; Morris and Sigurdson, 1989). A similar observation has been reported on both SA cation channels from crayfish stretch receptors (Erxleben, 1989) and SA K^+ channels from snail heart muscles (Brezden and Gardner, 1986).

C. Other properties of SA channels

Several SA cation channels exhibit adaptation, appearing as a time-dependent decrease in P_{open} in response to a sustained mechanical stimuli. Adaptation has been reported in ascidian oocytes (Moody and Bosma, 1989), *Xenopus* oocytes (Hamill and McBride, 1992), and yeast (Gustin et al., 1988). Adaptation can be distinguished from inactivation because the channel remains sensitive to mechanical stimuli but with a reduced stretch sensitivity. The response of SA cation channels in ascidian oocytes to a step change in suction was shown to be highly phasic, with channel P_{open} initially increasing rapidly then decreasing over several hundred ms to a non-zero steady-state (Moody and Bosma, 1989). In yeast protoplasts, SA cation channels showed an adaptation in response to pressure steps at the high pressures (Gustin et al., 1988). SA cation channels in *Xenopus* oocytes also showed a rapid adaptation, within tens of ms, which then decays over the next second (Hamill and McBride, 1992). This adaptation and decay process is similar to the previously demonstrated SA channels in yeast and ascidian oocytes (Moody and Bosma, 1989; Gustin et al., 1988). The adaptive behaviour has been shown to be due to a decreased P_{open} rather than a reduced channel conductance (Hamill and McBride, 1992). Based on the rapid adaptation and its fragility to patch recording conditions, Hamill and McBride (1992) proposed that the abolished adaptation after

strong suction is due to decoupling of the membrane-cytoskeleton interaction by mechanical stress. Thus, a gentle seal (<5 mmHg and less than 10 s) is essential to observe the MS channel adaptive behaviour and to avoid mechanical damage to the patch membrane (Hamill and McBride, 1992).

Despite of using gentle patches which may minimize mechanical disruption, a different kinetic property, delayed activation, is observed for SA K^+ channels from snail neurons (Small and Morris, 1994). Unlike the rapid adaptation of SA cation channels in gentle patched oocytes, SA K^+ channels show a delayed (1- to 4 s) mechanical response after rapid application of the suction step. Similar to the adaptation, the delayed activation was also fragile and dependent not only on the pressures applied but also on the patch history. This delay decreased with increasing suction and could be irreversibly lost with repeated stimuli (Small and Morris, 1994).

III. Membrane tension and pipette pressure

A. Laplace's law

Membrane tension can be estimated from Laplace's law which states that for a thin-walled sphere, the membrane tension is proportional to the applied suction:

$$T = Pd/4 \text{ (or } Pr/2) \qquad \text{Equation 1-1}$$

where T is the in plane tension of the membrane, P is the applied pressure, d is the diameter of the patch curvature and r is the radius of curvature of the patch (Sokabe et al., 1991). According to Laplace's law, if continuous or repeated suction draws more membrane deeper into a tapered pipette, the increased patch membrane area with a larger radius of curvature would generate higher membrane tension for the same applied pressure. On the other hand, if the patch perimeter stayed fixed, but more lipid bilayer was added with suction, the same pressure would give a lower tension

because the radius of curvature would be decreased. It is thus essential to monitor the membrane capacitance, as it reflects directly on the changing membrane area. If capacitance increases with time at the same pressure, it is likely that new membrane was sucked into the pipette. Fortunately, the co-existence of distinct SA and SI channel behaviour in the same patch (Morris and Sigurdson, 1989) indicates that the simplest scenario (where there is no changing capacitance) probably applies, at least some of the time.

B. Membrane tension controls gating

Early studies on MS channels suggested that the effective stimuli was membrane tension (Guharay and Sachs, 1984). This hypothesis has been confirmed by the fact that MS channels can be activated by either positive or negative pressures (Sachs, 1990). In particular, direct evidence was obtained by monitoring the shape of the membrane while changing the pipette pressures (Sokabe et al., 1991). They observed a low channel activity when the patch was flat but a high channel activity when the patch was stretched in the opposite directions by either suction or blowing. This direct correlation between membrane tension and channel activity strongly supports the hypothesis that MS channels are activated by membrane tension (Sokabe et al., 1991).

The perfectly round shape of yeast spheroplasts provided an excellent opportunity to test if Laplace's law applies to MS channel gating (Gustin et al., 1988). By measuring the whole cell current density ($pA/\mu m^2$) on various sizes of yeast spheroplasts, the plots of MS current versus applied pressure exhibited a clear dependence on spheroblast diameter whereas plots of current as a function of the tension (calculated from Laplace's law) were independent of the diameter. According to the Laplace's law, for channels regulated by membrane tension, current density is dependent on both the applied pressure and the cell size. Had the channels been regulated by

pressure, then channel current density would be cell-size independent. Since authors showed that the pressure-dependence of yeast SA channel current density is inversely dependent on the cell diameter, it was concluded that membrane tension generated gating energy that regulated MS channel activity (Gustin et al., 1988).

C. Mirror images of pressure activation curve for SA and SI channels

Insofar as the applied tension within a membrane patch increases symmetrically as a function of positive and negative pressures, both pressures should provoke the same mechanical effect on either SA or SI channels. In agreement with this, the sensitivity to positive and negative pressures of chick skeletal muscle SA channels are the same (Yang and Sachs, 1990).

For both SA and SI channels, the characteristic P_{open} profile can be determined from their sigmoidal responses to a series of positive and negative pressures. However, SA channels are functionally distinguishable from SI channels by the opposite activity profiles in response to changing pipette pressures. SA channels display a U-shaped activation curve with a minimum channel activity occurring near 0 mmHg, whereas for SI channels, the pressure dependence of channel activity show a bell-shaped form with a maximum channel activity at 0 mmHg (**Fig. 1-4**, Bourque, 1996).

IV. How much tension is required to change channel P_{open}?

When applying pressures to a patch pipette, ±200 mmHg is usually excessive and will rupture the cell membrane. Most SA channels of animal cells are reported to be maximally activated at -10 to -120 mmHg (Morris, 1997, also see **Table 1-2**) whereas more than -100 mmHg (-150 to -250 mmHg) pipette suction is required for activating bacterial MS channels (Sukharev et al., 1994).

Figure 1-4. Idealized symmetrical does-responses of SA and SI channels

Blowing into a pipette causes the membrane patch to become concave (relative to the cell interior), whereas suction causes a patch convexity. But in both situations, the patch of the membrane is stretched. If channel activity increases (SA) or decreases (SI) as a function of absolute pipette pressures in a dose-dependent manner, then SA channels should display a U-shaped activation curve, whereas SI channels exhibit a characteristic bell-shaped activation profile when both suction and blowing pressure stimuli are used (from Bourque, 1996).

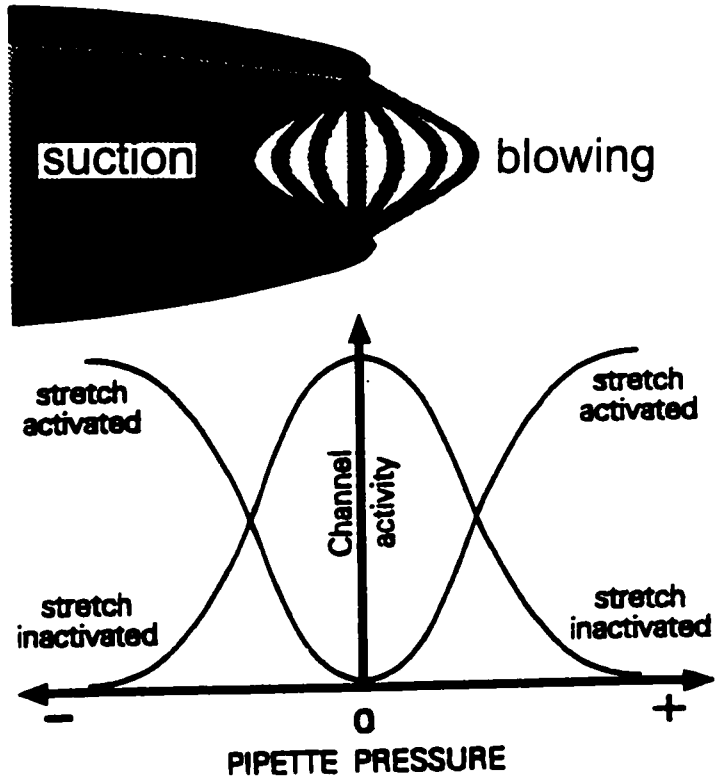
suction
blowing
stretch activated
stretch activated
Channel activity
stretch inactivated
stretch inactivated
−
0
+
PIPETTE PRESSURE

Table 1-2 Membrane stimuli relevant for MS channels

Resting membrane tensions	Tensions that activate MS channels	Lytic membrane tensions	Pressures that activate MS channels
0.12 mN/m (plant protoplast membrane)[A]	1 mN/m (yeast)[D] (muscle)[E]	4 mN/m (plant protoplast)[A]	-60 mmHg; 50% maximum P_{open} (SA K^+ channels in snail neurons)[L]
0.4 mN/m (normal molluscan neurons)[B]	≤ 8 mN/m (alamethicin)[C]	2 - 10 mN/m (lipid bilayer and cell membranes)[H]	-40 mmHg; threshold (SA Cl^- channel in snail neurons)[L]
0.2 mN/m (swollen molluscan neurons)[B]	>0.07 mN/m (turn on SA channel)[F]	6 to 11 mN/m (yeast whole-cell recording)[I]	<15 mmHg; 50% maximum P_{open} (SA cation channel in crayfish receptor)[M]
0.5-4 mN/m (lipids)[C]	5-10 mN/m (half max. level) (chick skeletal and heart muscle)[G]	3 - 4 mN/m (phospholipid vesicles)[J]	~ 15 mmHg (SI K^+ channel) ~-30 mmHg (SA K^+ channel) (*Lymnaea* neuron)[N]
		6 - 12 mN/m (erythrocyte)[K]	~15 mmHg, half maximum P_{open} (SA K^+ channel in heart cells)[O]
		5-12 mM/m (*Lymnaea* neuron)[B]	-10 to -100 mmHg; half-maximum (any SA channels)[P]

A. Kell and Glaser, 1993
B. Dai et al., 1998
C. Opsahl and Webb, 1994a
D. Gustin, 1992
E. Sokabe et al., 1991
F. Sackin, 1995
G. Sokabe et al., 1993
H. Sheetz and Dai, 1996
I. Gustin et al., 1988
J. Kwok and Evans, 1981
K. Evans et al., 1976
L. Bedard and Morris, 1992
M. Erxleben, 1989
N. Morris and Sigurdson, 1989
O. Kim, 1992
P. Morris, 1997

Pressure Conversions

1 kPa = 7.5 mmHg
100 mmHg = 13.3 kPa = 133 mbar
1 mmHg = 1.36 cm H_2O

Tension Conversions

mN/m = dyne/cm = pN/nm

To calculate membrane tension T, it is necessary to know both the pipette pressure P and the radius of patch r according to Laplace's law. However, since the patch curvature can only be determined by directly visualizing and measuring the geometry of the stimulated patch, very few studies have made a quantitative estimation of the tension during membrane stretch (Sokabe et al., 1991 and 1993). In one study which used video microscopy (Sokabe et al., 1991), the radius of the membrane curvature was determined by digitizing the patch image and fitting the data to a geometric model of the patch. By simultaneous measurements of the tension in the patch according to Laplace's law and calculation of single SA channel P_{open} from patches of chick skeletal muscle, Sokabe et al. (1991) reported that the slope sensitivity is 3.3 dyne/cm/e-fold change in P_{open}. In comparison, spherical protoplasts from yeast (Gustin, 1991) has a slope sensitivity of about 0.05 dyne/cm/e-fold with a midpoint at 0.7 dyne/cm. The difference between the high slope sensitivity of the yeast compared to the low slope sensitivity of the chick muscle may reflect shunting of tension around the channels in the muscle.

Furthermore, with human epithelial cells cultured on an elastic thin silicon membrane, mechanical stretch was applied in a controllable manner at the whole cell level without using a patch pipette (Naruse and Sokabe, 1993). The tension generated in the cell membrane was estimated from Hook's law based on the measurement of the two-dimensional deformation of the cell at stretch. The whole cell SA channel activity was estimated from the measurement of intracellular Ca^{2+} using the fluorescent calcium sensitive dye fura-2. Upon a mechanical stretch, the intracellular Ca^{2+} increased rapidly. The increased influx of Ca^{2+} was found to be dependent on the magnitude of the mechanical stretch. By using Hook's law with a known elastic constant (k = 20-40 dyn/cm), tension required to activate 50% of the SA channels was estimated to be 8-16 dyne/cm, comparable to that for the SA

channels in in endothelial cells (5-10 dyn/cm, Naruse and Sokabe, 1993) and SA channels in chick skeletal or heart muscle cells (5-10 dyn/cm, Sokabe et al.,1993). These half maximum tension values are comparable to the lytic tension for lipid bilayers and cell membranes (2-12 dyn/cm) (Nichol and Hutter, 1996; Dai et al., 1998), indicating near lytic tension is required to activate 50% of the SA channels.

V. Mechanisms of mechanosensitivity

A. Overview

Gating is the process of opening or closing of a channel and is an important aspect of ion channel function. Activation of ion channels in the patch-clamped membrane by mechanical force inevitably leads to questions about how the mechanical force reaches MS channels. Several models for MS channels activation have been proposed but no conclusion has been reached yet for most MS channels. Among these models, two have drawn extensive attention. They are the tethered model and the lipid bilayer model. The difference between these two models is whether or not a cytoskeletal element is required in the transmission of the mechanical force to the MS channels.

B. Gating energy transmitted via spectrin-like network

MS channels were first reported by Guharay and Sachs (1984) in chick skeletal muscles. In patch-clamp recordings they found that applying suction increased the P_{open} of the channel. To test the possible involvement of the cytoskeleton in MS channel function, muscle cells were treated with a actin depolymerizer, cytochalasin. Surprisingly, results showed that disrupting actin filaments significantly increased the sensitivity of MS channels. An e-fold increase in P_{open} required 7 $cmHg^2$ in untreated cells whereas only 0.2 $cmHg^2$ was required to produce a similar change in cytochalasin-

treated cells. In contrast, tubulin reagents (vinblastine and colchicine) exhibited no effect on stretch sensitivity (Sachs, 1988), indicating that tubulin integrity is not needed for MS channels. Thus, neither tubulin nor actin was required for conveying mechanical energy, or are essential for the mechanosensitivity.

Cytochalasin treatment increased the sensitivity by 30-fold (from 7 to 0.2 $cmHg^2$), almost 10 times larger than expected if tension is generated in the bilayer since area elasticity of the cytochalasin-treated membrane is only 3-4 times lower than that of the untreated cell membrane (Guharay and Sachs, 1984). To account for this extra 10 times stretch sensitivity, it has been proposed that the channels are linked in series to a submembranous cytoskeleton that serves to concentrate stress on the channel from a large area of membrane (Guharay and Sachs, 1984). The fact that disruption of actin or tubulin did not abolish mechanosensitivity of the SA channels in chick skeletal muscle indicates that components of the cytoskeleton other than actin or tubulin are involved in the channel gating. A tethered model (**Fig. 1-5** , see Sachs and Sokabe, 1990) was thus proposed based on the assumption that the stretch-sensitivity could only result from connections between the channel and the underlying spectrin-like cytoskeleton (Guharay and Sachs, 1984). According to this model, mechanical stress is thought to be funneled into widely-spaced channels through the spectrin-like network, similar to that of an anion exchanger tethered to spectrin in red blood cells. When the parallel network of actin is disrupted (i.e., by actin depolymerization with cytochalasin), the effective mechanical stress on the spectrin network is increased and hence increased on the individual channels. This model received supports from several research groups (Sokabe et al., 1991; Sheetz and Dai, 1996) who showed that tension exerted on the lipid bilayer was too small to activate eukaryotic MS channels. Thus, most eukaryotic MS channels are gated by membrane tension

Figure 1-5. Cartoon of a tethered channel model for MS channels

MS channels are proposed to be interconnected via cytoskeletal proteins. Spectrin is a likely candidate for the cytoskeletal component. The hypothesis is that the continuous spectrin network, rather than the in-plane bilayer, would be the major load-bearing entity (from Sachs and Sokabe., 1990).

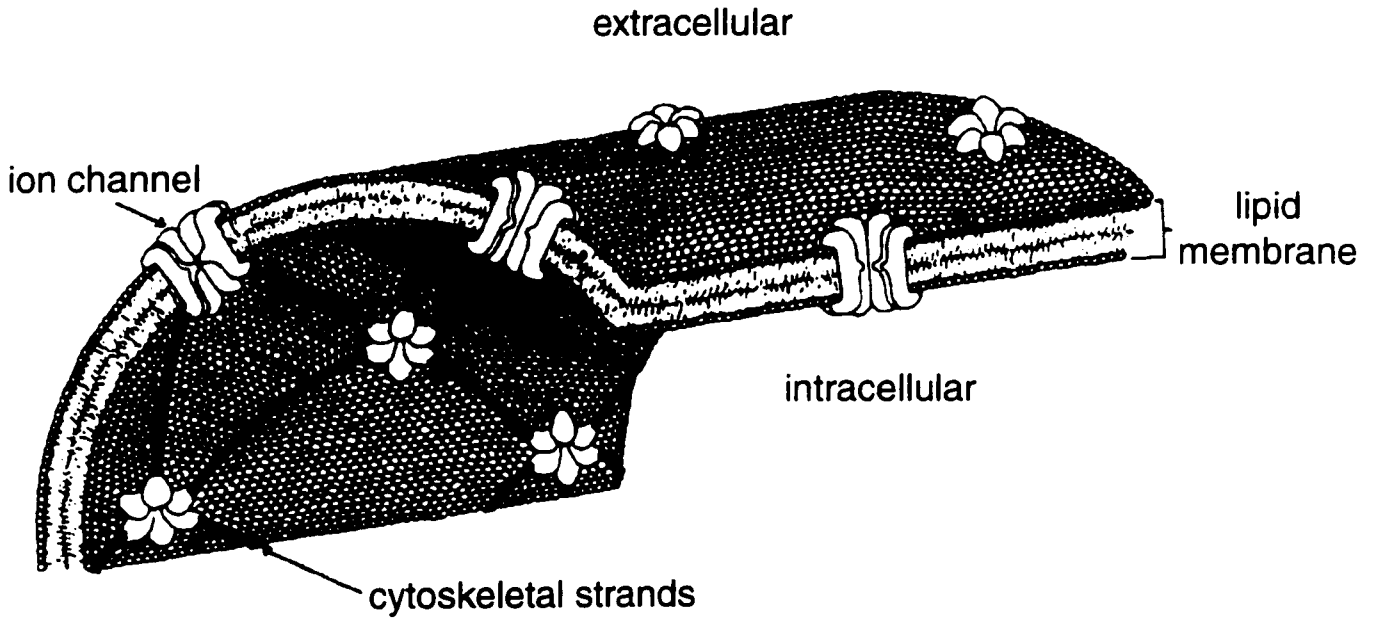
extracellular
ion channel
lipid
membrane
intracellular
cytoskeletal strands

probably transmitted via the cytoskeleton elements, similar to that of the hair cell MT channels. It is now known many channels such as Shaker-like K^+ channel (Kim et al., 1995) and NMDA channels (Kornau et al., 1995, 1997) are linked to cytoskeletal proteins like PSD-95.

C. Integrity of the cortical cytoskeleton and mechanosensitivity

The dramatic increase of the single MS channel mechanosensitivity in chick skeletal muscle by cytochalasin treatment suggests that at least part of the cortical cytoskeleton F-actin is mechanoprotective (Guharay and Sachs., 1984). In line with this notion, Terakawa and Nakayama (1985) reported that voltage-gated Na^+ and K^+ channels rely on the submembranous cytoskeleton for mechanoprotection. For internally perfused squid axons, electron microscopy together with current and voltage clamp studies (Terakawa and Nakayama, 1985) showed that after removal of the submembranous cytoskeleton by chaotropic anions, inflation (intracellular pressure with 15 cm H_2O or 11 mmHg) reversibly abolished the action potential and the voltage-gated currents were suppressed. The naked axon membrane became extremely sensitive to mechanical inflation when submembranous cytoskeleton were dissolved by chaotropic anions: a 1 cm H_2O (0.7 mmHg) rise resulted in a significant depolarization of the axon and a complete impairment of the voltage-gated currents. By contrast, for axons perfused with KF (non-chaotropic), where membrane cytoskeleton were intact, the same mechanical inflation had very little effect on either the action potential or voltage-dependent currents. These mechanical effects on excitability were unexplained, but the observation suggests that an intact membrane skeleton protects the function of channel proteins by absorbing mechanical energy that would otherwise create tension in the bilayer. This idea was articulated by Vandorpe and Morris (1992): *"MS channels are predisposed to act as mechanotransducers and in some cases do so, but the cortical actin cytoskeleton can shield channels*

from mechanical stimuli, allowing them to serve other cellular roles. Disruption of the cortical cytoskeleton makes the channels more susceptible to mechanical stimuli. Depending on circumstances, this can lead to useful MS signalling or it can engender pathology".

Increasing evidence supports that mechanical stress is probably shielded by the integral membrane cytoskeleton, and that mechanical tension can be better transmitted to MS channels when the cortical cytoskeleton is traumatized. In snail neurons, Small and Morris (1994) reported that SA K^+ channel became more readily activated by repeated suction or when actin filaments were abolished by cytochalasin, similar to the findings in chick skeletal muscles (Guharay and Sachs, 1984). This can be explained by Hamill and McBride (1992) who showed that sustained membrane stress induces a progressive decoupling of the membrane from the cytoskeleton in *Xenopus* oocytes. This phenomenon is also evident for NMDA channels in cultured mouse central neurons (Paoletti and Ascher, 1994). In the cell-attached configuration, repeated mechanical stimuli caused a progressively larger mechanical response, presumably due to decoupling of the membrane from the cytoskeleton which increased stretch sensitivity of NMDA channels. Consistently, in the same study but using the whole cell recording mode, mechanosensitivity is difficult to be demonstrated. And the mechanical effect only becomes visible after a prolonged osmotic challenge. These results suggest that in an intact cell, membrane cytoskeleton may protect the NMDA channels by dampening any tension exerted in the plane of the lipid bilayer. When cytoskeleton is traumatized either by depletion of ATP, patch excision or suction-induced damage to the membrane patch, NMDA channels became mechanosensitive (Paoletti and Ascher, 1994). In agreement with this idea, Small and Morris (1994) and Wan et al. (1999) showed that procedures that traumatize the membrane skeleton increased the mechanosusceptibility of TREK-like K^+ channels. More mechanoprotective role of the membrane

cytoskeleton can be found in **Chapter 6**.

D. Evidence supporting the lipid bilayer model

1. Gating energy conveyed by bilayer tension

As discussed in the previous section, it has been shown that disrupting cytoskeletal elements provokes a greater mechanosensitivity. Moreover, there are several pieces of evidence indicating that mechanosensitivity does not require the involvement of cytoskeleton coupling and that tension generated in the lipid bilayer may be transmitted directly to channels. The first and best evidence for MS channels to be activated via the lipid bilayer was from MscL, the cloned *E. coli* MS channels (Sukharev et al., 1994). These MscL channels were initially studied in native bacterial membranes, where excised patches from giant spheroplasts (Martinac et al., 1987) revealed two types of MS channels: a large conductance of 3 nS (MscL) and a small conductance of 0.9 nS (called MscS) and suction reproducibly provoked MscS and MscL channel activities. MscS channels are activated at -30 to -70 mmHg whereas MscL channels require -150 to -250 mmHg of suction (Sukharev et al., 1994). Upon detergent solubilization and purification to remove bacterial cell wall, the individual protein fractions were analysed for MS channel activity by reconstituting them into large, patch clampable liposomes. This lead to the strategy used for cloning the MS channels and also made it possible to test the hypothesis that the bilayer alone suffices to convey gating energy. The bacterial channel MscL remains fully functional in the lipid bilayer; gating in essentially the same way as it does in giant spheroplasts (Sukharev et al., 1994; Hase et al. 1995). Moreover, the amount of suction required to activate the MS channels is much lower than those in spheroplasts (Sukharev et al., 1994), indicating that the more complex membrane structures in spheroplasts may restrain some tension that would otherwise be felt by the channel protein. Taken together, these results show that

mechanosensitivity is an inherent property of these MscL channels, and that the bacterial cell wall components may be mechanoprotective. This, incidentally provides further support to the idea that channels are mechanically protected by association with cytoskeletal elements.

The alamethicin channel has also been shown to exhibit mechanosensitivity in simple bilayers (Opsahl and Webb, 1994). Alamethicin forms a peptide ring surrounding a central conducting pore when reconstituted into pure lipid membranes in the absence of cytoskeletal proteins. Using combined voltage clamp and microscopic techniques, the conductance changes were measured at increasing pipette pressures and the applied membrane tension was calculated (Opsahl and Webb, 1994). Single channel recordings indicate that membrane tension causes addition of alamethicin monomers to the channel perimeter (Opsahl and Webb, 1994). This demonstrates that membrane tension directly energizes mechanical force associated with the changes of membrane area (i.e. channels), accompanying changes of the conductance state. Two models, a fixed aggregate model and a barrel-stave model, have been proposed for mechanical signal transduction of alamethicin channels (Opsahl and Webb, 1994). The fixed aggregate model assumes a fixed number of polypeptides, with increased membrane tension causing an internal rearrangement of channel polypeptides. On the other hand, the barrel-stave model (**Fig. 1-6**) suggests that tension increases the aggregate conductance by addition of a peptide stave into the pore-forming barrel perimeter.

2. Activation by amphipaths (changing membrane curvature)

(i) Overview

A second line of evidence for lipid bilayer tension underlying MS gating is that channel mechanosensitivity can be mimicked by changing the properties of the lipid bilayer in the absence of cytoskeleton elements. Amphipath-induced membrane curvature, first shown to mimic the

Figure 1-6. Model of a MS gating transition in an alamethicin channel

Alamethicin is an antibiotic channel that forms a conducting pore with variable number of monomers (indicated by M). In the presence of tension, larger diameters of alamethicin channels are favoured; here one monomer is shown inserting (left) to increase the diameter of the pore, and thus the conductance (From Sachs, 1997).

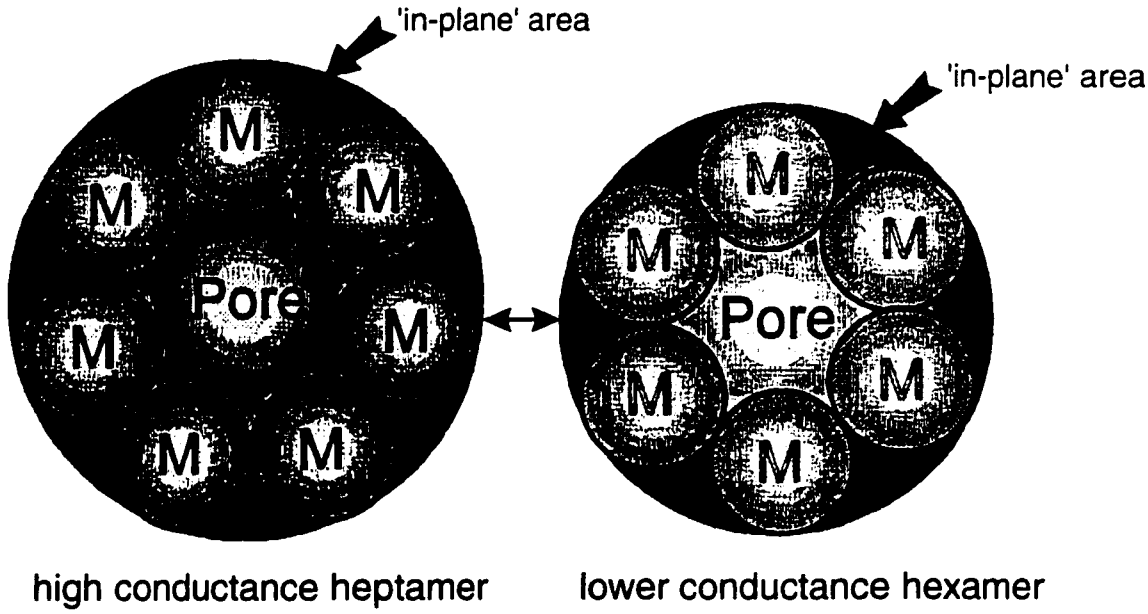
'in-plane' area
'in-plane' area
M
M
M
M
Pore
M
M
M
M
M
M
M
M
Pore
M
M
M
high conductance heptamer
lower conductance hexamer

mechanical effects on *E. coli* MS channels (Martinac et al., 1990), is now known to do the same on NMDA channels (Casado and Ascher, 1998) and on TREK, the S-like K^+ channels (Patel et al., 1998). It has long been known that amphipathic compounds can induce membrane curvature in opposite directions (Sheetz and Singer, 1974), changes thought to be due to the compounds preferentially inserting into the inner or outer leaflet of the bilayer (Martinac et al., 1990). This would expand one monolayer relative to the other and produce a microscopic bending of the bilayer that would transmit tension to MS channels. In this model, hydrophobic cationic amphipaths would insert into the relatively negatively charged inner leaflet, causing a concave bending (form cups). Conversely, hydrophobic anionic amphipaths would insert into the less negative leaflet, expanding it and creating a convex region of the cell membrane (form crenators). This bilayer couple model (**Fig. 1-7a**) may be important in transducing membrane tension into changes in channel P_{open}.

A cartoon (**Fig. 1-7b**, Sachs and Morris, 1998) about the formation of tension in one leaflet shows that the bilayer's two monolayers could have different tensions. Inserting amphipath molecules into the outer monolayer causes it to expand. If the outer and inner monolayers were limited in the number of available lipids, then expansion of the outer layer would stretch the inner monolayer and thereby activate the channel. An analogy for this coupled expansion effect would be pulling on a pair of elastic ropes (the monolayers), and then adding extensions (amphipaths) to one of the them. The load would be transferred to the shorter ropes (without amphipaths), increasing its tension. When both monolayers contained equal amounts of amphipath, the membrane area would increase equally in both monolayer. Thus, no tension would be created in either monolayer and the channel would not be activated (**Fig. 1-7c**).

Figure 1-7. Amphipaths changing the bilayer curvature and the MS channel behaviour

(a) Although both leaflets are negatively charged, the inner leaflet of the lipid bilayer has a higher density of negative charges. Hydrophobic cations (amphipaths) are preferentially inserted into the inner leaflet to form a concave curvature whereas hydrophobic anions (also amphipaths) are inserted into the outer leaflet to form a convex curvature. **(b)** If curvature is prevented and the number of lipid molecules in each layer is fixed, amphipaths added to the outer leaflet would expand the outer monolayer and this would put the inner monolayer under tension. The outer monolayer, in contrast, is not stressed because the amphipaths do the work of keeping the lipids apart. An MS channel in the bilayer is shown to be activated by the tension generated in the inner monolayer. **(c)** When amphipaths are inserted into both monolayers, the expanding tension is cancelled out and the MS channel tends to be closed (**a** is from Martinac et al., 1990; **b** and **c** are from Sachs and Morris, 1998).

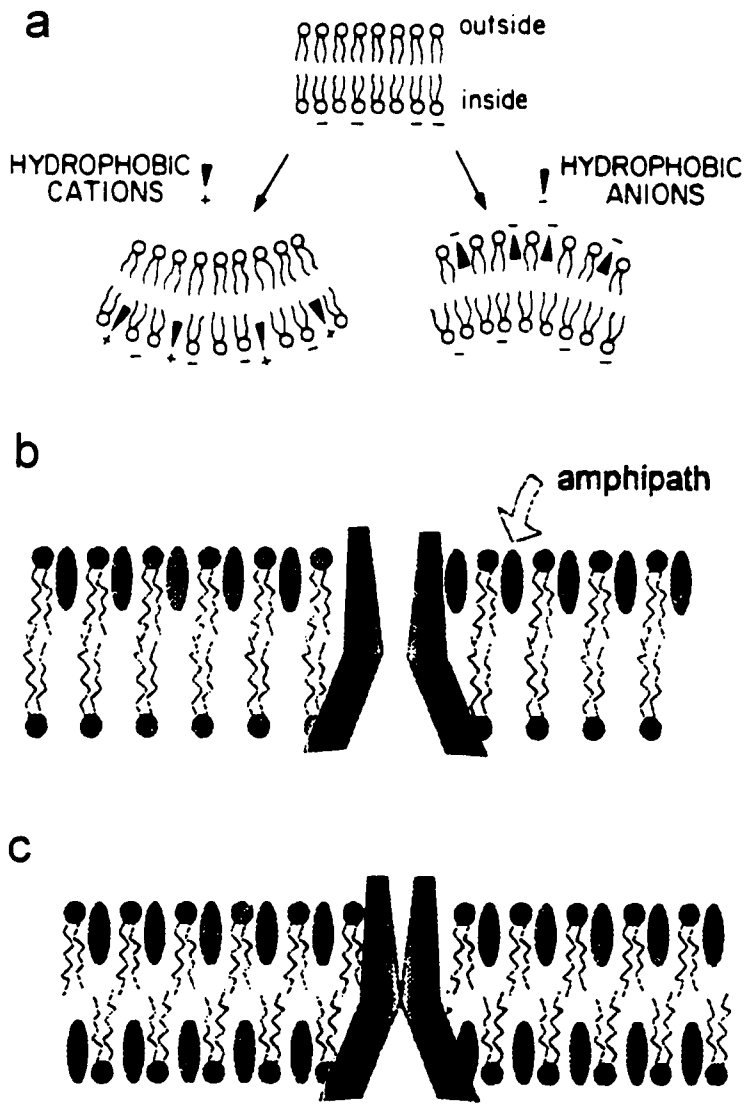
a
outside
inside
HYDROPHOBIC CATIONS
HYDROPHOBIC ANIONS
b
amphipath
c

(ii) Evidence from E. coli MS cationic channels

With the intent of modifying the lipid structure, Martinac et al. (1990) applied both cationic and anionic amphipaths and observed the gating of MS cation channels in *E.coli*. These experiments suggest that when amphipaths were inserted on either side of the bilayer, MS channels would be activated. When the amphipaths were inserted into both sides, MS channel activity returned to control levels. This observation was explained in that both convex and concave curvatures of the membrane would create a bilayer tension on the channel (Martinac et al., 1990) and induce an increased channel activity.

(iii) Evidence from cloned mammalian MS S-like K^+ channels

Evidence for curvature induced mechanosensitivity was also found in a recently cloned mammalian MS S-like K^+ channels, TREK-1 (Patel et al., 1998). Increased membrane tension augments P_{open} of TREK-1 channels expressed in *Xenopus* oocytes or mammalian cell-lines. In whole-cell patch clamp recordings, internally applied anionic as well as the neutral amphipaths (in the pipette solution) increase TREK-1 activity and mimic the effect of arachidonic acid metabolites. In contrast, cationic amphipaths inhibit its activity. These data suggest that bilayer curvature modification by various amphipaths exerts effects on channel activity. Consistent with this finding, TREK-1 retains its mechanosensitivity under conditions of cell-free patch in the presence of internal application of cytoskeleton-disrupting agents, colchicines (500 μM) and cytochalasin D (1 μg/ml). It is concluded that mechanical force is transmitted directly to the TREK-1 via the lipid bilayer without requirement of the cytoskeletal elements (Patel et al., 1998).

(iv) Evidence on NMDA receptor

The amphipath-induced effect was also evident for the mechanosensitivity of NMDA

channels (Casado and Ascher, 1998). Besides glutamate, this channel responds specifically to the agonist NMDA (McBain and Mayer, 1994). The NMDA response was recorded alternatively in the absence and in the presence of the amphipathic compounds (bath application) using a variety of patch clamp configurations: 1) nucleated patch on cultured mice embryonic neuron; 2) whole-cell recordings on NMDA channels expressed in HEK cells and 3) single channel recordings on outside-out patches from *Xenopus* oocytes expressing NMDA channels. Results are identical in all configurations and two pieces of evidence were provided in favour of the bilayer model. First, by varying amphiphilic compounds known to produce opposite deformations of the lipid bilayer, it was shown that lipid shape rather than charge is critical in determining membrane curvature and hence, the "MS" effect. For example, an amphiphilic compound with a large hydrophilic head decreased the NMDA response, mimicking the effects of patch compression. In contrast, an amphiphilic compound with a small hydrophilic head tended to increase the NMDA responses, mimicking the effects of stretch. Second, the NMDA channel has been previously shown to be connected to cytoskeletal elements (Kornau et al., 1995), it argues that the cytoskeleton was involvement in the NMDA mechanosensitivity (Paoletti and Ascher, 1994). More recent experiments designed to exclude this possibility showed that a mutant NMDA channel lacking the C-terminal residues that interact with cytoskeleton elements was still mechanosensitive even in excised cell-free patches. These results support the involvement of the lipid bilayer rather than linkage to cytoskeleton in the stretch sensitivity of NMDA channels (Casado and Ascher, 1998).

VI. Problems in studying MS channels

A. Lack of specific blockers

A major difficulty in studying MS channels is the lack of specific blockers. No compounds have been found with the high specificity and affinity of blockers used in structural and functional studies of, say, the voltage-gated Na^+ channels (e.g., tetrodotoxin). Three different classes of compounds, represented by amiloride, gentamicin and gadolinium, have been used for MS cation channel studies (Hamill and McBride, 1996). These compounds mainly act on SA cation channels, indicating a variety of "receptor sites" on MS channels. Of the various drugs that block MS channel, gadolinium (Gd^{3+}) is the most commonly used blocker with an effective concentration of 1-100 μM. In addition to SA cation channels (Yang and Sachs, 1989), Gd^{3+} also blocks SI cation channels (Franco et al., 1991; Oliet and Bourque, 1996). Unfortunately, it is also an excellent blocker of voltage-dependent Ca^{2+}, as well as Na^+ and K^+ channels (Boland et al., 1991; Lacampagne et al., 1994; Elinder and Århem, 1994a). More pharmacological features of Gd^{3+} can be found in **Chapter 3**.

B. Discrepancy between patch and whole cell study

Although almost every cell tested with patch clamp has revealed MS channels (see review of Sachs and Morris, 1998), very few have been reported to show MS currents at both the single channel and whole-cell macroscopic levels (e.g., Oliet and Bourque, 1993). This discrepancy underlies the controversy about the physiological role of most MS channels. Furthermore, despite numerous attempts made towards establishing a functional role for MS cation channels in *Xenopus* oocyte, there is no evidence to suggest that these endogenous MS cation channels are important for oocyte growth, maturation, fertilization or early embryogenesis (Steffensen et al., 1991; Wilkinson et al., 1998).

C. X-ray crystallography of a bacterial MS channel

The first gene encoding an MS channel (MscL) was cloned from *E. coli* (Sukharev et al., 1994). This bacterial MS channel comprised 136 amino acid residues (15 kD) arranged as a homomultimer, possibly a homohexamers (Blount et al., 1996a; Sukharev et al., 1997). Recently, the structure of the MscL homolog from *Mycobacteria tuberculosis* (Tb-MscL) was determined (Chang et al., 1998). From the x-ray crystallography at 3.5 angstroms resolution, the organization of Tb-MscL was established as a homopentamer, with each subunit containing two transmembrane α helices and a cytoplasmic α helice. The first transmembrane domain creates the bulk of the pore while the second transmembrane domain returns to the cytoplasm. A loop connecting two transmembrane domains dips into the pore region. This general pentameric organization and the pore architecture of Tb-MscL echo that of ligand-gated channels (e.g. NMDA channels). However, homologues of the MscL have not been found in eukaryotes. In addition to this, the intensive genetic, molecular, single-channel work (Blount et al., 1996b) has all failed to reveal the biological significance and physical basis for mechanosensitivity.

OUR APPROACH

In facing these unresolved problems and discrepancies in the study of MS channels, and prompted by the growing number of reports of mechanosensitivity in a variety of channel types, we decided to test the mechanosensitivity of a voltage-dependent channel. This decision was made because there were no cloned eucaryotic MS channels available at the time when this project was started. In the following section, the basic properties of voltage-dependent channels will be reviewed

and the emphasis will be put on voltage-dependent activation as it is most relevant to the channel that we studied.

OVERVIEW OF VOLTAGE-DEPENDENT CHANNELS

I. Voltage-dependent activation

Voltage-dependent ion channels, a superfamily of proteins including mainly K^+, Na^+ and Ca^{2+} channels, are exquisitely sensitive to membrane potential. They mediate action potentials in electrically excitable cells and play important roles in signal transduction in other types of cells (Armstrong and Hille, 1998). The general organization of all voltage-dependent channels is as follows: four homologous peptide subunits, each containing six transmembrane α-helices (S1-S6) surrounding a central ion conducting pore (Jan and Jan, 1989). A model for voltage-dependent channel is illustrated in **Fig. 1-8**. The highly conserved region among voltage-dependent channels is located on S4, the fourth of the six transmembrane segments. The S4 segment in each subunit (or domain) contains positively charged amino acid residues, either arginine or lysine, at every third position and is followed by two hydrophobic residues (**Fig. 1-9a**; Catterall, 1988).

Activation of voltage-dependent ion channels is proposed to result from a multiple voltage-driven conformational change that must precede the opening of a transmembrane pore. Hodgkin and Huxley first proposed that voltage-dependence may arise from voltage-sensitive components in the membrane, which they called gating particles (Hodgkin and Huxley, 1952). Armstrong and Bezanilla (1973) further predicted that collections of charged amino acid residues may be these gating particles. They showed that during voltage-dependent activation, charges associated with the channel

Figure 1-8. The structures of voltage-dependent channels

(a) Topology of the voltage-dependent Na^+ and K^+ channels. The topology for the voltage-dependent Ca^{2+} channel is similar to that of the Na^+ channel (not shown). Repeating motifs of Na^+ channels are labelled as I, II, III and IV (left), each homologous domain comprising six α-helical transmembrane segments (S1-S6, from N to C-terminus). The pore-region between segments S5 and S6 is indicated in the figure as a "V" shaped loop. The structure of the voltage-dependent K^+ channel showing one of the four identical subunits (right). **(b)** The generalized motif of voltage-dependent channels. The fourth of six transmembrane segment, S4, is enriched in positively charged residues for sensing the membrane potential, and intracellular N- and C-terminus for channel inactivation. In addition, voltage-dependent channels contain a pore loop responsible for ion conduction and selectivity. **(c)** Three dimensional arrangement of the six membrane-spanning domains of a voltage-dependent channel with pore loop indicated. **(d)** Tetrameric organization of a channel protein in membrane illustrates four subunits surrounding a central ion conducting pore (arrow, from Purves et al., 1997).

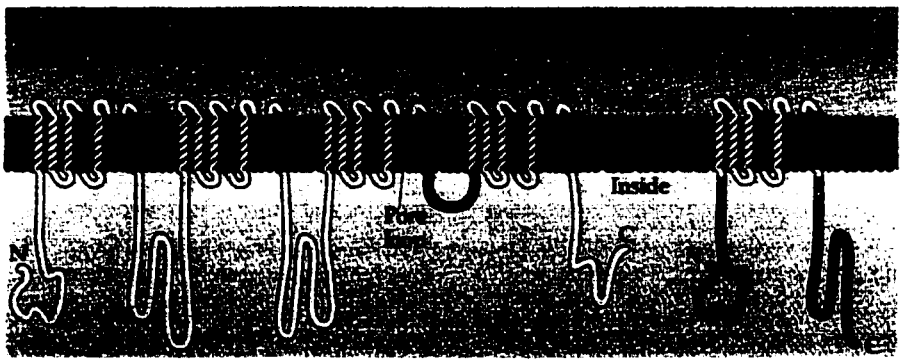
Inside

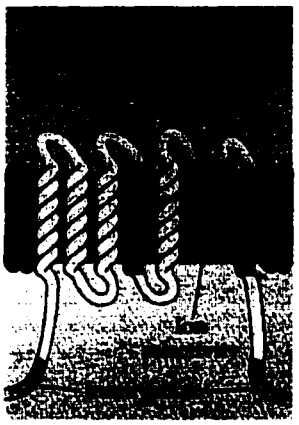

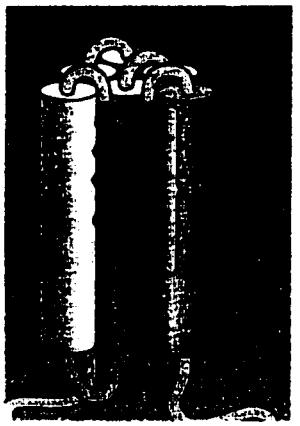

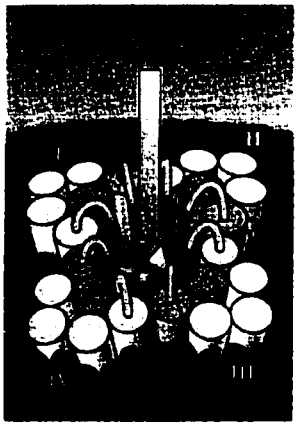

Figure 1-9. The S4 segment serves as voltage sensor for the voltage-dependent channels

(a) A comparison of the S4 sequences from the rat brain Na^+ channel, the rabbit muscle calcium channel, and the Shaker potassium channel. Positively charged amino acids, either lysine (K) or arginine (R) occur at every third position followed by two hydrophobic residues. **(b)** A model for the S4 region of voltage-dependent ion channels indicating how it could act as a voltage sensor. The transmembrane S4 helix is illustrated as a cylinder with a spiral ribbon of positively charged residues located on the outside of the helix where they are presumed to form ion pairs with the adjacent fixed negative charges contributed by the other transmembrane segments. During membrane depolarization (ΔV), the positively charged residues in S4 move outward by rotation of the helix, leaving unpaired negative charges on the inner surface of the membrane (from Hall et al., 1992).

a

Sodium channel (III S4)	G A I **K** S L **R** T L **R** A L **R** P L **R** A L S **R** F E
Calcium channel (III S4)	S L V **K** I L **R** V L **R** A L **R** P L **R** A I N **R** A K
Shaker potassium channel	**R** V I **R** L V **R** V F **R** I F **K** L S **R** H S K G L Q

b

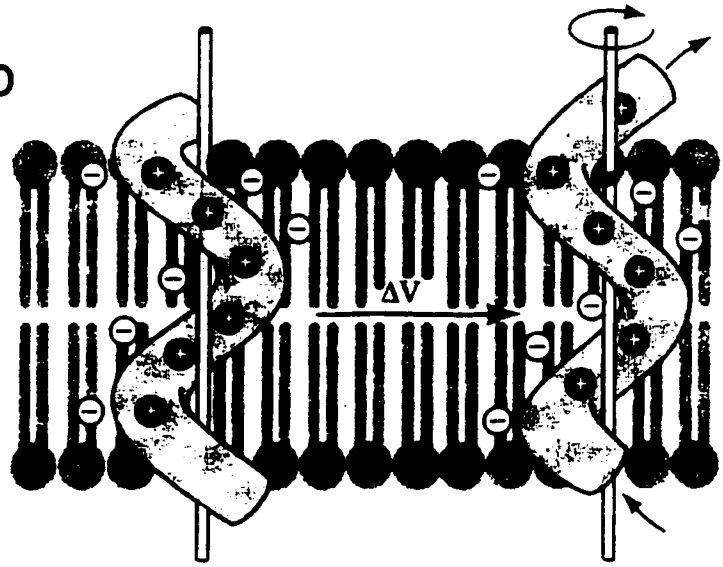

sense a change in the transmembrane voltage, and under voltage clamp, charge movement can be detected as gating currents. A "sliding helix" model of voltage-dependent gating was thus conceived (Armstrong and Bezanilla, 1973).

Since voltage-gated ion channels were first cloned, it has been postulated that they share a common mechanism of activation, in which the conserved S4 sequence acts as the primary voltage sensor (Noda et al., 1984; Catterall, 1986; Tempel et al., 1987). This hypothesis was based on the following points, although there was no direct physical evidence at that time. First, the S4 sequence is a highly conserved motif among different types of voltage-gated channels (Noda et al., 1984). Second, since the largest transmembrane voltage drop is in the region of low dielectric constant and high hydrophobicity, these charged voltage sensors would have to be buried within the membrane. Third, being in the membrane, these regularly arranged basic residues could thus feel transmembrane voltage changes (Catterall, 1986). According to an updated version of this model (**Fig. 1-9b**), the S4 sequence of positively charged amino acids may be the charged gating particle. At the resting potential, S4 may be stabilized by forming ion pairs with the nearby negative charges contributed by the other transmembrane segments (Catterall, 1993). In response to transmembrane depolarization, the S4 segment may move roughly perpendicularly towards the outer membrane surface, along a spiral path, and form a new set of ion pairs. Sequentially, the net transfer of gating charges across the membrane and thermal energy is sufficient to open the channel.

II. The voltage sensing S4 segments move outward during channel activation

A. Overview

Several authors have independently demonstrated that activation occurs as a result of the

outward transmembrane movement of these S4 segments on both voltage-dependent Na^+ and K^+ channels (Larsson et al., 1996; Mannuzzu et al., 1996; Yang and Horn, 1995; Yang et al., 1996). That is, an approximately 10 amino acid stretch of S4 residues that, at rest, is buried in a transmembrane protein canal and undergoes outward transmembrane movements in response to membrane depolarization, as would be expected for a voltage sensor (Larsson et al., 1996; Mannuzzu et al., 1996; Yang et al., 1996). Supporting evidence discussed below from a combination of three approaches demonstrates that S4 segments indeed move outward in response to changes of membrane potential. These approaches are: site-directed mutagenesis, cysteine-substituted mutagenesis and site-specific fluorescent labelling, all of which are used in combination with measurements of ionic or gating currents recorded by voltage-clamp techniques.

B. Site-directed mutagenesis

1. Overview

Via site-directed mutagenesis, each S4 basic residues has been replaced with either uncharged polar residues (neutralization mutations) or charged acidic residues (charge reversal mutations). Mutants were then expressed in *Xenopus* oocytes and electrophysiological properties of the channel were subsequently studied. In such studies, the voltage-dependence of channel activation is characterized by measuring the peak or steady-state conductance as a function of voltage to obtain conductance-voltage (G-V) curves. The slope (e-fold / mV) of these curves provides the basis for an estimate of gating charge, z. V_{50} (in mV) from the same curve indicates the 50% activation voltage.

2. The basic residues in S4 serve as gating charges

Site-directed mutagenesis and voltage-clamp recordings for the voltage-gated K^+ channel

Shaker demonstrated that neutralization of the positively charged residues in S4 caused an apparent reduction in the gating charge, z, and shifted the voltage-dependence of activation, as measured by V_{50} (Logothetis et al., 1992). For example, neutralization of one of the seven charged residues, an arginine, resulted in a ~50% decrease in z, indicating a larger movement of this charge across the electric field than one would predict if all 7 charged residues responded equivalently to the electric field. By contrast, neutralizing two arginine residues only produced an additional 11% decrease in z, it did not double the single neutralization effect. Such results suggest that each charged residue does not contribute equally to the total gating movement. In addition, all mutations including neutralization, conservative and charge reversal mutations of the same arginine shifted V_{50} to the right, with the charge reversal mutation having the most dramatic effect, up to 39 mV. These shifts suggest that these mutations reduced the voltage sensitivity and decreased the relative stability of the open conformations, as if this arginine favours the stability of the open state of the channel. Similarly, neutralization or charge reversal mutations of other charged residues in the S4 sequence not only decreased z but also shifted the G-V curve to more positive or more negative membrane potentials. All the above observations provide strong support that S4 is involved in voltage-dependent activation (Logothetis et al., 1992). Similar effects were also observed in the S4 segment of a Na^+ channel (Stühmer et al., 1989).

3. The hydrophobic residues in S4 also contribute to the voltage-dependent activation

Though the S4 segment is characterized by the positively charged residues at every third position, the interspersed hydrophobic residues are also important. If the S4 segments must move through the protein structure provided by the other transmembrane segments during the process of channel activation, the size and shape of the hydrophobic residues should also have a direct influence

on voltage-dependent activation. In support of this hypothesis, the mutation of a single leucine residue to phenylalanine (size change) in one S4 segment of a Na^+ channel shifts the voltage-dependence of gating by 20 mV (Auld et al., 1990). Similarly, the mutation of hydrophobic residues in the S4 segment of Shaker K^+ channels also causes significant shifts in the voltage-dependent activation. In this experiment, the six hydrophobic residues (five leucine and one alanine) in the S4 segment of Shaker (Lopez et al., 1991) were mutated individually. However, two of the six mutations gave a hyperpolarizing shift and the remaining four S4 mutations gave a positive shift in the G-V curve, with the most dramatic shift being 86 mV.

In contrast to the profound effects on S4 mutations, substituting highly conserved leucine residues with alanine in transmembrane segments other than S4 had little effect on the voltage-dependence of channel activation. Therefore, the S4 sequence appeared to be more importantly involved in voltage-dependent gating than the other five membrane-spanning segments (Lopez et al., 1991).

Thus, at this point, historically, the principle evidence that S4 functions as a voltage sensor came from the site-directed mutagenesis results showing that neutralizing or reversing charges in S4 reduced the gating charge and shifted the voltage range over which activation occurs (Logothetis et al., 1992). However, these studies did not prove that basic residues in S4 are the gating charges because activation of the channel was also affected by substituting hydrophobic residues in the S4 segment (Lopez et al., 1991). According to the S4 hypothesis, a number of charges within the S4 segment have to be moved across the membrane for the channel to open.

C. Cysteine-substitution mutagenesis

To test the hypothesis that the S4 segment moves outward during channel activation, it was

necessary to monitor the position of individual amino acids in S4. To achieve this goal, the positively charged residues were each substituted by a non-charged amino acid, cysteine. Subsequently, the accessibility of the cysteine to a bulky cysteine-modifying reagent methanethiosulfonate (MTS) could be tested. The MTS reagents mainly consist of the positively charged MTS-ethyltrimethylammonium (MTS-ET) and the negatively charged reagent MTS-ethylsulfonate (MTS-ES) which are capable of adding either positively (-SET) or negatively (-SES) charged groups to cysteine residues by disulfide bonds. Hence, these procedures are named "cysteine-substitution modification, or cysteine modification". Once the reaction had occurred, S4 should be stuck in place and voltage-activation should be impaired. By prediction, cysteine modification is voltage dependent and occurs only during the depolarization process, since depolarization pulls S4 along with this cysteine residue into the extracellular space. The rate of cysteine modification increases with depolarization and has the voltage dependence and kinetics expected for the movement of a voltage sensor. In other words, the substituted S4 residue is accessible to extracellular MTS reagents only when the channel is depolarized (Yang and Horn, 1995).

The evidence from cysteine-substitution experiments suggests that S4 segments move outward during activation. In this study, each of the eight basic residues in domain IV of the skeletal muscle Na^+ channel was substituted individually by cysteine. The properties of these mutants and effects of MTS modifications were tested with two-electrode patch-clamp recordings (Yang et al., 1996). In these experiments, since the S4 segment in domain IV was used, the voltage dependence of inactivation (rather than activation) was studied. If depolarization causes an outward movement of S4, then strong hyperpolarization should keep the residues buried in the membrane making them inaccessible to reagents applied extracellularly. By applying MTSET either internally or externally

while varying the membrane potential, Yang et al. (1996) showed that upon depolarization, two S4 basic residues move completely from an inwardly accessible to an outwardly accessible location. Evidently, a stretch of the S4 residues moves outward during depolarization. The modification rate increases with the greater depolarization. To exclude the possible effects of the positively-charged components from either arginine or -SET moiety on the rate of inactivation, a negatively charged MTSES was also used and showed a similar effect as that of positively charged MTSET. Therefore, the changes of inactivation kinetics by MTSET are not due to the restoration of a positively-charged residue, but, rather, to the bulkiness of the moiety. Using a similar approach, Larsson et al. (1996) showed the outward movement of the S4 segment in Shaker K^+ channel.

D. Site-specific fluorescence labelling

It has therefore been established that membrane depolarization causes an outward movement of positively charged residues in the membrane electric field. The movement of these charged residues (gating charge, Q) in S4 should be detectable as gating currents (i.e., dQ / dt). Although results from the cysteine-substituted mutagenesis have provided strong evidence that S4 segments indeed move outward during depolarization, these experiments failed to reveal how S4 moves or at which gating transition states (activation, opening, inactivation) S4 is moved. To further explore the molecular mechanism of S4 movement, a correlation between the movement of S4 and the displacement of the gating charge need to be established.

To address this question, site-specific fluorescence labelling of the Shaker K^+ channel combined with voltage-clamp measurements were used to study conformational changes of S4 during gating in *Xenopus* oocytes (Mannuzzu et al., 1996). Residues of S4 were substituted with cysteine and subsequently labelled with the membrane-impermeant fluorescent dye

tetramethylrhodamine-maleimide (TMRM) whenever cysteine became exposed to the extracellular side during depolarization. Both fluorescence and whole-cell gating current were measured with series of depolarizing voltage steps. To avoid the potential interference from native cysteine on fluorescence labelling, two native cysteines which could be accessible to the external solution in the Shaker channel proteins were substituted with two non-polar residues (alanine and valine) and cysteine present in endogenous oocyte plasma membrane proteins were blocked by non-fluorescent impermeant maleimide (Mannuzzu et al., 1996). Since the fluorescence of TMRM is sensitive to the polarity of its environment and has a short lifetime in the excited state, its conjugation to residues in S4, in the form of TMRM-cysteine complex (TMRM-C), could therefore report changes of the channel environment if TMRM-C moves from a position buried in the membrane to a more polar environment of extracellular fluid or *vice versa* (Mannuzzu et al., 1996).Thus, the gating currents reflecting the gating charge movements were assayed by voltage clamp and the accessibility of S4 residues to the extracellular TMRM were detected by confocal microscopy to quantify fluorescence intensity. From these two simultaneous recording techniques, the fluorescence-voltage (F-V) and the gating charge-voltage curves (Q-V) were obtained and compared. Depolarizing voltages caused a graded decrease in fluorescence which coincided with the kinetics of the gating current (Mannuzzu et al., 1996). The decrease in fluorescence during depolarization most likely reflects a polarity change of TMRM bound to cysteine residues when they move into extracellular solution. In addition, the increased outward exposure of S4 residues correlated in time and in voltage-dependence with the gating current, providing physical evidence in support of the hypothesis that S4 is the voltage sensor (Mannuzzu et al., 1996).

RATIONALE FOR EXAMINING MECHANOSENSITIVITY OF A VOLTAGE-GATED CHANNEL

I. Attachment of a voltage-dependent channel to the membrane cytoskeleton

We originally hypothesized (see **Appendix**) that a voltage-dependent channel may exhibit mechanosensitivity in its voltage-dependent gating when rigidly tethered to the membrane cytoskeleton, since mechanical gating energy might be transmitted to the channel via the cytoskeletal network. This "tethered channel" hypothesis was supported by two pieces of evidence. First, the morphological and physiological complexity of both hair-cell transduction and putative MT channel transduction in *C. elegans*, where mechanosensory structures are composed of a complex assembly of proteins. Second, the tethered MS gating model as proposed by Guharay and Sachs (1984) for eucaryotic cells and indeed many channels have attachments to the cortical cytoskeleton.

II. MS channels are ubiquitous and diverse

MS channels have been found in all cell types across five living kingdoms (Sachs and Morris, 1998). A recurrent finding is that the existence of MS channels is patch-related, almost every cell has one or two types of MS channels. For example, snail neurons have SA K^+ and SI K^+ channels (Morris and Sigurdson, 1989); chick heart muscle cells have five distinct SA channels (three K^+ selective and two cation selective) (Ruknudin et al., 1993) and three distinct non-selective MS channels have been reported in *E. coli* and identified by their conductance, stretch sensitivity as well as gating kinetics (Gu et al., 1998).

Shaker is both voltage-dependent and K^+ selective, there are examples of voltage-gated and

K^+ channels that exhibit mechanosensitivity. The voltage-dependent L-type Ca^{2+} channels from rat arteries, for example, are stretch sensitive (Langton, 1993); by applying either positive or negative pressures (via the patch electrode) or by changing the cell volume (via osmolarity), the authors showed that increases in membrane tension potentiated the Ca^{2+} current while decreases in membrane tension reduced it. This Ca^{2+} channel was also found to be sensitive to flow-induced mechanical stress (Ben-Tabou et al., 1994). These findings indicate that membrane tension can modulate the Ca^{2+} channel activities independent of its principle stimuli, the depolarized membrane potential (Langton, 1993). Various K^+ channels have been shown to respond to mechanical stimulation. These include the Ca^{2+}-activated K^+ channel (Taniguchi and Guggino, 1989), the ATP-sensitive K^+ channel (Van Wagoner, 1993), the G-protein regulated K^+ channel (Ji et al., 1998) as well as the S-like K^+ channel, TREK (Patel et al., 1998).

III. An unifying explanation for MS gating

Since many channels, from various cell types, display mechanosensitivity, it is reasonable to suggested that mechanosusceptibility is a common feature of different channel types, with diverse molecular structures. Since studies on cloned MS channels have not revealed a conserved mechanosensitive gating motif, even with X-ray crystallography, it is possible that a specialized motif may not be required for mechanosensation. It is possible that MS gating represents the inherent mechanosusceptibility of multimeric membrane proteins.

IV. Hypothesis

A. Global hypothesis

Based on the above rationale, a unifying explanation for the wide-spread manifestation of MS gating is that mechanosusceptibility is an inherent property of many transmembrane proteins, that became evident when a membrane's mechanoprotective features are circumvented as in patch clamp. Mechanosusceptibility may be a difficult to avoid feature for integral membrane proteins, unlike features such as K^+-selectivity and voltage sensing which can be regarded as highly conserved solutions to difficult evolutionary design problems.

B. Specific hypothesis

Under experimental conditions where native cellular mechanoprotection is absent, mechanosusceptibility can be demonstrated in an arbitrarily chosen channel with no known mechanotransducer function.

C. General approach

The well-studied, simplified voltage-gated homotetramer channel, Shaker-IR, was heterologously expressed and studied under the patch clamp conditions commonly used to characterize MS channels.

CHAPTER 2

General Methods

PREPARATION OF OOCYTES

I. Overview

The *Xenopus* oocyte is a good expression system for ion channels because of its large size and because it has only a few types of endogenous channels in the membrane. Injection of exogenous cDNA into the oocyte nucleus or cRNA into the cytoplasm can lead to expression of functional ion channels or receptors. Shaker cRNA injected into *Xenopus* oocytes give rise to new K^+ currents, confirming that the Shaker gene encodes a potassium channel (Zagotta et al., 1989). Although it generally works well, the oocyte system has certain problems. One is the variability of expression level either from toad to toad, from oocyte to oocyte, or with the change of seasons (Boyle et al., 1987). Another problem is an inhomogeneous distribution of heterologously expressed channels over the oocyte membrane (Goldin, 1991). This inhomogeneity can be a serious problem during single-channel recording; one might patch and finding nothing simply because the density was too low in that particular region. To compensate for these drawbacks, we initially recorded whole cell currents by two-electrode voltage clamp (TEVC) to screen for a good batch of Shaker-IR expressing oocytes, then switched to patch recording for further studies.

II. Maintenance of *Xenopus laevis*

Adult females of the South African clawed toad, *Xenopus laevis* **(Fig. 2-1a)**, were obtained from either NASCO (Fort Atkinson, Wisconsin, USA) or Xenopus I (Ann Arbor, Michigan, USA). Once they arrived, we generally waited at least 1 month before using them. The light cycle, room temperature as well as the water temperature are important factors in providing healthy oocytes (Sive et al., 1996). Although toads can withstand large variations in temperature, the quality of the oocytes decreases as the temperature is raised. Therefore, toads were maintained at ~ 20°C and exposed to a continuous light-dark cycle of 12 hours each. The toads were fed with frog brittle nuggets as per manufacture's instruction (Nasco, Fort Atkinson, Wisconsin, USA), three times per week.

III. Isolation of single oocytes

A. Surgery

Oocytes were prepared according to the method of Kushner et al. (1989). The isolation procedure started with surgical removal of the oocytes from the *Xenopus* ovarian lobe. A toad was placed in a container with ice/water in a ratio of about 1:1. After 20-30 min, the "drowsy" toad was placed on its back on an ice bed in a pyrex tray and covered completely with ice. Once anesthesized by the cold, a small area in the abdomen was cleared from ice for the incision. A sterile carbon steel surgical blade (#15, Becton Dickinson, Franklin Lakes, NJ, USA) was used to make a 1 cm lower abdominal incision through the skin and the underlying fascia. The ovarian lobes were gently pulled out from the abdominal cavity. Several clumps of oocytes were cut with scissors and placed immediately in Ca^{2+}-free OR2 solution (see **Solution** for recipe). After collecting approximately 200 oocytes, the remaining ovarian lobes were pushed back into the abdomen, and the incision was

Figure 2-1. *Xenopus laevis* and oocyte

(a) The clawed African toad, *Xenopus laevis*. **(b)** A single oocyte (stage VI) from an ovarian lobe of *Xenopus*. **(c)** A cartoon of an individual oocyte showing its two-toned colour scheme: the animal pole hemisphere is dark, while the vegetal pole is light coloured. Besides the oocyte plasma membrane, there are two additional layers: a layer of vitelline membrane surrounding the oocyte and a layer of follicle cells surrounding the vitelline membrane (modified from Purves et al., 1997 and Axon Guide [Axon instrument, 1993]).

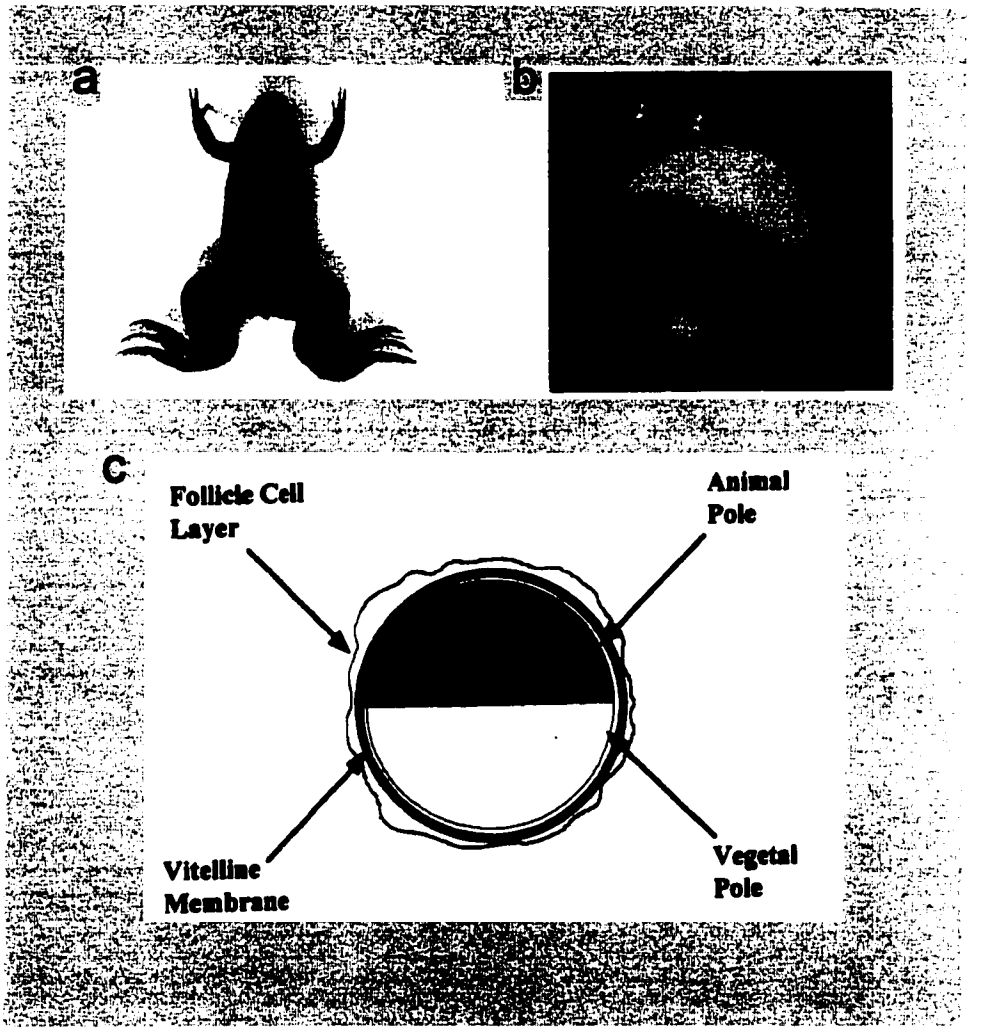
a
b
c
Follicle Cell Layer
Animal Pole
Vitelline Membrane
Vegetal Pole

closed with a synthetic absorbable suture (Cat. J422, Ethicon Inc. USA).

Under a dissecting microscope (Nikon, SMZU, Japan), the clumps of oocytes in Ca^{2+}-free OR2 were teased apart with a pair of fine No. 5 Dumont forceps (Electron Microscopy Sciences, Fort Washington, PA, USA) so that each clump opened into a single sheet of oocytes. After surgery, toads were left to recover in shallow water for a few minutes and then returned to their regular tank. Toads were repetitively operated on (up to four times) for harvesting of oocytes, but were allowed to rest for at least 2 months between surgeries. It was noticed that if the toad produced "good oocytes" (see below) last time, it would usually produce good oocytes the next time also.

B. Defolliculation of oocytes

Oocytes are encapsulated in several layers. From the inner to outer layer, they are, the vitelline membrane, follicle (**Fig. 2-1c**) and a connective tissue layer. The follicle layer as well as the connective tissue layer were removed to eliminate the endogenous channels or receptors on the follicle layer which may interfere with the assay of the expressed channels and to facilitate an easier penetration during injection. In brief, the freshly harvested oocytes were first rinsed in Ca^{2+} free-OR2 solution, then transferred to a 2 mg/ml collagenase (Type I, Cat. C130, Sigma, St. Louis, MO, USA) in Ca^{2+} free-OR2 solution and shaken at low speed (60 rpm) on an orbital shaker. After 2-3 hours of shaking at room temperature, the ovarian sheets began to separate into individual oocytes. The exact time of the enzyme treatment needed to loosen the follicle layer varied with different toads; the treatment was ended when the majority of oocytes were freed from the follicle layer. These individual oocytes **(Fig. 2-1b)** were then washed thoroughly in Ca^{2+}-free OR2 solution, placed in Ca^{2+} containing OR2 solution before injection. In cases when the follicle layer was partially removed by collagenase treatment, a pair of forceps was used to completely remove the follicle layer.

C. Selection of "good" oocytes

Oocytes from *Xenopus laevis* can be classified into 6 developmental stages; stages I to VI (**Fig. 2-2**) based on the size and general appearance of the oocyte (Dumont, 1972). Oocytes in stages I to III are small, with diameters ranging from 50 to 600 μm, and do not have a clear separation of the margin between the animal and vegetal hemisphere. Oocytes in the latter stages (stages IV to VI) are generally larger with differentiated hemispheres. At these stages, the animal pole is marked by a high concentration of melanin-containing pigment granules while the vegetal pole has a cream/white colour (**Figs. 2-1c and 2-2**). In addition to the homogeneous pigmentation uniformly throughout the animal pole, stage V or VI oocytes can be distinguished by an unpigmented equatorial band between the two hemispheres.

For expression purposes, the healthy, mature, stage V or VI oocytes are the best choice because they are large, 1000-1300 μm in diameter, can easily be injected with up to 100 nl solution and have significant translational capacity (Stühmer and Parekh, 1995). The quality of oocytes is graded according to their shape, size and appearance. For all experiments, "good" stage V or VI oocytes were selected based on the criteria that they are big, round cells with a smooth surface. The selection process usually starts after the collagenase treatment and the selected oocytes are maintained in Ca^{2+}-free OR2 (or ND96) solution at 21 °C. Generally, oocytes were left to recover overnight (at least 4 hours) before injection. As collagenase would damage oocytes to a certain degree, longer enzyme treatments required longer recovery time.

Figure 2-2. Six developmental stages of *Xenopus* oocytes

Xenopus oocytes of different stages after defolliculation. The smallest transparent oocyte is at stage I, while oocytes of increasing size represent stages II-VI, respectively. Stage VI oocytes are the largest cells, with a diameter 1.0 - 1.2 mm. These were selected for experimental study (from Smith et al., 1991).

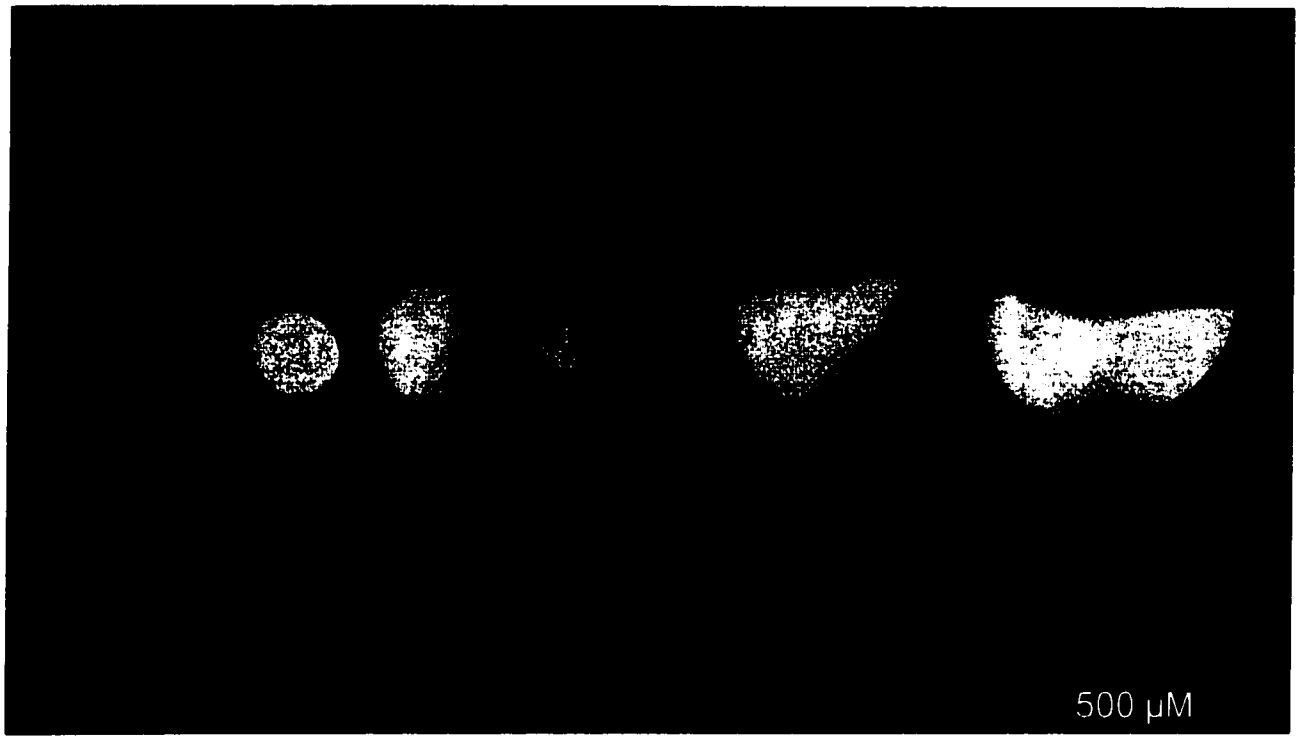
500 µM

PREPARATION OF SHAKER-IR cRNAs

The following information in part I (A, B) and II (A, B) of this section is provided but the work was accomplished by Dr. Peter Jurunka in Dr. Morris' laboratory. Part II (C) was done by myself.

I. Subcloning of Shaker-IR into pcDNAI/Amp

A. Overview

The Shaker-IR (inactivation removed) cDNA clone (1845 bp) was provided by Dr. C. Miller at Brandeis University (Waltham, MA, USA) in a pBluescript vector (pBS-KS+, Stratagene, USA). This cDNA clone encodes a modified Shaker-IR protein with an amino acid segment (Δ6-46) deleted from its N-terminus to remove the fast inactivation (Hoshi et al., 1990). In addition, the encoded Shaker-IR protein also has an 8 amino acid epitope (1D4) from bovine rhodopsin at the C-terminus.

The Shaker-IR cDNA in the pBS-KS+ vector was subcloned into the pcDNA1/Amp eukaryotic expression vector (InVitrogen Inc., Carlsbad, CA, USA) for expression in *Xenopus* oocytes by nuclear injection. The pcDNA1/Amp has the transcription enhancer and promoter elements from the immediate early gene of the human cytomegalovirus (CMV) for high level expression followed by a versatile multiple cloning site for cloning inserts.

B. Subcloning

The Shaker-IR pBS construct was digested with SacII and XhoI restriction enzymes and the ends were filled in with Klenow DNA polymerase and 4 dNTPs to create blunt ends. The blunt-ended Shaker-IR DNA [which contains the complete Shaker-IR coding sequence as well as 183 bp of the 5' untranslated region (5'UTR)] was separated from the pBS vector by electrophoresis

on a 0.8% agarose gel. The DNA band for Shaker-IR was then excised from the gel and purified using the GeneClean II kit (Bio 101 Inc., La Jolla, CA, USA). The pcDNAI/Amp vector was digested with BamHI and XhoI, blunt-ended and gel purified as above. The vector was then treated with calf intestinal alkaline phosphatase (CIP) to remove 5' phosphate groups from the ends of the DNA in order to prevent recircularization of the vector. The gel purified blunt-ended Shaker-IR DNA was ligated to the CIP-treated blunt-ended pcDNAI/Amp vector in an overnight reaction at 16°C with T4 DNA ligase and ATP.

The ligation products were transfected into *E.coli* XL1-blue cells by electroporation. These cells were then plated onto LB agar plates containing 50 μg/ml ampicillin (which selects for cells that have taken up the plasmid) and the plates were incubated overnight at 37°C to form colonies. Individual colonies were picked and put into LB broth with ampicillin and cultured overnight at 37°C. The plasmid DNA was prepared using the Wizard prep DNA isolation kit (Promega, Madison, WI, USA). The orientation of the Shaker-IR DNA with respect to the CMV promoter was determined by digestion with the restriction enzyme HinDIII. Finally, the plasmid Shaker-IR cDNA was dissolved in injection buffer (see Solution for recipe) to a final concentration of 0.1 mg/ml for nuclear cDNA injection.

II. Subcloning of Shaker-IR into pSP64TM vectors

A. Overview

The Shaker-IR cDNA clone was subsequently subcloned into a modified "Melton" expression vector (provided by Dr. Johne Liu, Loeb Research Institute, Ottawa, Canada) pSP64TM (Krieg and Melton, 1984) from the pcDNAI/Amp vector for two reasons. First, pSP64TM contains

the sequences of the 5' and 3' UTR of a *Xenopus* gene β-globin as well as a poly(A) tail, which enhances the stability of RNA transcripts in *Xenopus* oocytes. Second, this vector has the bacteriophage SP6 promoter which can be used to synthesize large amounts of cRNA *in vitro* for injection into oocytes cytoplasm.

B. Subcloning

The Shaker-IR-pcDNAI/Amp was digested with HinDIII which removed the Shaker-IR cDNA and Shaker-IR 5'UTR from the plasmid. The DNA was again blunt-ended and gel purified as above. The pSP64TM vector DNA was linearized between the 5' and 3' UTR ß-globin with BglII, blunt-ended and CIP-treated as above. The blunt-ended Shaker-IR and blunt-ended CIP-treated vector were ligated overnight, transfected into *E.coli* XL1-blue cells and the DNA was prepared from colonies as previously described. Importantly, this initial construct then had two possible initiator methionine codons in the context of good Kozak sequences (Kozak, 1987) that would result in translation initiation at the first, albeit " incorrect" ATG. Schematically the two Kozak construct appear as:

5'*Xenopus* β-globin UTR....Xenopus β-globin Kozak-ATG....5' *Drosophila* Shaker-IR UTR ....*Drosophila* Shaker-IR Kozak-ATG..... Shaker-IR coding sequence..... 3' *Xenopus* β-globin UTR.

Since both of the ATG initiator codons are within a NcoI restriction enzyme site (CCATGG) we simply digested this construct with NcoI and then re-ligated at this site to produce the Shaker-IR-pSP64TM clone with the correct Shaker-IR initiation methionine codon and no 5' Shaker-IR UTR sequences.

C. *In Vitro* transcription cRNA

In vitro transcription was performed by me using an Ambion kit according to manufacturers instruction (Ambion Inc., Austin, TX, USA). Shaker-IR cRNA was generated from the EcoRI linearized plasmid using SP6 RNA polymerase (Ambion SP6 mMESSAGE kit, Ambion Inc., Austin, TX, USA). After removing the template DNA with RNase-free DNase I, cRNA was precipitated, resuspended in RNase-free H_2O to give a final concentration of 1 mg/ml. It was important not to thaw and refreeze the Shaker-IR cRNA, as we noticed that such treatment produce low expression of the Shaker-IR protein. The suspended Shaker-IR cRNA was aliquoted into 2 µl volumes and stored at -80°C.

MICROINJECTION

I. Preparation of transferring and injection pipettes

For transferring oocytes, tips of 9" Pasteur pipettes were shortened and fire polished, yielding a large smooth-rimmed opening which was necessary to prevent damage during oocytes transfers. Injection pipettes were prepared shortly before injection, using a programmed pipette puller (Sutter Instrument Co. Model P-87, Novato, CA, USA) and 30 µl Microcaps pipettes (Cat. 1-000-0300OD, Lambdas, Drummond Scientific Co. Broomall, PA, USA). The pulling protocol was varied to give a fine-tipped pipette with a long, thin shank. To give the injection pipettes an ellipsoid opening, the tips of the pipettes were gently broken at an 45° angle with a pair of Dumont No. 5 forceps. This procedure was performed under a microscope until the opening diameter was approximately 10 to 15 µm. The pipettes were stored in a dust-free lidded container.

II. Sample preparation and pipette calibration

Extreme care was taken when handling Shaker-IR cRNA to prevent contamination with RNases. Shaker-IR cRNA was taken out from -80°C freezer and allowed to thaw for approximately 2 min at room temperature. To precipitate insoluble debris present in the RNA solution, the Shaker-IR cRNA was centrifuged 25 g at room temperature for 5 min and then placed on ice. This process reduced the likelihood of clogging the injection pipette. The injection pipette was inserted into a pipette holder and mounted on a hand-driven 3-D coarse manipulator (Narishige, Japan). 2 μl of Shaker-IR cRNA solution was then placed on a piece of parafilm (Greenwich, CT, USA) and the pipette tip was inserted into this droplet. Using a Pico-Injector PLI-100 (Medical Systems Corporation. Greenvale, NY, USA) (**Fig. 2-3**), the Shaker-IR cRNA was taken up into the injection pipette by applied negative pressure. The same Pico-Injector was also used to inject Shaker-IR cRNA into oocytes by applied positive pressure.

Prior to injection, each pipette was calibrated individually. The following procedure was used in determining the injection volume. First, the amount of cRNA injected was estimated by injecting a droplet of water onto a polyethylene calibration mesh (5 μl / division). The injection time (duration) was adjusted via the injector device setting until the droplet gave the appropriate volume. For example, 10 μl corresponded to approximately 2 divisions on the mesh.

III. Microinjection of Shaker-IR cRNA into the cytoplasm

As oocytes have a tendency to move away when the pipette touches them, it was essential to stabilize the oocytes during injection. To achieve this, oocytes were placed onto sterilized gauze in Ca^{2+}-free OR2 solution or onto an injection vessel prepared from a 60 mm plastic petri dish with

Figure 2-3. Microinjection set up

Pico-injector (PLI-100) (1) with pedal control (2); Micromanipulator (3); Injection pipette (4) connected to Pico-injector with nitrogen-filled 3 mm tubing; Binocular with fiberoptic illuminator (5); Injection solution drop on Parafilm (6); Injection chamber (7) with black tape for better viewing; stable support for hand (8); Wide opening transfer pipettes and fused pipettes for adjusting oocyte position (9); Dumont #5 fine forceps (10). I, injection; A, aspiration; P, purge (from Bertrand et al., 1991).

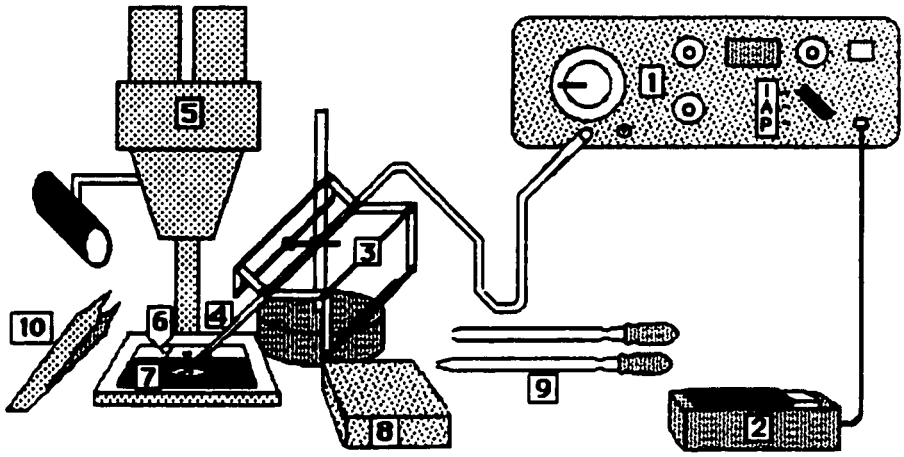
1
5
3
10
6
4
7
8
9
2

a piece of polyethylene Nitex mesh (Fisher Scientific, Pittsburgh, PA, USA) glued to the bottom. The grid wells of the mesh are similar in dimension to the diameter of the oocyte, and the sheet of Nitex was fixed permanently to the bottom of the petri dish with a few drops of chloroform.

The selected oocytes were placed under a dissecting microscope illuminated with a non-heat transferring Fiber Optic Illuminator (Model 9745-00, Cole-Parmer Instrument, Chicago, Illinois, USA) (**Fig. 2-3**). The binocular (eye piece) was set at a low magnification (0.7 x 10) to ensure a wide field of view. Approximately 10 oocytes were placed in the injecting chamber which had black adhesive taped to the back to permit better visualization. To inject cRNA into the cytoplasm, the vegetal hemisphere of the oocytes were oriented upward with a fire-polished (fused-tip) Pasteur pipette, so that the nucleus would be avoided.

Once the injection pipette was filled with Shaker-IR cRNA, it was positioned over each oocyte and lowered at a 70° angle until it pierced the oocyte. 10-30 nl of 1 mg /ml cRNA solution was injected into the cytoplasm at the vegetal pole of each oocyte. The amount of injected cRNA was varied to control the level of expression (10 nl for single channel recording and 30 nl for macro-patches). After injection, the oocytes were transferred into a small petri-dish with Ca^{2+}-containing OR2 (with 1 mM $CaCl_2$) solution supplemented with 100 U/ml antibiotics (penicillin/streptomycin, Sigma, St. Louis, MO, USA) and 2.5 mM sodium pyruvate (BDH Inc., Toronto, Canada). The solution was changed and the injected oocytes were inspected daily under a microscope. Dead oocytes were discarded. The oocytes were maintained in Ca^{2+}-containing OR2 solution at 20°C to allow for translation. Non-injected control oocytes were set aside in each batch. Sometimes, an equal volume of H_2O was injected into oocytes as controls.

IV. Microinjection of Shaker-IR cDNA into the nucleus

Although cytoplasmic injection described above was the major injection method, a nuclear injection method was used initially to explore the optimum method to increase the rate of expression. Nuclear injections require aligning the nucleus on the top surface of the oocyte so that the injection pipette could be inserted into the appropriate location. To achieve a higher success with the nuclear injections, the oocytes were centrifuged (Kressmann et al., 1978) at 2,000 rpm for 5 min. This process draws the nucleus to the animal pole of the oocyte, giving a whitish appearance in the black animal pole. This whitish spot marks the position of the nucleus for injection. When injecting, it was important to place the micropipette near the centre of the pigmented hemisphere and to drive the tip into approximately one fifth of the diameter of the oocyte.

Individual oocytes were injected with 100 pg/nl Shaker-IR or ShanX cDNA (see **Appendix** for constructs). Since the nucleus has a volume of approximately 50 nl, only about 10 nl of cDNA was injected, corresponding to 1 ng DNA (Bertrand et al., 1991). After injection, the oocytes were transferred to fresh Ca^{2+}-containing OR2 or ND96 solutions with antibiotics and maintained at 19°C to allow for translation.

ELECTROPHYSIOLOGY

Two to six days following the injection, voltage-dependent currents associated with the heterologously expressed channels were recorded at three levels of resolution using either the TEVC or patch clamp technique. All experiments were performed at room temperature (20 - 23°C). TEVC technique was used to study whole cell currents in the oocyte. A detailed description of the TEVC

technique will be presented in **Chapter 3**. Patch clamp was used to study channel properties at both macro- (many channels) and single- (or a few) channel levels depending on the number of channels in the patch and the size of the recording pipette tip. In the following section, an overview of the patch clamp technique is provided, starting with manufacturing of recording pipettes followed by a detailed description of cell membrane preparation and how to achieve a gigaohm seal between the pipette and the cell membrane.

I. Patch clamp overview

Patch clamp is an extreme powerful technique developed by E. Neher and B. Sakmann (Neher and Sakmann, 1976). Instead of controlling the voltage across the membrane of the whole cell as required for TEVC, this technique clamps or holds the voltage across an isolated piece of membrane (patch) while the currents from all channels in that patch are recorded. This configuration provides a low-noise level recording so that the opening and closing of single channels can be observed. Moreover, it allows for current recordings in small cells which may not be accessible by the TEVC technique where two electrodes need to be inserted into the cell. Since the main goal of this project was to study the MS channel behaviour on a voltage-dependent channel, patch clamp recording was optimum because mechanical stimulation could be applied through a recording pipette and the cell membrane could be stretched to various extents by varying pipette pressures.

Several patch clamp configurations can be applied, such as cell-attached, or inside-out recordings (**Fig. 2-4**). The cell-attached and inside-out (sometimes termed "excised" patch) configurations used in this study will be discussed in the following sections. The cell-attached or inside-out patch can each be subdivided into macro- and single-channel patch clamp configuration

Figure 2-4. Various patch clamp configurations

Top: cell-attached patch. Lower left: whole-cell recording. Lower right: inside-out excised configurations. Relationship between three patch configurations are shown by arrows, from cell-attached, strong suction ruptures the membrane to form whole-cell recording (not used in this thesis) whereas retraction of the pipette from cell-attached patch forms an inside-out configuration (from Purves et al., 1997).

Various configurations in patch clamp

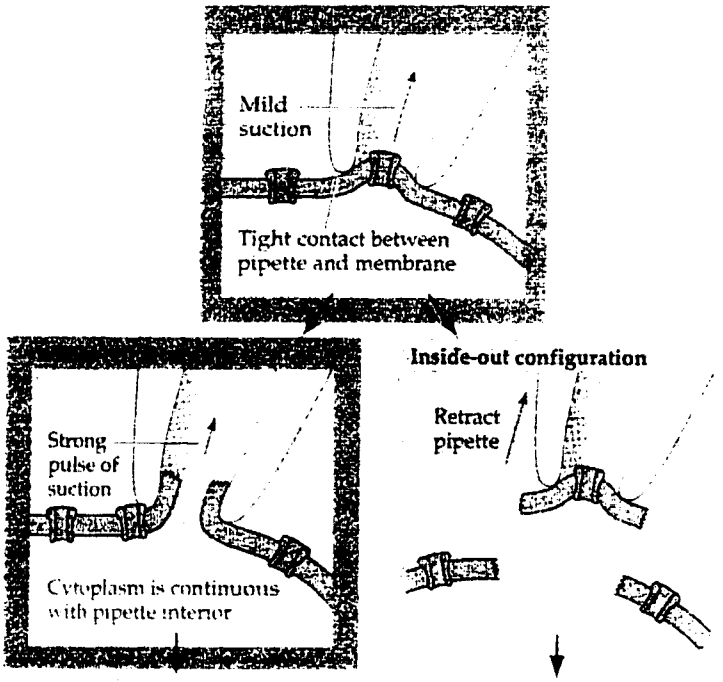

according to the number of channels in the patch.

II. Manufacturing of recording pipettes

Electrode pipettes for patch-clamp were pulled on a two-stage L/M-3P-A vertical puller (Darmstadt, Germany) using thick-walled borosilicate glass N51A (OD 1.65 mm, ID 1.15 mm; Garner Glass, Claremont, CA, USA). For large macropatches, pipettes had shorter taper tips in order to reduce the access resistance. In order to reduce electrode capacitance and decrease recording noise, the pipette tips were coated with Sylgard 184 (Dow Corning, Midland, MI, USA) and a minimal volume of solution (just enabling the electrode wire to contact the electrode solution) was used in the recording pipette. Uncured Sylgard was applied to the pipettes with a small applicator and then solidified by heat exposure immediately prior to use. For single channel recordings, almost the entire pipette shank was coated with Sylgard to about 100 μm above the pipette tip. The pipette tips were fire polished. Macropatch pipettes had a diameter of 3 - 6 μm and single-channel patch pipettes of 1 - 2 μm. The pipette resistances, when filled with normal frog Ringer (saline solution), were 2-5 MΩ for single channel and 0.4-2 MΩ for macropatch recordings. For filling the pipette, a small quantity of filtered pipette solution was stored in a covered 500 μl eppendorf tube and backfilled into the pipette using a drawn-out (by heat) 1 ml plastic syringe. The connection between the solution in the recording pipettes and the patch clamp amplifier was made by using chlorided Ag/AgCl wire. Intermittently, one or twice per week, the Ag/AgCl electrode wire was cleaned with emery paper and re-chloridated.

III. Preparation of the surface of the oocytes

The vitelline membrane of the oocytes, which prevents seal formation, was removed manually with fine No. 5 Dumont forceps under 40x magnification using a Wild M8 dissection microscope (Wild Leitz Canada, Willowdale, Ontario, Canada). Devitellination was usually performed on one oocyte at a time by placing it in a hyperosmolar solution (see section of Solution) for 3-10 min. In this solution, oocytes shrink and the vitelline membrane can then be separated from the plasma membrane and removed manually with forceps under the dissecting microscope. Only those oocytes that exhibited a clear separation between vitelline and plasma membranes were used and others were discarded. Two pairs of forceps were used to take the vitelline membrane off. One was fairly sharp, with the points slightly bent towards each other to give a pincer for grabbing the vitelline membrane. The other pair with slightly blunt tips, was used to hold on the other end of vitelline without poking through. Usually, the vitelline membrane came off in a complete shell.

Once the vitelline membrane was removed, oocytes were extremely fragile and ruptured easily when exposed, even briefly, to an air-water interface. They also became very sticky and adhered strongly to the plastic petri dish in just a few min. To minimize manipulation, the stripped oocytes were immediately transferred to the centre of the recording chamber (35 x 10 mm petri-dish, Becton Dickinson Labware, Lincoln Park, NJ, USA) with an appropriate bath solution for either cell-attached or inside-out patch clamp recording.

IV. Seal formation

Both the bath and the patch pipette solutions were filtered prior to use using a 0.2 μm syringe filter (Nalge company, Rochester, NY, USA). This is because dust and other suspended particles can

prevent seal formation. Positive pressures (4-7 mmHg) were maintained in the pipette as it passed the air-water interface into the bath solution to prevent exchange of the bath and pipette solutions and to prevent particles from clogging the pipette prior to seal formation. The pipettes were then sealed onto the oocyte by gently pressing the pipette against the oocyte membrane, while applying gentle suction to the back of the patch pipette (see **Fig. 2-4**). Gigaohm seals on devitellinated oocyte were readily formed using mouth suction by slowly increasing the suction from 5 to 10 mmHg for less than 10 s. Sometimes, gigaseals formed spontaneously when releasing the positive pressure and touching the membrane. Gentle suction was used throughout this project because a stronger suction may cause disruption of the cortical cytoskeleton associated with the patched membrane (Hamill and MacBride, 1992).

V. Two patch clamp configurations

A. Cell-attached patch configuration

The cell-attached configuration (**Fig. 2-4**) is formed when a gigaseal is obtained with the oocyte membrane. An advantage of this configuration is that normal intracellular constituents are less disrupted than in any other configurations and patches are electrically stable, sometimes enabling recording for nearly an hour without breaking the gigaohm seal. To study the MS channel behaviour, either negative (suction) or positive (blowing) pipette pressure was applied to the oocyte membrane via the side port of the recording pipette. However, it was difficult to maintain cell-attached patches with large, repetitive suctions. Thus, small (about 20 mmHg) and short (2 second) mechanical stimuli were generally used in order to complete the experimental requirements. These requirements included observing responses when stretching the membrane curvature using either suction / blowing

or by using a series of pressure steps.

A disadvantage of this configuration is that the exact membrane potential is unknown. In cell-attached patches, the net electrical potential across the membrane (V_m) is equal to the resting transmembrane potential of the cell (V_{rest}), minus the pipette potential (V_p), according to a formula of $V_m = V_{rest} - V_p$. The polarity of the pipette potential is opposite to what the membrane "feels", a negative potential applied to the pipette depolarizes the membrane patch. Positive currents are defined as positive charge flowing outward through the membrane into the pipette (illustrated as upward current deflections). And negative currents are positive charges flowing inward from the pipette into the cell. V_{rest}, obtained from TEVC recordings with normal frog Ringers solution in the bath, was -48.9 ± 0.43 (SEM, n = 107). Thus, V_{rest} = -50 mV was used in calculations for cell-attached patch experiments.

B. Excised inside-out patch configuration

The inside-out patch configuration (**Fig. 2-4**) was achieved by rapidly withdrawing the pipette from the oocyte after a gigaseal had been formed. A standard excised patch solution was used (Hoshi et al., 1994), except that Ca^{2+} was omitted from bath. It was thought that Ca^{2+} may activate endogenous Ca^{2+}-activated Cl^- channels during the excision process (Methfessel et al., 1986). Also, it was noticed that Ca^{2+} promotes membrane fusion and vesicle formation when forming inside-out patches. The success rate for obtaining excised patches was almost 90%. Excised patches were more fragile than cell-attached patches. Mechanical stimuli could easily break the seal, especially for the larger patches. About one quarter of the excised patches were unable to sustain the first suction even with a low level of suction (~10 mmHg).

In most experiments, the inside-out excised patch configuration was used because it allowed

for accurate V_m measurements and for control of ionic gradients across the patch. The V_m is no longer influenced by the V_{rest} and is simply opposite in polarity to the pipette potential (V_p), $V_m = -V_p$. Thus V_m can be defined without knowing V_{rest} of oocyte. The convention for polarity of membrane currents is identical to that in cell-attached patch configurations.

For the experimental design, the excised patch provides several additional advantages. First, it has minimal cytoskeleton attachment and cytoplasmic components. This is a useful feature as we can largely exclude the possible influence of a well-organized membrane cytoskeleton, as well as cytoplasmic second messengers as an explanation for any observed mechanical effects. Second, in this configuration, the patch has limited membrane area which should not change largely during suction.

MECHANICAL STIMULATION OF THE CELL MEMBRANE

When mechanical stimulation was applied to the plasma membrane, patch clamp was preferred over TEVC because hydrostatic pressure can be applied easily through the patch pipette as either sustained suction or dynamic suction steps. Changes of pipette pressure were achieved as described previously (Small and Morris, 1994) using two pressure transducers DPM-I (Biotek Instrument, Winooski, VT) arranged in series.

One transducer (T1) was located as close as possible to the pipette, connected with a 75 cm TYGON plastic tubing R3603 (Fisher Scientific, Pittsburgh, PA, USA) to the side-port of the pipette holder. The pressure at T1 was amplified with a home-made device to use the full range of the TL-1 analog (A)-to-digital (D) converter. The other transducer (T2) was more remote from the pipette but

linked to the T1 via a manually controlled 3-way stopcock valve. In this way, the two transducers were mechanically uncoupled and it was possible to operate a 3-way valve manually to initiate and terminate the pressure steps without provoking mechanical perturbations. During experiments, pressure applied by mouth or by a 3 ml syringe was delivered to T2. After opening the stopcock valve between these two transducers, the pressure was delivered to the oocyte membrane via T1 and recorded on-line by a PC 486 computer using pCLAMP software (version 6.04, Axon instrument, Foster City, CA, USA).

DATA ACQUISITION AND DATA ANALYSIS

I. Data acquisition

Voltage commands, generated by the PC 486 computer using pCLAMP software and a TL-1 interface (Axon Instruments, Foster City, CA, USA) for D/A conversion, were applied to the patch pipette and the elicited channel currents were recorded using an Axopatch 200B amplifier (Axon Instruments). Current signals were sampled at 10 kHz, lowpass filtered at 2 kHz with an 8-pole Bessel filter and stored directly on the computer hard drive via the TL-1 interface for A/D conversion. The current signals were corrected for capacitive transients with the fast and slow pipette capacitance compensation circuit of the amplifier and the remaining linear components (ionic leak) were uncompensated unless otherwise indicated.

Data analysis was carried out using Clampfit (Axon Instruments) for primary analysis, then exported to Origin 4.1 (Microcal Software, Inc., Northampton, MA, USA) for further analysis, graphing and exported to PowerPoint 97 (Microsoft Coporation, Redmond, WA, USA) or Coreldraw

7.0 (Corel, Ottawa, ON, Canada) for graphical display.

Continuous single channel recordings acquired by Fetchex (a pCLAMP software, Axon instrument) were initially stored on VHS videotape using a JVC video cassette recorder (Model No. BR-9050U, Japan). The recorded signal was filtered at 1 kHz through a built-in Gaussian digital filter and digitized off-line using the Fetchan (pCLAMP) program. The continuous single channel recordings were then analysed with other pCLAMP programs such as pSTAT (see below).

II. Conductance-voltage (G-V) curve

Conductance values (G) were calculated by dividing the steady-state current over the driving force and plotted as a function of the membrane potential (V_m), i.e., G-V. The driving force is the difference between the equilibrium potential for Shaker-IR (calculated from the Nernst equation) and the applied pipette potential:

$$G = I / (E_K - V_m) \qquad \text{Equation 1}$$

where I is the current amplitude at a given membrane potential V_m. To generate G-V curves, the experimental data sets were fitted to a Boltzmann equation of the form:

$$G/G_{max} = 1 / [1 - \exp(V_m - V_{50}) / dx] \qquad \text{Equation 2}$$

using a sigmoidal fitting program from Origin 4.1, where G is the conductance (in mS), G_{max} is the maximum G representing the open channel conductance multiplied by number of channels in a given patch. V_m is the membrane potential (in mV), V_{50} is the midpoint potential of the G-V curve (in mV) at which G reaches 50% of its maximum and dx is the slope of the curve (in mV per e-fold change). From this fit, the slope parameter (dx), midpoint potential (V_{50}) and the maximum conductance (G_{max}) were obtained for voltage-dependent channel characterization. Normalized G-V curves were

generated by dividing conductance values at each membrane potential by the maximal value from the Boltzmann fit (G_{max}) then plotted against V_m.

III. Open probability (P_{open}) and pressure activation curves

A. Calculation of P_{open}

The non-dimensional parameter, P_{open}, measures the fraction of time (relative duration) that an ion channel spends in the open state, thus providing a quantitative description of the activation of the channel. Plotting P_{open} as a function of the pressure applied to the recording is used to characterize the pressure dose-response data for ion channels. Because the number of channels in the patch (N) is often not known, it is more common to plot NP_{open} (normalized P_{open}) as a function of pressure. The procedures for P_{open} and NP_{open} determinations were as follows.

Single channel recordings acquired with Fetchex were scanned by an automatic event detection pCLAMP6 program (Fetchan). The Fetchan determines the amplitude of the channel events by setting a base line level (level 0, i.e. closed channel state, needs to be readjusted sometimes) and then set up other levels (multiple channels up to 5) using a 50% amplitude criteria. In this way, the event list was generated by reading through the open channel current amplitude.

From the resulting events list, P_{open} was computed by another pCLAMP6 program, pSTAT, for a defined time interval. To ensure an accurate measurement of P_{open}, a 20 s continuous current recording was obtained for each sustained pressure step. Since pSTAT has a limit on the number of total events, the channel events computed from the 20 s recordings often broke the limit of pSTAT when suction induced more opening events. Thus, the 20 s interval was divided into 4 segments and P_{open} was measured at 5 s intervals. Because the number of channels varied from patch to patch and

from time to time, P_{open} was normalized to the maximal number of simultaneously activated channels in the given patch at maximal pressure step. For each 5 s interval, normalized P_{open} was calculated as P_{open} (P) times the maximum activated channels (N) in this patch. Finally, the average P_{open} over 20 s was given by P_{open} = (NP 1 +NP 2 + NP 3 + NP 4) / 4.

B. All-point amplitude histograms

An all-point current amplitude histogram is a histogram of the single channel and multiple channel amplitude from all time points (with the baseline current value subtracted), so that the closed channel will produce a zero amplitude signal. Ideally, a patch with one active channel, has a resulting histogram with two Gaussian peaks, one with a mean of zero (one Gaussian peak corresponds to the baseline noise) and the other with a mean at the unitary current level for the channel (the Gaussian about this mean corresponds to the single channels current amplitude).

Amplitude measurements were used to characterize channel types because different channel types have different single channel amplitudes. Even for so-called single channel recordings, there is often more than one channel in the membrane patch from which the recording is made. In the case where more than one channel was open at the same time, the current amplitudes that are integer multiples of the single channel current will be revealed.

All-points amplitude histograms were constructed using Fetchan (pCLAMP 6) and fitted with a sum-of-Gaussians function using pSTAT. The interval between peaks (means) of the fitted curve give the amplitude of the single channel events, whereas the number of peaks (minus one, for the baseline) gives the number of activated channels in a given patch. Thus, all-points amplitude histograms obtained from single channel recordings showed how many channels are present in the patch and whether they are the same channels, i.e., whether they have the same amplitude.

SOLUTIONS

Oocytes were maintained in OR2 solution [(in mM): 82.5 NaCl, 2.5 KCl, 1 $MgCl_2$ and 1 Na_2HPO_4, buffered with 5 HEPES, pH 7.5] supplemented with 2.5 mM sodium pyruvate, 100 IU of penicillin and 100 IU of streptomycin, per ml. In some cases, ND96 solution was used as an alternative, which contains (in mM): 96 NaCl, 2 KCl, 1 $MgCl_2$ and 2.5 pyruvate, buffered with 5 HEPES to pH 7.6. The hyperosmolar solution contained (in mM): 200 KAspartate, 20 KCl, 1 $MgCl_2$, 5 EGTA, 10 HEPES (pH 7.4).

Cell-attached recordings were made on oocytes bathed in normal frog Ringers solution which contains (in mM): 115 NaCl, 2.5 KCl, 1.8 $CaCl_2$ (omitted in some cases), 1 $MgCl_2$, 10 HEPES (pH 7.2). This same frog solution was also used as a pipette solution. To suppress the activity of native MS cation channels in the oocyte membrane, 100 μM gadolinium chloride hexahydrate (Aldrich Chemical Co., WI, USA) was routinely included in the pipette solutions. Gadolinium chloride hexahydrate is very hydroscopic and therefore was made daily to a 200 μM concentration in 10 ml of pipette solution, diluted to a final concentration of 100 μM with an equal volume of pipette solution. As usual, the pipette solution was filtered with a 0.2 μm sterile syringe filter and backfilled to pipettes.

For inside-out configuration, all recordings were made with the following solutions. The pipette (external, in mM): 140 NaCl, 2 KCl, 6 $MgCl_2$, 5 HEPES, pH 7.2 with 100 μM Gd^{3+} . The bath (internal, in mM): 140 KCl, 2 $MgCl_2$, 11 EGTA, 10 HEPES, pH 7.2.

Injection buffer (in mM): 88 NaCl, 1 KCl, 15 HEPES, pH 7 (filtered).

CHAPTER 3

Shaker-IR K^+ Channel Expression and Characterization

INTRODUCTION

I. Shaker - a voltage-dependent K^+ channel

A. Overview

Voltage-dependent K^+ channels are present in most eukaryotic cells and play an important role in the control of cellular excitability and synaptic transmission. When voltage-dependent K^+ channels were first cloned from the fruit fly *Drosophila melanogaster* (Tempel et al.,1987), it was found that the structure of these channels bears a striking homology to the four slightly varying tandem repeats in the α-subunits of voltage-dependent Na^+ and Ca^{2+} channels. Therefore, it seemed likely that Shaker belongs to the superfamily of voltage-dependent channels (Ellis et al., 1988). Evidence for a homotetrameric structure of the Shaker channel has been obtained by examining its sensitivity to a high affinity peptide pore blocker (a modified form of CTX) when the channels were formed either by co-expression of both wild type subunits and mutant subunits with altered blocker affinity, or by expression of concatenated subunits (MacKinnon et al., 1988; MacKinnon, 1991). Furthermore, the block of the external pore by tetraethylammonium (TEA) has been shown to involve the coordination of TEA with all the four subunits (Heginbotham and MacKinnon, 1992).

B. Structural basis of Shaker channel function

1. Topological arrangement

The hydropathy analysis of the primary amino acid sequence suggests that Shaker has six membrane-spanning α-helical segments, denoted S1 through S6, with both the amino and carboxyl terminals located intracellularly (Chua et al., 1992). Evidence for the topological arrangement was further supported by functional studies in which antibody epitopes were inserted into various regions of the protein (Shih and Goldin, 1997).

Shaker has been extensively used for structural and functional studies because of its homotetramer structure. **Figure 3-1** illustrates what is currently known about the topology of Shaker channel protein. Some of the functional regions that have been well characterized at the molecular level will be briefly highlighted in the following.

2. S5-S6 linker: the pore region

The major feature of voltage-dependent K^+ channels is that it has a central ion-conducting pore composed of a region (variously termed the P or H5 region) between S5 and S6 transmembrane segments. The accepted working model of the pore region (**Fig. 3-1**) is that the S5-S6 loop first extends partly into the membrane to form the ion selectivity filter then loops back out to join the transmembrane segment S6. Each P region is highly conserved, consisting of approximately 20 uncharged and mostly hydrophobic residues (Armstrong and Hille, 1998; Dolly and Parcej, 1996). These residues are thought to be precisely what is required to narrow the pore and to form the selectivity filter. Alignment of the cloned sequences from all major K^+ channels revealed a homologous stretch of eight residues (TXXTXGYG, the signature sequence) in the pore region (Heginbotham et al., 1994). Mutagenesis studies on Shaker demonstrated that three residues of the signature sequence, GYG (the selectivity filter), form the narrowest span of the channel and are critical for K^+ selectivity (Dolly and Parcej, 1996; Armstrong and Hille, 1998).

Figure 3-1. A model for the membrane topology of a Shaker K^+ channel subunit

Six putative transmembrane segments, S1-S6, and the P region which contributes to the pore for ion conduction, are shown. Many features of Shaker are illustrated: the intracellular N-terminal region contains an inactivation ball (black box) that is responsible for blocking the pore during N-type inactivation (Hoshi et al., 1990). The intracellularly located C-terminal end contains a motif X-Thr/Ser-X-Val for binding to the PDZ domain of cytoplasmic proteins like PSD-95 (Kim et al., 1995). The approximate locations of the ionizable residues, comprising the voltage sensor, are labelled: the positively charged residues of either arginine (R) and lysine (K) in S4 segment and negatively charged residues of glutamic acid (D) and aspartic acid (E) in S2 and S3 (Tiwari-Woodruff et al., 1997). The electrostatic interactions between these charged residues are shown as solid lines, but not including negatively charged residue (D447) in the pore region (Papazian et al., 1995). The sequence before S1, about 100 amino acids in length, called the T1 domain, mediates subunits tetramerization (Li et al., 1992; Shen et al., 1993; Kreusch et al., 1998). In the extracellular S1-S2 loop of the Shaker protein, two asparagine residues (N-259 and N-263) are modified by N-linked glycosylation (branched structures, Santacruz-Toloza et al., 1994) (modified from Tiwari-Woodruff et al., 1997).

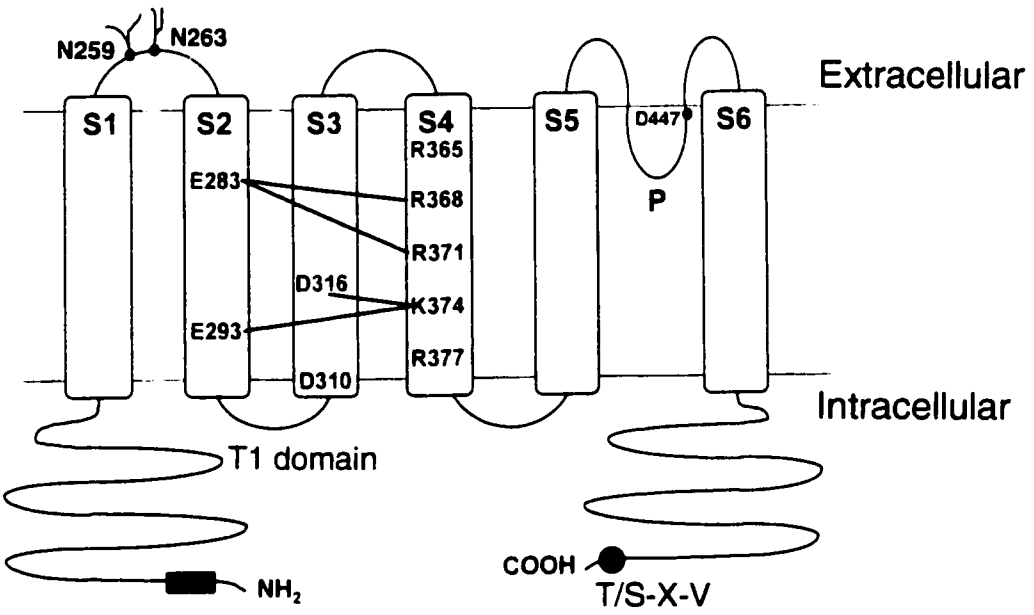
N259
N263
S1
S2
S3
S4
S5
S6
D447
P
Extracellular
Intracellular
R365
E283
R368
R371
D316
K374
E293
R377
D310
T1 domain
NH2
COOH
T/S-X-V

The direct observation of the pore region of a K^+ channel was achieved on a small but highly conserved bacterial K^+ channel, which yielded X-ray crystallographic data at 3.2 Å resolution (Doyle et al., 1998). This bacterial K^+ channel is also a homotetramer. Although it lacks four of the transmembrane segments found in Shaker, each subunit has two transmembrane segments corresponding closely to S5, P region and S6 of eukaryotic Shaker-like K^+ channels. As the pore region sequence of the bacterial K^+ channel is nearly identical to that of the corresponding segment in Shaker (Heginbotham et al., 1997; Doyle et al., 1998), the major features of the bacterial K^+ channel pore can be applied to Shaker. Each subunit of the bacterial K^+ channel has two transmembrane α-helices connected at the extracellular face. The connecting region consists of a "turret", pore helix and selectivity filter (**Fig. 3-2**). One α-helix (inner helix) faces the central pore while the other (outer helix) faces the lipid membrane. The inner helix is tilted with respect to the membrane by about 25° and is slightly kinked, such that the four subunits open like petals facing the extracellular medium. The selectivity filter region is located not in the centre of the bilayer, but near the extracellular surface of the membrane. The X-ray structure revealed that the K^+ channel selectivity filter is a cavity about 10 Å in diameter composed of five conserved amino acids from the signature sequence of eight TXXTXGYG. These conserved amino acids turn their electronegative backbone carbonyls in towards the pore axis and their side chains outward (Doyle et al., 1998).

3. S4 segment: the voltage-sensor

The S4 segment of Shaker is highly conserved among voltage-dependent channels, every third residue (repeats of the motif Lys/Arg-X-X) is a positively charged arginine or lysine for a total of seven positively charged residues in Shaker (compared to five to eight positively charges in the various S4 domains of Na^+ and Ca^{2+} channels) (Armstrong and Hille, 1998). These evenly spaced

Figure 3-2. A representation illustrating a crystallized bacterial K^+ channel

For clarity, only two subunits of the K^+ channel tetramer are shown. Both N- and C-termini are located intracellularly. Each subunit has α-helices with an outer and an inner helix running almost in parallel through the membrane. The inner helix is slightly tilted relative to the outer helix and the loop connecting the two helixes forms a selectivity filter, a pore helix and a turret (as shown). The selectivity filter (in sequence GYG) is shown as a sawtoothed dark line (redrawn from Doyle et al., 1998).

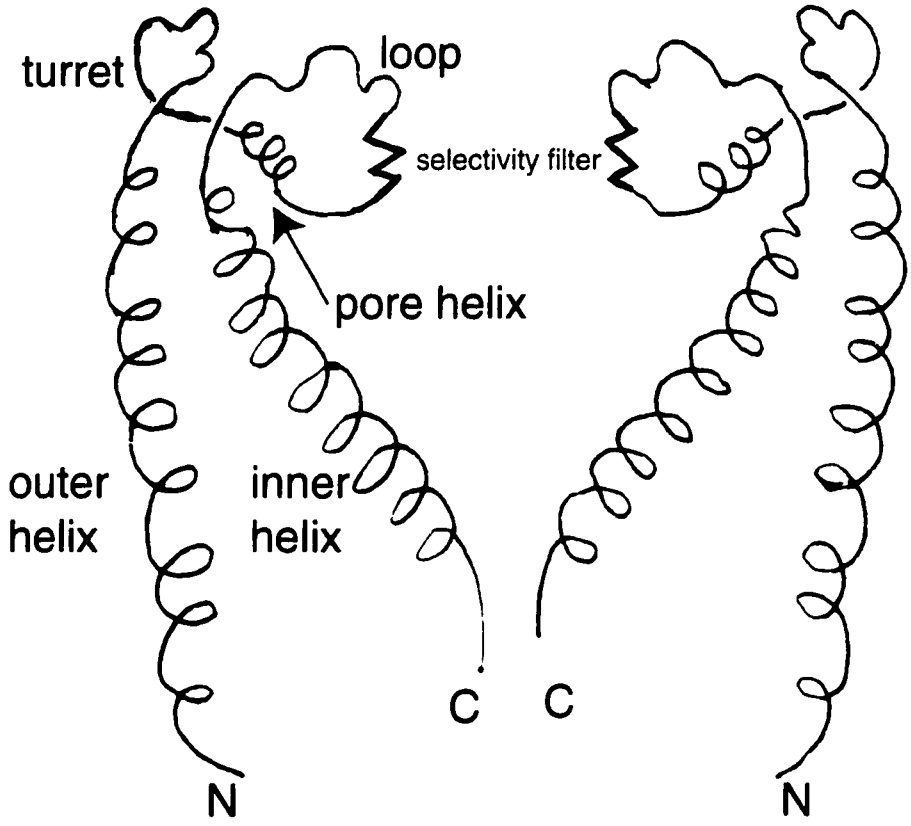
turret
loop
selectivity filter
pore helix
outer
helix
inner
helix
C
C
N
N

residues in the S4 segment have been the primary candidate for the voltage sensor (Papazian et al., 1991) and there has been much experimental evidence supporting the gating role of the S4 segment in Shaker channels (see **Chapter 1**).

In addition to S4, the transmembrane segments S2 and S3 of Shaker also make significant contributions to the voltage sensor (Papazian et al., 1995; Seoh et al., 1996; Tiwari-Woodruff et al., 1997). Using an intragenic suppression strategy, it has been shown that positively charged residues in S4 interact specifically and electrostatically with the negatively charged residues in S2 and S3. For example, K374 in S4 interacts with E293 in S2 and D316 in S3 within the same subunit, rather than in adjacent subunits. Similarly, E283 in S2 interacts electrostatically with R368 and R371 in S4 (**Fig. 3-1**). These results raise the possibility that the S4 segment is tilted at an angle relative to S2 and S3 (Tiwari-Woodruff et al., 1997).

4. N- and C-terminal region: the inactivation gates

Three separate regions have been proposed to be responsible for the different inactivation processes (Loots and Isacoff, 1998). The fast, N-type inactivation is achieved by a "ball-and-chain" mechanism, blocking the internal mouth of the open channel by a compact structure (ball) formed by the N-terminal region. Functional analysis has revealed that the first 20 amino acids at this region are essential for rapid channel inactivation upon channel opening (Hoshi et al., 1990). Deletion of the N-terminal region (Δ6-46) effectively removes fast inactivation, producing a channel designated as Shaker-IR. The fast inactivation can be subsequently restored by adding synthesized ball peptides back to the intracellular side (Hoshi et al., 1990; Zagotta et al., 1990; Isacoff et al., 1991).

Slow inactivation, on the other hand, is subdivided into two components: 1) C-type inactivation is thought to be associated with the C-terminal region in S6 (Lopez-Barneo et al., 1993)

and 2) P-type inactivation is associated with the outer mouth of the pore region (Liu et al., 1996; Yang et al., 1997; Loots and Isacoff, 1998). Both types of inactivation may involve a single external gate adopting two sequential arrangements, the first arrangement shuts the gate making the channel behave as non-conducting state, whereas the second arrangement yields a stabilized closed conformation by stabilizing S4 in its deactivated position (Olcese et al., 1997; Yang et al., 1997).

5. Other regions

Within the S4-S5 linker region, there is a well conserved structure called the "leucine heptad repeat", or "leucine zipper" which is enriched in leucine residues (McCormack et al., 1991). It has been shown that substitution of the leucine by valine residues altered the voltage dependence of the resultant expressed Shaker channel conductance (McCormack et al., 1991), in a manner resembling the effects of S4 mutations. In Shaker, mutations of the leucine residues close to S4 shifted the activation curve to the left while mutations of leucine residues close to S5 shifted the activation curve to the right (McCormack et al., 1991; Schoppa and Sigworth, 1998), probably by disrupting its interaction with S4 segments. Nonconservative substitutions on the leucine residues at the end of the S4 segment influence the ability of Shaker subunits to assemble into functional channel complexes, indicating that leucine residues participate in protein-protein interactions that are important determinants in the conformational state of the channel. These results suggest that hydrophobic groups outside S4 are also important in the gating process of Shaker (McCormack et al., 1991).

A cytoplasmic region of about 100 amino acids in length before the S1 segment, called the T1 domain, may mediate subunit interactions for tetramerization (Li et al., 1992; Shen et al., 1993). The crystal structure of the T1 domain of Shaker has recently been determined (Kreusch et al., 1998).

In addition, a conserved sequence (Thr/Ser-X-Val) on the C-terminal of a Shaker-type K^+ channel has been shown to be essential for binding to cytoplasmic membrane-associated proteins such as post-synaptic density protein 95, PSD-95 (Kim et al.,1995) which are associated tightly with the neuronal cortical cytoskeleton (Cho et al., 1992). In brain sections, immunostaining distribution analysis showed striking overlap of Shaker-type K^+ channels with PSD-95. This overlap is probably a functional co-localization, since when PSD-95 and Shaker-type K^+ cDNAs are expressed together in the same cell, they colocalize apparently on the cell surface; whereas expressed individually, PSD-95 is distributed throughout the cytoplasm while Shaker-type K^+ channel is mainly on the cell surface. Furthermore, deletion mutations from the N-terminus of PSD-95 completely abolished Shaker-type K^+ channel binding. Taken together, these findings suggest that the clustering of Shaker-type K^+ channels in neurons may be directly mediated by the binding of its C-terminal tail to the N-terminal of PSD-95 (Kim et al., 1995).

C. General properties of Shaker-IR

1. Shaker-IR and Shaker

As mentioned above, Shaker is a voltage-dependent K^+ channel originally isolated from the *Drosophila* genome (Tempel et al., 1987; Papazian et al., 1987). The native Shaker channel was so named because fruit flies with a mutant Shaker phenotype were found to shake or jerk their legs when anaesthetized with ether. Shaker-IR, on the other hand, is a modified Shaker channel with its fast inactivation ball removed (Hoshi et al., 1990; Zagotta et al., 1990). Most structural and functional studies referred to in this thesis have used Shaker-IR as their channel model. To avoid confusion, Shaker-IR will be consistently used to refer to any Shaker construct with the inactivation ball removed. The following properties of Shaker-IR expressed in *Xenopus* oocytes are compiled

from the literature, in order to provide a comparison for data shown in this and the subsequent chapters.

2. Biochemical features

Shaker-IR proteins expressed in *Xenopus* oocyte (Santacruz-Toloza et al., 1994; Papazian et al., 1995) and transfected in HEK 293 cells (Schulteis et al., 1995) can be detected on SDS gels as two glycosylated bands. One is a sharp band at about 70 kD, representing partially glycosylated precursor and the second, representing the mature glycosylated protein, is a broad band at about 110 kD.

3. Voltage-dependent activation profile

(i) Macroscopic channel behaviour

Recorded from inside-out excised patches, Shaker-IR K^+ channels produce outward K currents and activate with a sigmoidal time course (Hoshi et al., 1994; Zagotta et al., 1994a). The sustained Shaker-IR current is evident up to +100 mV during 50-150 ms depolarizing pulses (Zagotta et al., 1994a). Although lacking fast N-type inactivation, the whole-cell and single-channel currents of Shaker-IR exhibit a "rundown" or slow inactivation process, namely C- and P-type inactivation (Hoshi et al., 1994). Although not discernible on the time scale of 50-150 ms, slow inactivation is evident as a decreasing current amplitude for voltage pulses longer than 2 s, especially at the more depolarized potentials (Hoshi et al., 1990).

Hodgkin and Huxley (1952) first deduced that the changes in conductance of the voltage-dependent channels are functions of time and membrane potential. The voltage-dependence of K^+ channel activation is characterized by measuring steady-state conductance as a function of voltage (G-V curve). Like other voltage-dependent channels, Shaker-IR also has a sigmoidal G-V curve

which can be fitted to the Boltzmann function (Zagotta et al., 1994a, see **Chapter 2** for equation 2). From the Boltzmann fitting, the slope of the curve and the mid-point potential V_{50} can be extracted. According to Papazian et al. (1995), the activation parameters for Shaker-IR are: V_{50} = -28 mV and slope steepness = 8.4 mV per e-fold change.

As mentioned in **Chapter 1**, mutations on S4 basic residues shift the G-V curve along the voltage axis and alter its slope (Papazian et al., 1991). The shifted G-V curve suggests that the residues affect the relative stabilities of the open and closed conformations of the channel protein (Papazian et al., 1991). Since the slope of the G-V curve provides an estimate of gating charge, any change in the charge of the voltage sensor or in the electric field that the voltage sensor traverses would be expected to change the slope (Perozo et al., 1993). Accordingly, neutralization mutants reduce the steepness of the activation curve (yielding a larger value for the slope steepness), as expected if the charged residues contribute to gating charge (Papazian et al., 1995).

(ii) Single channel behaviour

Typically, at the single channel level, Shaker-IR channels open in bursts (Shao and Papazian, 1993) after a delay ("latency") in response to depolarizing steps. This latency to first opening becomes shorter as the voltage step becomes more depolarized (Hoshi et al., 1994). Consistent with the sustained macroscopic Shaker-IR currents at depolarized voltages, Shaker-IR generally continues to burst for the duration of entire voltage pulses and does not enter long duration closed states.

As expected, since Shaker-IR is K^+-selective, the single channel amplitude increases as driving force (i.e., $V_m - E_K$) increases. For instance, the single channel amplitudes of Shaker-IR (in pA) are: 0.4, 0.5, 0.6, 0.7, 1.0 and 1.3 pA using normal excised patch solution (see **Chapter 2**) in response to depolarizing voltage pulses at -50, -40, -30, -20, 0 and +50 mV, respectively (Hoshi et

al., 1994). The single channel conductance for Shaker-IR, determined from the slope of single channel current-voltage relationships, is 7.8 pS (Shao and Papazian, 1993).

The open probability (P_{open}, probability of a channel being open) of Shaker-IR can be obtained using single channel current data at steady-state and plotted as a function of voltage. Reflecting the G-V curve from macroscopic currents, this probability increases steeply in a sigmoidal fashion between -50 and +50 mV. Moreover, the time course of achieving the steady state P_{open} becomes more rapid as the voltage is more depolarized (Zagotta et al., 1994a).

4. Conduction profile of Shaker-IR

As discussed above, Shaker-IR has two conserved structural segments, a voltage-sensor in the S4 segment and a K^+ selectivity filter in the S5-S6 loop. Therefore, Shaker-IR can be identified both by its voltage-dependent gating properties and its K^+ selectivity. The V_{rev} of Shaker-IR is about -80 mV (2 mM KCl [pipette] / 140 mM KCl [bath]) determined from instantaneous tail-currents measurements (Hoshi et al., 1994), and is equivalent to the equilibrium potential for K^+ channels. Based on bi-ionic reversal measurements (determined when a test monovalent cation is replaced on one side of the membrane and the comparison ion, K^+, is on the other side), the Shaker-IR channel displays a relative permeability sequence of $K^+ > Rb^+ > Cs^+ \gg Na^+$, indicating that the conduction properties of the Shaker-IR are similar to those traditionally described in other K^+ channels (Heginbotham and MacKinnon, 1993).

D. Reasons for using Shaker-IR

Shaker-IR offers many advantages for fundamental studies of voltage-dependence, and these advantages are important in testing the mechanosensitivity on this well-characterized channel (detailed discussion will be presented in **Chapter 4**).

First, Shaker-IR is advantageous for kinetic studies of the voltage-activated state as it exhibits maintained outward currents with sustained membrane depolarization (Hoshi et al., 1994). Second, the cloned Shaker-IR channel has been well characterized biophysically at the molecular level (Papazian et al., 1995; Mannuzzu et al., 1996; Baker et al., 1998). Third, there are specific antibodies and peptide toxins available for recognition and purification of the Shaker-IR protein (Goldstein and Miller, 1992; 1993). Fourth, unlike other voltage-dependent channels, such as Na^+ or Ca^{2+} channels, Shaker-IR is a homotetramer of four identical subunits rather than a single large polypeptide chain. The smaller size makes Shaker-IR more amenable for *in vitro* genetic manipulations and its 4-fold symmetry structure (compared to for example, the Na^+ channel where each of the 4 domains is a little different) simplifies interpretation.

II. Gadolinium (Gd^{3+})

Gadolinium (Gd^{3+}), a trivalent lanthanide, is the most commonly used pharmacological tool in blocking mechanosensitive (MS) cation channels. It was first reported that Gd^{3+} block endogenous MS channels in *Xenopus* oocytes (Yang and Sachs, 1989). Subsequent patch clamp studies confirmed that Gd^{3+} indeed blocks single MS channel currents not only in plant cells (Ding and Pickard, 1993) but also in fungi, bacteria and a variety of animal cells (see review by Hamill and MacBride, 1996). As the ultimate goal of this study is to test the effects of mechanical stimuli on the Shaker-IR channel expressed in *Xenopus* oocytes, it was essential to block any endogenous MS cation currents in *Xenopus* oocytes. Yang and Sachs (1989) have demonstrated that 10 μM Gd^{3+} completely and reversibly blocks endogenous MS cation channel activity in patches of *Xenopus* oocytes. Because the K^+-selective MS channel in snail neurons is not blocked by Gd^{3+} (Small and

Morris, 1995), Gd^{3+} may be an appropriate pharmacological inhibitor to study possible mechanical effects on a K^+-selective channel like Shaker-IR.

Although Gd^{3+} is known as an effective blocker for MS cation channels, it is not highly selective. Besides MS channels, Gd^{3+} also blocks voltage-dependent L-, T- and N-type Ca^{2+}channels at concentrations used to block endogenous MS cation channels (Caldwell et al., 1998). Additionally, because Gd^{3+} is similar in size to Ca^{2+} and it has long been recognized that multivalent ions like Ca^{2+} can exert modulatory effects on voltage-dependent channels (Cukierman et al., 1988; Moczydlowski et al., 1985), it was proposed that Gd^{3+} may also effect the gating properties of Shaker-IR by shielding membrane surface charge and by modifying the electric field across the membrane. In fact, previous studies in myelinated nerves have shown that 100 μM Gd^{3+} can diminish voltage-dependent Na^+, K^+ as well as voltage-independent leak currents (Elinder and Århem, 1994a). If the underlying mechanism for these non-specific blockages is surface charge shielding by Gd^{3+}, this effect may abolish Shaker-IR currents as well. The effects of Gd^{3+} on Shaker-IR have not, however, been previously characterized, neither had its effect on other recombinant K^+ channels been studied prior to starting this project.

III. Objectives

The aims of this chapter are two-fold. First, to confirm the functional expression of Shaker-IR by electrophysiological recordings, and to demonstrate the presence of Shaker-IR protein by Western-blotting. Second, to characterize the voltage-dependent gating properties of Shaker-IR in the presence of the MS cation channel blocker, Gd^{3+}. It was essential, to determine if Shaker-IR still exhibits typical voltage-dependent gating in the presence of Gd^{3+}, before testing the mechanical

effects on this voltage-dependent channel.

MATERIALS AND METHODS

I. Oocytes preparation and microinjection (see **Chapter 2** for details)

II. Biochemical analysis of Shaker-IR protein made in oocytes

Drosophila Shaker-IR cDNA clone in the pBluescript vector and monoclonal anti-1D4 antibody were generously provided by Dr. Chris Miller at Brandeis University (Waltham, MA, USA). Shaker-IR cDNA was subcloned into a pSP64TM expression vector and Shaker-IR cRNA was obtained by *in vitro* transcription by Dr. Peter Juranka in our lab. Alkaline phosphatase-conjugated secondary anti-mouse antibody was kindly provided by Dr. David Brown (University of Ottawa, Ottawa, Canada).

Western blots of oocyte membrane extracts were made as follows: two days after cytoplasmic injection of 25-50 ng of Shaker-IR cRNA, oocytes were collected and homogenized in oocyte lysis buffer (10 μl per oocyte) which contained: 150 mM NaCl, 1% triton X-100 and a protease inhibitor cocktail in 10 mM sodium phosphate (PH 7.4). The protease inhibitor cocktail contained: 10 mM benzamidine, 0.2 units / ml aprotinin, 10 μg / ml leupeptin, 10 μg / ml antipain, 0.2 μg / ml soybean trypsin inhibitor and 1 mM phenylmethanesulfonyl fluoride. The oocyte lysate was clarified by centrifugation for 20 min. at 4°C at 15,000 rpm and the middle layer was collected. Protein concentration was determined using the BioRad Bradford reagent (Cat. No. 500-0001, Bio-Rad,

Hercules, CA). 50 μg lysate protein (from approximately 20 oocytes) was diluted in sample loading buffer (10% glycerol, 125 mM Tris-HCl, 500 mM mercaptoethanol and 0.3% SDS with 4% bromophenol blue) and boiled for 5 min. The sample was subjected to electrophoresis on denaturing 8% polyacrylamide gels with 4% polyacrylamide stacking gels (Laemmli, 1970). The proteins were transferred to a nitrocellulose membrane by electroblotting using the Electroblotting Trans-Blot cell (Bio-Rad). First, the membrane was rinsed in TNT (10 mM Tris -HCl, pH 8.0; 140 mM NaCl; 0.05% Tween-20) several times and blocked overnight at 4°C with 3% BSA (Sigma; A-9647) in TNT. Second, the membrane was incubated with the primary antibody, anti-1D4 (1:5,000), which is directed against an 8 amino acid 1D4 epitope at the C-terminal end of Shaker-IR. Third, the protein-bearing nitrocellulose membrane was washed three times (10 min each) in TNT buffer and incubated with secondary antibody, alkaline phosphate-conjugated anti-mouse antibody (1:2,000) in TNT. Finally, the protein was visualized by alkaline phosphate detection buffer containing nitroblue tetrazolium chloride and 5-bromo-4chloro-3-indolylphosphate.

III. Electrophysiological testing of Shaker-IR expression

A. Overview

Functional expression of Shaker-IR K^+ currents was assayed by two-electrode voltage clamp (TEVC). An amplifier system designed for rapidly charging the large capacitance of the oocyte plasma membrane was used (OC -725, Warner Instrument, New Haven, CT, USA). TEVC measures the current that is needed to keep the cell at a particular voltage by using two intracellular electrodes; one electrode measures the membrane potential (the voltage electrode) and compares this via an operational amplifier circuit to the desired holding potentials. The difference between these two

potentials is amplified using a feedback circuit and fed to the second electrode (the current-injecting electrode), which passes just sufficient current to the cell to maintain the desired voltage level. The injected current is measured by a current-to-voltage converter placed in the ground connection.

B. Electrode pipette preparation

Electrode pipettes were made from borosilicate glass (GC150F-10, OD 1.5 mm, Warner Instrument) with a thin internal filament that ensures that electrode solution reaches the tip. To smoothly insert the pipette into a pipette holder, the pipettes were fire polished by heating the back end of the pipette in a Bunsen flame then they were pulled on a programmable electrode puller (Model P87, Sutter Instrument Co. Novato, CA, USA). The puller was programmed to produce voltage pipettes with a long, thin shank because this inflicts less damage when impaling the cell. A slight change was made when pulling the current electrode which had a bit wider tip to achieve the low resistance required for a fast clamping. Generally, the voltage electrode had a relatively smaller opening (3-5 μm) in comparison with the current electrode (7-9 μm). For minimizing electrode resistance, both electrodes were backfilled with sterile filtered 3 M KCl and had pipette resistances of 1-2 MΩ and 0.5 -1 MΩ respectively for voltage and current electrodes. Air bubbles lodged near the tip were removed by holding the pipette straight (tip down) and tapping on the shank. Because of their low resistance, the electrode did not clog frequently and were reused sometimes for several cells.

Unlike the pipettes used as patch electrodes, pipettes for TEVC recordings required neither fire polishing nor coating with Sylgard (silicone curing agent RTV615). However, Sylgard-coated electrodes were occasionally used to reduce electrode capacitance. The recording electrodes' Ag/AgCl silver wire, that was in contact with the electrode solution, was regularly chloridated to

reduce drift, noise and to prevent exposure of the oocytes to toxic silver ions. Possible capacitive coupling between the two recording electrodes was minimized by shielding the electrodes from each other. This was accomplished by mounting a grounded aluminum plate between the two pipettes.

C. Recording chamber

As oocytes tend to roll away while being impaled, a dental drill was used to carve a pit on the bottom of the recording chamber (petri-dish 35 x 10 mm, Falcon 1008, Becton Dickinson Labware, Lincoln Park, NJ, USA). In addition, the coarse manipulator which held the pipettes was adjusted so that the angle of the two electrodes was steep enough to hold the oocyte in the drilled depression. The recording chamber was grounded with a fine coiled Ag/AgCl silver wire. The oocytes were selected and injected as described in **Chapter 2**. During an experiment, one oocyte at a time was transferred to the recording chamber.

D. Current recording

Recordings were made 24 hours post-cRNA injection as well as on the following 2-6 days. Under a Wild M5A dissection microscope, the voltage electrode was inserted into the oocyte while the oocyte was held in place by the current electrode (not yet impaled) from the opposite direction. Successful impalement of the voltage electrode was monitored by recording the resting membrane potential (V_{rest}, see below). The current electrode was then inserted and the V_{rest} was read from the voltage electrode meter. Once the oocyte was clamped at a holding potential, series resistance was compensated for both fast and slow components. Data acquisition and analysis were performed on a PC486 computer using pCLAMP software and a TL-1 A/D converter (Axon instrument, Foster City, CA, USA). Current signals were low-pass filtered at 2 kHz with an 8-pole Bessel filter. No leak or capacitative current subtractions were made. All experiments were performed at 21-23°C with the

oocyte membrane held at -100 mV unless otherwise indicated.

E. Perfusion of oocytes with 100 μM Gd^{3+}

The oocytes were perfused with standard frog Ringer solution (see **Chapter 2** for recipe) with or without 100 μM Gd^{3+}. The impaled oocytes tolerated well with the process of changing bath solutions; there was no lowering of the input resistance as indicated by the size of leak currents. Shaker-IR currents could be measured for up to an hour without any noticeable leak currents. The V_{rest} measured prior to current recording was used as an indirect indication of the oocytes wellness. The V_{rest} for Shaker-IR injected oocytes was -48.9 ± 0.4 mV (mean ± SE; n = 107). V_{rest} was routinely rechecked at the end of each experiment. If V_{rest} was found to be less than 40 mV, the data was discarded.

A simple gravity driven solution exchange system was used to perfuse the recording chamber and a Pasteur pipette was used to manually draw off solution and control the solution level in the recording chamber. To ensure a complete solution exchange, a 20 ml petri dish was washed with approximately 200 ml bath solution (with or without Gd^{3+}). To avoid sequence related effects, some experiments started with normal frog Ringer without Gd^{3+} in the bath, while others started with normal Ringer with Gd^{3+} followed by a double exchange. Occasionally, changes in fluid level altered the electrode shunt capacitance and hence readjustment of capacitance compensation and neutralization was required.

RESULTS

I. Electrophysiological evidence for expression of Shaker-IR in *Xenopus*

oocytes

TEVC provided a quick and reliable method for detecting the exogenously expressed Shaker-IR currents. Because of between-batch differences in expression levels, this technique was routinely used to screen for a good batch of oocytes and to determine if a particular oocyte had appropriate channel densities for patch recording.

Shaker-IR is a voltage-dependent K^+ channel that activates during membrane depolarization, therefore, to detect voltage-dependent outward Shaker-IR currents with TEVC, a series of voltage steps were applied to Shaker-IR-injected oocytes. Non-injected or water-injected control oocytes from each batch were used as controls. At least three control oocytes were tested per day. This provided day-to-day comparisons between Shaker-IR and control oocytes. As seen from the representative examples shown (**Fig. 3-3**), Shaker-IR-injected oocytes exhibited typical voltage-dependent outward currents by two days after injection (**Fig. 3-3a**). These currents had no inactivation during sustained (50 -150 ms) depolarizing pulses, as expected for the inactivation-removed Shaker-IR. In contrast, no visible currents were elicited from the non-injected oocytes with the same depolarization pulses over the same period of expression, a typical example is shown in the **Fig. 3-3b**.

II. Biochemical evidence of expressed Shaker-IR protein in oocytes

Western blot analysis was performed on *Xenopus* oocytes injected with Shaker-IR cRNA to detect the presence of Shaker-IR protein. Non-injected or water-injected oocytes were used as controls. Immunoblots were probed using an anti-1D4 antibody which recognizes the 8 amino acid epitope (1D-4 tag, Glu-Thr-Ser-Glu-Val-Ala-Pro-Ala) inserted at the C-terminal end of Shaker-IR.

Figure 3-3. Expression of Shaker-IR in *Xenopus* oocytes

Current recordings were from two electrode voltage clamp. Shaker-IR currents were recorded from a Shaker-IR mRNA injected oocyte **(a)** whereas no current responses were elicited from an non-injected oocyte **(b)**. A series of 100 ms voltage pulses was applied in 5 mV increment yielding steps from -110 mV to +50 mV. A holding potential of -100 mV was applied for 1 s between successive pulses.

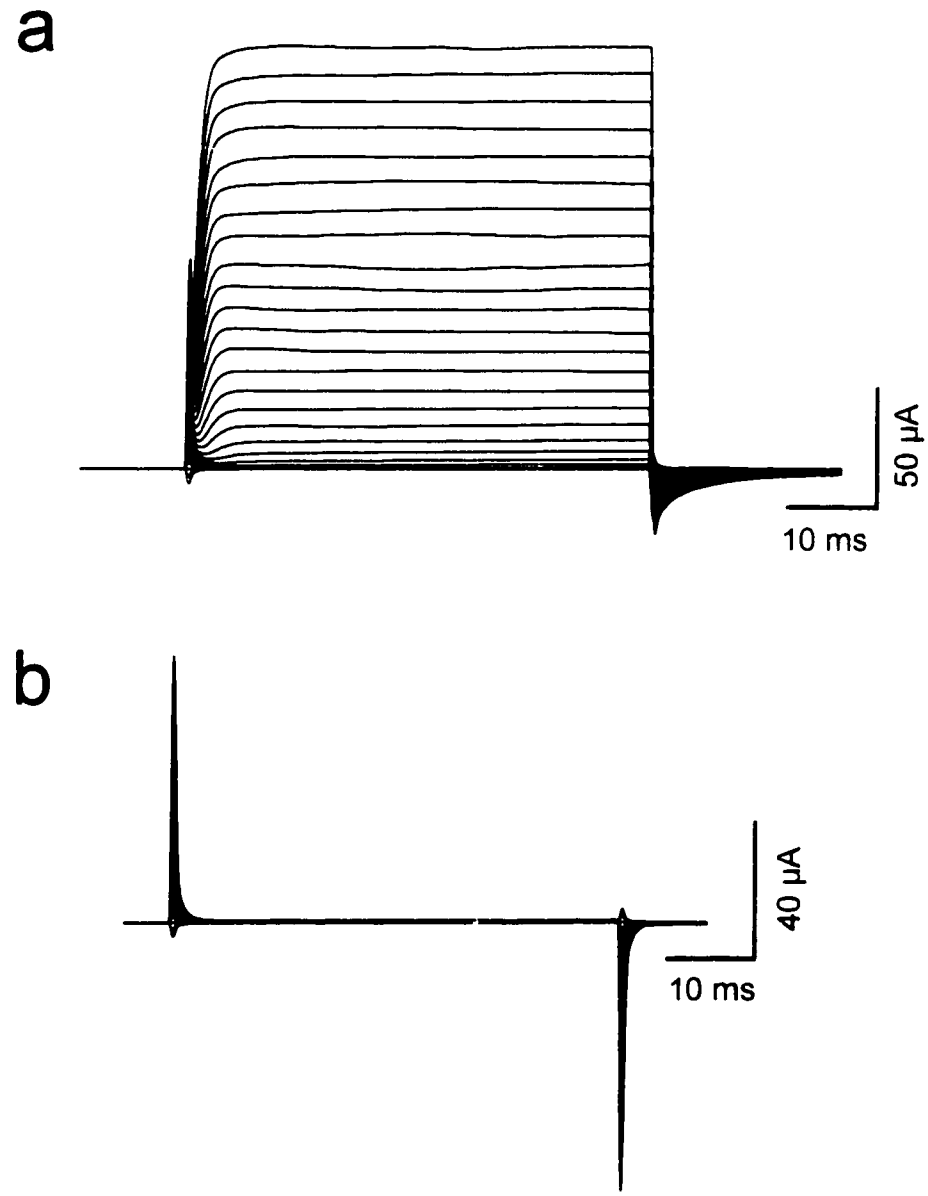
a
50 µA
10 ms
b
40 µA
10 ms

As expected, oocytes injected with Shaker-IR produced prominent immuno-reactive bands (**Fig. 3-4**, lane 2) while no bands were detected from either non-injected (not shown) or water-injected oocytes (lane 1, in this case, it was from a water-injected oocyte). As shown, three protein bands were detected with the anti-1D4 antibody, almost identical to the protein profile of immunoblots using an antibody against the carboxyl (C)-terminal of Shaker-IR (data not shown). According to Schulteis et al., 1995, the heavy band of approximately 113 kD represents the glycosylated form of the Shaker-IR protein while a lighter band of approximately 73 kD is the unglycosylated form. The identity of the third low molecular weight band was unknown but it may be a C-terminal break-down product **(Fig. 3-4, lane 2)**.

III. Characterization of Shaker-IR in the presence of 100 μM Gd^{3+}

A. Overview

Because Gd^{3+} has been reported to shift the voltage-dependent gating parameters for both voltage-dependent Na^+ and K^+ channels along the voltage axis (Elinder and Århem, 1994a), and because there is evidence that lanthanum (La^{3+}) affected the gating of a Shaker-like K^+ channel (Tytgat and Daenens, 1997), it is reasonable to propose that Gd^{3+} may also affect the voltage-dependent gating parameters of Shaker-IR. In the present study, the three parameters (V_{50}, slope steepness and G_{max}, see **Chapter 2**) were compared in conditions with and without Gd^{3+} application. For each parameter indicated below, the mean, standard error, and number of oocytes (n) are given. Paired t-test was used for statistical analysis since the comparison is valid only within each given patch.

Figure 3-4. Detection of Shaker-IR protein in *Xenopus* oocytes by anti-1D4 antibody

Each lane represents approximately 50 μg protein from a Triton X-100 solubilized oocyte lysate. Lane 1: water-injected oocytes; lane 2: oocytes injected with Shaker-IR mRNA. The 1D4 epitope tag in Shaker-IR was detected with a monoclonal antibody (anti-1D4: 1:5,000). Three bands were detected, a very broad band of about 113 kD (top) represent glycosylated form of Shaker-IR and a sharp band (73 kD, in the middle) is the unglycosylated form. The bottom band is thought to be degradation product. These molecular weights were estimated by comparing the protein profile on SDS-PAGE gel by Santacruz-Toloza et al (1994).

Lane 1
Lane 2
- 113
- 71
k D
water-injected
Shaker-IR

B. Effect of Gd^{3+} on V_{50} and slope of the G-V curve

Fig. 3-5a shows Shaker-IR channel currents (I_{Sh}) elicited in response to a series of depolarizing voltage pulses (5 mV increments) at a holding potential of -100 mV. The I_{Sh} was recognized by their outwardly rectifying current-voltage (I-V) relations (**Fig. 3-5b**). Steady-state G-V curves (**Fig. 3-5c**) were generated by calculating the conductance (from the steady-state I_{Sh} for data obtained with or without 100 μM Gd^{3+}) and plotted as a function of V_m. The plotted G-V curves were fitted to the Boltzmann equation. From this fit, conductance G at given V_m were normalized to the G_{max} under each experimental condition (**Fig. 3-5d**). From the normalized G-V curve (e.g. **Fig. 3-5d**), we found that Gd^{3+} shifted the V_{50} of Shaker-IR by 23 ± 3 mV (from -19 to +3 mV, n = 9, P <0.01) and decreased the slope steepness by 6 ± 2 mV (from 14 to 20 mV, n = 9, P <0.01).

C. Partial inhibition of G_{max} by Gd^{3+}

The third parameter for characterizing Shaker-IR, G_{max}, could not be obtained from the normalized curves. Instead, G_{max} with and without 100 μM Gd^{3+} were taken from the Boltzmann fittings before normalization (as in **Fig. 3-5c**). As shown, Gd^{3+} decreased I_{Sh} at all test potentials and hence decreased the fitted G_{max} from 0.5 to 0.3 mS (62 ± 9%, n = 9, P<0.01). This decrease was reversible as G_{max} completely recovered after Gd^{3+} washout.

D. Reversal potential (V_{rev})

A primary intention in this chapter was to establish whether the expressed currents, in the presence of Gd^{3+}, were still recognizable as Shaker-IR. The ion-selectivity of Shaker-IR enables it to discriminate among monovalent cations and to be highly selective for K^+ ions (Hoshi et al., 1994). One way to check this is to measure V_{rev} (also called zero-current potential). If the V_{rev} is close to the equilibrium potential (E_K) expected for the experimental K^+ composition, then we would argue that

Figure 3- 5. Effects of Gd^{3+} on I_{Sh} expressed in *Xenopus* oocytes

(a) Whole-cell I_{Sh} elicited in response to a series of voltage pulses (5 mV increments) from -110 mV to + 80 mV at a holding potential of -100 mV. **(b)** Superimposed current-voltage relationship for Shaker-IR at control (○), during (△) and after (✳) 100 μM Gd^{3+} perfusion. **(c)** Conductance-voltage (G-V) curves for data in **(b)** set. **(d)** Normalized version of **(c)**. The solid curves are fits to the Boltzmann equation.

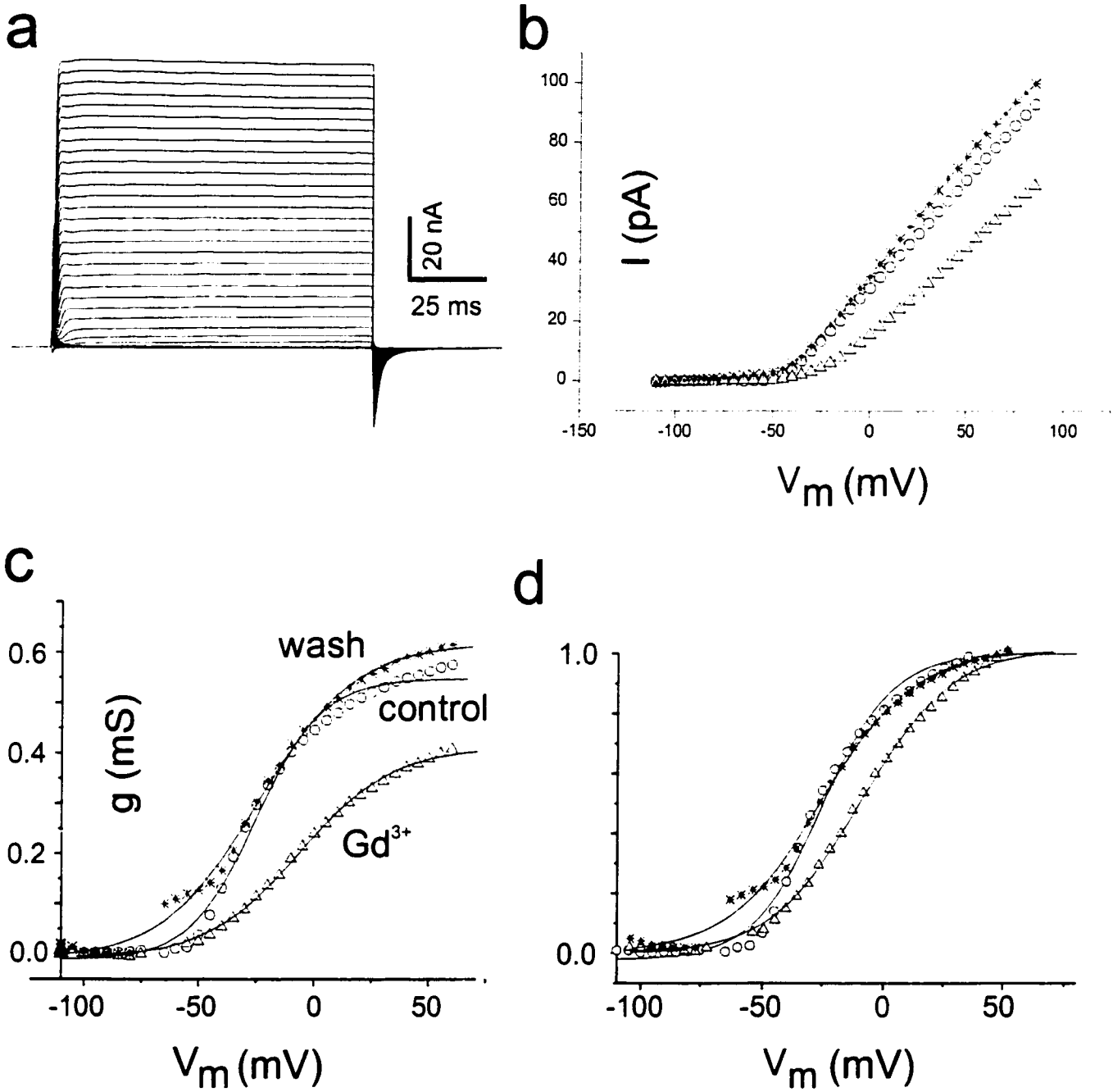
a
20 nA
25 ms
b
I (pA)
100
80
60
40
20
0
-150
-100
-50
0
50
100
Vm (mV)
c
g (mS)
0.6
0.4
0.2
0.0
wash
control
Gd3+
-100
-50
0
50
Vm (mV)
d
1.0
0.0
-100
-50
0
50
Vm (mV)

the Gd^{3+}-sensitive conductance would likely be K^+ selective. To test whether Gd^{3+} had any effect on V_{rev} of Shaker-IR, currents from Shaker-IR-injected oocytes were compared with and without 100 μM Gd^{3+}. V_{rev} was determined by evoking tail current in 5 mV increments in the voltage range that encompasses the equilibrium potential for K^+ ions. For some channels (such as for the voltage-dependent Na^+ channel), V_{rev} can be determined from "regular" I-V relations because the V_{rev} falls within test potentials which generate currents at either side along the voltage axis of the V_{rev}. The currents are either positive or negative or zero relative to V_{rev}. However, for Shaker-IR, this method was not applicable since, for the solutions we used, Shaker-IR expressed in healthy oocytes should have had a V_{rev} of approximately -80 mV (Hoshi et al., 1994), so that currents can only be elicited when the membrane is depolarized ($V_m > E_K$). To circumvent this problem, a tail current protocol was used. Briefly, the protocol was started by stepping the membrane potential to a depolarizing voltage at which approximately 50% of the total channels would be activated, then the membrane potential was stepped back to a series of test voltages including V_{rev}. V_{rev} was determined either directly from the instantaneous tail currents or from interpolation of the tail current I-V relations. A typical example of Shaker-IR tail currents can be found in the Appendix (**Fig. A-6**).

Evidently, application of Gd^{3+} reduced I_{Sh} at all test potentials and shifted V_{rev} in the positive direction [from -82 mV to -77 mV (5 ± 0.7 mV, n = 7), paired t-test $P < 0.01$]. Thus, the slightly affected V_{rev} during Gd^{3+} application indicates that Shaker-IR retains its selectivity for K^+ ions. The mechanism of Gd^{3+}-induced changes in gating parameters were not analyzed further because the main purpose of using Gd^{3+} was to suppress endogenous MS cation channels while studying the effects of mechanical stimuli on the voltage-dependent gating of Shaker-IR. Since Shaker-IR was still functional in the presence of Gd^{3+}, we were able to pursue our main investigation.

DISCUSSION

I. Shaker-IR expression

Two independent pieces of evidence from this study confirmed that Shaker-IR was successfully expressed in *Xenopus* oocytes. First, voltage clamped *Xenopus* oocytes revealed the characteristic voltage-dependent Shaker-IR K^+ current (**Fig. 3-5**) and the voltage-dependent gating properties of this channel are similar to those described by others (Papazian et al., 1995; Larsson et al., 1996). Second, biochemical evidence confirmed the presence of 1D4 epitope-tagged Shaker-IR in *Xenopus* oocytes; two bands with molecular weights of 113 and 73 kD were detected on SDS-PAGE (**Fig. 3-4**). This protein profile of Shaker-IR-injected oocytes is virtually identical to the results from other studies (Schulteis et al., 1995; Santacruz-Toloza et al., 1994). We are confident that these bands are products of Shaker-IR expression for the following reasons. 1) They were not present in oocytes that were injected with water instead of Shaker-IR cRNA; 2) Both of the major bands expected (i.e. for immature and mature form of Shaker-IR) were detected by the anti-1D4 antibody that recognizes a 1D4 epitope tag on the Shaker-IR construct. Hence, biochemical detection of Shaker-IR corroborates electrophysiology evidence for successful expression of Shaker-IR in *Xenopus* oocytes.

II. Mechanisms of surface charge on the voltage-dependent gating

Most multivalent metal ions shift the gating parameters of voltage-dependent conductance

(Hille, 1992) in a manner similar to what we observed for Gd^{3+} on Shaker-IR. This has been explained by several theories, including the surface charge theory. The surface charge theory proposes that local potentials of multivalent ions are what affect the voltage-dependent gating. This theory was first introduced by Frankenhaeuser and Hodgkin (1957) who showed that increasing the external Ca^{2+} concentration shifted the squid axon Na^+ channel's activation curve towards more depolarized transmembrane voltages. Based on these observations, the authors proposed that there is probably a localized potential on the surface of the cell. Later, Gilbert and Ehrenstein (1969) pointed out that the membrane surface bears fixed negative charges that are the major source of a surface potential, and that Ca^{2+} ions could reduce this potential by electrostatically screening these surface charges, thus polarizing the membrane electric field across the channel's voltage sensor. Since the voltage sensor of voltage-dependent channels is confined to the membrane, it can not distinguish a change in the electric field caused by altered membrane voltages from that of screening surface charges.

Bell and Miller (1984) suggested a second possibility, namely that divalent cations may interact directly with channel proteins in ways other than by screening membrane surface charges. This conclusion is based on charge density studies on the membrane surface by introduction of charged lipid-like amphipaths. These amphipaths can insert into the inner or outer monolayer of the membrane, so that the surface potential is directly changed by reconstituting channels into membranes with the different surface charge densities, then observing the resulting differences in single channel currents (Bell and Miller, 1984). Using a similar approach, Cukierman et al. (1988) reported effects of Ca^{2+}-induced V_{50} shifts in voltage dependent Na^+ channels reconstituted in neutral or charged lipid bilayers. In the absence of Ca^{2+}, the V_{50} did not depend on which phospholipid was

used, whereas Ca^{2+} (7.5 mM) gave rise to a +17 mV shift with neutral membranes and a +25 mV shift with negatively charged membranes. The negatively charged membrane did not itself shift V_{50}, yet had a greater Ca^{2+}-induced shift than the neutral membranes. Therefore, the Ca^{2+}-induced shift cannot be attributed to surface charge alone. The overall effects of Ca^{2+} would be due to direct interactions between Ca^{2+} and the Na^+ channel proteins, plus interactions with the negatively charged phospholipid (Cukierman et al., 1988). This combination theory seems plausible and in fact has been used (Elinder and Århem, 1994a; 1994b) to explain Gd^{3+}-induced voltage-dependent gating shift. Recently, by using a saxitoxin (STX) to block Ca^{2+} and Na^+ movements into or out of the Na^+ pore, without preventing access of Ca^{2+} to the membrane surface, Armstrong (1999) elegantly distinguished the surface charge effect of Ca^{2+} from the direct interaction of Ca^{2+} on the voltage-dependent Na^+ channels. In the presence of STX, the effects of Ca^{2+} on gating properties are small, and much larger effects are seen in the absence of STX (Armstrong, 1999). These results indicate that neutralizing surface charge of Ca^{2+} is not an important component on Na^+ gating, rather, Ca^{2+}-occupancy seems to be a favoured mechanism responsible for the gating interference of Ca^{2+} on Na^+ channels (Armstrong, 1999).

III. Effects of divalent or trivalent ions on voltage-dependent channels

A. Overview

In this section, Gd^{3+}-induced effects on gating and conduction parameters of Shaker-IR are compared with the effects of the multivalent Ca^{2+} and La^{3+} ions on voltage-dependent channels (as reported by others). This comparison is relevant since: 1) trivalent Gd^{3+} is similar in size to the divalent Ca^{2+} (ionic radius: 1.1 Å for Gd^{3+} and 1.0 Å for Ca^{2+} [Elinder and Århem, 1994a]); and 2)

as a lanthanide, Gd^{3+} (0.938 Å) is closely related to La^{3+} in series (ionic radius 1.061 Å), both are trivalent (Armstrong and Cota, 1990; Cukierman et al., 1988; Elinder and Århem, 1994a; 1994b). Thus, theories used to explain modulatory effects of trivalent La^{3+} and divalent Ca^{2+} ions on other voltage-dependent channels may also apply to the Gd^{3+} effects on Shaker-IR.

Based on our observation, Gd^{3+} (100 μM) not only affected the voltage-dependent gating in Shaker-IR (shifting V_{50} to a more depolarized potential by 23 mV and decreasing the slope steepness by 6 mV), but also affected its conductance (decreasing G_{max} by 62%). These results are comparable to the magnitude of Ca^{2+}-mediated V_{50} shift (17 mV for neutral or 25 mV for negatively charged phospholipids) in a voltage dependent Na^+ channel (Cukierman et al., 1988). Moreover, Shaker-IR still maintained the characteristic sigmoidal G-V curve in the presence of Gd^{3+} (**Fig. 3-5c and 3-5d**); G_{max} was partially inhibited by Gd^{3+} (**Table 3-1**) but did not abolish voltage-dependent I_{Sh}.

B. Effect of La^{3+} on Shaker-like K^+ channels

The most direct comparison comes from studies of La^{3+} on voltage-dependent gating of a Shaker-like K^+ channel (the mammalian neuronal Kv 1.1). This study used a similar approach as in our experiment, i.e. TEVC on expressed Kv 1.1 channels in *Xenopus* oocytes (Tytgat and Daenens, 1997). As eluded to in the results section, it was demonstrated that 100 μM Gd^{3+} induced an approximately 23 mV V_{50} shift for Shaker-IR. Similarly, 100 μM La^{3+} for Kv 1.1 was found to shift the V_{50} of the membrane voltage by approximately 20 mV (Tytgat and Daenens, 1997). In addition, La^{3+} also decreased the K currents in Kv 1.1 expressing oocytes (Tytgat and Daenens, 1997), consistent with our finding that Gd^{3+} reduced G_{max}. Furthermore, La^{3+} had a much larger inhibition on inward currents than for outward currents for Kv 1.1 (Tytgat and Daenens, 1997). If Gd^{3+} also exhibited a larger effect on the inward Shaker-IR, then the positive shift of V_{rev} for Shaker-IR is

Table 3-1 Effects of Gd^{3+} on Shaker-IR gating parameters*

Parameter	Unit	Control	Gd^{3+} perfusion	Wash	"Gd^{3+}"- control **or** (G_{max}) "Gd^{3+}"/control	n
V_{50}	mV	-9.1 ± 2.7	3.4 ± 4.4	-15.2 ± 4.1 n = 4	23 ± 3.0	9
Slope	mV per e-fold	14.3 ± 0.5	20 ± 1.4	15.1 ± 1.3 n = 5	5.7 ± 1.7	9
V_{rev}	mV	-82.6 ± 2.0	-77.4 ± 1.6	82.1 ± 2.4 n = 6	5.1 ± 0.7	7
G_{max}	mS	0.5 ± 0.04	0.3 ± 0.10	0.4 ± 0.05 n = 6	62.4 ± 0.1 %	9

* Mean ± SE

reasonable.

C. Effect of Gd^{3+} on the voltage-dependent channels in *Xenopus laevis* axons

Consistent with our finding that Gd^{3+} affects the voltage-dependent gating of Shaker-IR, Gd^{3+} has also been shown to block voltage-dependent Na^+ and K^+ channels in *Xenopus laevis* axons (Elinder and Århem, 1994a). Using voltage-clamp techniques, all ionic currents including voltage-dependent Na^+, K^+ as well as the leakage currents, were found to be affected dose-dependently by Gd^{3+}. In addition, the voltage-dependent parameters such as activation, inactivation and activation time constant curves of both Na^+ and K^+ channels were all shifted by Gd^{3+}. Particularly, for the voltage-dependent K^+ channel, Gd^{3+} shifted the steady-state K^+ activation curve to the positive direction in a dose-dependent manner,. For example, 60 μM Gd^{3+} caused a 18 mV shift after 100 ms perfusion whereas 200 μM Gd^{3+} caused a 26 mV shift after 80 ms perfusion. These values are comparable with the V_{50} values obtained with Shaker-IR in our study.

It has also been shown that Gd^{3+} slows down the time course of the K^+ channel activation (Elinder and Århem, 1994a). For example, 60 μM Gd^{3+} increased the half-activation time about 5 fold and 200 μM Gd^{3+} about 7 fold. Since we did not perform a time course study of the Gd^{3+} effect, a comparison can not be made at this point. Furthermore, although not performed on K^+ channels, Gd^{3+} has been shown to induce a reversibly negative shift on V_{rev} of Na^+ channels, an approximately 8 mV shift by 100 μM Gd^{3+} and ~13 mV shift by 1 mM Gd^{3+} (Elinder and Århem, 1994a), comparable with the 5 mV positive shift for Shaker-IR. As V_{rev} represents the ion selectivity for the channel, one explanation might be a Gd^{3+}-induced modification of selectivity for Shaker-IR K^+ channels, as proposed to explain the Ca^{2+}-effects on K^+ channels (Armstrong and Miller, 1990) and Gd^{3+} effects on voltage-dependent Na^+ channels (Elinder and Århem, 1994a). Elinder and Århem

(1994b) tentatively interpreted the action of Gd^{3+} on voltage-dependent Na^+ and K^+ channels in terms of: 1) pure surface potential screening (no binding) of fixed charges on the bilayer; 2) the modulation by binding to modulatory sites on the channels; and 3) binding to a blockage site in the pore.

CHAPTER 4

Stretch-activation of Shaker-IR

INTRODUCTION

In the cell membrane of native *Drosophila* somatic muscle, wild-type Shaker was not reported to be mechanosensitive under conditions which activated the *Drosophila* SA K^+ channel (presumably a TREK homologue, see **Table 1-1**) (Zagotta et al., 1990; Gorczyca and Wu., 1991). It was generally accepted that Shaker was a typical voltage-dependent channel. We initially intended to test the hypothesis that Shaker-IR may acquire mechanosensitivity when modified by tethering to the spectrin cytoskeleton in *Xenopus* oocytes (see **Appendix**). In the course of these studies, it was found that even without this modification, Shaker-IR alone, responded to mechanical stimulation when expressed in *Xenopus* oocytes. In this chapter, the results of testing the mechanosensitivity on the heterologously expressed (non-modified) Shaker-IR will be presented.

RESULTS

I. Shaker-IR has mechanosensitive (MS) channel properties

A. Endogenous SA cation channels in *Xenopus* oocytes

To examine the mechanosensitivity of Shaker-IR expressed in oocyte membrane, which was known to have endogenous SA cation channels, it was important to distinguish these two types of

channels by electrophysiological recordings. For this purpose, non-injected or H_2O-injected (control) oocytes in the absence of Gd^{3+} were used to record the endogenous SA cation channels, and Shaker-IR-injected oocytes in the presence of 100 μM Gd^{3+} were used to record Shaker-IR currents (I_{Sh}).

The endogenous SA channels were distinguished from the exogenously expressed Shaker-IR channels by several criteria, including the V_{rev}, single channel conductance and different gating properties. In the absence of Gd^{3+}, the control oocytes (n = 20) showed low levels of spontaneous channel opening events which could be dramatically increased by suction. Under given experimental conditions (see **Chapter 2** for Na^+ and K^+ concentrations on both sides of the membrane), cell-attached patch clamp recordings showed that these endogenous SA channel currents reversed at about 0 mV and had a single channel conductance of ~30 pS at -60 mV. When there was only one active SA channel in the patch, the single channel current was characterized by brief flickery bursts lasting in the order of a few ms. The bursts continued for few tens of ms at higher open probability (P_{open}) when several channels were simultaneously activated. **Fig. 4-1** (left trace) shows an example of spontaneous inward currents (indicated by the downward deflections in the current trace) before application of suction. Upon suction (middle trace), the P_{open} increased but the amplitude of the current jumps remained the same, indicating an increase in P_{open} rather than activation of another channel type. After releasing suction (right trace), the channel activity returned to the original level, therefore exhibiting a reversible stretch-activation behaviour. This stretch-activation was reproducible when suction was re-applied. In several experiments, both negative (suction) and positive (blowing) pressures were applied to the same patch and each induced stretch-activation of the endogenous SA channels. Since blowing tended to break the seal, suction was used to stretch the patches in most experiments. When similar experiments were performed on control oocytes (n

Figure 4-1. Mechanical effects of endogenous SA cation channels

In the absence of Gd^{3+}, cell-attached patch-clamp recordings on a non-injected oocyte show a stretch activation of endogenous SA channels (V_m = ~ 60 mV). Three non-continuous single channel recordings are taken before, during sustained suction of -10 mmHg and after suction was released. Stretch activation events are shown at higher time resolution.

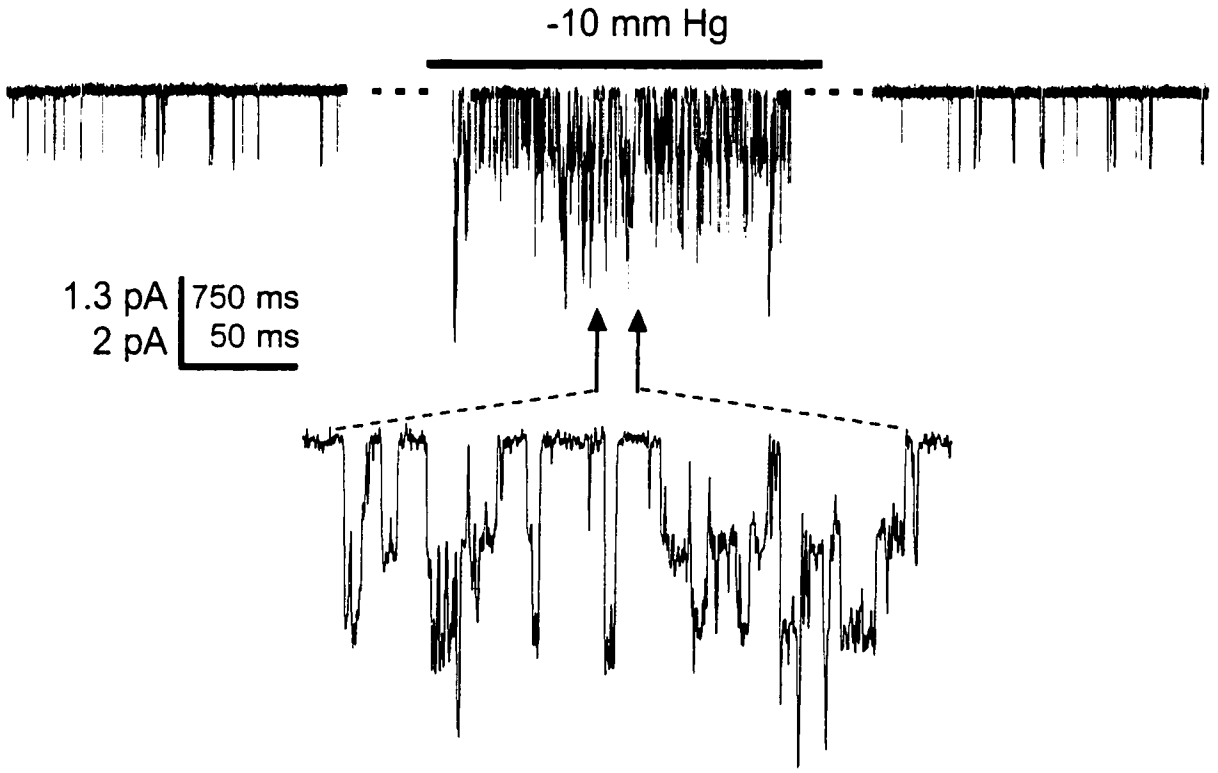
-10 mm Hg
1.3 pA
2 pA
750 ms
50 ms

=20) in the presence of 100 μM Gd^{3+}, no detectable spontaneous or suction-induced ionic currents were observed (data not shown). Various batches of oocytes on different days after surgery were tested.

B. Expression of Shaker-IR channels in *Xenopus* oocytes

To record I_{Sh} from oocytes expressing Shaker-IR, a series of depolarizing voltage steps (family protocol, see legend of **Fig. 4-2**) were applied to either cell-attached or excised patches. 100 μM Gd^{3+} was added to the pipette solution to block the endogenous SA cation channels. As previously shown, the Shaker-IR channels (see **Chapter 3**) exhibited outward currents which showed voltage-dependent activation and kinetics (**Fig. 4-2b**). These steady-state currents remained constant during prolonged depolarizing pulses, up to several hundred ms. However, when very long pulses (2 s) were used, the slow "C-type" inactivation (Hoshi et al., 1991) became evident, especially at more depolarized potentials (not shown). That these currents were carried by Shaker-IR channels was confirmed by the tail currents (see **Appendix**) which reversed at the predicted equilibrium potential for the K^+ ions (E_K). As a routine, both the family protocol and the tail protocol were conducted on every Shaker-IR-injected oocyte to confirm the expression of Shaker-IR. In other words, the family protocol was used to characterize the voltage-dependent gating parameters of Shaker-IR (see **Chapter 3**) by plotting the G-V activation curves while the tail protocol was followed to determine the V_{rev} for the recorded channels.

In comparison, when the same family protocol (**Fig. 4-2a**) and tail protocol were used on non-injected or water-injected control oocytes, they elicited no voltage-dependent ionic currents but only passive leak and capacitive currents. As a rule, three control oocytes were tested along with Shaker-IR-injected oocytes. We were confident that 100 μM Gd^{3+} was both appropriate for observing

Figure 4-2. Expression of Shaker-IR and mechanical effects on I_{Sh}

Representative examples from inside-out excised patches on **(a)** non-injected control oocyte and **(b)** Shaker-IR injected oocyte encoding Shaker-IR protein. I_{Sh} was elicited in response to a series of 100 ms voltage pulses from -110 mV to +70 mV in 10 mV step. A holding potential of -100 mV was applied for 1 s between successive pulses. The identical series of 100 ms voltage pulses were also applied to non-injected oocytes over the same period of expression time, with electronic compensation to remove the initial capacitance transient. **(c)** Cell-attached patch-clamp recordings on Shaker-IR-injected oocyte in the presence of Gd^{3+} to show first steady state currents (V_m = -20 mV), then stretch activation during application of -12 mmHg suction.

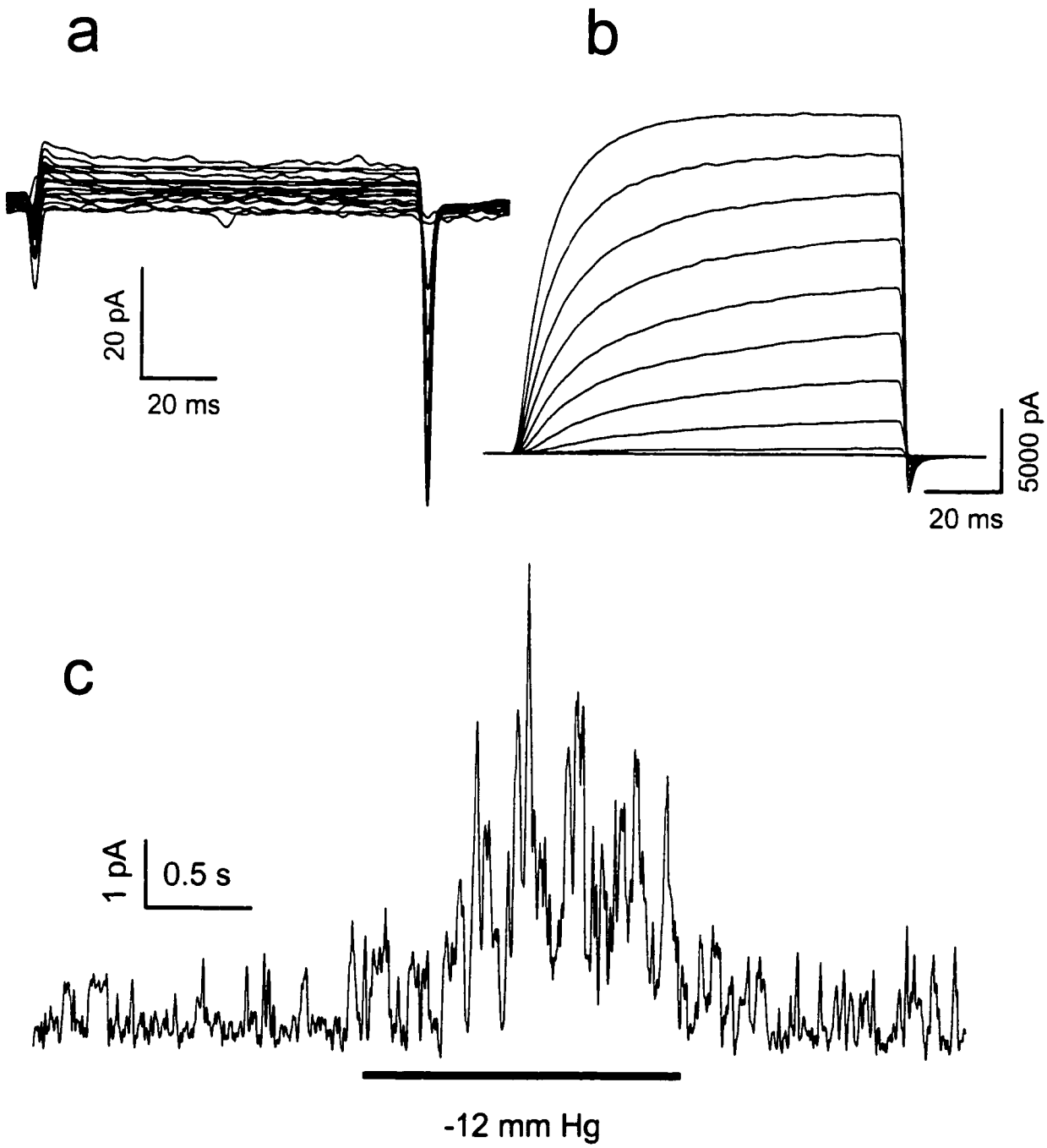
a
b
20 pA
20 ms
5000 pA
20 ms
c
1 pA
0.5 s
-12 mm Hg

the I_{Sh} and also sufficient for blocking the endogenous SA channels since I_{Sh} was recorded from Shaker-IR-injected oocytes but no ionic currents were recorded from the control oocytes. To exclude the possible contamination from endogenous SA channels and to study the response of Shaker-IR to mechanical stimulation, all subsequent experiments were carried out in the presence of 100 μM Gd^{3+} unless otherwise indicated.

C. Selecting a voltage range for recording single I_{Sh}

Since Gd^{3+} caused a substantial rightward shift of the G-V curve for Shaker-IR (**Chapter 3** and **Appendix**), the voltage used to elicit the first detectable I_{Sh} was relatively depolarized (~-20 to -10 mV) compared to others (e.g., -50 to -40 mV, Zagotta et al., 1994a). This shift turned out to be fortuitously advantageous given that the main goal of this study was to examine the mechanical effects on Shaker-IR channels at both single channel and macroscopic current levels. First of all, there were too many simultaneously active channels at voltages in the mid-region of the G-V curve, the best chance to record unitary I_{Sh} was at the foot of the G-V curve where the channel had a very low P_{open}. If G-V had not been shifted, the foot would have been very close to the V_{rev} of Shaker-IR, making it hard to resolve single Shaker-IR channel events. Second, the Gd^{3+}-induced shift (see **Discussion** of this chapter) provided an additional 30 mV driving force, allowing single I_{Sh} to be recorded at a larger signal-to-noise ratio. The third advantage of the Gd^{3+}-induced shift was that the voltage (at the foot of the G-V curve) used to elicit single I_{Sh} was coincidently near 0 mV, being around the V_{rev} for the two main types of endogenous channels in *Xenopus* oocytes: SA cation channel as well as Ca^{2+}-activated Cl^- channels (Cl^- concentration was approximately symmetrical in excised patches). This coincidence would minimize any sporadic contributory currents from these endogenous channels that reverse around zero. Thus, when 100 μM Gd^{3+} was added to the pipette

solution and V_m was stepped to the foot of the G-V curve, the recorded currents would be expected from expressed Shaker-IR.

D. Mechanical effects on Shaker-IR channels

The voltage value at the foot of the G-V curve was used also because the preliminary data suggested that stretch-activation was consistent at this voltage region. Patches were first subjected to a series of voltage steps to determine the foot of the G-V curve. Ideally, this procedure would be unnecessary since the foot of the curve should be fairly characteristic for all Shaker-IR channels in the same expression system under the same experimental conditions. In practice, however, the location of the G-V curve varied considerably from patch to patch presumably due to variations in Gd^{3+} concentration and oocyte-to-oocyte variance due to their specific surface chemistry (see **Discussion** for details). To examine if mechanical stress had any effects on I_{Sh}, the I_{Sh} elicited by the voltages near the foot of the G-V curve was subjected to mechanical stimulation. Under these conditions, the Shaker-IR-injected oocytes showed outward currents (sometimes with evident unitary events, see **Fig. 4-2c**) in all patches (n=18). When patches were subjected to a -10 to -20 mmHg suction, the P_{open} immediately increased and the channel activity recovered to its previous level upon release of suction.

As shown in **Fig. 4-2c**, the membrane potential was held at -20 mV for 10 s in the presence of 100 μM Gd^{3+}. Since P_{open} was low at this voltage (< 0.001) based on the macroscopic G-V relationship, there were only a few spontaneous outward channel events, indicated by the upward deflections. When the patch was transiently subjected to -12 mmHg suction (bar), P_{open} transiently increased by about 20-fold. Since 100 μM Gd^{3+} was more than sufficient to block the endogenous SA channels in oocytes, these channels could not have carried outward currents at -20 mV, the

mechanically responsive channels are likely Shaker-IR.

II. Stretch-activation of Shaker-IR at the foot of the G-V curve

A. Establishing a step pair protocol

One approach to confirm whether SA currents are indeed carried by Shaker-IR, would be to generate G-V curves (by a family protocol) before, during and after mechanical stimulation. Parameters such as V_{50} and G_{max} could then be extracted from the G-V curves to characterize the voltage-dependent gating properties of Shaker-IR. This approach did not, however, prove to be practicable since the family protocol takes about 2 min to complete and stretch must be held throughout this period. Our preliminary experiments showed that the patches frequently ruptured during prolonged stretch. Additionally, such prolonged suction may also increase the likelihood of changing the membrane patch area by adding bilayer material (Sokabe et al., 1991). A "truncated" G-V approach was therefore preferred. Instead of generating the entire family of currents, a pair of voltages (step pair) near the foot of the known G-V curve was applied. By stepping to the paired voltage steps, I_{Sh} was recognizable by its sigmoidal activation at either one or both of the test voltages (depending on the current magnitude) and by the voltage-dependent outward K^+ currents that were maintained during the sustained depolarizing voltage steps. Step 1 was chosen to minimally activate I_{Sh} (in a voltage range from -20 to 0 mV) and step 2 was set at 10 mV more depolarized voltage (in some experiments, 5 mV). Each of the two successive voltage pulses was applied for 150 ms followed by a return to the holding potential of -100 mV for 500 ms (**Fig. 4-3b, top**). The long duration (150 ms) step was necessary to allow I_{Sh} to approach steady-state. The step pairs were repeated 6 times (with ~1 s intervals between pairs) on the same patch before, during and

Figure 4-3. Stretch-activation of Shaker-IR by paired-step protocol

(a) Inside-out excised patch recording from a non-injected oocyte using voltage pairs (steps to -10 mV and then to 0 mV from a holding membrane potential (V_{hold}) of -100 mV, the paired-step protocol is illustrated above **(b)**. The step pairs (applied 6 times) elicited currents from a control oocyte were given before (top trace), during (middle trace) and after (bottom trace) suction. Suction bar is indicated in mmHg. Applied pressure and V_{hold} were maintained during the middle trace-breaks (2 s). The two upward current spikes indicate the capacitive currents in response to the step from -100 to -10 mV and then from -10 to 0 mV, and the downward spike was the capacitive transient when the membrane was stepped back to -100 mV. **(b)** The step pairs voltage protocol is illustrated at the top. I_{Sh} recorded from an inside-out excised patch of Shaker-IR-injected oocyte before (top trace), during (middle trace, suction bar) and after (bottom trace) suction. Sustained suction applied to the patch is indicated by the bars. The same protocol was used as in **(a)** but with a different paired-step (-20 mV and -10 mV). All pipette solutions contained 100 μM Gd^{3+}.

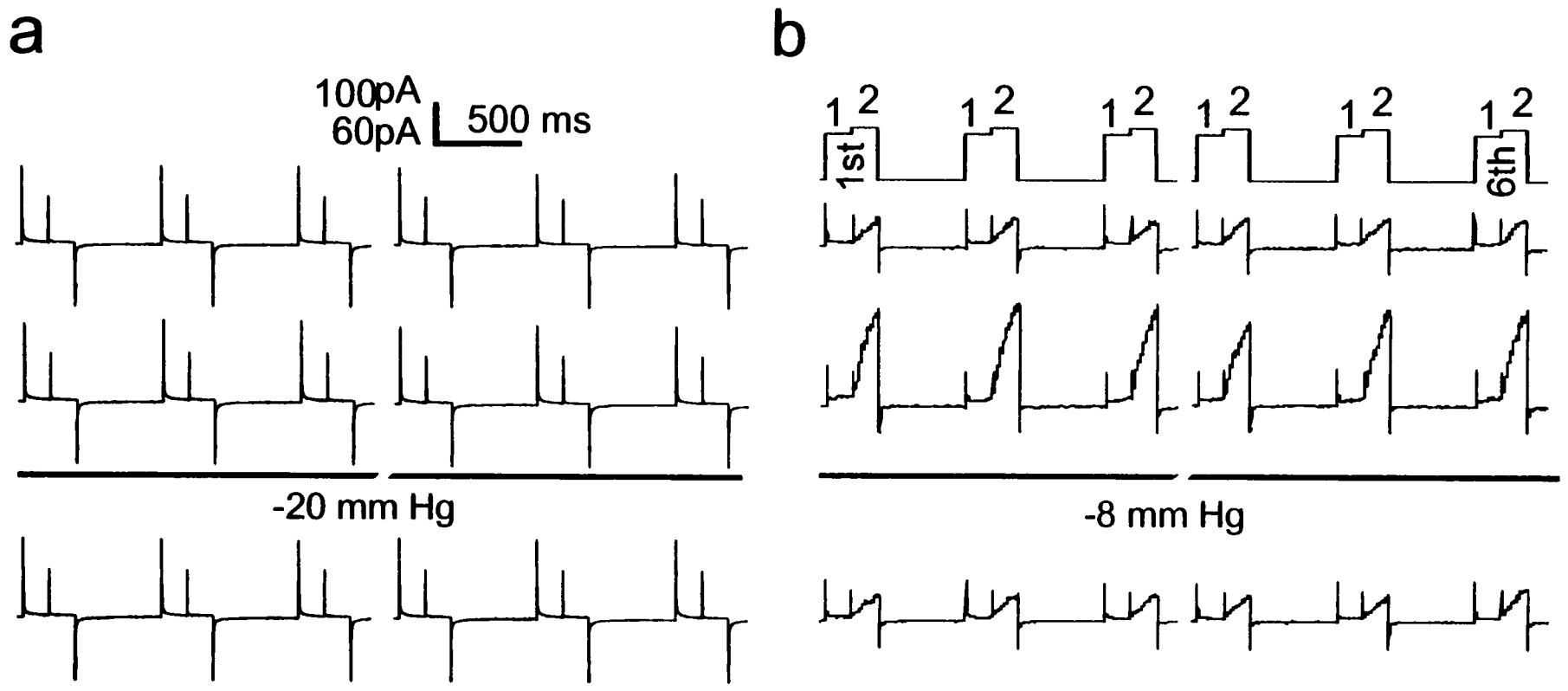
a
100pA
60pA
500 ms
-20 mm Hg
b
1 2
1st
6th
-8 mm Hg

after mechanical stimulation. This is to test the repeatability and/or trends of the mechanical response. Then mechanical effects were assessed by comparing the steady-state I_{Sh} for step 1 and step 2 at, before and during mechanical stimulations (**Fig. 4-3**).

B. Applying step pairs to non-injected and Shaker-IR-injected oocyte patches

To exclude the possibility that suction may draw more membrane into the patch, the excised patch configuration was preferred. Not only does the excised patch configuration have a limited membrane area, it also allows for direct control of V_m (see **Chapter 2**). Every step pair used for studying the mechanical effects on Shaker-IR-injected oocytes was tested on non-injected control oocytes. With 100 μM Gd^{3+} in the pipettes, control oocytes (n = 15) exhibited no visible ionic currents at voltage steps from -20 to +20 mV (in 10 mV steps) and suctions sufficient to rupture the patch (>40 mmHg) did not detectably alter the capacitive currents or leak currents. As shown in **Fig. 4-3a**, on an uninjected oocyte, a step pair (-10, 0 mV) elicited only capacitative currents (indicated by the transient spikes at both voltage steps) and tiny leak currents from a non-injected oocyte. With -20 mmHg suction, both currents remained unchanged and no detectable ionic currents were observed. These results from control oocytes suggested that 100 μM Gd^{3+} completely blocked the endogenous SA channel activity and that suction did not enlarge the membrane area in the patch.

By comparison, for Shaker-IR-injected oocytes (n = 22), the same step pairs elicited voltage-dependent outward I_{Sh}, and suction (from -10 to -20 mmHg) reversibly and reproducibly increased I_{Sh} at both voltage steps. Because the characteristic kinetic and voltage-dependent gating features of Shaker-IR was observed, it was assumed that the suction-induced currents were indeed carried by Shaker-IR. A typical example of such an excised patch is shown in **Fig. 4-3b**. In a few cases when the patches (n =5) held out without rupturing, the same procedure was repeated at a different step

pairs and stretch-enhanced currents with the characteristics of I_{Sh} were again evident.

C. Disproportionate increase of I_{Sh} at different step pair voltages

1. Reversible mechanical effects

The steady-state I_{Sh} elicited by a pair of voltage steps (as described earlier) was measured to quantify the effects of mechanical stimulation on the Shaker-IR channels. Baseline was set at the current trace elicited by the holding membrane potential of -100 mV. Then I_{leak} was measured as the difference between the baseline and the current trace in response to the first voltage step when the time dependent I_{Sh} became evident. The baseline was then reset to the I_{leak} level and the steady-state I_{Sh} elicited by the first (e.g., -10 mV) and second voltages (e.g., 0 mV) were measured. Any additional I_{leak} on the second step was considered trivial because the I_{leak} on step 1 was due to a large 90 mV voltage difference (-100 to -10 mV) whereas additional I_{leak} produced by step 2 was only 1/9 of the I_{leak} produced by step 1. Thus, unsubtracted I_{leak} at the second voltage step would have caused only a small underestimation of the stretch sensitive component of I_{Sh}.

In this way, the means of the steady-state I_{Sh} from six repeats (± SD) were calculated and plotted for each patch before (control), during (stretch) and after (release) suction. As shown in **Fig. 4-4a**, suction (indicated by the solid bar at the bottom) reversibly increased the current amplitude of Shaker-IR at both steps (step 1, -20 mV and step 2, -10 mV). Similarly, for all patches tested with the same step pairs (-20 and -10 mV, n = 17), suction increased I_{Sh} at both voltages (paired T-test, $P<0.01$). Because amplitudes varied from patch to patch, presumably due to variation of the number of channels in each patch, data like that in **Fig. 4-4a** for each of 17 patches were normalized against the means (n = 6) of each patch's suction-augmented currents in order to display the general trend of the reversible stretch-activation with a common scale (**Fig. 4-4b**). When the fold increase of I_{Sh}

Figure 4-4. Stretch-activation at one pressure in one or all patches

(a) Analysed steady-state I_{Sh} (Mean ± SD of the six repeats) were plotted before (control), during (stretch) and after (release) mechanical stimulation at voltage steps of -20 mV (step 1) and -10 mV (step 2). Steady-state I_{Sh} was obtained with a cursor measurement (Clampfit). Baseline was reset to the leak current level where this was evident and then the steady state current amplitudes activated by steps 1 and 2 were measured. **(b)** Summarized data for 17 such excised patches under the same experimental condition. For each patch, the steady-state I_{Sh} were normalized against the mean value during suction. The difference of suction to control ratio between the step 1 and step 2 was significant (Student's paired t-test, $P < 0.01$, $n = 17$).

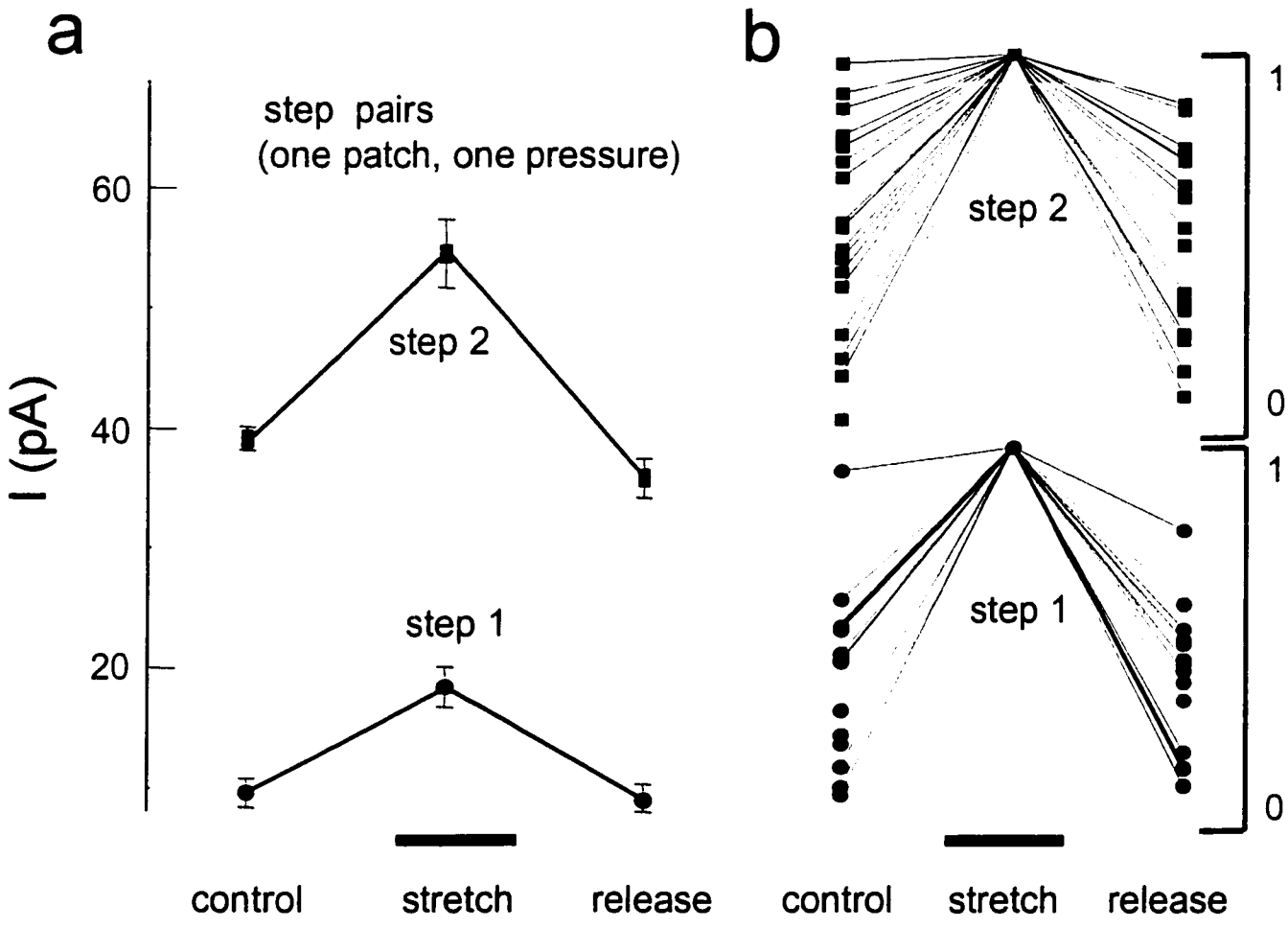
a
step pairs
(one patch, one pressure)
60
40
20
I (pA)
step 2
step 1
control
stretch
release
b
step 2
step 1
1
0
1
0
control
stretch
release

was expressed as ratios of $I_{stretch}/I_{control}$ for each voltage step, the ratio of step 1 [$I_{stretch}/I_{control}$] was greater than the ratio of step 2 [$I_{stretch}/I_{control}$] ($P<0.01$). The averaged ratio (or fold increase) is 3.76 ± 0.35 (mean±SE, n=17) for step 1 and 2.56 ± 0.3 for step 2 ($P<0.01$). Thus, suction induced a disproportionate fold-increase at the two adjacent voltages within the same patch, with the larger increase near the foot of the G-V (i.e. at the relatively more hyperpolarized potential).

2. Dose-response of stretch-activation

Fig. 4-5a further illustrates the disproportionate increase of Shaker-IR at paired voltage steps by replotting the ratios as bar graphs. This analysis was done to help clarifying the procedure involved in generating step pair dose responses, one of which is illustrated in **Fig. 4-5b**. The means and SD of I_{Sh} for a sample patch (**Fig. 4-5a**, left) were calculated and plotted as control (0 mmHg), stretch (-15 mmHg) and release (0 mmHg) for two voltages (left panel), then the same data were plotted as a bar graph showing the ratio of fold increase ($I_{stretch}/I_{control}$ and $I_{release}/I_{control}$, with control (0 mmHg) designated as 1. As shown in the right panel of **Fig. 4-5a**, suction caused an almost 2-fold increase in current amplitude at -20 mV (step 1), whereas at -10 mV (step 2), approximately 1.5-fold increase is shown. Similar observation was found in all patches (n =50) tested with a series of step pairs from -25 to +20 mV (from the foot of the G-V curve where I_{Sh} become evident to the voltages near V_{50}). For example, -25; -20 mV (n=2); -10, 0 mV (n=18); -10, -5 mV (n=2); 0, +5 mV (n=1); 0, 10 mV (n=15); 10, 15 mV (n=2); 10, 20 mV (n=10). Consistently and significantly larger ($P<0.01$) fold increase was always found with step 1 than with step 2, indicating the disproportionate increase of I_{Sh} at different voltages pairs.

If there was undetected residual pressure in the pipettes following the gigaseal formation, application of one pressure could either increase or decrease the actual pressure applied on the cell

Figure 4-5. Disproportionate increase of I_{Sh} over one pressure or a range of pressures

(a) Left: mean of the six repeats (± SD, standard deviation) plotted at voltage pairs -20 mV (step 1) and -10 mV (step 2) before (0 mmHg), during (-15 mmHg) and after (return to 0 mmHg) stretch. Where no error bar is shown, the SD is smaller than the control. Right: the same data was plotted as the fold increase of I_{Sh}, a ratio of stretch to control and of release to control with control designated as 1. **(b)** A pressure-response curve for Shaker-IR at voltage pairs -10 mV (step 1) and 0 mV (step 2).

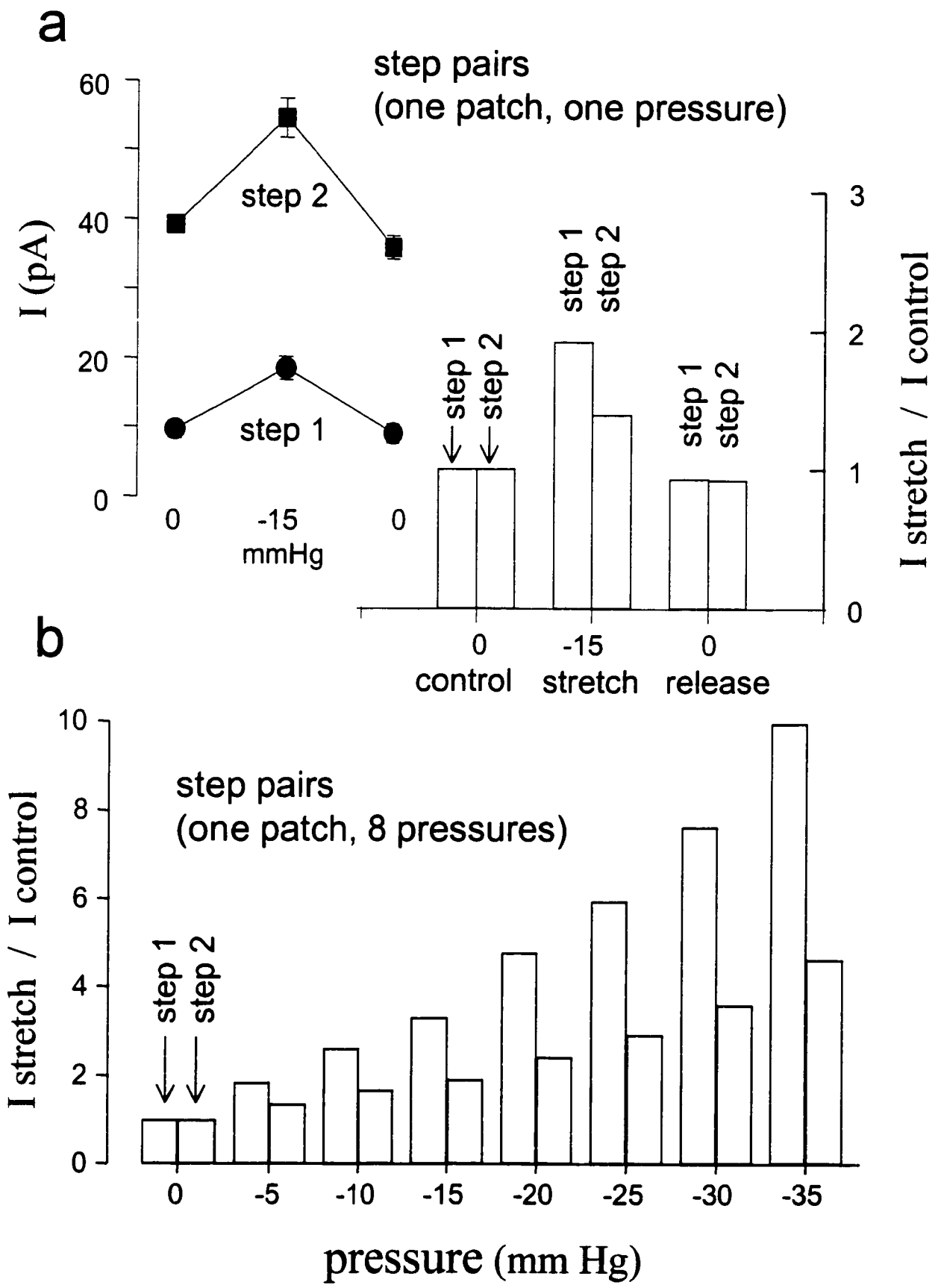
a
step pairs
(one patch, one pressure)
I (pA)
60
40
20
0
step 2
step 1
0
-15
mmHg
0
step 1
step 2
step 1
step 2
step 1
step 2
3
2
1
0
I stretch / I control
0
-15
0
control
stretch
release
b
step pairs
(one patch, 8 pressures)
I stretch / I control
10
8
6
4
2
0
step 1
step 2
0
-5
-10
-15
-20
-25
-30
-35
pressure (mm Hg)

membrane. Thus, it was important that the characterization of stretch-activation of Shaker-IR be made not only at one but at a series of pressures. For this purpose, the fold increases from two voltage steps were obtained for a series of increasing negative pressures. Patches from 3 oocytes showed that the mechanical responses of Shaker-IR were stretch dependent, and that higher stretch induced larger mechanical responses. As illustrated in **Fig. 4-5b**, the fold increase for both voltages (step 1 and step 2) increased with the increasing pressures from 0 to -35 mmHg (in 5 mmHg steps), in a dose-dependent manner. Consistent with the disproportionate increase on each given pressure (see **Fig. 4-5a**), a larger fold-increase was observed at the lower voltage (step 1) over the whole pressure range.

III. Stretch-activation of Shaker-IR at the single channel level

Single-channel recordings provide a quantitative description of how changes in P_{open} account for the mechanical effects seen on macroscopic currents. Since we established at the macroscopic current level that the stretch-affected currents were I_{Sh}, the effect of mechanical stimuli on Shaker-IR was further examined at the single channel level. The single I_{Sh} was identified by the burst openings which continued (as expected, given the absence of an inactivation ball) for an extended period of time and which was distinct from the single endogenous SA channels in oocytes (see **Fig. 4-1**).

To further test the mechanical effects at the single channel level, single I_{Sh} elicited by voltages near the foot of the G-V curve were subjected to mechanical stimulation. In these experiments (n=6), a series of increasing negative pressures (from 0 to -100 mmHg) resulted in more and more channel openings until the isolated single channel events could no longer be resolved. This finding is consistent with the dose-dependent stretch-activation at the macroscopic level and the

representative data is shown in **Fig. 4-6**. Similar to the mechanical effects on macroscopic I_{Sh} (**Figs. 4-2c and 4-3**), stretch-activation at the single channel level was reversible and the single channel activity resumed completely when the suction was released (**Fig. 4-6**, bottom trace). Like the example shown in **Fig. 4-6**, results from five other patches suggested that suction increased the P_{open} in a pressure-dependent manner.

To verify that suction-induced channel activity was from Shaker-IR channels rather than from contamination by other channel types, all-points current amplitude histograms were produced that allowed us to identify different channel types by comparing their single channel amplitudes (see **Chapter 2**). The all-point amplitude histogram (**Fig. 4-7**) was plotted before and during a series of suction steps (same data set as in **Fig. 4-6**). An equal interval between amplitude peaks (0.6 pA at V_m = -30 mV) is seen either within each histogram trace at a given pressure or between histogram traces at different pressures, suggesting that increasing suction does not affect the current amplitude. For example, the histogram at -17 mmHg shows that the increased opening events were from the same kind of channel as seen at 0 mmHg since they have the same unitary current. The single channel current amplitude obtained from these all-point amplitude histograms was comparable to the values reported by Hoshi et al. (1994, i.e. 0.6 pA at -30 mV and with similar ionic conditions), further confirming that the suction indeed increased the P_{open} of Shaker-IR channels.

IV. P_{open} of Shaker-IR channel is a sigmoidal function of applied pressure

MS channels are characterized by changes of their P_{open} in response to mechanical stimulation (Morris, 1990) and MS gating is described by the sigmoidal P_{open} as a function of applied pressure (Hamill and McBride, 1994; Sachs and Morris, 1998). The pressure-dependence of the

Figure 4-6. Effect of increasing suction on single I_{Sh}

Single channel currents were recorded from an excised patch exposed to a series of negative pressures as indicated. Each pressure was applied for 20 s then switched to the next pressure level and each trace represents a continuous recording of 5 s. Bottom current trace represents the recording after suction was released from -20 mmHg. V_m = -30 mV.

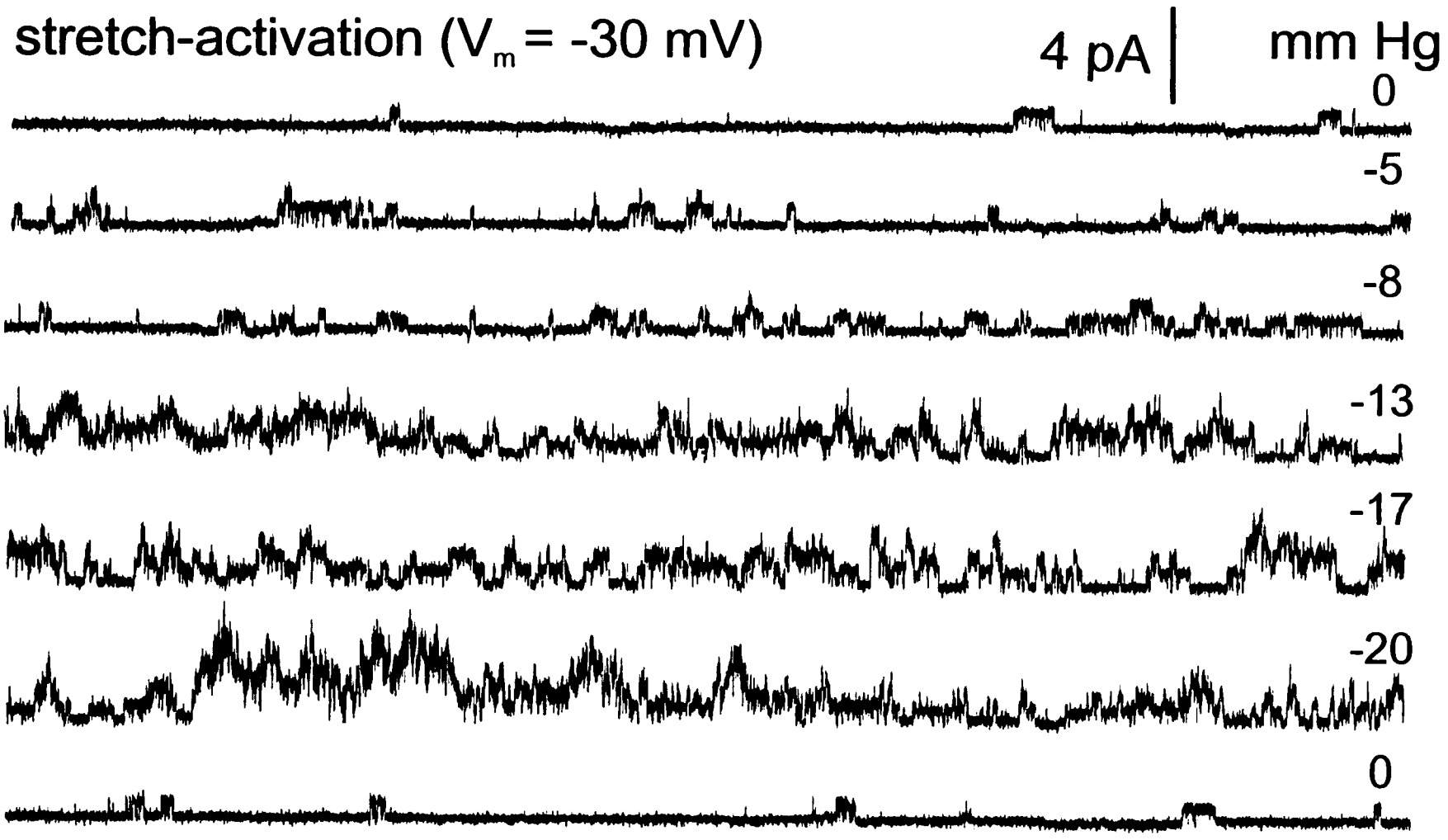
stretch-activation (V_m = -30 mV)
4 pA
mm Hg
0
-5
-8
-13
-17
-20
0

Figure 4-7. All-points histogram of I_{Sh} events over a range of pressures

Superimposed all-points current amplitude histograms were from five suction steps (same data set as in **Fig. 4-6**). Abscissa represents the current amplitude, with "0 pA" being the baseline current (no open channels).

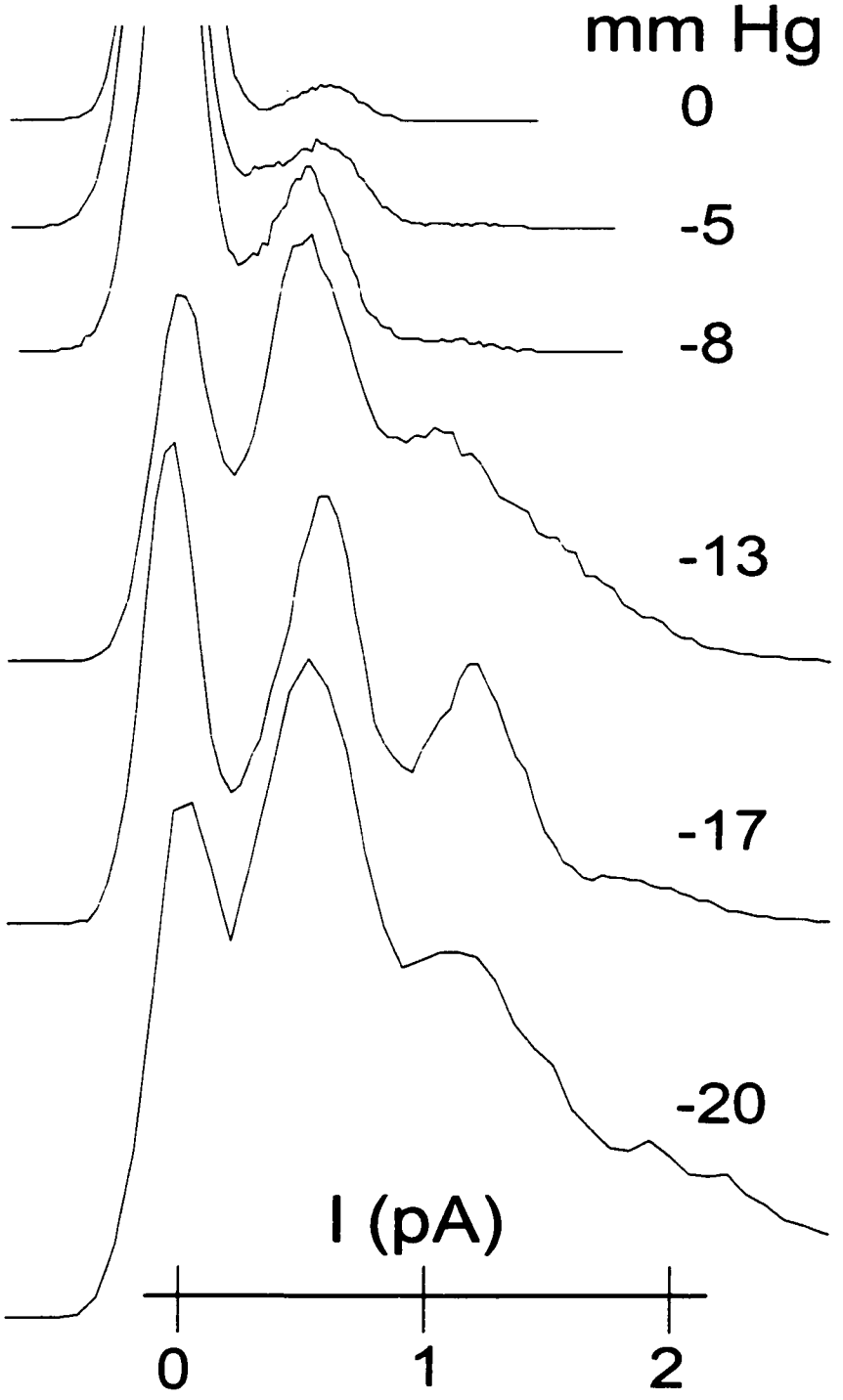
mm Hg
0
-5
-8
-13
-17
-20
I (pA)
0
1
2

Shaker-IR channel activity has already been demonstrated at the macroscopic level (**Fig. 4-5b**) as well as at the single channel level (**Fig. 4-6**).

To further characterize the stretch-activation behaviour of Shaker-IR, the P_{open} of single I_{Sh} was calculated (see **Chapter 2** for P_{open} measurements), plotted as a function of applied pressure and fitted to the Boltzmann function (**Fig. 4-8**). As expected for a SA channel, an increase in negative pressures caused a significant ($P<0.01$, $n=6$) augmentation of Shaker-IR P_{open} and resulted in a steep P_{open} / pressure activation curve (**Fig. 4-8**). The fold-increases (ratios of P_{open} at highest pressure compared to the pre-stretch P_{open} within a given patch) for six patches were as follows: 4.4, 8.5, 9.3, 37, 118 and 358.

As mentioned previously, application of Gd^{3+} caused a rightward shift of the G-V curve and thus the position of each G-V curve was dependent on actual Gd^{3+} concentration. Thus, V_m was varied for each patch to optimize the recording condition for single channel studies. Six patches were each held at different V_m and the elicited single I_{Sh} was subjected to a series of increasing negative pressures. Although the position of each plot varied from patch to patch along the pressure axis, it can be seen (**Fig. 4-8**) that the P_{open} of Shaker-IR was non-linear, increased steeply as a function of the applied pressure.

For reasons given in the **Discussion**, the Shaker-IR P_{open} / pressure activation curves were not constrained to a minimum P_{open} of zero before application of pressure. However, P_{open} was normalized against maximum P_{open} in each patch at the maximal suction step. This was done to observe the general trend of stretch-activation for all the six patches with the same plot scale (from 0 to 1). This normalization was based on the assumption that P_{open} reached saturation at maximal stimulation in each patch.

Figure 4-8. Effect of suction on the P_{open} of Shaker-IR

NP_{open} (number of channels times the P_{open}) of Shaker-IR channel versus applied pressures from single-channel recordings of six inside-out excised-patches. Each point represents an averaged P_{open} computed for the entire 20 s segment of continuous recording. The holding V_m were: -30 mV (▽); -30 mV (■); -20 mV (○); -10 mV (▲), 0 mV (●) and 5 mV(❐). Pressure was increased progressively with no release between successive pressures. All patches were subjected to a sequentially increased pressure from low to high except one patch (□) which was done in a reverse order. The curve (○) was generated from the same data set as shown in **Fig. 4-6**.

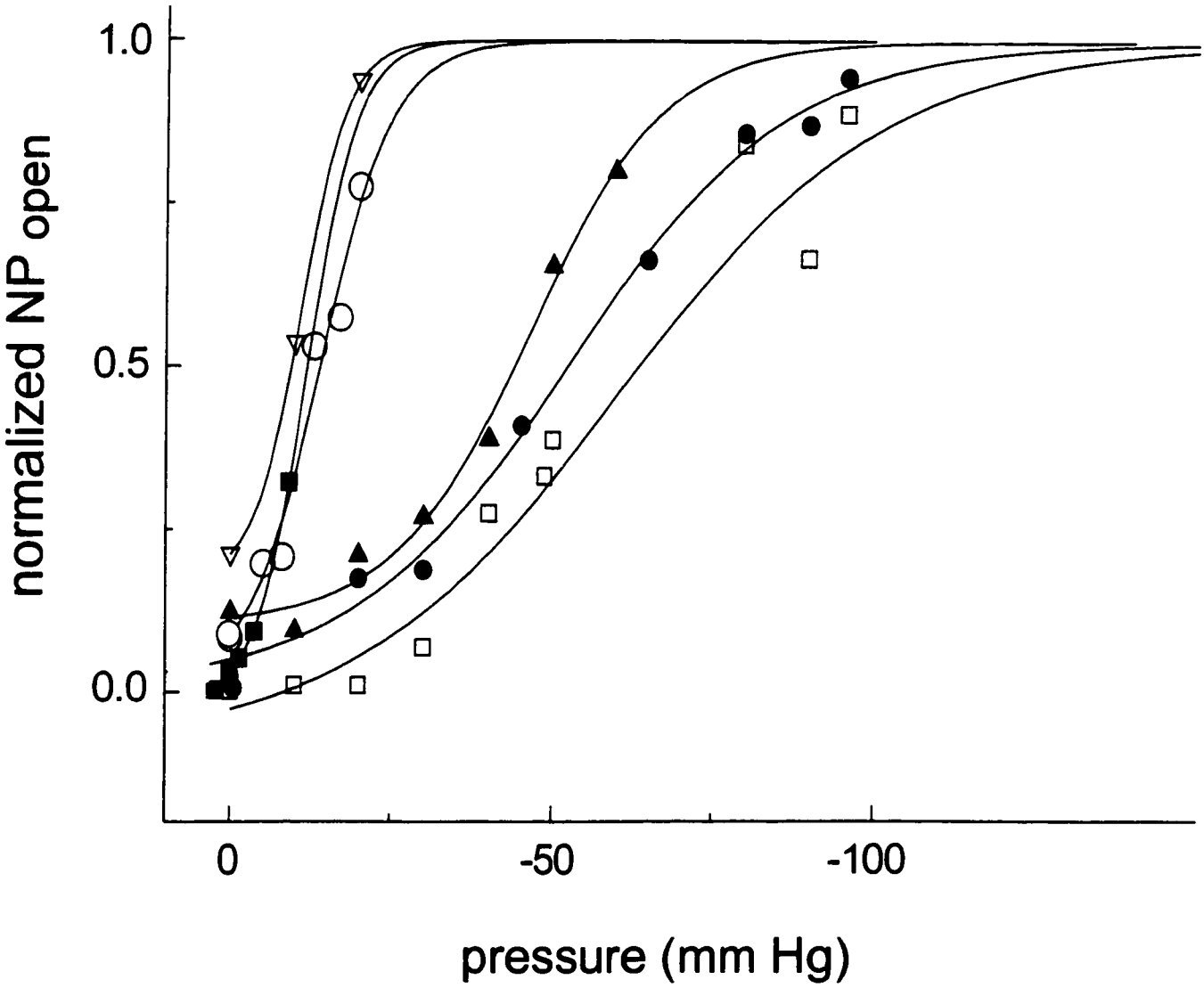
1.0
0.5
0.0
normalized NP open
0
-50
-100
pressure (mm Hg)

V. Shaker-IR is activated by membrane tension

Most SA channels are known to be gated by membrane tension rather than membrane curvature (Hamill and McBride, 1996). It was thought that if the P_{open} of Shaker-IR is increased by membrane tension, then the channel activity should be insensitive to the membrane curvature and a U-shaped activation curve in response to stretch would be expected, the characteristic feature for SA channels (Bourque, 1996). To test whether the P_{open} of Shaker-IR was modulated by membrane tension, both suction and blowing were applied to the patch to vary the membrane curvature. Theoretically, both suction and blowing should have generated membrane tension although negative pressure would produce a concave curvature whereas positive pressure produce a convex curvature. If the stretch-activation is due to gating interference on Shaker-IR channels, it is expected that both stimuli would produce the same mechanical effect. Moreover, to exclude the possibility that membrane area is increased by suction, the same approach (suction and blowing) is applied. If suction-induced an increase in membrane area, then blowing would not be expected to exhibit a similar effect.

V_m was varied to record single I_{Sh}, then the patch was subjected to a series of 20 s sustained pressure steps. Between each pressure step, suction was released for about 2 s for recovery from the stimulus. The oocyte membrane was first subjected to a series of increasing negative pressures (suction) then to a series of increasing positive pressures (blowing). The single Shaker-IR P_{open} was measured as previously described (**Chapter 2**), normalized against the maximum P_{open} at either the highest suction step or the highest blowing step, then plotted against the applied pressures. As blowing was far more likely to break a patch than suction, only a few patches (n = 4) showed stretch-activation with <+20 mmHg (data not shown). **Fig. 4-9** illustrates that both blowing and suction

Figure 4-9. U-shaped P_{open} / pressure activation curve

Effects of membrane tension on Shaker-IR is plotted as the channel P_{open} versus a series of positive and negative pressures. Each point represents the mean value of NP_{open} from 2 to 3 recordings under the same experimental conditions and fitted with non-linear regression. V_m = -30 mV.

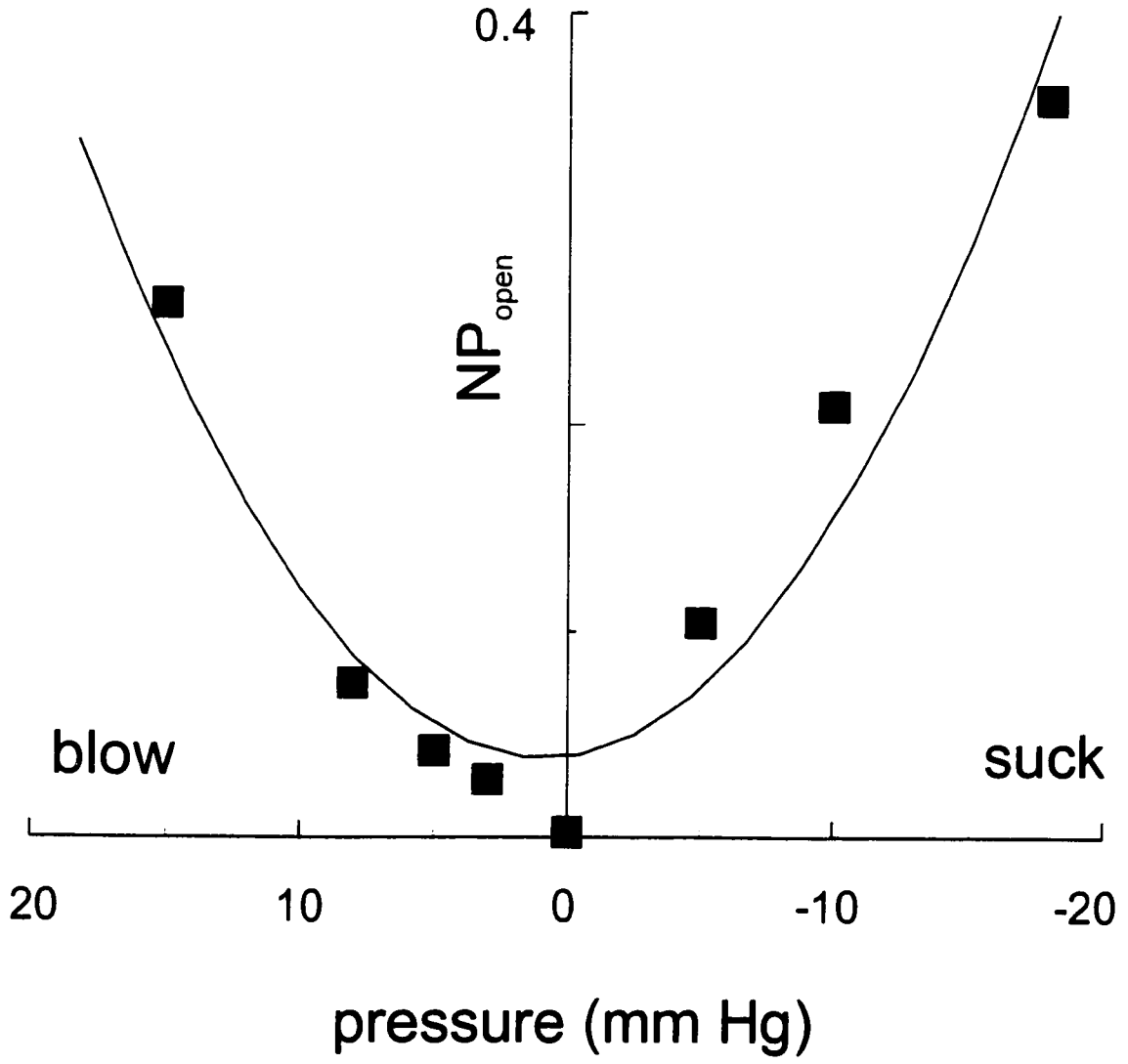
0.4
NP open
blow
suck
20
10
0
-10
-20
pressure (mm Hg)

increased the P_{open} of Shaker-IR and the increase was roughly symmetrical about the zero pressure point, yielding the classical U-shaped pressure activation curve. In this experiment, the mechanical effect was reversible. Each pressure was repeated 2 to 3 times before going to the next pressure step, further confirming that transient pipette pressure yielded a transient membrane tension. It is unlikely that membrane area increased with increasing suction because blowing produced the same transient stretch-activation of I_{sh}. Moreover, mechanical response is dependent on the net pipette pressure, regardless of membrane curvature, both suction and blowing could exert mechanical forces which could regulate Shaker-IR channel's activity.

DISCUSSION

I. Stretch-activation of Shaker-IR

The present study was initiated by preliminary data (**Appendix**) that Shaker-IR was susceptible to mechanical stimulation. Results presented in this chapter demonstrated that Shaker-IR exhibited "typical" responses of SA channels; at voltages where it had a low P_{open}, a sustained suction consistently increased P_{open}. As with other SA channels, these effects were reversible in that channel activity recovered rapidly after suction was released (**Figs. 4-2 and 4-3**). Thus, Shaker-IR can be added to the growing list of voltage and ligand-gated channels that display mechanosensitivity. Moreover, Shaker-IR seems to be even easier to be activated by stretch than some SA channels reported in the literature (discussed below).

Direct comparisons of mechanosensitivity among different preparations are difficult because tensions are almost never known. Correlating the pressure applied to the patch pipette with any

estimate of membrane tension is impossible without visualizing the patch (see **Chapter 1**). But in general, one can compare the mechanosensitivity between channels by threshold pressure values. For example, the "threshold" pressure for activating Shaker-IR was much lower (from -10 to -20 mmHg, see **Fig. 4-3; 4-6**) than that of the SA K^+ channel in *Lymnaea* neurons, typically ranging from -30 to -50 mmHg (Morris and Sigurdson, 1989; Morris, 1990) or SA Cl^- channels (-40 mmHg) in snail neurons (Bedard and Morris, 1992, see **Table 1-2**). TREK channels in cell-attached patches have a threshold pressure range of -30 to -80 mmHg at different holding membrane potentials (Patel et al., 1998) under similar experimental condition used in this study. Most strikingly, the cloned MS channel from *E. coli*, MscL, requires near lytic-pressure (-100 mmHg) to show stretch-activation (Sukharev et al., 1994). In contrast to MscL, Shaker-IR was activated by much smaller pressures (as above) and its lytic pressure was -20 to -30 mmHg for excised patches and -30 to -40 mmHg for cell-attached patches. The lytic pressures for K_{ACh} are -80 mmHg for cell-attached and -100 mmHg for excised patches (Pleumsamran and Kim, 1995). The differences in threshold suggest that the Shaker-IR is more sensitive to mechanical deformation. Finally, it is possible to compare the fold increase in response to mechanical stimulation between Shaker-IR and NMDA channels. In these experiments, suction produced from 5 to 358-fold increase at -20 mmHg stretch whereas ligand-induced NMDA currents in cultured mouse neurons, as well as NMDA expressed HEK cells (Paoletti and Ascher, 1994; Casado and Ascher, 1998), can be further augmented only by up to a 3-fold increase (-50 to -150 mmHg) in single-channel recordings. Taken together, Shaker-IR is at least as stretch-sensitive as the other MS channels listed above.

II. Modulation of Shaker-IR P_{open} by mechanical stimulation

For "typical" SA channels such as the endogenous SA channels in oocytes, a closed channel ($P_{open} \approx 0$) can be activated by membrane tension alone. In contrast, NMDA (Paoletti and Ascher, 1994) and GIRK channels (Ji et al., 1998; Pleumsamran and Kim, 1995) have to be "primed" with their appropriate agonists to observe their mechanosensitivity. In the presence of specific agonists such as NMDA plus glycine, NMDA channels are at an equilibrium among several closed states and a double-liganded open state. A simplified kinetic scheme can be depicted as:

$$\begin{array}{ccc} & OAg & AgOAg \\ & \updownarrow & \updownarrow \\ C1 \leftrightarrow & C2 \leftrightarrow C3...Cn \leftrightarrow & CnAg^* \leftrightarrow AgCnAg \end{array}$$

where Ag represents the bound agonist, C1-C3 represent the closed conformations, n represents the number of transitions and O represents an open conformation.

Paoletti and Ascher (1994) showed that NMDA channels need first to be primed with a low concentration (10 μM) of agonist. Although not discussed in their paper (Paoletti and Ascher, 1994), we proposed that the priming might be able to get most of the channels into a single ligand bound form (CAg, shown as*). From the single-liganded closed state, channels may be either transitioned to the single liganded open state (OAg) or transitioned to the two agonist liganded open state, AgOAg, via an intermediate state, AgCAg. Although both the single and double liganded NMDA channels (AgC and AgCAg) are required for the open state of the channel, AgCAg has a long, stable open state (higher P_{open}) while AgC has a short-lived open state (lower P_{open} relative to AgCAg). Thus, at the AgCAg state, mechanical stimuli may, relatively easily, bias the open and closed equilibrium transitions and affect the P_{open} of NMDA channels. For channels at gating states in the absence of agonist (C1...Cn), P_{open} is extremely low and suction may not be sufficient to lower the

energy barrier and to induce a detectable change in P_{open}. This might be the reason that NMDA channels need to be primed by a low concentration of agonist in order for its activity to be further increased by stretch. Although my data do not specifically address any particular model, a similar scheme may apply for Shaker-IR channels. They may also have to be "primed" by depolarizing membrane potential to that close to the foot of the G-V curve, so stretch affects the P_{open} of Shaker-IR. At voltages far away from the foot of the established G-V curve, for instance, at holding membrane potential of -80 or -100 mV, no current events were detected and suction did not induce any detectable I_{Sh}. This was as expected since there was too little driving force; Shaker-IR has a V_{rev} of -80 mV while stretch-induced effects, if any, would not be detectable at these holding potentials.

During membrane depolarization, Shaker-IR goes through a number of voltage-dependent closed states followed by a final voltage-independent open transition (Zagotta et al., 1994a). Thus, a simplified activation process involving "n" sequential conformational transitions may be summarized by the following gating scheme, at depolarized voltages (modified from Zagotta et al., 1994a):

$$\begin{array}{ccccccc} & \alpha 1 & & \alpha 2 & \alpha 3 & & \alpha n \\ & \updownarrow & & \updownarrow & \updownarrow & & \updownarrow \\ C1 & \leftrightarrow & C2 & \leftrightarrow & C3 & \leftrightarrow \ldots\ldots & Cn^* \leftrightarrow ON \end{array}$$

where $\alpha 1$ to αn represent the rate constants for the indicated conformational changes; C1-Cn represent closed conformations, n is the number of transitions and O represents an open conformation. At depolarized voltages, the rate constants for the reversed transitions would be expected to be much slower than the rate constants for the forward transitions, and are thus ignored here.

Depolarization moves the Shaker-IR channel through many of its closed transitions and pushes it closer to the open state. For example, if Shaker-IR was initially at closed state 1 (C1), depolarization (below the foot of the G-V curve) might put Shaker-IR at C3 state. With mechanical stimulation, membrane tension may bias the free energy difference between these transitions and shift the occupancy of these states closer (e.g., Cn-1) to an open state (ON). However, at voltages far below the foot of the G-V curve, this might still be insufficient since P_{open} is undetectably low and channel shows no mechanical responses. Whereas at the foot of the G-V curve, depolarizing voltages might have changed the equilibrium so that the average occupancy of the Cn state is much higher (higher P_{open}). Under this condition, suction would be sufficient to lower the relative level of energy wells, and the channel would tend to open, resulting in stretch-activation.

III. Stretch-activation of Shaker-IR is not due to an increased membrane area

If suction draws more channel-containing membrane into the patch, then the total channel number in the patch and hence the current amplitude would be increased. For example, if the amount of channel bearing membrane, and hence the number of channels doubled by suction, the fold increase of I_{Sh} after suction for step 1 and step 2 would both be doubled. Hence, increasing the membrane area should produce a proportionate change at two adjacent voltages. Since the results in this study (e.g., **Fig. 4-5**) showed that suction induced disproportionate fold-increase at the two adjacent voltages, the stretch-activation of Shaker-IR is not due to an increase in membrane area (more evidence to exclude this artifact can be found in **Chapter 5**).

IV. Half-maximum activation curve depends on how a curve is fitted

Ideally, P_{open} /pressure activation curves can be fitted to a Boltzmann function under the following conditions: 1) the number of channels in the patch is known; 2) the data show convincing saturation at high pressures; and 3) the channel has 0 activity at 0 stimulus and is activated to P_{open} of N at maximal stimuli (N is a known channel number in the patch). From the Boltzmann fitting, four parameters can be extracted if the above three criteria are met: slope factor, half-maximum P_{open} pressure, minimum and maximum P_{open}. The first two parameters (plus measurements of patch curvature during applied pressure) are needed for characterization of the stretch-sensitivity of a given MS channel. These two parameters can be accurately estimated if the other two parameters are fixed, the minimum and maximum P_{open}.

Without an accurate knowledge of the total channel number in the patch, the maximum P_{open} is unknown. Even if Shaker-IR channel activity continues to increase with changing pressure until the patch breaks, the maximum P_{open} is not necessarily known. At the best, we might be able to know it for one voltage (i.e., the holding potential). Moreover, the number of channels in one patch is not necessarily the same as the number of stretch-activatable Shaker-IR channels in the patch. The presence of Gd^{3+} exacerbated the problem since the effective V_m was not necessarily the same as the nominal V_m. The maximum P_{open}, therefore, can only be crudely underestimated by the overlapping events at the highest suction before membrane rupture.

To illustrate that it is important not to trivialize these difficulties, one data set (P_{open} /pressure activation curve from **Fig. 4-8**) was constrained to the lower (0) and/or upper bound (maximum P_{open}). Two constrained values for maximum P_{open} were used: 1 (the ideal, with all channels continuously in the open state) and 0.8 x N (according to Zagotta et al. (1994a), P_{open} for Shaker-IR saturating at ~0.8 above +30 mV). To take into consideration that data were from a multi-channel

patch (e.g., 4 channels), the maximum P_{open} were constrained to 4 and 3.2 (1 and 0.8, multiplied by 4). In addition, the minimum P_{open} of the curve was also forced to the observed value of the pre-stretch P_{open} for the given patch.

The resulting fits (not shown) suggest that both the slope factor and half-maximum P_{open} varied depending on how the constraint values are given. For these reasons, P_{open} /pressure activation curves shown in **Fig. 4-8** were not constrained to a minimum P_{open} of zero (all channels in the closed states) or a maximum of P_{open} (all channels are at the open states). Each data set was normalized to its largest P_{open} and fitted by Boltzmann function. Although the Boltzmann fitting of our P_{open} / pressure data (**Fig. 4-8**) were in a sigmoid-like shape, the fitting should be considered not much more than a "fit-by-eye". However, the fitting demonstrated a good dose-response relationship, and the P_{open} rose steeply with the increase of pressure above each patch's threshold, even though it would be inappropriate to extract the main parameters from the curves.

V. Gd^{3+} shifted the G-V curves of Shaker-IR

A. General considerations

Gd^{3+} at 10 μM completely blocks the endogenous SA non-selective cation channels in oocytes (Yang and Sachs, 1989) but does not block snail neuron SA K^+ channels at 100 μM (Small and Morris, 1995). Since the main purpose of this thesis was to study the mechanosensitivity of Shaker-IR K^+ channels, an even higher Gd^{3+} concentration (1 mM) was initially used but then had to be reduced to 100 μM Gd^{3+} because of the difficulties in obtaining a seal with 1 mM Gd^{3+} in the pipette. The possible explanation for this difficulty could be from the precipitation of Gd^{3+} at the pipette tip. In addition, numerous experiments with or without Gd^{3+} on both control and Shaker-IR-

expressed oocytes showed that 100 μM Gd^{3+} should be sufficient to block the endogenous MS cation channels over the voltage range between -60 mV and +40 mV in patch-clamp recordings.

B. Variations of V_{50} from patch to patch

In patch clamp studies, a larger variation in V_{50} measurements was seen which was in contrast to that seen in TEVC. This difference may be due to the accuracy of making up the Gd^{3+} solutions. A relatively larger volume of bath solution (>200 ml) was required each day for TEVC and 100 μM Gd^{3+} could be accurately obtained. Whereas in excised patch-clamp recordings, only small quantities of Gd^{3+} are required in the pipette solution. Because of its hygroscopic property, Gd^{3+} was extremely difficult to accurately measure (i.e. 0.372 g $GdCl_3.6\ H_2O$ in order to make a 5 ml 100 μM Gd^{3+} solution). To increase accuracy, a 200 μM Gd^{3+} solution (10 ml) was made and an equal volume of pipette solution was added to make the dilution. Although this volume was more than required, it may reduce the likelihood of differing Gd^{3+} concentrations. Gd^{3+} was made fresh each day since Gd^{3+} is unstable and easily forms precipitates in solutions (Caldwell et al., 1998). However, this may have added to the day-to-day variations in the actual Gd^{3+} concentration. Moreover, since pipettes need to be changed frequently in patch-clamp experiments, it is inevitable that the actual pipette Gd^{3+} concentration varies from batch to batch solutions or from time to time in the same pipette due to Gd^{3+} precipitation. Even with the same concentration of Gd^{3+}, its effects could also vary from oocyte to oocyte if different amounts of glycoproteins on the surface of different oocytes, which may respond differently to the same concentration of Gd^{3+}.

Because Gd^{3+}-induced shifts are concentration dependent (Elinder and Århem, 1994a) and because of the variable Gd^{3+} concentrations, the location of the G-V curve may vary considerably from patch to patch. The unavoidable variations in pipette Gd^{3+} concentrations probably increased

the between-patch variations of V_{50} for Shaker-IR channels. For this reason, the foot of the G-V curve was defined for each patch by running a series of voltage steps.

C. Discrepancy in V_{50} measurements

A discrepancy of 15 mV in the V_{50} measurements was found between excised patch clamp (+19 mV; **Appendix**) and TEVC recordings (+4 mV; **Chapter 3**) in the presence of Gd^{3+}. Two possible explanations for this discrepancy are discussed below.

There were several differences between excised patch clamp and TEVC recordings. One is that for patch clamp recordings, the vitelline membrane of the oocyte was removed to obtain a smooth surface in order to obtain gigaohm seals. In contrast, the vitelline membrane was left intact for TEVC recordings. To block endogenous SA channels and exert its effects on expressed Shaker-IR channels, Gd^{3+} has to pass the vitelline membrane and act directly on the oocyte surface or on the channel proteins. Since the vitelline membrane has high permeability to many molecules, including large molecules and La^{3+} (Steffensen et al., 1991), permeation to Gd^{3+} is also feasible. Based simply on this argument, it is unlikely that Gd^{3+} would have a different impact on "naked" or devitellinized oocytes than on intact oocytes. However, vitelline membrane proteins may sterically and/or electrostatically protect some surface charge from Gd^{3+}.

A second difference between the two recording configurations is that Ca^{2+} was excluded from the pipette solutions in inside-out patches because it caused baseline instability of the current recording. Conversely, Ca^{2+} (1.8 mM) was included in the bath solutions in TEVC recordings. Since both Ca^{2+} and Gd^{3+} have been shown to shift the voltage-dependent activation curve by shielding surface charges (see **Chapter 3**), this shielding effect by 100 μM Gd^{3+} may be altered by the presence of 1.8 mM Ca^{2+} in a competition-like manner. Since the concentration of Gd^{3+} used was

approximately 20 times smaller than that of Ca^{2+}, the shielding effect may be predominantly from Ca^{2+} in TEVC recordings. Since the shielding effects are dependent on charge density, the trivalent Gd^{3+} alone may produce a greater shift in the G-V curve than when there is an abundance of a divalent Ca^{2+} to "compete". There may, for example, be "sites" near Shaker S4 where such competition might be expected.

CHAPTER 5

Stretch-activation and stretch-inactivation of Shaker-IR

INTRODUCTION

I. Overview

MS (mechanosensitive) channels have been classified into two types, stretch-activated (SA) and stretch-inactivated (SI) channels, depending on their responses to mechanical stimulation (Morris, 1990). Although there are numerous examples of SA channels (i.e., channels that exhibit an increased open probability (P_{open}) during mechanical stimulation)), a few MS channels show the opposite effect, stretch-inactivation (i.e., decreased P_{open} when patched membrane is mechanically stimulated).

II. SI channels coexist with SA channels

SI channels were first identified in snail neurons where they coexist with SA channels (both types are K^+-selective) and can be detected electrophysiologically in the same patch (Morris and Sigurdson, 1989). For reasons which are not understood, the SI K^+ channels are only sporadically present whereas most patches exhibit SA K^+ channels. In single-channel recordings, suction not only increased P_{open} of the ubiquitous SA channels but simultaneously reduced the P_{open} of the SI channels. This was, therefore, not only the first evidence for SI channels, but also the first indication that channels with reciprocal responses to mechanical tension can be obtained from channels

experiencing the same stimulus within the same patch.

Spontaneous SI K^+ channel currents are evident in the absence of applied suction and "disappear" when suction is applied. After releasing the suction applied to the patch pipette, the P_{open} of the SI channels is restored to high levels. Apart from having opposite mechanical response during suction, the SI K^+ and SA K^+ channels can be distinguished from each other on the basis of conductance level (SI channels have a several fold smaller conductance) and sensitivity to quinidine, suggesting that SI channels are a distinct K^+ channel type from that of the SA K^+ channels. Like SA K^+ channels, suction does not affect the single SI channel current amplitude. The open time of SI K^+ channels is insensitive to membrane tension. Rather, the stretch-dependent decrease in the SI channel P_{open} is due to a tension-induced decrease in the rate of leaving a closed state (longer closed time). Interestingly, this kinetic profile is comparable to that of the SA cation channels first reported by Guharay and Sachs (1984): membrane stretch acts to shorten a closed time rather than increasing an open time.

As mentioned in **Chapter 1**, most MS channels are activated by membrane tension, induced by either positive or negative pressures. When examined over a broad range of pressures (from negative to positive), the SI channels show a bell-shaped P_{open} versus pressure activation curve centred around zero applied pressure (Morris and Sigurdson, 1989). The explanation is that tension increases whether the membrane is stretched in a concave or convex orientation. This type of activation curve can be considered as a characteristic profile for SI channels, similar to U-shaped activation curve for SA channels.

III. SI channels in dystrophic muscles

Shortly after the first report of SI channels in snail neurons (Morris and Sigurdson, 1989), SI channel behaviour was described in dystrophic myotubes (Franco and Lansman, 1990). This study generated interest because this SI channel may play a role in the pathophysiological process of muscular dystrophy. Immunochemical studies have shown that dystrophin is present in normal muscle but is absent from muscular dystrophy patients (Arahata et al., 1988). Based on the speculation that dystrophin binds to channels (Campbell and Kahl, 1989), it has been proposed that the presence of dystrophin provides a counter force to changes of resting membrane tension. The absence of dystrophin may alter the resting membrane tension so that some MS channels are in the open state (Franco and Landsman, 1990). Since spontaneous MS cation channel activity is higher in dystrophic myotubes, it was suggested that dystrophin, a cytoskeletal protein associated with muscle membrane, may have a role in regulating the activity of MS channels in skeletal myotube membrane. SA channels were observed in 42% of the patches on normal myotubes and 19% of the patches on dystrophic myotubes. By contrast, high spontaneous activity SI channels were observed in 2% of the normal myotube patches and 21% on dystrophic myotube patches. Thus, there is a greater proportion of SI channels in dystrophic myotubes than in normal myotubes.

For SI channels in dystrophic myotubes, -20 mmHg suction reduces the spontaneous P_{open} by more than half (from 0.3 to 0.1) and -40 mmHg suction virtually abolishes channel activity (P_{open} reduced to 0.004). A subsequent study (Franco-Obregón and Landsman, 1994) confirmed that channels with a higher spontaneous P_{open} have a tendency to show stretch-inactivation in dystrophic myotubes, whereas the same channel type with lower spontaneous P_{open} has a tendency to show stretch-activation in normal myotubes. This observation seems to suggest that the spontaneous P_{open}

prior to mechanical stimulation may play a role in the stretch-sensitivity.

IV. SI cation channels in osmosensory neurons may be mechanotransducer (MT) channels

SI channels raised interest again as Oliet and Bourque (1993) reported that a SI cation channel in mammalian hypothalamic osmosensory neurons was a good candidate for mediating the osmotransducer currents in both single-channel and whole-cell current recordings (Oliet and Bourque, 1993; reviewed in Bourque and Oliet, 1997). In whole-cell current clamp recordings obtained from isolated hypothalamic osmosensory neurons, cell shrinkage (a hypertonic perfusion at +30 mOsm) provokes a reversible depolarization and an increased action potential frequency. Such activity causes release of vasopressin from osmosensory neurons of the supraoptic and paraventricular nuclei. In contrast, increasing cell volume by a hypotonic perfusion (-30 mOsm) induces the opposite effect; cell hyperpolarization and inhibition of action potential firing frequency. When negative pressure is applied to the inside of whole-cell pipettes to produce a decreased cell volume, a reversible depolarization and accelerated firing results, mimicking the hypertonic perfusion effect. For whole-cell recordings, hyperosmotic perfusion increases the overall channel activity, as does applying suction through the recording pipette. Cell-attached patch clamp recordings show that the MS channels have a V_{rev} at about -40 mV and a slope conductance of 32 pS. These channels discriminate poorly between monovalent cations and seem to be inhibited by both positive or negative pipette pressures. This latter property led the authors to categorize the MS channels as SI channels. Overall, the picture is that these supraoptic channels are sensitive to cell volume at the

whole-cell level and changes in membrane tension associated with osmotically evoked volume changes modulate their activity in a manner that makes the SI cation channels the likely basis for cellular osmosensitivity. This constitutes the first report that MS activity can be followed from the single-channel level all the way to the whole-cell level in a physiologically relevant context (reviewed in Bourque and Oliet, 1997).

V. Molecularly identified SI channel

Although different SI channels are found in snail and mammalian neurons as well as in mammalian muscle cells, the molecular nature of all these SI channels remains unknown. Recently, however, a molecularly identified mammalian K^+ channel, G-protein gated inward rectifying K^+ channel (GIRK, see **Table 1-1**, also known as K_{ACh} because it is activated via acetycholine) has been shown to exhibit stretch-inactivation after expression in *Xenopus* oocytes (Ji et al., 1998). Cardiac muscarinic K_{ACh} channels regulated by $G_{\beta\gamma}$ are preferentially expressed in atrial tissues. They are heterotetramers (Krapivinsky et al., 1995). Using the two-electrode voltage clamp (TEVC) technique, Ji et al. (1998) found that expressed heterotetrametic Kir3.1/3.4 (GIRK) channels and homotetrameric Kir.3.4 channels are rapidly and reversibly inhibited by a 50% hypo-osmolar stress. The effect is comparable in magnitude to that of mechanical stimulation of the native K_{ACh}: after potentiating the whole-cell rabbit atrial myocyte K_{ACh} currents with carbachol, a large positive pipette pressure (10 cmH_2O) causes a reversible decrease (15%) in the carbacol-sensitive K_{ACh} currents (Ji et al., 1998). Interestingly, in a different experimental condition, a similar K_{ACh} channel from rat heart has been shown to exhibit stretch-activation, so that application of negative pressure (cell-attached and inside-out excised patches) increases the channel activity (Pleumsaran and Kim, 1995).

This raises the possibility that the same channel type can be both SA and SI, echoing the finding in dystrophic muscles (Franco-Obregón and Lansman, 1994).

RATIONALE

Because we began seeing evidence of stretch-activation in Shaker-IR, it was important to explore the phenomenon in more detail. It was already known that different K^+ channels could show stretch-activation and stretch-inactivation in the same patch (Morris and Sigurdson, 1989). It was also apparent that the same cation channel type (molecular identity unknown) could show either stretch-activation or stretch-inactivation in different muscle cell variants (Franco and Lansman, 1990) and that GIRK variants in different cell types could exhibit either stretch-activation or stretch-inactivation under different experimental conditions (Ji et al., 1998; Pleumsaran and Kim, 1995). Shaker-IR allowed us to ask if a given population of channels in the patch could show both responses to mechanical stimuli. Specifically, we hypothesize that stretch-activation dominates when pre-stretch P_{open} is low and that stretch-inactivation dominates when pre-stretch P_{open} is high.

METHODS

Stage V-VI *Xenopus* oocytes were prepared and injected with Shaker-IR cRNA as described in **Chapter 2**. Immediately before patching, oocytes were devitellinated and fire-polished pipettes were prepared and used for either cell-attached or excised patches. The cell membrane was stretched by either negative (suction) or positive (blowing) pressures through the side port of the recording

pipette. For detailed procedures of patch clamp recordings and for solutions used, see **Chapter 2**.

RESULTS

I. Stretch-activation and -inactivation of Shaker-IR at the macroscopic level

A. Voltage-dependent mechanical effects on Shaker-IR

As described in **Chapter 4**, stretch-activation is evident near the foot of the G-V curve. To test the hypothesis that the net effect of mechanical stimulation on Shaker-IR current (I_{Sh}) depends on its pre-stretch P_{open}, the effects of mechanical stimulation were tested at various membrane potentials from the foot to the top of the G-V curve.

As a preliminary procedure, a series of voltage steps was applied to each patch to establish the voltages corresponding to the foot and top of the G-V curve. In a given patch, the steady-state I_{Sh} was then elicited by a depolarizing voltage near the foot or top, then the patch was subjected to mechanical stimulation. In order to determine the repeatability of any mechanical effects, two suction pulses were applied during a 10 s depolarizing voltage step. This is termed the "voltage-tension protocol".

Both inside-out excised and cell-attached patch configurations were used. For both configurations, stretch-activation and -inactivation were found to occur in the same patched membrane with -10 to -20 mmHg suction. This is illustrated for an excised patch (**Fig 5-1**) and for a cell-attached patch (**Fig. 5-2a**); note that for cell-attached patches, V_m is approximated assuming V_{rest} = -50 mV. At voltages nearer the foot of the G-V curve, suction reversibly induced an increased I_{Sh} (an outward deflection) whereas at voltages nearer the top of the G-V curve, suction caused a

Figure 5-1. Suction effects on I_{Sh} at various V_m by excised patch clamp

Excised patch clamp traces were recorded from a Shaker-IR-injected oocyte with Gd^{3+} in the pipette. V_m was varied as indicated. C-type inactivation occurred at large depolarizations (+40, +60 mV). The amplitude of steady-state current changed with the different V_m, as expected for voltage-dependent I_{Sh}. Solid bars below each trace indicate about -15 mmHg suction.

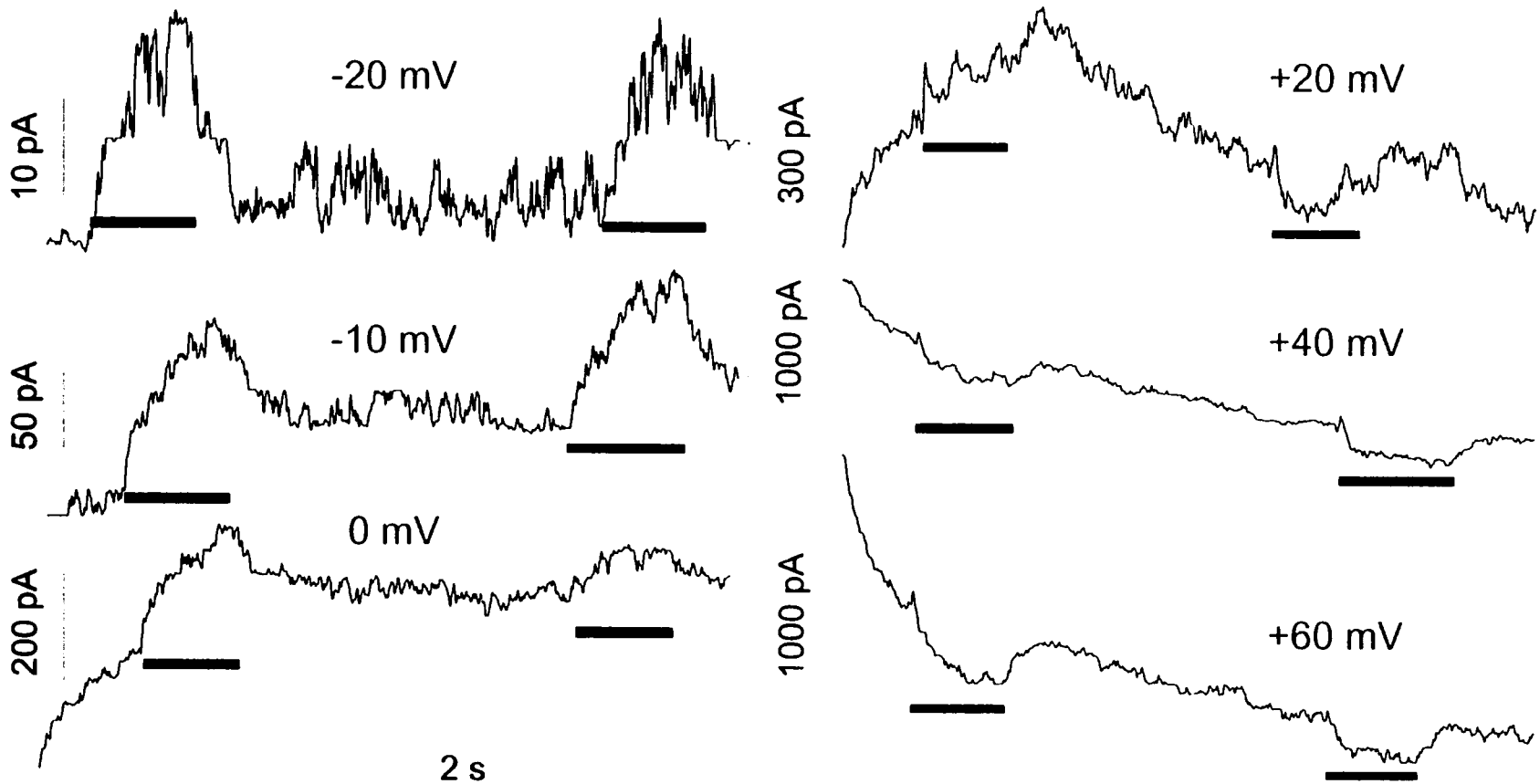
-20 mV
10 pA
-10 mV
50 pA
0 mV
200 pA
2 s
+20 mV
300 pA
+40 mV
1000 pA
+60 mV
1000 pA

decreased I_{Sh} (downward deflection). In the mid-region, there was no detectable response to suction (e.g. **Fig. 5-1**, +20 mV). Similar results were obtained in 11 other patches (6 cell-attached and 5 excised patches). Regardless of what mechanical effects were elicited by suction, the induced channel activity persisted during sustained suction and returned to baseline levels upon releasing of suction. Moreover, the effects were repeatable when suction was reapplied. The repeatability of the stretch-activation and -inactivation and the fact that such effects were not seen in control patches (i.e. non-Shaker-IR injected but with Gd^{3+} in the patch, same range of voltage and same mechanical stimuli applied in both cell-attached and excised patches; data not shown), indicates that the effects were not an artifact of the recording system during these prolonged depolarization and sustained suction. Rather, we attributed them to an altered Shaker-IR P_{open} in response to mechanical stimulation.

Although Shaker-IR (Δ6-46) had its inactivation ball removed from its N-terminus, when expressed in oocytes, it exhibited a slow C-type inactivation, a phenomenon especially evident at highly depolarized membrane potentials (see **Chapter 4** or Hoshi et al., 1994). For reasons we did not explore, the relative magnitude of C-type inactivation was variable among different oocytes. In the last two traces of **Fig. 5-1**, C-type inactivation was assumed to be responsible for the gradually decreasing I_{Sh} over the 10 s of the sustained depolarizing voltage pulse ($V_{m:}$ +40 and +60 mV, **Fig. 5-1**). As C-type inactivation can be used as a signature characteristic for Shaker-IR, the "drooping" currents, while "messy", are fully consistent with the interpretation that the stretch-sensitive currents are carried by Shaker-IR channels.

In summary, by stepping through the voltage range and then mechanically stimulating in these experiments, our results showed that Shaker-IR-injected oocytes exhibited a net stretch-

activation when pre-stretch P_{open} was low and a net stretch-inactivation when pre-stretch P_{open} was high. In contrast, while stepping through the same voltage range using patches from non-injected control oocytes (with Gd^{3+} in the pipette), mechanical stimuli did not elicit any detectable ionic currents even with larger pressures (> -40 mmHg) that sometimes ruptured the patches. These results suggest that Shaker-IR acts like a typical MS channel except that it can exhibit both stretch-activation and stretch-inactivation in a given patch. In the intermediate voltage range (P_{open} is about 0.5), it is simplest to assume that both processes were occurring at about the same frequency during stretch, thus yielding no net effect on the current. This possibility is particularly noteworthy because it is the first evidence, to our knowledge, that the same channel type can be both stretch-activated and -inactivated in the same patch.

B. Comparison of mechanical effects between Shaker-IR and endogenous MS channel

Since *Xenopus* oocytes contained endogenous non-selective cationic SA channels (Yang and Sachs, 1989; Ackerman et al., 1994), it was necessary to verify that the observations described above and ascribed to gating effects on Shaker-IR were not the "contamination current" from inadequately blocked endogenous *Xenopus* oocyte SA cation channels.

For this purpose, three types of control experiments were performed. First, non-injected oocytes were routinely (n = 3 per day) tested in the presence of 100 μM Gd^{3+}; there was no trace of ionic currents while stepping through the voltage range under the same experimental condition as those used for Shaker-IR-injected oocytes. Second, the depolarizing voltages used to study Shaker-IR were near the V_{rev} for the endogenous SA channels, this could also minimize the interference from SA cation channels. Third, the possibility of contamination from endogenous MS channels was further excluded by directly demonstrating that the endogenous MS currents from an non-injected

oocyte in the absence of Gd^{3+} could not explain the stretch effect in Shaker-IR patches in the presence of Gd^{3+}. This last point is illustrated in **Fig. 5-2b** where SA currents are shown (control oocytes in the absence of Gd^{3+}) over a voltage range similar to the SA and SI I_{Sh} (**Fig. 5-2a**). Re-iterating, Shaker-IR is a voltage-dependent channel, so depolarizing potentials elicited progressively larger steady-state I_{Sh}. At more hyperpolarized potentials where P_{open} was low (left panel), stretch increased I_{Sh} (stretch-activation) whereas at more depolarized potentials when P_{open} was high (right panel), stretch decreased I_{Sh} (stretch-inactivation). Both effects recovered rapidly upon releasing suction and reoccurred when the suction was re-applied. By comparison, for an non-injected oocyte (in the absence of Gd^{3+}), **Fig. 5-2b** shows only stretch-activation of the endogenous MS channels with -20 mmHg suction in response to a series of voltages from -30 mV to +20 mV. As the endogenous *Xenopus* MS channel is cation non-selective with a V_{rev} at about 0 mV, inward stretch-induced currents were observed at more hyperpolarized potentials ($< V_{rev}$) whereas stretch-induced outward currents were detected with more depolarized potentials ($>V_{rev}$).

With the direct comparison between current traces of Shaker-IR and the endogenous SA channel at each corresponding voltage, it is evident that the endogenous SA channel openings could not have been responsible for the mechanical effects on Shaker-IR for the following reasons. Because of their different V_{rev} (~ 0 mV vs ~ -80 mV), the current direction for SA channel and Shaker-IR was different at the corresponding voltages. Voltage-dependent I_{Sh} were exclusively in the outward direction at all test voltages ($V_m > E_K$, reversal potential for Shaker-IR) (**Fig. 5-2a**), whereas endogenous SA channel exhibited inward currents when $V_m < V_{rev}$ and outward currents when $V_m > V_{rev}$ (**Fig. 5-2b**).

More than ten patches for each case (with or without Gd^{3+} in the pipettes), were tested on

Figure 5-2. Suction effects on I_{Sh} and endogenous SA currents

(a) Cell-attached patch clamp current traces were recorded from a Shaker-IR injected oocyte at the indicated voltages. Simultaneous pressure recordings are shown below each current trace; downward deflection indicates a negative pressure (suction). C-type inactivation is evident in the last trace. **(b)** Endogenous MS cation currents were elicited by suction from an non-injected oocyte. Four current traces are shown at the indicated voltages. Suction of -20 mm Hg is indicated by bars located either above or below each current recording. Cell membrane potential (V_m) were calculated on the assumption of V_{rest} = -50 mV [from intracellular recordings, V_{rest} =-51 +/- 1.9 mV (SEM), n = 32]. Gd^{3+} was omitted from the pipette solution.

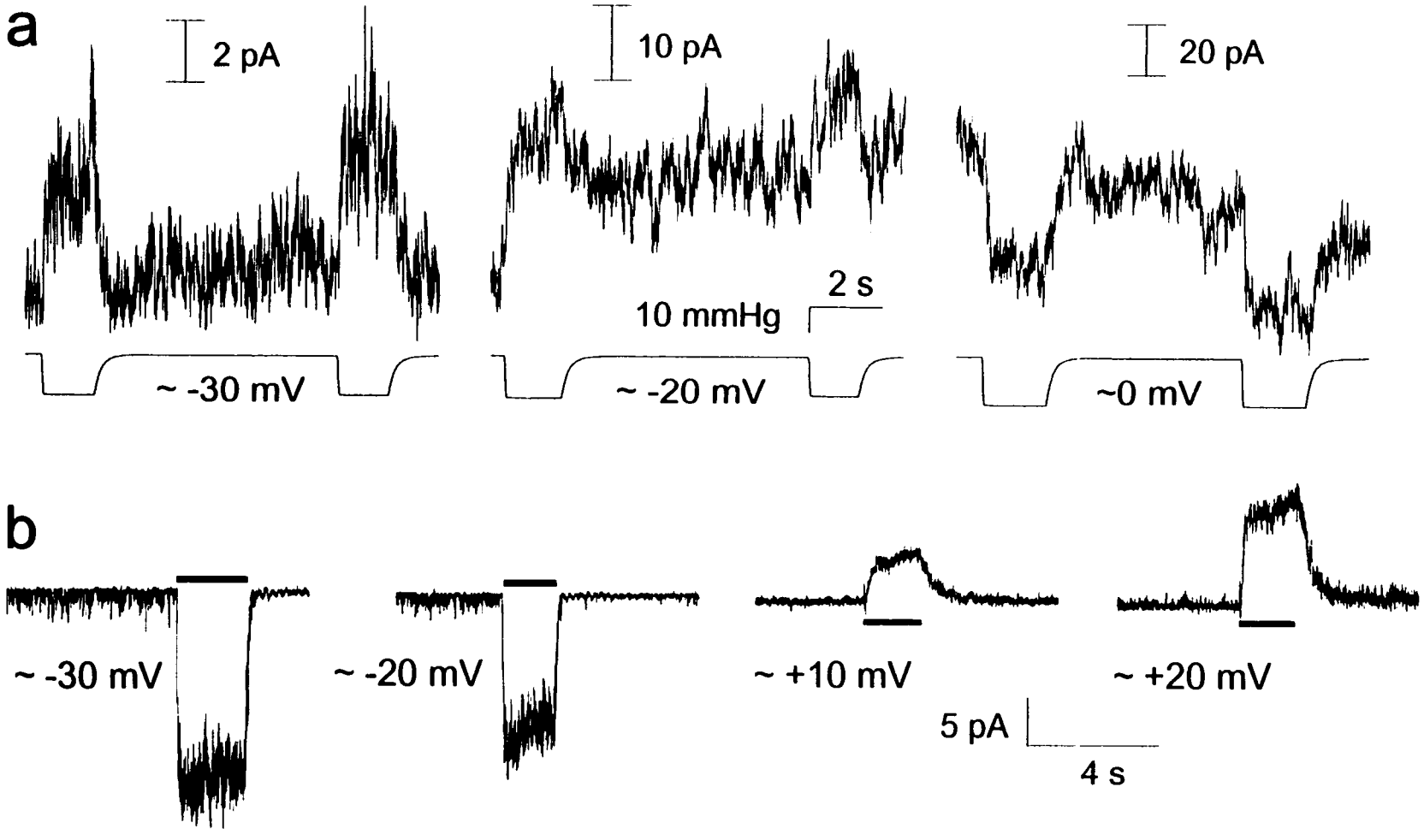
a
2 pA
10 pA
20 pA
2 s
10 mmHg
~ -30 mV
~ -20 mV
~0 mV
b
~ -30 mV
~ -20 mV
~ +10 mV
~ +20 mV
5 pA
4 s

non-injected oocytes using a voltage-tension protocol as in **Fig. 5-2b**. Patches with Gd^{3+} exhibited no currents and suction did not elicit any effect whereas for patches without Gd^{3+}, the endogenous SA currents were elicited at all test potentials. Thus, the apparent stretch-activation of Shaker-IR at more hyperpolarized potentials can not be explained by a contamination from the inward endogenous SA currents at the similar voltage range. Likewise, the sum of the two synchronous currents (outward SA cation current and outward Shaker-IR current) could not produce the decrease in current amplitude at more depolarized potentials, that we interpreted as stretch-inactivation. Therefore, the mechanical effects appeared to be truly gating effects on Shaker-IR, not contributions from the endogenous SA cation channels.

C. Tension-induced mechanical effects

Having excluded the possible contribution from the endogenous MS channels, it was then essential to examine the possibility that more channel-containing membrane was drawn up into the patch by suction and that this might be responsible for the increased channel activity of Shaker-IR. For this purpose, excised patches were used to eliminate a possible source of increased membrane area. In such a configuration, the patch was formed by stripping off a piece of sealed membrane from the cell. Additionally, the protocol was modified by the use of positive pressure (blowing) for the second mechanical stimulus, rather than a repeat of the suction as in **Fig. 5-1** and **Fig. 5-2a**. The rationale for using the blowing was three-fold: first, if mechanical effects on I_{Sh} were due to increasing the patch membrane area by suction, then blowing would produce an opposite effect. Second, it was unlikely that blowing would draw membrane deeper into the pipette causing an increased membrane area without breaking a seal. Third, by varying the membrane curvature of the patch using either suction or blowing, the experiment was designed to test the hypothesis that

mechanical effects were mediated by membrane tension rather than by the direction of membrane curvature.

Control oocytes were first tested on a daily basis using a similar approach as described in **Fig. 5-2b** but solely on excised patches. Neither suction nor blowing yielded any trace of ionic current when 100 μM Gd^{3+} was present in the pipette solution. The excised patches were very fragile and many were lost during suction. Thus, less than -20 mmHg suction was generally used for excised patches. However, to make sure that there was a complete blockage of endogenous MS currents by 100 μM Gd^{3+} and that no "breakthrough" of these currents could occur during mechanical stimulation, even higher pressures (> 40 mmHg) were used. This often broke the patch and yet prior to rupture, there were still no signs of ionic currents. In contrast, on Shaker-IR-injected oocytes, suction and blowing elicited qualitatively the same response on the steady-state I_{Sh} at any given voltage in a given patch, regardless of the membrane curvature.

Data from two representative patches are shown in **Fig. 5-3**. Here, suction induced stretch-activation at a more hyperpolarized potential (**Fig. 5-3a**) while stretch-inactivation was induced at a more depolarized membrane potential (**Fig. 5-3b**). Both these effects were also elicited by applying a positive pressure to the same extent. As expected, the stretch-induced changes in I_{Sh} terminated with the release of pressure; the current returned rapidly toward the original current level (**Fig. 5-3**). Comparable results were found in 8 patches recorded under the same experimental conditions.

As suction would produce a convex curvature of the membrane whereas blowing would produce a concave curvature, these results suggest that Shaker-IR is not sensitive to the direction of membrane curvature, and the effects on I_{Sh} upon application of both positive and negative pressure are due to elevated in-plane tension from a patch's convexity or concavity. Moreover, the stretch

Figure 5-3. Suction and blowing produce the same effects at given voltages

The effects of both suction and blowing on I_{Sh} from two excised patches of Shaker-IR injected oocytes are shown. Two current traces were elicited by the indicated voltages. The simultaneous recordings of the pressure traces are shown below each current trace. The downward deflection represents a negative pressure (suction) whereas a upward deflection represents a positive pressure (blowing). C-type inactivation is shown in the right panel.

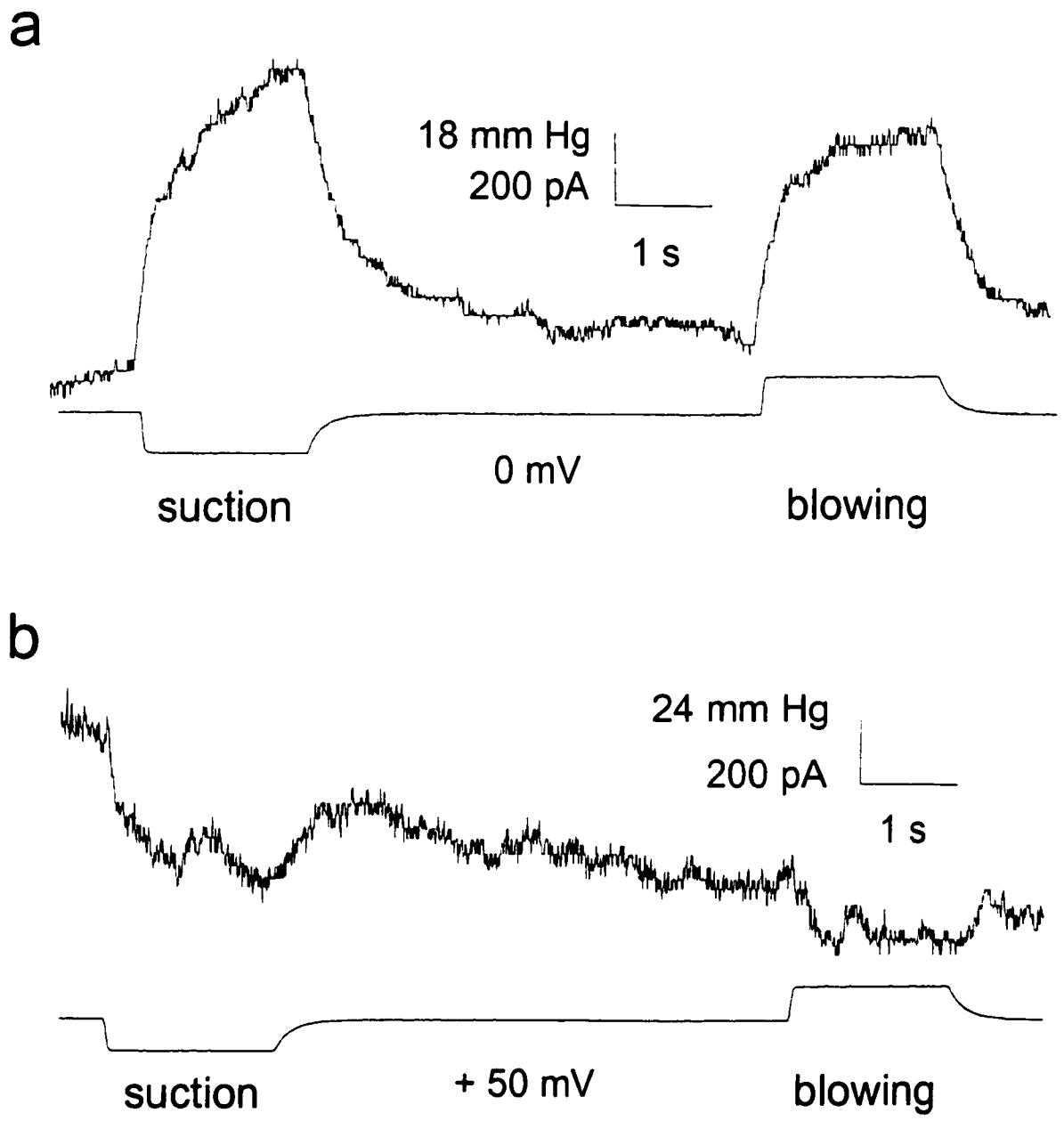
a
18 mm Hg
200 pA
1 s
0 mV
suction
blowing
b
24 mm Hg
200 pA
1 s
suction
+ 50 mV
blowing

blowing and suction produced the same mechanical effects and because stretch could also induce inactivation. For an excised patch, it is hard to imagine that blowing could increase the area of channel-bearing membrane (yielding increased I_{Sh} amplitudes). Also, if the total number of Shaker-IR channels in the patch increased, one would not expect to obtain a decreased I_{Sh}. Taken together, these results support the concept that mechanical effects on I_{Sh} are mediated by changes in membrane tension, and do not arise from changes in the channel number or patch area.

D. Pressure-dependence of stretch-activation and -inactivation

While the mechanosensitivity of Shaker-IR shown in **Figs. 5-1, 2, 3** represents its net responses to a pressure step of a single magnitude, it is important to test further whether, as hypothesized, the two opposite mechanical effects, stretch-activation and stretch-inactivation, were being induced simultaneously during the same mechanical stimulation (although to different extents except where there is no net effect). In addition, because an unknown amount of residual tension may exist following seal formation (Morris and Sigurdson, 1989), application of a single pressure step might either increase or, decrease the net pressure on the patch by opposing this residual value. For this technical reason, it was also essential to know whether the opposite mechanical effects (i.e., stretch-activation and stretch-inactivation) were induced with a series of different pressure steps. The pressure dose-response experiments were done using a pair of extreme voltages, i.e. near the foot and the top of the G-V curve. This contrasts with the earlier use of two adjacent (10 mV apart) voltages, here the two test voltages differed by 60 mV. In addition, also different from the step pairs protocol of **Chapter 4**, the voltages were not repeated for fear of losing the patch as tension increased. Results are shown in **Fig. 5-4** (n = 3). The between patch variations in absolute current amplitude reflect different levels of channel expression in patches from different oocytes. In each

Figure 5-4. Pressure dose-responses by extreme step pairs

Data were obtained from three excised patches at the indicated voltages (+60 mV apart). Steady-state I_{Sh} elicited by these voltage pairs was measured and plotted as a function of negative pressures applied. ■: I_{Sh} from step 1. □: I_{Sh} from step 2.

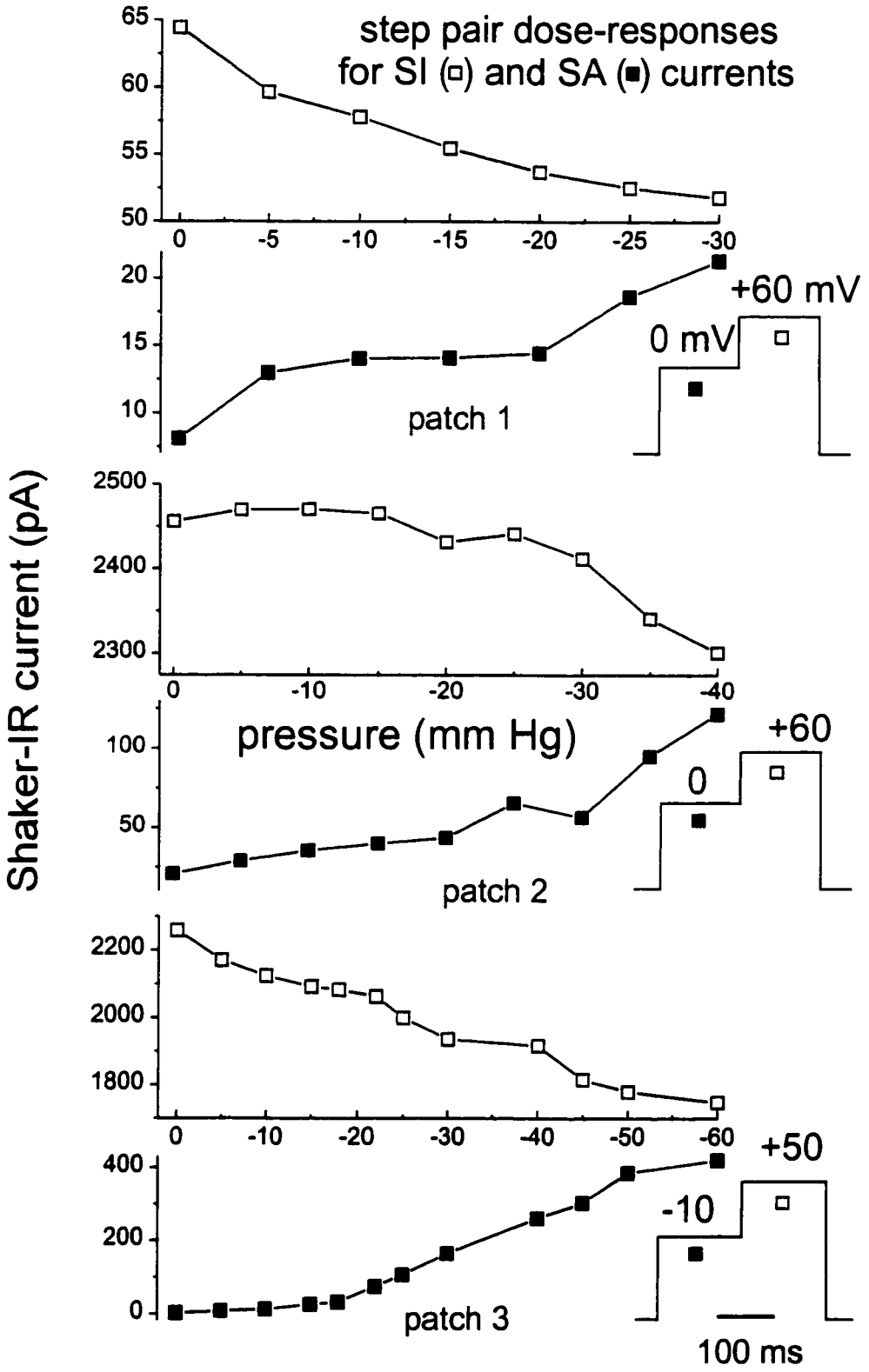
step pair dose-responses
for SI (□) and SA (■) currents
Shaker-IR current (pA)
65
60
55
50
0
-5
-10
-15
-20
-25
-30
20
15
10
+60 mV
0 mV
patch 1
2500
2400
2300
0
-10
-20
-30
-40
pressure (mm Hg)
100
50
+60
0
patch 2
2200
2000
1800
0
-10
-20
-30
-40
-50
-60
400
200
0
+50
-10
patch 3
100 ms

patch, however, the same mechanical stimuli that increased I_{Sh} (stretch-activation) for low pre-stretch P_{open} (step 1) also decreased I_{Sh} (stretch-inactivation) for high pre-stretch P_{open} (step 2), and both effects were dependent on the amount of suction applied to the patch, in a pressure-dependent manner.

Thus, we observed that stretch-activation and -inactivation could both be induced by the same mechanical stimulus. This was true for a set of suction pressures that would have far exceeded any inadvertent residual positive pressures that may have existed in the pipette. Evidently, a given mechanical stimulus does not have the same effect on every channel in the patch. This result therefore suggests that the mechanical environment of channels is not homogeneous for the entire population in a patch. This finding also essentially eliminates the possibility that the patched membrane area transiently increased during suction. This argument is supported by the finite membrane area in excised patches and the reversible changes of I_{Sh} by either suction or blowing. Presumably, the membrane containing Shaker-IR channels was stretched by the mechanical stimuli and an inhomogeneous tension exerted forces on the channels, which interfered with their voltage-dependent gating.

II. Stretch-inactivation in a multichannel patch

If macroscopic currents could be SI, the phenomenon should be demonstratable at the single-channel level. The main factors for achieving the desired recording levels (e.g., macropatch or single patch) were the channel density of expressed Shaker-IR and the patch size. If decreasing I_{Sh} was due to suction-induced closure of channels, then, in a patch with, say 10-20 channels active at large depolarization (i.e., a patch with a "small" macroscopic current level), it may be possible to stretch-

inactivate enough of the channels, that those remaining active are discernible at the single-channel level. In other words, it should be possible to observe a suction-induced recording-level switch from "macro" to "single-channel" current. To make such a demonstration, a pipette size normally for macro-patch recording was used. Macroscopic I_{Sh} was recorded at a relatively depolarized potential on an excised patch, then suction was applied. **Fig. 5-5** shows that suction reversibly inactivated most of the I_{Sh}. As shown, the macroscopic I_{Sh} elicited by a depolarizing voltage (V_m = + 20 mV) was sharply attenuated when -20 mmHg suction was applied for approximately 10 s. At most, only one channel was active at a time during the portion of the record shown, yielding ideally single-channel data with unitary current level. Upon releasing suction, the I_{Sh} recovered gradually and eventually approached the original macroscopic current amplitudes, indicating that the number of channels are the same within the patch before and after mechanical stimulation. The suction-induced change was due to decreased P_{open}, yielding a reduced number of channels simultaneously in the open state. The full relaxation to the initial (0 mmHg) level of channel activity required a time on the order of seconds (**Fig. 5-5**). The rapid switch from multiple to single-channel recording strongly suggests that the suction-induced change in P_{open} also accounts for the stretch-inactivation observed on strictly macroscopic recordings. Compared to **Fig. 4-2c** of **Chapter 4** which showed a single to multiple openings by suction (V_m at ~-20 mV), this opposite effect was seen at a more depolarized potential (V_m at +20 mV), consistent with the idea that stretch-induced effects on Shaker-IR are pre-stretch P_{open} dependent.

III. Stretch-inactivation of Shaker-IR at the single-channel level

A. Stretch-inactivation coexists with stretch-activation in the same patch

Figure 5-5. Reversible macroscopic to single I_{Sh} by suction

I_{Sh} from an excised patch before, during and after suction, reveals an abrupt I_{Sh} change from macroscopic (multichannel) to single channel. The solid bar at the bottom indicates applied suction (trace interrupted for ~10 s). V_m is as indicated.

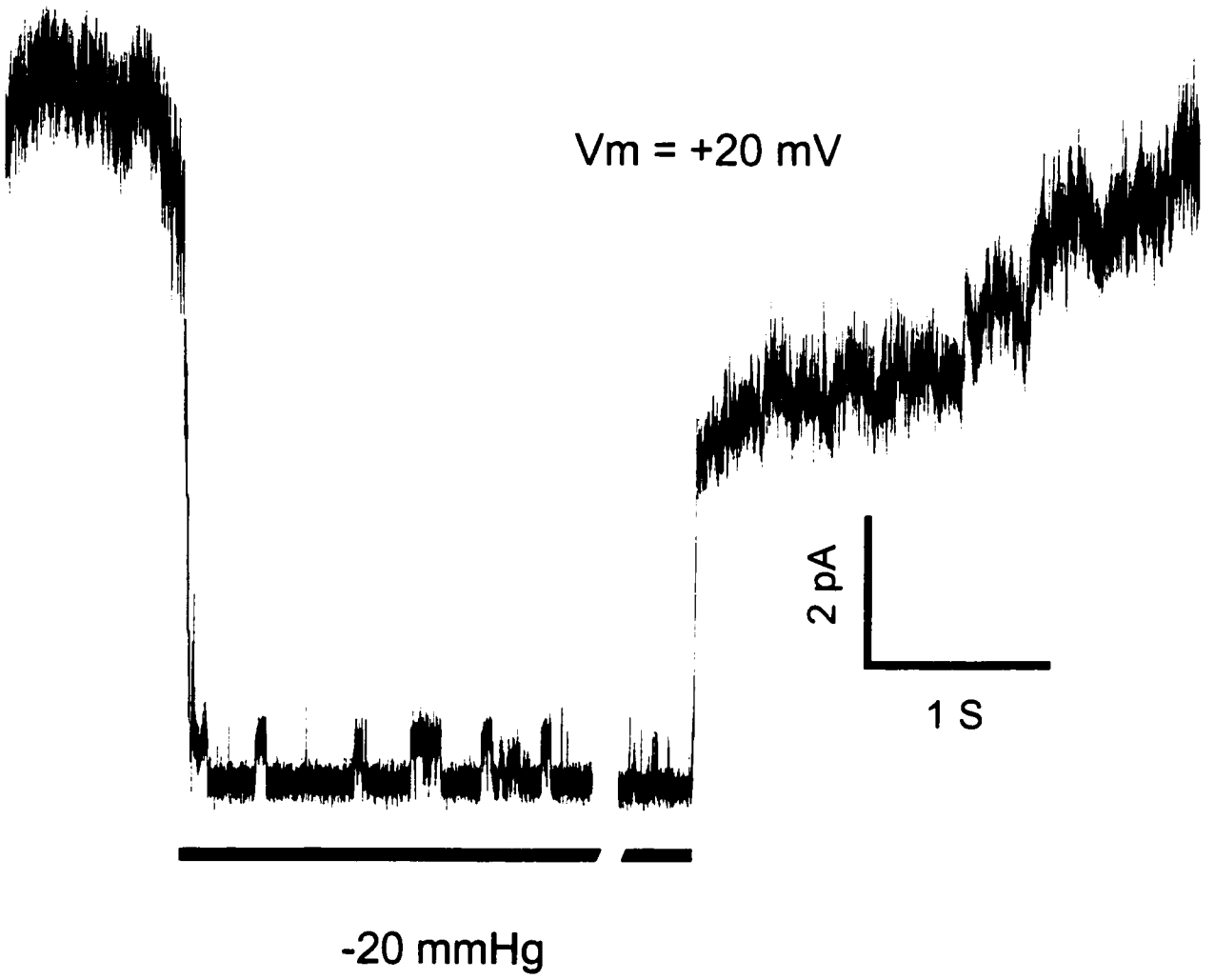
Vm = +20 mV
2 pA
1 S
-20 mmHg

If the above interpretation of the macroscopic effects is correct, the two opposite mechanical effects of Shaker-IR should be detectable within a given patch at single-channel recordings. Single-channel recordings of steady-state I_{Sh} were performed on excised patches at two widely-spaced voltages, one at the foot and one at the top of the G-V curve. First the patch was stepped to the voltages at the foot of the G-V and the elicited I_{Sh} was measured, then the patch was subjected to a series of increasing negative pressures. After this, the same patch was stepped to the second voltages at the top of the G-V, I_{Sh} was measured and the patch was subjected to the same range of pressures.

There were difficulties in maintaining these excised patches while applying long-duration suctions. Only one patch survived such treatment and showed both stretch-activation and stretch-inactivation whereas most patches either lost their seal or became very leaky after repeated mechanical stimulations. Consistent with the observations at the macroscopic level, suction induced not only stretch-activation but also stretch-inactivation in the same patch and both were evident at the single-channel level. **Fig. 5-6** shows single-channel recordings from this patch recorded at two potentials 30 mV apart. As shown, a series of increasing negative pressures from 0 to -50 mmHg diminished the Shaker-IR P_{open} at V_m = +20 mV while augmenting it at V_m = -10 mV. For simplicity, only two current traces at 0 and -50 mmHg are shown at V_m = -10 mV (**Fig. 5-6a**). It is striking to compare the 0 mmHg I_{Sh} traces for +20 and -10 mV as those traces represent obvious differences in pre-stretch P_{open}. Similar differences are also seen for the -50 mmHg I_{Sh} traces for these same two voltages. The opposite response to suction within a given patch demonstrated that Shaker-IR channels could be either SA or SI, depending upon the pre-stretch P_{open} of the channel. Together with results from other patches in which either stretch-activation at low V_m (e.g. **Fig. 4-8**) or stretch-inactivation at high V_m was recorded (see below), these data make it evident that at high pre-stretch

Figure 5-6. Suction effects on single I_{Sh} at two different V_m

(a) Segments of 5 s current trace from 20 s continuous recordings were collected in the sequence shown, on an excised patch. The patch was subjected to a series of suctions (as indicated) at V_m of +20 mV and then from 0 to -60 mmHg in 10 mmHg steps at V_m of -10 mV. For simplicity, only two current traces are displayed for V_m of -10 mV. **(b)** Stretch-activation and -inactivation pressure-response curves are shown from the above patch [V_m of +20 mV (▽) and V_m of -10 mV (▲)]. Normalized NP_{open} was plotted as a function of the applied suction, from 0 to -60 mmHg for ▲ and 0 to -50 mmHg for ▽.

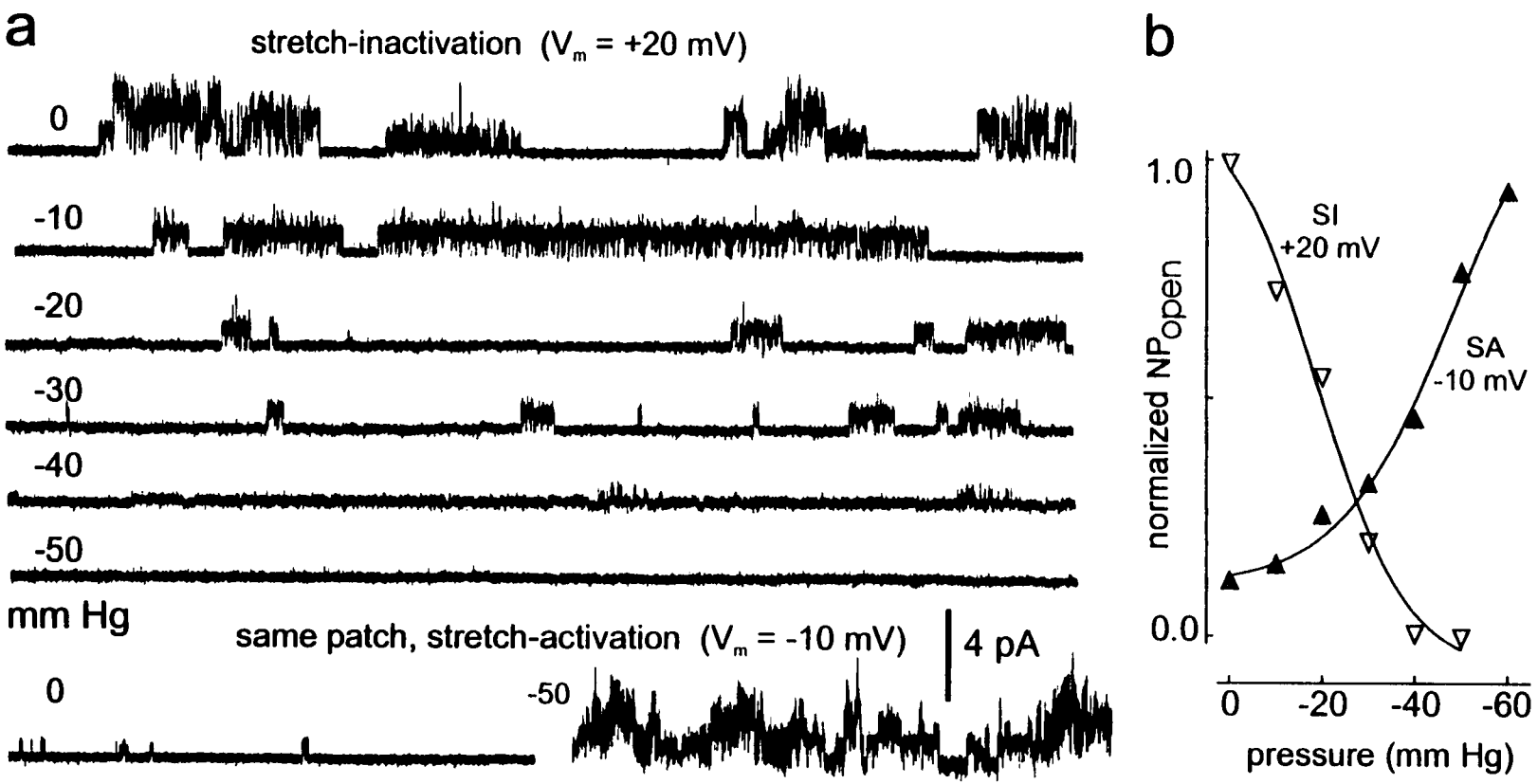
a
stretch-inactivation (V_m = +20 mV)
0
-10
-20
-30
-40
-50
mm Hg
same patch, stretch-activation (V_m = -10 mV)
4 pA
0
-50
b
1.0
0.0
normalized NP_{open}
SI
+20 mV
SA
-10 mV
0
-20
-40
-60
pressure (mm Hg)

P_{open}, channels tended to exhibit stretch-inactivation, whereas at low pre-stretch P_{open}, channels tended to exhibit stretch-activation.

As expected for a typical MS channel, the stretch-inactivation of Shaker-IR also exhibited a non-linear (Boltzmann-like) pressure-dependence. **Fig. 5-6b** is a normalized P_{open} plotted as a function of applied suction using the same data set as in **Fig. 5-6a**. It shows that the P_{open} of the same Shaker-IR channels in a given patch can have opposing responses to mechanical stimulation. In other words, suction can either increase P_{open} (stretch-activation:▲) or decrease P_{open} (stretch-inactivation: ▽) in a pressure-dependent manner (**Fig. 5-6b**), depending on whether channels are mostly quiescent or mostly active prior to stimulation. This phenomenon is consistent with our interpretation of the macroscopic data with the two extreme step pairs as shown in **Fig. 5-4**. The pair of curves from the same patch is, it should be noted, fundamentally different from those obtained for SI and SA K^+ channels in snail neurons, where the assumption was that two different populations of channels were represented by the two curves. Here, a single population of channels is represented by the two curves.

B. P_{open} decreases with increasing suction

To further illustrate pressure-dependent stretch-inactivation, the P_{open} was plotted as a function of applied pressure for several patches held at potentials between +20 mV and +60 mV. Patches rupture before P_{open} could reach a plateau (conductance saturation) was a recurring problem. Thus, five non-saturating does-response curves are shown in **Fig. 5-7** that the P_{open} of Shaker-IR was inversely related to the applied suction, as expected for SI channels.

Figure 5-7. Pressure dose-response of stretch-inactivation

Single-channel dose-responses were recorded from five excised patches at depolarized voltages of +60 mV(✱); +40 mV (○); +60 mV (◆); +20 mV(▽); +60 mV (■). NP_{open} was normalized according to the maximum number of activated channels in the patch. Each point represents an NP_{open} calculated from a 20 s segment of recording. The pressure-response curve (▽) corresponds to the same patch as in **Fig. 5-6b**.

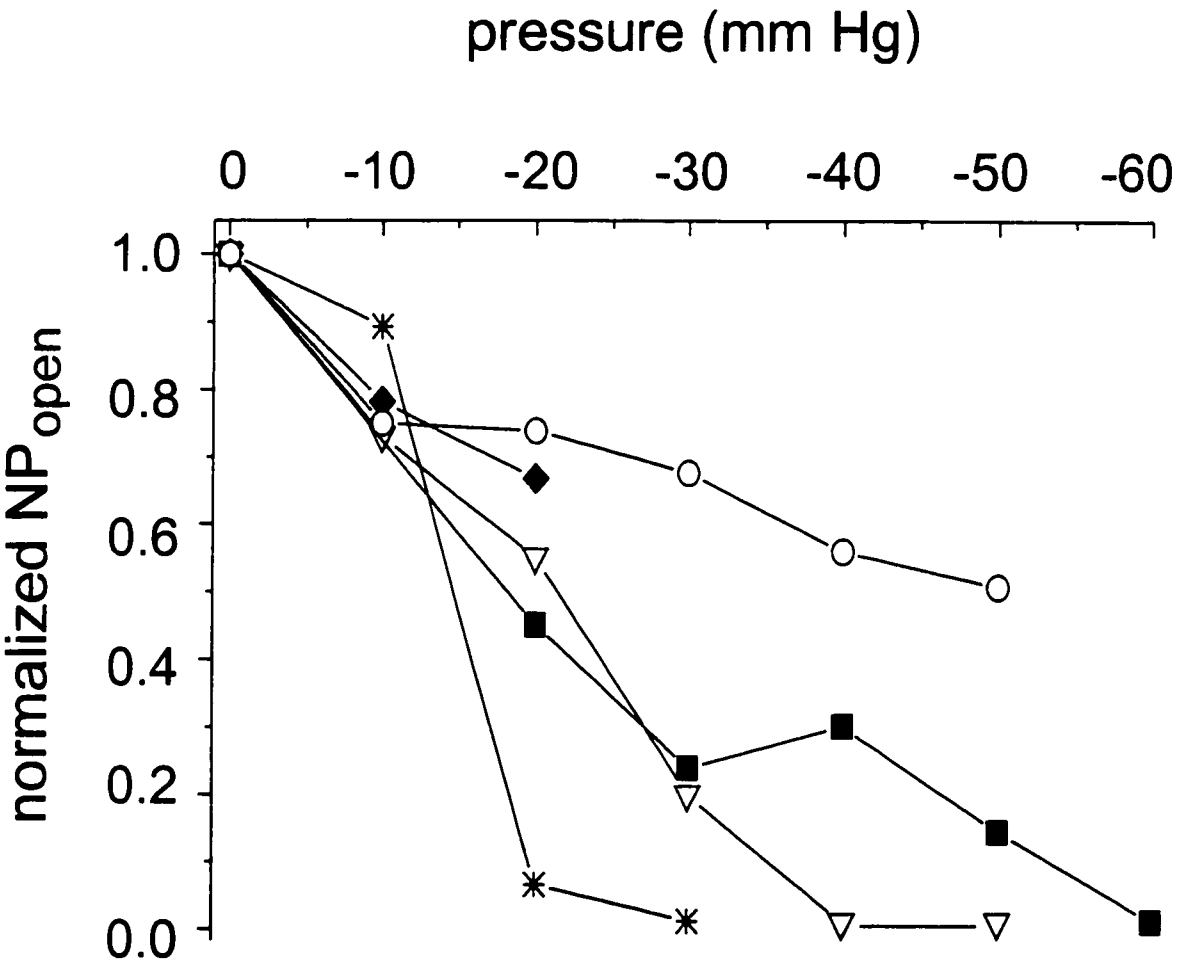
pressure (mm Hg)
0
-10
-20
-30
-40
-50
-60
1.0
0.8
0.6
0.4
0.2
0.0
normalized NP$_{open}$

DISCUSSION

I. Summary

Results presented in this chapter suggest that gating of the voltage-dependent channel Shaker-IR can be modulated by membrane tension. Shaker-IR was either activated or inactivated by increases in membrane tension depending on pre-stretch P_{open}. As presented above, there was a consistent trend that stretch-inactivation occurred at more depolarized potentials while stretch-activation occurred at more hyperpolarized potentials.

In the following, evidence is compiled from the combined results of this chapter and of **Chapter 4**. The two concerns about the validity of the mechanical effect, a possible increase in membrane area or a contamination from the endogenous MS currents, which might have contributed to the observed mechanical effects in Shaker-IR are further discussed and ruled out. Mechanical effects on Shaker-IR are therefore assumed to be truly a gating interference rather than artifacts. A theory that incorporates pre-stretch P_{open} is proposed as a general explanation of stretch-activation and stretch-inactivation of Shaker-IR.

II. Are mechanical effects on Shaker-IR truly gating interference

A. Contamination of endogenous MS currents

The endogenous MS cation channels in oocyte may complicate the detection of mechanical effects on other channels. However, the mechanical effects that we have attributed to Shaker-IR can not be due to the contamination from the endogenous MS cation channels based on the following

pieces of evidence.

First, families of voltage-dependent outward K^+ currents were detected in oocytes injected with Shaker-IR mRNA whereas only passive currents (capacitative and leak currents) were elicited from non-injected oocytes in the presence of 100 μM Gd^{3+} (**Figs. 3-3, 4-2a and 4-2b**). 100 μM Gd^{3+} was effective at blocking the endogenous MS channels since, with its presence, the non-injected oocyte patches exhibited no background ionic currents and suction at a pressure even up to rupturing the membrane, did not elicit any detectable currents. Using a paired-step protocol (see **Fig. 4-3**), I_{Sh} exhibited characteristic activation time courses, and these currents were reversibly augmented by suction < -20 mmHg whereas, with the same protocol, control oocytes showed no detectable stretch-augmented currents even with suctions up to rupturing the patch (>-40 mmHg). Thus, the mechanical effects on Shaker-IR-injected oocytes could not be from breakthrough of unblocked endogenous MS currents.

Second, the endogenous SA cation channels produced inward currents at hyperpolarized potentials and outward currents at depolarized potentials. In contrast, heterologously expressed Shaker-IR channel exhibited voltage-dependent outward currents at all test potentials. If stretch effects ascribed to Shaker-IR were really from contamination of some unblocked endogenous MS channels superimposed on I_{Sh}, then the outward I_{Sh} should be decreased at more hyperpolarized potentials and increased at more depolarized potentials. Instead, as shown in **Figs. 5-1, 5-2a and 5-3**, suction elicited stretch-activation at more hyperpolarized potentials and stretch-inactivation at more depolarized potentials. The two opposite effects in the same patch were consistent throughout the experiments under the same conditions.

Third, both stretch-activation and -inactivation were reversible and repeatable within a patch

and were broadly reproducible from patch to patch, suggesting a specific mechanistic correlation between pipette pressures, elevated membrane tension and mechanical effect on the voltage-dependent Shaker-IR channels gating.

Fourth, Shaker-IR could easily be distinguished from the endogenous MS channels by the single-channel kinetics. Shaker-IR was characterized by prolonged openings (**Figs. 4-6 and 5-6**), contrasting sharply with the much briefer openings of the endogenous MS cation channel (**Figs. 4-1 and 5-2b**).

Finally, the V_{rev} of Shaker-IR remained the same either with or without suction (see **Appendix**), which further supports that the stretch-affected current was truly Shaker-IR. The possibility that the mechanical effects might be from non-specific breakdown of the membrane can also be excluded since these mechanical effects were reversible and repeatable. Taken together, the data from our experiments demonstrate that the susceptibility to mechanical interference is an intrinsic property of Shaker-IR.

B. Gating interference versus drawing in more membrane

Sokabe et al. (1991) used high resolution video microscopy in conjunction with cell-attached patch clamp and showed that suction caused a reversible 10% increase in the patch membrane area without breaking a seal, presumably due to an influx of new lipids. Therefore, there was a possibility that small increases in Shaker-IR channel activity in response to suction might be from recruitment of new Shaker-IR channel-bearing lipid bilayer into the patch membrane. However, the following evidence indicates that the effects of suction on I_{Sh} are due to an increased membrane tension effects on the P_{open} of existing Shaker-IR channels within the patch.

The membrane capacitance can be used to measure the membrane area. Capacitance is

directly proportional to the patch membrane area and an increased membrane area should be reflected by an increment in capacitance current. Neither internal membrane stores which are not continuous with the surface membrane nor the stretching out of existing folds of membrane may contribute to the capacitance (Ross et al., 1994). As mechanical stimulation did not elicit detectable changes in capacitance currents, as shown in **Fig. 4-3a** and examined at higher time resolution, these results indicate that stretch-activation of Shaker-IR was not due to an increase in membrane area. Similarly, if suction causes "micro-ruptures" of the membrane or loss of the gigaohm seal, then any conductance change would likely be non-specific, and would show up as increased I_{leak}. As there was no evidence that suction produced nonspecific I_{leak}, it was evident that the applied pressure did not disrupt the bilayer membrane structure.

Second, we have demonstrated that the same mechanical effect could be elicited in excised patches by either suction or blowing and that this effect was immediately reversible upon release of the stimulus, as shown in **Fig. 5-3**. Also shown in **Fig. 4-9**, both suction and blowing produced the same mechanical effects and the extent of the increase was dependent on the amount of the applied pressure. It is also unlikely that blowing would have increased membrane area. These results suggest that membrane area remained constant during and after mechanical stimulation.

Third, if mechanical stimulation caused an increase in channel-containing membrane area, this increase should only give rise to irreversible "stretch-activation". In contrast, a decrease in membrane area would produce an irreversible "stretch-inactivation". However, at a low or high pre-stretch P_{open}, stretch reversibly activated or inactivated Shaker-IR, respectively. If membrane area had changed with stretch, it would also be difficult to explain how the identical mechanical stimulus produced a net activation of I_{Sh} at one voltage and a net inactivation of I_{Sh} at the other (**Fig. 5-4**).

Fourth, as shown in the cell-attached patch (**Fig. 4-2c**), suction could quickly induce, in this case, a 20-fold increase in P_{open}. If the stretch effects as illustrated in **Fig. 4-2c** were due to an increase in membrane area, this increase would have to be over 20-fold to account for the increased P_{open} of Shaker-IR and it would have to be increased reversibly. Although we did not measure the patch membrane area, a 20-fold capacitance current increase would not have gone unnoticed. Such a large increase in current amplitude by suction was also seen in excised patches. For example, in single-channel recordings of excised patches (**Fig. 4-6**), we observed over 15-fold increase in P_{open} upon application of -20 mmHg suction. Moreover, the stretch-activation effects on P_{open} (or fold-increases) in excised patches ranged from 4.4 to 358 fold (see **Fig. 4-8**). In general, excised patches with a good gigaseal stay fixed in position (Sokabe et al., 1991), the 15-fold area increases would be highly impossible. For example, considering a milder 9-fold area increase: a flat 2 μm diameter patch has an area of $\pi r^2 = 3.14 \times 1^2 = 3.14\ \mu m^2$ and a flat 6 μm diameter patch has an area of $3.14 \times 3^2 = 28.26\ \mu m^2$, to reach a 9-fold difference. Thus, to get a reversible 9-fold increase in membrane area, a patch would have to quickly relocate from a position in the pipette where its diameter was 2 μm (**Fig. 5-8**, location **a**) to a location where its diameter was 6 μm (**Fig. 5-8,** location **b^1**), then back to a location upon release of suction. Or, it would have to stay fixed at location **a** and reversibly elongate to a sac-like shape with 9 times the area (**Fig. 5-8,** location **b^2**). Neither of these behaviours have been reported for gigasealed patches (Sokabe and Sachs, 1990).

Fifth, since both stretch-activation and -inactivation on Shaker-IR were successfully repeated in both excised patches and cell-attached patches (**Figs. 5-1 and 5-3**), these results strongly argue against the possibility that suction may draw up more channel-containing membrane into the sealed patch.

Figure 5-8. Schematic diagram of hypothetical changes in membrane area

The diagram depicts two positions that can result in a 9-fold patch area change (equivalent to a 3-fold patch diameter change from 2 to 6 μm). **(a)** a patch of 2 μm diameter. **(b^1)** and **(b^2)** indicate two other patch positions with a 9-fold area greater than **(a)**.

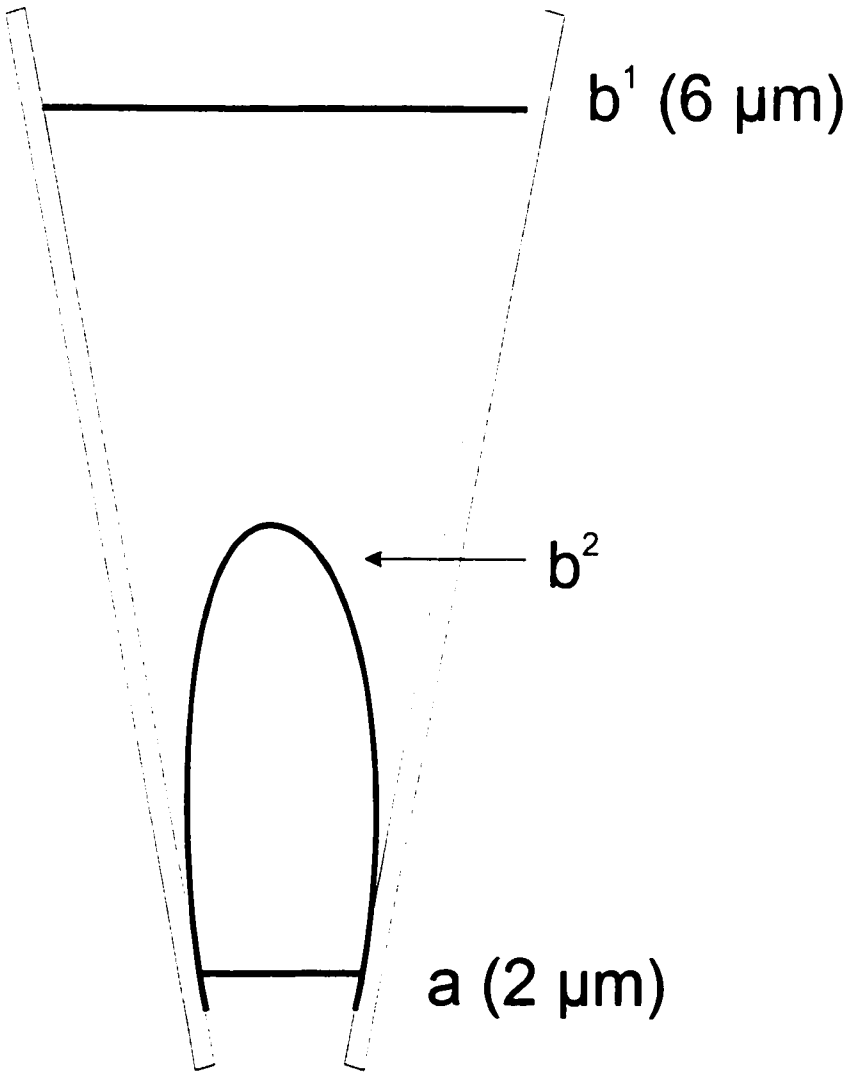
b1 (6 µm)
b2
a (2 µm)

Sixth, if mechanical effect on I_{Sh} was due to an increased membrane area, the increasing I_{Sh} should increase proportionately at all voltages. Thus, one would expect to see the same fold increase either at two adjacent voltage steps or at two widely-spaced voltage steps upon mechanical stimulation. In contrast, a disproportionate increase should be observed if tension interfered with the gating of fixed population of Shaker-IR channels. Using the paired-step protocol, responses on Shaker-IR were consistently disproportionate (**Figs. 4-3, 4-5 and 5-4**). Altogether, for closely adjacent voltages near the G-V foot, about 50 patches were tested. Seven paired voltages from -25 to +20 mV in every adjacent 5-10 mV step were tried, and it was evident that I_{Sh} elicited by the more hyperpolarized potential (the lower P_{open}) always had the larger fold increase with stretch. Therefore, suction-induced effects are thought to be the gating interference on I_{Sh}. Somehow, stretch bias the gating transitions between the open and closed states. Recruitment and loss of channels is not a tenable explanation.

Finally, if the stretch effects on Shaker-IR were due to recruitment or loss of channels, and not due to the membrane tension, then the P_{open}-pressure curve should be shallow with a small difference in P_{open} between pre-stretch (0 mmHg) and the maximum values obtained either at saturation or patch rupture [keep in mind that area increase in excised patches are small, (<< 2 fold)]. Instead, the steep non-linear stretch-activation (**Fig. 4-8**) and stretch-inactivation (**Fig. 5-6b**) curves obtained suggest that they are sigmoidal or as one part of a sigmoidal relationship (Boltzmann), as expected for gating energy effects on the Shaker-IR protein. These results further confirm that the effect of mechanical stimulation is on the gating of Shaker-IR.

III. Why does Shaker-IR exhibit both stretch-activation and -inactivation?

A. Channel microenvironments are "granular", so microstresses may differ among channels

Several channels such as bacterial MS channel (Sukharev et al., 1994), ENaC (Awayda et al., 1995) and alamethicin (Opsahl and Webb, 1994) exhibit mechanosensitivity after being incorporated into pure lipid bilayers. In this cases, it is evident that mechanical gating energy must be conveyed to the channel via the lipid bilayer constituents. As was shown in this chapter, stretch can activate Shaker-IR channels in cell-free excised patches. Thus, it is feasible that the bilayer model may also apply to Shaker-IR. However, the oocyte patches are far more complex than pure lipid patches. A sense of the compositional complexity of a typical non-excitable cell membrane can be gleaned from **Table 5-1**. Not only are the lipid compositions of the inner and outer leaflets of the membrane diverse, but also a multitude of proteins (only a few of which are indicated), add complexity to the cell membrane. There may easily be a hundred types of molecules to consider. In addition, lipids and proteins are not fully independent components of the membrane but rather, the two supplement each other: lipids form the microenvironment of the integral membrane proteins which in turn can modulate the specific composition and properties of lipid domains. Also, peripheral proteins (**Table 5-1**) such as glycosylphosphatidylinositol (GPI) are attached to the outer leaflet through a covalent bond to the glycolipids. GPI proteins have been proposed to cause lateral assemblies of glycolipids and cholesterols (called rafts). As a result, GPI-attached proteins will be anchored at the raft which are important in membrane trafficking, signal transduction and cell adhesion (Harder et al., 1998). On the other hand, G protein variants are located at the inner leaflet of the plasma membrane, and act as a link between receptors and the enzymes that generate second messengers; some G proteins interact directly with channels.

Table 5-1 Complex composition of the cell membrane

Lipids [A]	Proteins	
	Peripheral proteins	Integral proteins
Outer leaflet glycosol-phosphatidyl-inositol (GPI) phosphatidylcholine (PC) sphingomyelin (SM) glycolipids	GPI-anchored proteins [B] prenylated $G_{\alpha\beta}$ proteins [C]	**Specifically demonstrated for oocyte membrane [D]** 1. Ca^{2+}-activated Cl^-channels 2. hyperpolarization-activated Cl^- channels 3. voltage-dependent Ca^{2+} channels 4. pool-depletion-activated current 5. stretch-activated channels 6. tetrotoxin-insensitive Na^+ channels 7. minK-regulated K^+ channels
Inner leaflet phosphatidylserine (PS) phosphatidylinositol (PI) phosphatidylethanolomine (PE) cholesterol fatty acid diacylglcerol (DAG) inositol trisphosphate (IP3)		**Ion channels in non-excitable cells [E]** 1. Amiloride-sensitive Na^+ channels 2. Ca^{2+}-activated nonselective cation channels 3. ATP-activated nonselective cation channels 4. cyclic nucleotide-activated cation channels 5. Ca^{2+}-activated K^+ channels (maxi K^+ channels) 6. inwardly rectifying K^+ channels 7. cAMP-activated Cl^- channels 8. voltage-dependent Cl^- channels (CIC family) 9. volume-activated Cl^- channels 10. mechanically activated ion channels 11. Ca^{2+}-entry and store-operated Ca^{2+} channels **Other integral proteins** Ca^{2+} / ATPase Na, K^+-ATPase Na-H antiporter Na^+ dependent-glucose transport kinases; phosphatases; lipases cytosolic cholesterol-carrier proteins glycoproteins glycolipids receptors

A. Schroeder et al., 1998
B. Turner, 1994; Casey, 1995
C. Clapham and Neer, 1997
D. Stühmer and Parekh, 1995
E. Nilius, 1998

Using video microscopy, the cytoskeletal remnants has been shown to present even in excised patch membrane (Sokabe and Sachs, 1990; Sokabe et al., 1991). Thus, the microenvironment of a channel protein in a patch is composed of a group of diffusible or anchored lipids, plus other proteins including membrane skeleton remnants (Horber et al., 1995). Variations in the mix of these molecules would produce a different microenvironment from one channel protein to the next. Thus, even in excised oocyte patches, it is inappropriate to imagine channels with a surrounding uniform bilayer. Native membrane patches are unavoidably complex. And so, correspondingly, are the microenvironments of channels. Under mechanical stimulation, a macroscopic uniform membrane tension could create non-uniformly distributed mechanical force at the individual channel-bilayer interfaces. Consequently, channels in the same patch may feel the same mechanical stimulation differently: some channels may be stimulated to move towards the open state while others are stimulated to move away from the open state. Likewise, some channels in the patch may not experience the particular mechanical "micro-forces" that can bias their P_{open}. Therefore, the coexistence of stretch-activation and stretch-inactivation in the same patch may be due to the complex structure and interactions of the plasma membrane components. Whether stretch-activation or -inactivation dominated in current recordings would reflect the sum of different channel responses at different pre-stretch P_{open} determined by the prevailing membrane potential.

B. Shaker-IR occupies multiple states at any voltages

Added to the microenvironment complexity of the channel, there is the fact that Shaker-IR is kinetically complex. This needs to be taken into consideration when thinking about how membrane tension might affect the channel's gating. Although we simplify the gating process of Shaker-IR by referring to "activation" and "inactivation", Shaker-IR is not a two-state (closed $\Leftrightarrow$

open) channel. Gating transitions occur within a rather complex kinetic scheme for Shaker-IR As indicated in **Table 5-2** (also see **Chapter 3**), the gating of single Shaker-IR channels involves a number of distinct open and closed states (Hoshi et al., 1994). For example, analysis of the time course of Shaker-IR channel opening in response to a voltage step suggests a minimum of five to seven sequential closed-state transitions must occur prior to opening (Zagotta et al., 1994b; Schoppa and Sigworth, 1998). In addition, although Shaker-IR has its rapid N-type inactivation deleted, it still exhibits two distinct forms of slow inactivation, identified as the P- and C-type inactivation (**Chapter 3**). Moreover, a mutant Shaker-IR (Zheng and Sigworth, 1997) and a Shaker-like K^+ channel (Chapman et al., 1997) have been reported to have two subconductance levels, presumably corresponding to two voltage-dependent conformational changes for each of the four subunits. All these features constitute a complex "energy barrier terrain" for a Shaker-IR channel finding its way into or out of its open state.

As Shaker-IR channels gate through many states, each channel population is at an equilibrium among these multiple kinetic states at a given steady-state P_{open}. Thus, a mechanical stimulus may either activate or inactivate Shaker-IR channels depending on 1) its favoured kinetic state(s) prior to mechanical stimulation and 2) what state(s) is stabilized by mechanical stimulation. Of course, depolarizing voltages also profoundly affect some of the energy barriers separating the open and closed states. When channels are at a steady state P_{open} at some voltage, membrane stretch would stabilize some channels in their current states, while destabilizing others, causing them to switch states. If macroscopically uniform membrane tension exerts non-uniform mechanical forces at individual channels, stretch could decrease closed-state stability at some channels while increasing it at others.

Table 5-2 Kinetic complexity of Shaker* and Shaker-IR

Zagotta and Aldrich, 1990	Activation is modelled as a voltage-dependent conformational change in each of the four subunits, followed by a final voltage-independent opening transition.
Zagotta et al., 1994a	Estimation from activation delay and sigmoidal activation time course, yield a minimum of five kinetic transitions between resting and open states.
Stefani et al., 1994 Bezanilla et al., 1994	The voltage dependence of charge movement (Q-V) relation is shallow at hyperpolarized voltages but is steeper over the voltage range where channels open.
Schoppa et al., 1992; Seoh et al., 1996;	Total gating charge associated with the activation of Shaker-IR is about 12 electronic charges.
Aggarwal and MacKinnon, 1996	The activation conformational changes are associated with the movement of charge equivalent to 12 to 16 electronic charges through the membrane electric field.
Loots and Isacoff, 1998	The slow, C- and P-type inactivation processes were suggested to be associated with the outer mouth of the pore region.
Baukrowitz and Yellen, 1995	Permeant ions not only interact with the activation gating, they can also affect C-type inactivation where it seems that the depletion of K^+ from the conducting pathway allows the outer mouth of the pore to collapse.
Bezanilla et al., 1994	The time course of the "ON" gating current induced by a step depolarization has a rising or plateau phase, implying that the initial kinetic steps in channel activation are slower or less voltage dependent than subsequent steps.

..... continues on next page

Table 5-2 *continues*

Bezanilla et al., 1991; Zagotta et al., 1994a	After large depolarization, the time course of the "off" gating current induced by a voltage step back to the holding potential has a rising phase and also decay kinetics that match the time course of channel deactivation. Thus, the first kinetic steps in channel deactivation are slower than subsequent steps.
Bezanilla et al., 1994 Zagotta et al., 1994a	At intermediate voltages, the gating currents display a fast component that is followed by a slow exponential component that is correlated with channel opening. At these voltages, the ionic currents have a relatively short delay, followed by a very slow rise to the peak currents. These phenomena imply that channel opening at these voltages is much slower than the rate that the channel traverse through early closed states.
Chapman et al., 1997	In a mammalian Shaker-like K^+ channel (Kv 2.1), four sub-states have been identified which correspond to channels with one, two and three subunits in the open state.
Zheng and Sigworth, 1997	Subconductance was thought to couple with Shaker-IR activation, mutation of the pore-region residues show two subconductance levels, 37% and 70% of the full conductance.
Schoppa and Sigworth, 1998	The partial charges correspond to an average charge movement of 0.5 e_0 during each transition in the activation process, this value implies that activation gating involves a large number of transitions to account for the total gating charge displacement of 13 e_0.
Schoppa et al., 1992 Perozo et al., 1994	Components of charge in the Q-V relation have been shown to be differentially affected by some mutations in the S4 region and also by drug binding. The differential effects suggest that the existence of different types of voltage-dependent conformational changes.

* Excluding N-type inactivation

- The description here are essentially brief excerpts from the listed papers

C. Pre-stretch P_{open} and mechanical effects on Shaker-IR

Although most of the kinetic states of Shaker-IR are closed states, stretch-activation or -inactivation is defined in terms of increased or decreased contributions from the open (current carrying) state. The net effect of the perturbed state stabilities therefore appears in the current record as activation, inactivation or no net change, depending on the pre-stretch channel activity, or pre-stretch P_{open}.

At the most hyperpolarized potentials, when P_{open} is close to zero, only stretch-activation would be detectable since most channels are in closed states (the system has been pre-forced into a far corner of the energy terrain). Any further stabilization of the closed states would not alter the current record. In contrast, when P_{open} is initially near unity, most channels are in the open state and the only changes that contribute to the current record would be closures, with a net effect of stretch-inactivation. Similarly, at some intermediate pre-stretch P_{open}, both stretch-activation and stretch-inactivation would contribute to the record such that the two are balanced and no effect would be registered. This pre-stretch P_{open} concept can explain why stretch-activation is the major effect at the foot of the G-V curve, while stretch-inactivation is the dominant effect at the top of G-V curve.

IV. Pre-stretch P_{open} and other channels

The pre-stretch P_{open} may also provide an explanation for the long standing enigma that MS channels exhibit stretch-activation in normal myotubes whereas the same channel type exhibits stretch-inactivation in dystrophic myotubes. In addition, the pre-stretch P_{open} idea can be applied to GIRK, which is reported to show either stretch-activation or -inactivation under different experimental conditions.

In dystrophic myotubes (Franco-Obregón and Lansman, 1994), the pre-stretch P_{open} was 0.07 as mean channel activity, being higher than that of the normal myotubes (P_{open} = 0.04). The underlying reason for this difference is not known. Nevertheless, upon mechanical stimulation, dystrophic myotubes with the higher pre-stretch P_{open} channels exhibit stretch-inactivation (P_{open} is reduced to 0.02), whereas normal myotubes with lower pre-stretch P_{open} exhibit stretch-activation (P_{open} is increased to 0.07). In conclusion, the pre-stretch P_{open} determines the mechanical response.

A similar explanation might account for GIRK channels exhibiting opposite mechanical effects in different preparations. GIRK shows stretch-inactivation when it is maximally activated by exposure of rabbit atrial myocyte to 10 μM carbachol or when GIRK is coexpressed with the excess of $G_{\beta\gamma}$ subunits in *Xenopus* oocytes (Ji et al., 1998). In a different preparation (Pleumsaran and Kim, 1995), the pre-stretch P_{open} for the rat heart K_{ACh} was 0.17 (10 μM ACh applied in the pipette, cell-attached patches) and 0.32 (in the presence of 100 μM GTP plus 1 mM ATP applied in the bath / 10 μM ACh in the pipette, inside-out excised patches). These pre-stretch P_{open} values (0.17 and 0.32) are well below the maximum channel activity, and in these preparations, there was stretch activation, in which suction doubles P_{open} to 0.65 (Pleumsaran and Kim, 1995). A direct comparison can not be made between these two reports, but we suggest this may represents a similar pattern: when channels are maximally activated, stretch-inactivation dominates; when there is a lower pre-stretch P_{open}, stretch-activation dominates.

CHAPTER 6

General Discussion

WHAT MAKES SHAKER-IR AN MS CHANNEL

In this section, four possible mechanisms are presented to explain how the P_{open} of a voltage-dependent channel can be affected by mechanical stimulation. These speculative mechanisms may not be mutually exclusive.

I. Tension favors larger area conformation state(s)

Single channel kinetic analysis suggests that Shaker-IR undergoes multiple sequential kinetic conformational transitions before opening (Hoshi et al., 1994; also see **Table 5-2**). Since voltage activation of Shaker-IR depends on the movement of the voltage sensor S4 prior to the opening of the channel, it is plausible that different conformational states occupy different membrane area and so, would be differentially favored by different membrane tension (see **Chapter 1**).

There is some indirect evidence that would be consistent with Shaker-IR conformation state of different area. Spectroscopic studies, which use chemically synthesized peptides corresponding to hydrophobic segments S2, S3 and S4 of the Shaker K^+ channel, have demonstrated that while free S4 peptide orient itself parallel to the membrane surface, S3 tends to favour a more transmembrane orientation (Peled-Zehavi et al., 1996). Resonance energy transfer measurements, done in high

lipid/peptide molar ratios, revealed that S3 and S4 can not self-associate in phospholipid vesicles, but they can associate with each other and with the S2 segment of the channel (Peled-Zehavi et al., 1996). Thus, the S4 segments not only interacts with S2 and S3 segments in the lipid bilayer, they are also stable when tilted at an angle relative to S2 and S3 segments (Peled-Zehavi et al., 1996). Based on studies involving an intragenic suppression strategy, a tilting S4 model has also been proposed by Tiwari-Woodruff et al. (1997) to explain the electrostatic interactions between positively charged residues in S4 with negatively charged residues in its neighboring segments (see **Chapter 3**). Consistent with this proposition, in Shaker-IR K^+ channels with fluorescently labeled residues, preliminary data with quenching interaction study showed that the voltage sensing S4 segment undergoes two sequential outward transmembrane movements. In response to membrane depolarization, S4 seemed not only to move outward but also to tilt peripherally (Gandhi et al., 1998). With this structural orientation, it is possible that maximally tilted S4 in or prior to the open state may occupy a different membrane area compared with the closed states.

As tension favors protein conformations with larger area (Opsahl and Webb, 1994), any larger area states of Shaker-IR channels (e.g. one with S4 maximally tilted) would be stabilized by membrane tension. This kind of effect could be an underlying mechanism for both stretch-activation and -inactivation. As Shaker-IR undergoes many connected states from closed to open, depending on which state the channel is at, tension might affect any conformational changes that alter the protein size and the equilibrium between the states. If channel proteins occupy larger membrane area in the open state, tension would favor the open state and thus stretch-activation would be expected. On the other hand, if channel proteins occupy a smaller membrane area in the open state, it would be less favored by tension and stretch-inactivation would be expected (see Morris, 1990).

II. Tension leads to destabilization of S4 segments

The current model of Shaker channel protein proposes that S5, the P-region, and S6 of the four subunits line the channel pore [and correspond to the inner helix, pore and outer helix of the bacterial K^+ channel (Doyle et al., 1998)]. While S1, S2 and S3 are located peripherally facing and interacting with the lipid bilayer, S4 functions as a voltage sensor bridging the above two parts (S1 -S3 and S4-S6) and interacting with the neighboring transmembrane segments (Durell et al., 1998).

Upon mechanical stimulation, molecular stresses would distort or change the conformation of the lipid bilayer. This distortion would in turn affect Van der Waal's interactions with, presumably the hydrophobic S1, S2 and S3 segments of the transmembrane proteins. These stresses may be sufficiently intense to indirectly affect the conformation of the S4 segment via S1-S3 segments. If this is true, a disturbed gating would be expected since S4 acts as a gating sensor. This altered stability of S4 may yield an augmented or attenuated response to the transmembrane voltage, depending on which conformational states the channel favors prior to mechanical stimulation.

III. Tension thins the lipid bilayer, altering the electric field sensed by S4

Based on patch capacitance measurements, Sachs (1987) proposed that the lipid bilayer thins by <6 % under mechanical stimulation. The thinning bilayer would modify the local electric field, making it span a shorter distance where the intramembrane charged voltage sensors cross. In this way, the transmembrane voltage could act more intensely on the voltage sensors such that channels would show a higher P_{open} at the same V_m. Thus, a stretch-activation would be expected by altering the local electric field across the membrane.

The free energy of a bilayer deformation occurring as the result of a conformation change in

an inclusion (i.e., an integral membrane protein) has been described as the sum of three contributions: compression-expansion, splay-distortion, and surface tension (Nielsen et al., 1998). Using a (liquid-crystal) elastic model of bilayer deformations, it has been demonstrated that the first two components play a major role in the contribution of the free energy deformations. With mechanical stimulation, the thinning bilayer affects not only the compression-expansion energy but also the splay-distortion energy (Nielsen et al., 1998). This deformation due to protein-bilayer interactions may generate enough linear spring energy in the bilayer and may be sufficient to affect channel's function.

IV. Tension changes multimeric state of the channel

In a homogenous lipid membrane, alamethicin peptides insert and aggregate to form barrel shaped channels. Raising the membrane tension reversibly increases the conductance of the alamethicin channels (see **Chapter 1**). Presumably there is an enlargement of the pore size by incorporation of an additional peptide into the pore-forming subunits (Opsahl and Webb, 1994). Channel multimers that occupy larger area are thought to be increasingly favored as tension increases. This scenario can be ruled out for Shaker-IR since the all-point current amplitude histograms (**Fig. 4-7**) showed that different pressure steps showed no difference in single-channel amplitude, suggesting that suction did not affect the pore size of the Shaker-IR. Also, the tetrameric structure of Shaker-IR channels also rules out the possibilities that more subunits might come together to form a larger pore.

COUPLING OF MECHANICAL ENERGY TO THE GATING OF SHAKER-IR

I. Direct or indirect gating

Depending on how mechanical forces are delivered to the channels, mechanosensitivity can be divided into direct and indirect (see **Chapter 1**), and these two gating processes can each be subdivided into lipid bilayer or cytoskeleton mechanisms. To distinguish between direct and indirect mechanisms of gating, one can consider the time required for a channel to show altered MS gating. If the time scale is too short to allow for intermediate steps, the channel is probably directly gated. According to this criterion, the gating of Shaker-IR might coupled directly to the applied mechanical stimulation, since the onset of the mechanical effect on Shaker-IR occurs almost instantaneously when the stimulation is applied. Although this was not quantified specifically, the rise time of suction-altered current was clearly correlated to the rise time of pressure steps, at a time scale of hundreds of milliseconds. Also, if one can observe the mechanosensitivity in both cell-attached and cell-free patch configurations, this would help to further clarify whether cytoplasmic second messengers are required in the gating process. Since Shaker-IR exhibited mechanosensitivity in both configurations, and in the case when the mechanical effect is reversible, the involvement of cytoplasmic second-messengers in the gating process could be excluded.

II. Bilayer pathway vs cytoskeleton pathway

The direct gating of Shaker-IR is likely to be mediated via the lipid bilayer since we showed similar mechanical effects in both cell-attached and in excised patches; and the later should have had

minimal cytoskeletal constituents. Although it may be possible for cytoskeleton as well as organelle remnants to accompany the excised patches (Sokabe and Sachs, 1990; Ruknudin et al., 1991), it is unlikely for the cytoskeleton remnants to persist in the high Cl^- (140 mM KCl) that we applied to the excised patches. This argument is based on the observation that for squid axon cortical cytoskeleton, the Cl^- is chaotropic (Terakawa and Nakayama, 1985). Perfusion of 360 mM KCl (squid is a marine organism so this is a normal concentration) for one hour completely dissolved the submembranous cytoskeletal network as demonstrated by scanning electron microscopy (Terakawa and Nakayama, 1985). In contrast, no such a cytoskeletal protein dissolving effect was found with the non-chaotropic anion F^- (360 mM KF). Although higher KCl concentration and longer perfusion times were used in perfusion of the squid axon (Terakawa and Nakayama, 1985), their experiments were done on axons with intact cortical cytoskeleton. Our experiment with 140 mM KCl (normal for the amphibian) would also likely disperse the remaining cytoskeleton components from our excised patches.

Nevertheless, there are several isolated reports implicating cytoskeleton involvement in Shaker gating. For instance, a highly conserved PSD-binding sequence (**Fig. A-1**) is found at the C-terminus of Shaker-like K^+ channels, and this sequence binds directly to cytoplasmic ion channel clustering proteins such as PSD-95 (Kim et al., 1995). Recently, Jing et al., (1997) showed that microfilament disruption by cytochalasins enhanced a fast inactivating current component of a Shaker-like K^+ channel. Since their expression system was *Xenopus* oocytes, this would indicate an association of the Shaker-like K^+ channels with an endogenous oocyte protein resembling the members of the PSD-95 (Jing et al., 1997). Although for simplicity, we favour the hypothesis that mechanical gating energy is delivered through the lipid bilayer to Shaker-IR, we could not

completely rule out the cytoskeleton involvement. To do so, we would have to perform experiments on purified Shaker-IR inserted into lipid bilayer preparations, as has been done for ENaC in planar lipid bilayer (Awayda et al., 1995) and *E. coli* MscL in liposomes (Sukharev et al., 1994).

BROADER IMPLICATIONS

I. Channels are intrinsically mechanosusceptible

A. Widespread occurrence of mechanosusceptibility

Living cells constantly experience mechanical stress from their own activities, such as growth, migration or division, as well as from external sources, such as passive stretch, osmotic stress, or shear forces. Patch recordings have shown that plasma membrane proteins and, more specifically, ion channels, are susceptible to mechanical perturbation. These MS channels are not only ubiquitous, being found in a variety of organisms, from bacteria and fungi to plants and animals, but also diverse, constituting various unrelated channel types.

B. MS channels have no common structural motif

Ion channels have two major functional properties: permeation and gating (Armstrong and Hille, 1998). In the case of Shaker-IR, both permeation and gating processes are dependent on highly conserved structural motifs: the voltage sensor S4 and a highly conserved signature sequence G-Y-G, also known as the selectivity filter (see **Chapter 3**). In contrast, although MS channels are ubiquitous, they feature no conserved molecular motif that might be associated with mechanosensitivity. For example, MscL, TREK, NMDA and Shaker-IR, are very different (**Table 6-1**) in terms of amino acid sequences and proposed structures (none belong to the same family).

Table 6-1 The structural differences of MS channels

Channel types	Molecular structure	Monomer molecular weight
MscL[A]	one P*, two TM**, pentamer[B]	15 kD
TREK[C]	two P, four TM, dimer	41 kD[D]
NMDA[E]	one P, four TM, hetero-pentamer	120 kD[F]
Shaker[G]	one P, six TM, homo-tetramer	70 kD[H]

* Pore region
** Transmembrane domain

A. Sukharev et al., 1994
B. Chang et al., 1998
C. Patel et al., 1998
D. Fink et al., 1996
E. Planells-Cases et al., 1993
F. Benke et al., 1995; Chazot and Stephenson, 1997
G. Tempel et al.,1987
H. Santacruz-Toloza et al., 1994; Papazian et al., 1995

Seemingly, mechanosensitivity seen in patch clamp studies does not need a specialized molecular entity. In the case of specialized mechanoreceptor cells, (e.g. the auditory hair cells), long range cytoarchitecture (tip links) powerfully filter and focus the mechanical inputs onto channels (Jaramillo and Hudspeth, 1991; Gillespie and Corey, 1997), indicating that mechanical gating may be largely due to the presence of the tip links. The channel themselves, however, may be rather ordinary.

C. Conformational flexibility of channel proteins

Channel gating is based on protein structural rearrangements that occur stochastically in response to applied stimuli operating in the presence of thermal energy. These stimuli are widely varied and include membrane potential, the binding of ligands as well as mechanical stretch. Various channels have been shown to be sensitive to multiple stimuli although not all stimuli would exert physiological effects. For example, the NMDA receptor can be regulated by glutamate (or NMDA), glycine, Mg^{2+} and mechanical stimulation (Paoletti and Ascher, 1994). Also, the K_{ACh} channel activity can be regulated by a plethora of molecules such as G-proteins, ATP, arachidonic acid, and mechanical stimulation (Pleumsamran and Kim, 1995).

Like NMDA and K_{ACh} channels, Shaker or Shaker-like K^+ channels are also conformationally flexible and can be regulated by a variety of modulators, such as serotonin (Hevers and Hardie, 1995), cAMP-dependent protein kinase A (Drain et al., 1994), protein kinase C (Furukawa et al., 1995) as well as by the trivalent cations La^{3+} (Tytgat and Daenens, 1997). The conformational flexibility needed for responding to diverse modulators could thus explain the mechanosusceptibility and hence the ubiquitous mechanosensitivity on these diverse MS channel types.

II. Native channels may be protected from mechanical perturbation

A. Through tethering to the membrane cytoskeleton

Many channels and transporters are localized and clustered at specific subcellular sites by linking to the underlying cortical cytoskeleton (Bennett, 1990). Transporter-cytoskeleton interactions are important not only for restricting and clustering proteins to specific membrane domains, but also for protecting the bilayer from breaking down during large mechanical stimuli. This has been shown for circulating erythrocytes: cells are subjected to enormous stresses as they are continuously tugged, pulled or sheared while passing through tiny capillaries (Davies and Lux, 1989). Without its transporter-ankyrin-spectrin interactions, the erythrocyte bilayer would vesiculate (Lux et al., 1979). Presumably, the transporter-ankyrin linkage in erythrocytes has evolved to minimize disruptive mechanical energy transfer from the spectrin membrane cytoskeleton to the anion transporter by dissipating mechanical stress. The dual role of the linkage would be to strengthen the erythrocyte while providing mechanoprotection for the transport proteins.

The channel-cytoskeleton interactions might also be essential for the normal function of voltage-dependent Na^+ channels; clustering of channels at the nodes of *Ranvier* creates a low threshold zone for action potential generation (Srinivasan et al., 1988). Whether the linkage is also designed to protect Na^+ channels, either from being constantly subjected to mechanical stimulation in contracting muscles or from axoplasmic dynamics in neurons, is still unknown. Given the positive feedback scenario for V_m and G_{Na} (V_m) and the high channel density at nodes and neuromuscular junctions, the Na^+ channel-cytoskeleton interaction would need to be contrived to avoid any mechanical activation. Because the cytoskeleton could either promote mechanosusceptibility by focusing tension on the channel or provide mechanoprotection by absorbing the mechanical energy,

channels may have, as required, acquired either stiff or spongy linkages with the cytoskeleton. The mechanics of transporter-cytoskeleton linkages have not, however, to our knowledge, been studied.

B. Mechanoprotection

Channels may be protected from mechanical interference when the intact cortical cytoskeleton serves as an in-parallel "shock absorber" (Wan et al., 1999, also see review of Sachs and Morris, 1998). Any damage to the cortical actin-based cytoskeleton may allow mechanical perturbations to impact more strongly on the spectrin-based membrane skeleton and/or the lipid bilayer than they normally do (Wan et al., 1999). Weakened protection may allow mechanical impacts to act in such a way that mechanosensitivity is evident in channels which are not normally considered to be mechanosensitive. For example, mechanosensitivity is more readily detected in channels when cortical cytoskeleton is experimentally disrupted (Guharay and Sachs, 1984; Paoletti and Ascher, 1994; Wan et al., 1999) or when it is defective in diseases, such as in muscular dystrophy (Franco and Lansman, 1990).

In addition to evidence listed in **Chapter 1**, a mechanoprotective role of the membrane cytoskeleton has also been confirmed by studies in snail neurons, where the activation of SA K^+ channels in response to a "first hit" (a relatively large step of suction) occurs after a 1- to 4-s delay (Small and Morris, 1994; Wan et al., 1999). The first hit delay is both pressure and patch dependent and shortened under repeated suction steps, presumably due to various degrees of cytoskeleton damages (Wan et al., 1999). When various treatments that traumatized the cortical cytoskeleton were compared to the controls without such treatments, it was shown that all such treatments enhanced the mechanosensitivity, as measured by the shortened first hit delay and by the subsequent extent of channel activation (Wan et al., 1999). Some examples of these treatments are, 1) actin

depolymerization; 2) repeated suction which directly traumatized the cytoskeleton; 3) elevated intracellular Ca^{2+}; 4) application of a non-specific ATPase inhibitor which indirectly disrupts the integrity of cytoskeleton, and 5) hypo-osmotic shock. Taken together, it is now clear that a well-organized cytoskeletal network serves as a "shock absorber" and protects the channels from excessive mechanical interference. In other words, the channel would exhibit greater mechanosensitivity when its cytoskeleton has been disrupted.

A similar interpretation is used to explain the mechanoprotective role of an actin-binding protein ABP-280 (Glogauer et al., 1998). ABP-280 belongs to the spectrin superfamily and links actin to integral membrane proteins, thereby stabilizing cell membranes by facilitating interactions between the cortical actin cytoskeleton and the plasma membrane (Glogauer et al., 1998). In their study, both ABP-280 deficient and ABP-280 positive melanoma cell lines were incubated with collagen-coated magnetic beads which bind directly to the actin cytoskeleton via integrin receptors. Mechanical force was applied by changing the magnetic field to direct the beads on the cell surface, thus allowing forces to be transmitted to the actin cortical cytoskeleton. Using a microscope-based spectrofluorimeter, whole-cell $[Ca^{2+}]_i$ was measured as an indication of the SA channel activity. The results showed that ABP-280 deficient cells had a greater calcium influx in response to the same mechanical force application. In addition, to estimate the proportion of non-viable cells, iodide was added to denote the damaged cell membrane. It was shown that application of force significantly ($P<0.01$) increased the iodine-stained cells in ABP-280 deficient cells. Altogether, these results suggest that mechanosusceptible SA channels in human fibroblasts are protected by ABP-280, presumably by reinforcing the membrane cytoskeleton network and thereby desensitizing SA channels (Glogauer et al., 1998).

III. Evolution of Channels

Kim et al. (1998) have explored, by mathematical modeling, some of the consequences of the fact that embedded protein monomers impose a curvature on the surrounding lipid bilayer. Their study indicates that elastic forces produced by the bilayer curvature will cause protein monomers to aggregate and counteract the electrostatic repulsions between two identical proteins. In the case when the lipid bilayer component is excluded from the central regions of the energetically favored aggregates, these aggregates would conceivably open to form non-selective pores or primitive channels. Based solely on this concept, the first protein channels might have been formed through such aggregation process.

According to this concept, the stability of protein aggregates in turn should be sensitive to bilayer curvature. When a "protocell" was subjected to hypo-osmotic changes, swelling membrane stretch would reduce the lipid curvature. This reduction would favor a rearrangement of the protein aggregates. If this rearrangement results in opening of the central region of the aggregates, small organic solutes and electrolytes would efflux and thereby prevent protocell rupture and restore the cell volume. Protocells with such heritable aggregates (assuming the protein was encoded by the nucleotide sequence) would cope better with environmental osmotic shock than those without and thus have a selective advantage. It is thus reasonable to hypothesize that the first channels might be mechanosusceptible membrane protein aggregates that functioned as osmotic release valves, or as crude osmoregulators.

In modern representatives of ancient taxa, prokaryotic MS channels such as MscL in bacteria and MscA in archaea (Sukharev et al., 1994; Le Dain et al., 1998) have several properties consistent with the above proposed primitive channels, such as small sizes (MscA of ~37 kD and MscL ~15

kD); non-selective ionic pores; large conductance (3 nS for MscL and 0.4 to 0.9 nS for MscA) and activation by tension only at near-lytic levels (the threshold for activating MscA is approximately -140 mmHg and >100 mmHg for MscL channels). This last feature is important since an open non-selective pore with such a large conductance would be lethal. These prokaryotic MS channels are pentameric, in agreement with the prediction of protein aggregates in lipid bilayer (Kim et al., 1998).

FUTURE PERSPECTIVES

Further studies are needed to explore the molecular basis of mechanosusceptibility in Shaker-IR, and to determine how native Shaker is protected from mechanical perturbation in *Drosophila* cells.

I. Are gating currents affected by membrane tension?

We have demonstrated mechanical effects on Shaker-IR ionic currents both at the macroscopic and single channel level. Truly single channel patches are extremely rare and single channel studies can only provide functional information of a few channels; analysis of the single ionic currents may not be representative of the stretch effects. In contrast, recording of gating currents can be expected to reveal details of the conformational changes of the Shaker-IR proteins. Additionally, gating currents could be obtained from recordings from large macropatches (i.e. from a large population of channels). Since gating currents indicate the movement of charged particles associated with voltage sensors prior to channel opening (Armstrong and Bezanilla, 1973; Perozo

et al., 1994), we propose that stretch may affect gating current in a way that could explain the effects of stretch on the P_{open} of Shaker-IR.

Idealized gating currents are sometimes depicted as capacitative currents with an instantaneous rising phase followed by an exponential decay. In practice, however, gating currents arising from real proteins have a rising phase together with a more complex decaying phase. For both the "ON" and "OFF" responses, the total gating charge should be represented by the area enclosed by the gating current and the time axis. A hypothetical diagram of "ON" currents shows three possible stretch effects on gating charges. **Figure 6-1a** shows that stretch has no effect on gating currents. **Figure 6-1b** shows that stretch either speeds up or slows down the whole gating process without changing the total amount of the gating charge. **Figure 6-1c** show that stretch changes the total amount of the gating charge without affecting the time course of the gating currents. In reality, both the total gating charge and the gating kinetics could be affected by stretch.

Because the magnitude and time-course of the gating currents are a direct reflection of the conformational change in channel protein as a result of the movement of the S4-based voltage sensors (Bezanilla et al., 1994), altered gating currents indicate that stretch may have altered the stability of S4. If stretch destabilized S4, the peak of the gating current would occur sooner along the time axis; the rising and the falling phases would be faster. If stretch interfered with the proper S4 movement, the opposite would occur (**Fig. 6-1b**). If stretch allowed S4 to move further across the voltage field, an increased gating charge would be expected, and vice versa, if it reduced the distance S4 moved (**Fig. 6-1c**).

Since gating currents are very small in magnitude compared with the ionic currents (Bezanilla et al., 1991; Perozo et al., 1992), a Shaker-IR mutant, IR-W434F, which eliminates the ionic

Figure 6-1. Three hypothetical stretch-effects on gating currents

(a) No stretch effects. **(b)** Stretch accelerated and slowed down the gating process. **(c)** Stretch changed the total amount of the gating charge without affecting the time course of the gating currents. Solid trace: gating currents before stretch. Dotted trace: gating currents after stretch.

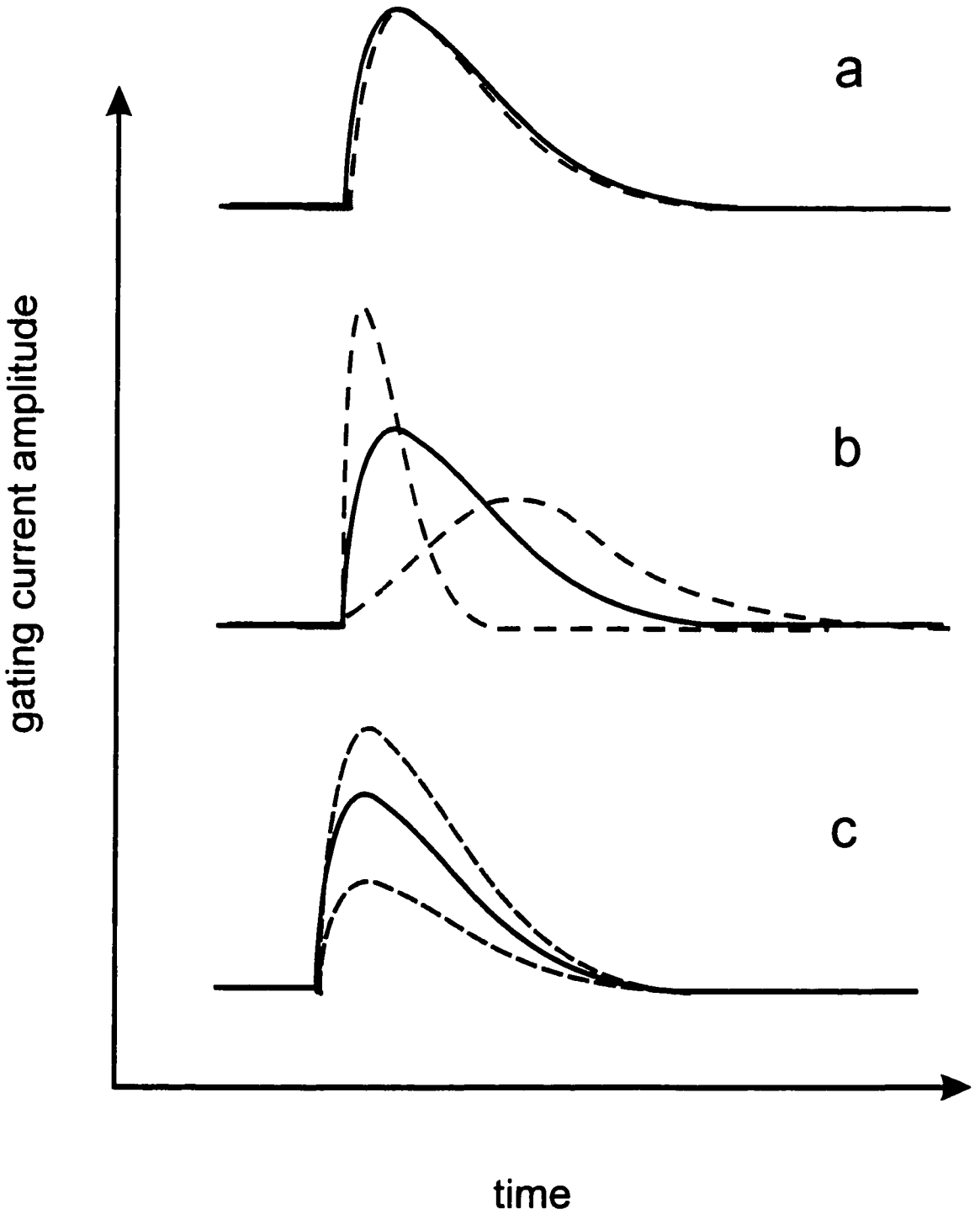
a
b
c
gating current amplitude
time

conductance without altering the gating currents (Perozo et al., 1993), should be expressed in *Xenopus* oocytes. In addition, gating currents should be measured in the absence of any permeant ions (Na^+ and K^+ ions should be replaced with N-methylglucamine NMG^+) (see Perozo et al., 1993). Furthermore, to maximize the resolution of gating current recording, a pre-hyperpolarized voltage pulse (-100 mV) should be given followed by a depolarized potential. The depolarized potential would be varied systematically to determine the proper experimental condition. As gating currents are very short, usually completed in a few milliseconds (Perozo et al., 1994), each voltage pulse duration will be set as 20 ms. Finally, 1s intervals should be used by returning V_m to the holding potential of -100 mV, which is necessary to allow the charged voltage sensor to get back to its resting state. During this 1s period, a series of small hyperpolarizing voltage steps will be applied. This recording procedure would be repeated six times to allow for signal averaging, and non-specific leakage currents and linear capacitive currents would be subtracted using the hyperpolarizing responses.

II. Does the native *Drosophila* cell environment provide mechanoprotection for Shaker?

It was observed that Shaker-IR is mechanosensitive when expressed in *Xenopus* oocytes by patch clamp recordings, but what makes a voltage-gated channel mechanosensitive under these conditions? Since wild-type Shaker and Shaker-IR are structurally different, it is necessary to test whether the wild-type Shaker exhibits mechanosensitivity when expressed in *Xenopus* oocytes. If no mechanical effect is found with the expressed wild-type Shaker, the structural differences between Shaker (with intact N-type inactivation) and Shaker-IR (without inactivation ball but with

1D4 epitope) may provide the structural basis in their different mechanical responses. Since the PSD binding motif TDV is located adjacent to the 1D4 epitope of Shaker-IR (**Fig. A-1** in Appendix), the presence of 1D4 epitope in Shaker-IR may prevent the PSD-TDV interaction. The different response to mechanical stimulation between these two constructs could indicate that Shaker-IR failed to be associated with the oocyte membrane cytoskeleton due to the presence of 1D4 epitope. This possibility could be tested by removing the 1D4 epitope from Shaker-IR or removing the TDV sequence from Shaker.

On the other hand, if Shaker (inactivation intact) is mechanosensitive when expressed in *Xenopus* oocytes, this would suggest that a different cellular environment in *Drosophila* muscle cells may provide the mechanoprotection. In our preliminary experiments (see Appendix), the addition of a linker (ankyrin) between the cytoskeleton and Shaker-IR seemed to attenuate mechanosensitivity. This finding could mean that in *Drosophila* muscle, some components (e.g. ß-subunit) may be required for linking Shaker to its cytoskeleton. The "*in situ*" condition in *Drosophila* could be reconstituted by coexpression of the Shaker ß-subunit together with Shaker α-subunit in *Xenopus* oocytes. If mechanosensitivity is abolished after ß-subunit expression, then ß-subunits may be required for protection of Shaker channels from the mechanical interference.

There are at least four classes of K^+ channels reported in *Drosophila* muscle, including Shaker, and one of the four, a voltage-insensitive channel was found to be stretch sensitive (Zagotta et al, 1988). However, the mechanosensitivity of Shaker was not specifically tested by the authors. Although Shaker may be protected from mechanical perturbation in its native environment, one needs to repeat the experiment in native *Drosophila* using the protocol established for oocytes. Based on our experience with Shaker-IR in oocytes, stretch effects should be examined at the foot of the

G-V curve. The foot of the G-V should be used for the two following reasons: first, we found that stretch-activation of Shaker-IR was most evident (see **Chapters 4** and **5**) in this voltage region, so the same might be true for Shaker. Second, native Shaker exhibits rapid inactivation at voltages near G_{max}, whereas the inactivation is relatively slow at the foot of the G-V curve (Zagotta et al., 1988).

Drosophila SA K^+ channels can be distinguished from SA components of Shaker using kinetic and pharmacological approaches. The kinetic approach utilizes Shaker's voltage- and time-dependent gating properties. Native Shaker is distinguished by the transient outward voltage-dependent current, which inactivates rapidly during sustained voltage pulses (Zagotta and Aldrich, 1990). In this way, Shaker currents can be distinguished from the endogenous SA K^+ (TREK-like) current in *Drosophila*. One of the pharmacological approaches can use a modified charybdotoxin (CTX, with high affinity for Shaker K^+ channel) to confirm that the stretch-induced currents are indeed carried by Shaker. The result would only be valid if a comparison is made within a given patch with or without CTX application, so an internally perfused pipette, allowing for exchange of external solution in inside-out patch recordings, would be needed. Also since Shaker is far more TEA sensitive than SA TREK-like channels (Small and Morris, 1995), these two channels could be distinguished by using a perfusion pipette with or without TEA added.

To test the mechanical effects on native *Drosophila* Shaker, V_m would be stepped to the foot of the G-V curve to elicit Shaker currents, then the same protocol would be repeated in response to mechanical stimulation. The stretch-activated component [a combination of endogenous SA K^+ (TREK-like) and Shaker, if it is stretch-activated] could be isolated by subtracting the Shaker currents. Since damage to the cortical cytoskeleton seems to enhance mechanosensitivity (Paoletti and Ascher, 1994; Small and Morris, 1994; Wan et al., 1999), chemical disruption by cytochalasin

or mechanical disruption through repeated mechanical stimulation could be tried to maximize the mechanical response of Shaker to stimulation. Again, this would maximize both SA K^+ and SA Shaker channel response, but the SA components of Shaker could be distinguished from other SA K^+ channels by their kinetic properties.

APPENDIX

Tethering a Voltage-gated Channel to the Membrane Skeleton: A Model for Studying the Mechanical Effects on Gating

INTRODUCTION

Mechanosensitive (MS) channels, found in almost all cell types tested with patch-clamp techniques, are those whose open probability (P_{open}) changes in response to mechanical stimulation (Morris, 1995). Although MS channels have been found ubiquitously distributed in various cell types, very few, if any, have been convincingly shown to function as a mechanotransducer. After over 10 years of study, the molecular mechanism of MS channel gating still remains unclear. Based on the biophysical and molecular biological studies in mechanosensory neurons of *Caenorhabditis elegans* and the acousto-vestibular system in vertebrates hair cells, it has been proposed that a channel's mechanosensitivity is dependent on channel-cytoskeleton interactions (Hudspeth, 1989; Huang et al., 1995). In brief, upon mechanical stimulation, the rigid connection between channel and cytoskeletal filamentous proteins (and/or extracellular attachment) is thought to produce a displacement that promotes channel opening. In other words, a specially tethered channel is thought to form the basis for the mechanosensory transduction (Bargmann, 1994).

It was further proposed that at least for eucaryotic MS channels, mechanical force might be transmitted to the channel via direct tethering to the membrane cytoskeleton (Sachs, 1997). Based on those studies, we hypothesized that a channel may acquire mechanosensitive components in its

gating when directly tethered to the membrane cytoskeleton. To test this hypothesis, a fusion protein named ShanX (**Fig. A-1**) was constructed using a voltage-gated channel tethered with a spectrin-binding moiety from the globular protein ankyrin. The entire spectrin-binding fragment of *Xenopus* ankyrin (~62 kD) was fused directly to the C-terminus of Shaker-IR, a voltage-dependent K^+ channel with its inactivation-ball removed from the N-terminal region (Δ amino acid 6-46).

The resulting Shaker-IR/ankyrin recombinant protein, called ShanX, and the "wild-type" Shaker-IR were then expressed in *Xenopus* oocytes and two-electrode voltage clamp was used to characterize the voltage-dependent gating properties. Although I consistently obtained a better expression with Shaker-IR than with the fusion protein ShanX, in the form of either earlier detection of channel activity or higher channel density, preliminary results showed that both Shaker-IR and ShanX expressed well in *Xenopus* oocytes and exhibited voltage-dependent outward currents. Since Shaker-IR channels are homotetramers, the successful expression of ShanX indicates that addition of 4 x 62 kD cytoplasmic globular proteins to Shaker-IR neither prevented the assembly of the channel nor disabled its fundamental gating behaviour.

After successful expression of Shaker-IR and ShanX in *Xenopus* oocytes, the voltage-dependent gating properties were characterized and compared between the two channel types. Some significant differences between Shaker-IR and ShanX in their voltage gating properties were found and are, reported here. In testing the possible acquisition of responses to mechanical stimulation by chimaeric ShanX, the cell-attached patch-clamp configuration was used with or without negative pressures applied to the recording pipette. Surprisingly, not only ShanX, but also the control Shaker-IR, exhibited responses to mechanical stimulation.

The observations reported in this **Appendix** led us to discontinue further studies on the

Figure A-1. Schematic diagram of primary structure for Shaker-IR and ShanX monomers

(a) The open reading frame of a Shaker-IR monomer is shown as a box. The Shaker-IR was modified by addition of an 8 amino acid epitope tag (1D-4) from bovine rhodopsin at the C-terminus for detection by a monoclonal antibody. Also adjacent AatII and SphI restriction enzyme sites were added at the C-terminus within the Shaker coding region (**, in box **a**) to provide convenient sites for the ligation of the spectrin-binding domain of ankyrin. Six membrane-spanning hydrophobic domains are shaded (S1-S6) and labelled. **(b)** ShanX is a combined construct with the entire 62 kD spectrin-binding domain of ankyrin from *Xenopus* oocytes fused at the C-terminal region.

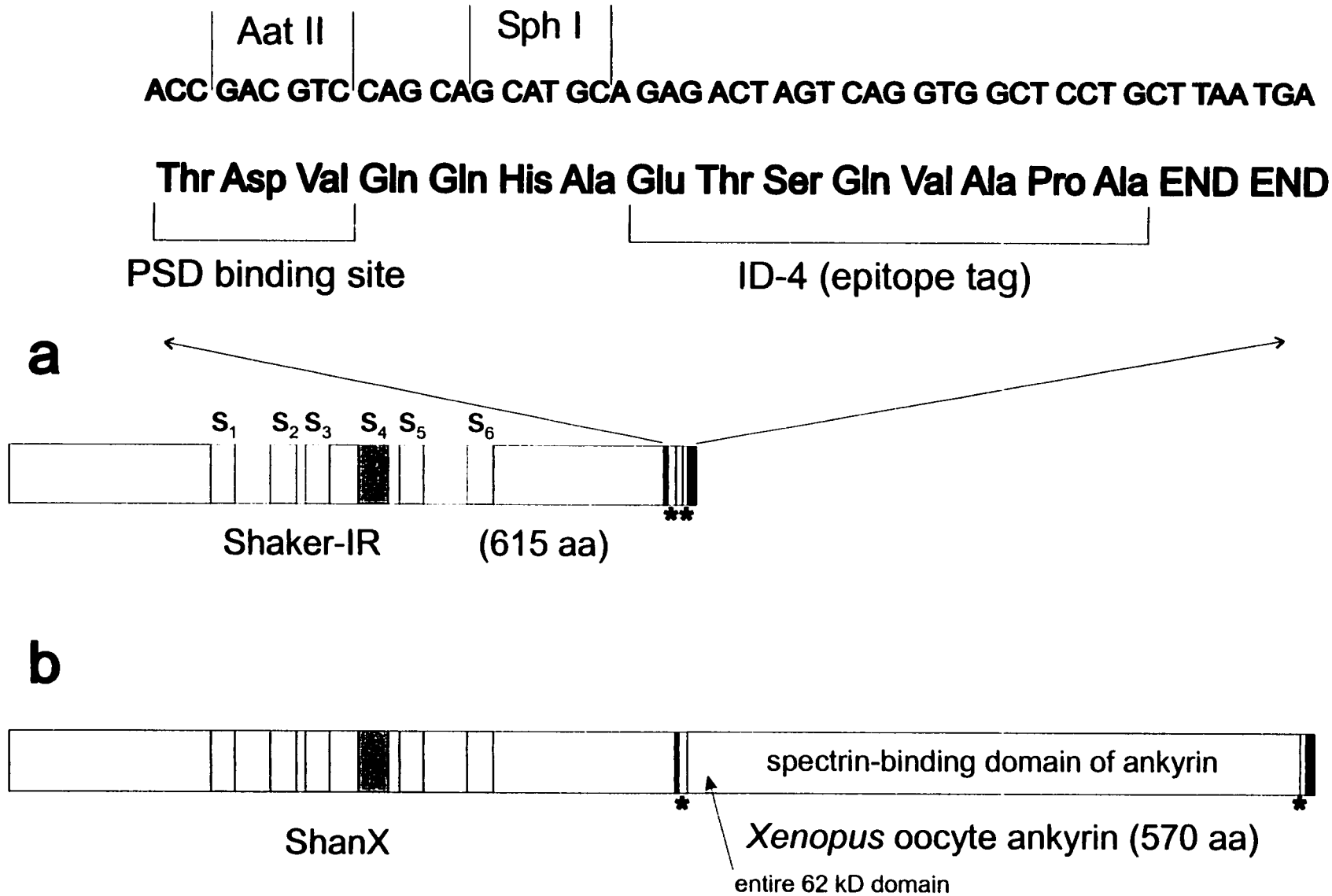
Aat II
Sph I
ACC GAC GTC CAG CAG CAT GCA GAG ACT AGT CAG GTG GCT CCT GCT TAA TGA
Thr Asp Val Gln Gln His Ala Glu Thr Ser Gln Val Ala Pro Ala END END
PSD binding site
ID-4 (epitope tag)
a
S1 S2 S3 S4 S5 S6
Shaker-IR
(615 aa)
b
spectrin-binding domain of ankyrin
ShanX
Xenopus oocyte ankyrin (570 aa)
entire 62 kD domain

chimaeric protein ShanX and inspired our interest in studying the effect of mechanical stimuli on Shaker-IR, as seen in the body of this thesis (**Chapter 3-5**). Nevertheless, I will report the major findings in this chapter of developing the chimaera and preliminary data regarding mechanical effects on both Shaker-IR and chimaeric ShanX since this approach may still have something to offer in the future.

COMPONENTS OF CHIMAERIC FUSION CHANNEL

I. Overview

For the purpose of testing electrophysiologically whether tethering would help to exhibit mechanosensitive gating components, it would be ideal to obtain a cloned MT channel to which a manipulable cytoskeletal filament attaches. Since there was no such channels available at the time, we developed a model system using available molecular components. The basic elements required for this artificial system include the filamentous proteins, a channel protein and a linker peptide in between. We chose the homotetrameric voltage-dependent channel Shaker-IR for the membrane channel based on the assumption that the endogenous spectrin in *Xenopus* oocytes would provide the filamentous tethering for a spectrin-binding protein, ankyrin, to be the linker between channel and spectrin cytoskeleton. All of these components were cloned about 10 years ago and have been well characterized at the molecular level (Schwarz et al., 1988; Winkelmann and Forget, 1993).

Interestingly, nature has made a somewhat comparable chimaera, a Shaker-like K^+ transport polypeptide from *Arabidopsis* (Sentenac et al., 1992). The predicted sequence of this K^+ transport system of 838 amino acid has three domains: a channel-forming region homologous to Shaker, a

cyclic nucleotide-binding domain and a large ankyrin-like domain of 195 amino acid at the C-terminus. Thus, the prospects of expression of a functional Shaker-ankyrin construct seemed good.

II. Spectrin: the filament

Spectrin (formally named fodrin in nonerythroid cells) is a linear filamentous α and β heterodimer, containing a 280 kD (α) subunit and a 246 kD (ß) subunit in human erythroid cells and in numerous other cell types (Giebelhaus et al., 1987). Each subunit is a chain of 22 (α spectrin) and 17 (ß spectrin) repeats of 106 amino acid (Luna and Hitt, 1992). There is a spectrin binding site on the N-terminal of the α-subunit for dimer association whereas binding sites for actin, band 4.1 and ankyrin are presented in three of the highly conserved regions in the ß-subunit, the N-, C- and the central 15th spectrin repeats respectively (Winkelmann and Forget, 1993).

The spectrin α- and ß-subunits are arranged in a head-to-head heterodimer. Without disassociating from one another, this heterodimer then forms a tetramer between the ß N-terminal and α C-terminal. Five or six tetramers are linked "radially" through a junction containing a rod of ≈ 13 actin monomers. Tetramers can produce oligomers and even supercoiled configurations through non-covalent interactions (**Fig. A-2a**). This structural characteristic is required for the flexibility and extensibility of the cytoskeleton (Luna and Hitt, 1992) and is crucial for maintaining the shape and integrity of the plasma membrane (Lambert and Bennett, 1993). However, this network is sensitive to mechanical stimulation, and can be transiently stretched and/or disrupted by tension (**Fig. A-2b**).

Figure A-2. Tension effects on erythrocyte membrane cytoskeleton

A portion of the intact erythrocyte membrane skeleton network is depicted: rope-shaped spectrin is composed of two structurally similar subunits, the α and ß subunits. White "ropes" represent α-spectrin and black "ropes represent ß-spectrin. Spectrin tetramers form a network using actin oligomers (beaded structure). On isolated spectrin skeleton oligomers, tension was induced during the process of critical point drying. Based on subsequent observation by transmission electron microscopy, schematic diagram **(a)** depicts the interactions between spectrin oligomers in the native membrane skeleton. Application of membrane tension **(b)** is indicated by the large arrows. Small arrows indicate the "torque" force on spectrin in response to the membrane tension and unwinding of spectrin. An integral membrane protein bound to, say, the ß-subunit of spectrin, should transmit torque forces it experienced to the membrane protein. At very high tension, laterally associated filaments separated completely; an arrowhead points to an α-spectrin filament that has detached at its tail end from ß-spectrin (from Ursitti and Wade, 1993).

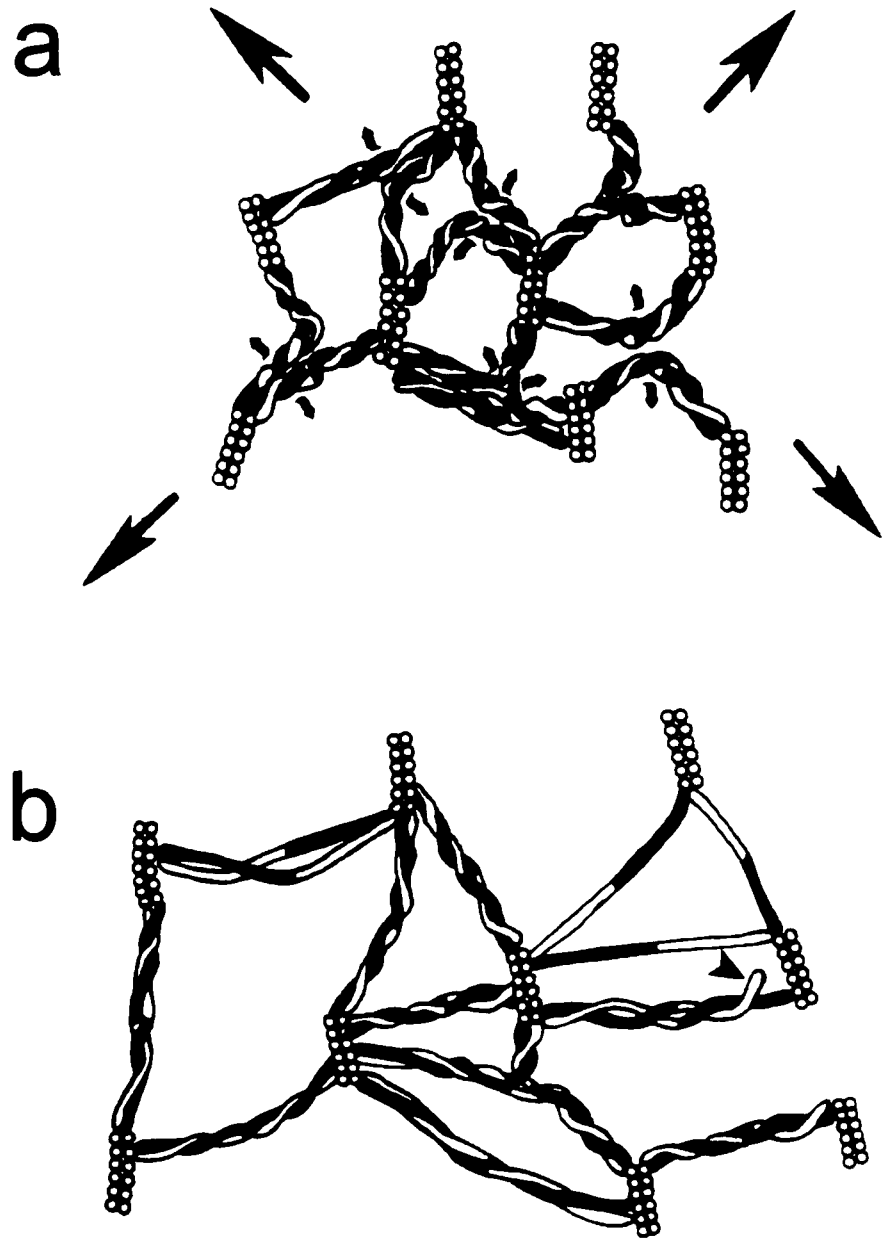
a
b

III. Ankyrin: the linker

Many channels and transporters are localized and clustered at specific subcellular sites by linking to membrane cytoskeleton via ankyrin-spectrin interactions. For instance, the segregation of voltage-dependent Na^+ channels to presynaptic terminals, and to nodes of Ranvier through the ankyrin-spectrin network can increase the channel density at these sites (Srinivasan et al., 1988).

Structually, ankyrins are spectrin-binding globular proteins located at the cytoplasmic surface of the plasma membrane with recognition sites for both membrane spanning integral membrane proteins and cytoplasmic spectrin-based network (Bennett, 1992). Functionally, the best studied example is the association of ankyrin with an erythrocyte anion exchanger, which provides a mechanical resilience and flexibility to the membrane. This linkage is crucial for protecting the structural integrity of circulating erythrocytes and enabling them to survive ~120 days in spite of the shear stress (Luna and Hitt, 1992).

Erythrocyte ankyrin is a globular 207 kDa monomer containing three major domains: a central 62 kD spectrin-binding domain, a N-terminal 90 kD membrane protein binding domain and a C-terminal 55 kD regulatory domain. The linear structure was mapped from ankyrin subfragmentation by proteolytic cleavage and binding assays (Lambert and Bennett, 1993). The ability of ankyrin to bind to the membrane skeleton is dependent on the central 62 kD peptide domain which binds to the ß-subunit of spectrin heterodimer. Therefore, the 62 kD spectrin-binding domain was used to ensure that ankyrin would bind to the *Xenopus* spectrin cytoskeleton. The *Xenopus* oocyte form of ankyrin was cloned from a *Xenopus* oocyte cDNA library and the DNA coding for the 62 kD domain was subcloned into the C-terminal of Shaker-IR to form our own chimeric channel ShanX. Platt et al (1993) tested the affinity of binding of the human 62 kD domain

to spectrin using a ligand blot assay. It was found that this 62 kD fragment competitively inhibits spectrin binding to the full length of ankyrin with a K_i of 10^{-7} M. Although the smallest ankyrin fragment known to bind spectrin is a 12-kD tryptic peptide within the 62 kD domain, we choose to use the 62 kD ankyrin fragment as the 12 kD fragment binds to spectrin with a 1/10 lower affinity (Platt et al., 1993).

The N-terminal 89 kD domain of ankyrin also exhibits special functional properties. Its conserved 22 tandem 33 amino acid repeats are important for interacting with a variety of integral membrane proteins. This 89 kD domain interacts with band 3, Na^+-K^+ ATPase (Morrow et al., 1989), Na^+-Ca^{2+} exchanger (Li et al., 1993) and most importantly, the voltage-dependent Na^+ channel with high affinity (K_d = 22 nM). A subdomain of this 89 kD N-terminal domain containing 11 of the 22 tandem 33 amino acid repeats binds to the Na^+ channel with a lower affinity (K_d = 63 nM, Srinivasan et al., 1992). Ankyrin not only associates with the voltage-dependent Na^+ channel *in vitro* but co-localizes with spectrin molecules at the nodes of Ranvier, axonal initial segments, and the neuromuscular junctions (Srinivasan et al., 1988). From the binding of Na^+ channels to spectrin via ankyrin, the channels are immobilized and clustered at the nodes of Ranvier with a high density (Lambert and Bennett, 1993). Because we artificially fused the spectrin-binding moiety of ankyrin directly to the channel protein, this 89 kD N-terminal domain was not included.

Neither included in our fusion protein was the C-terminal 55 kD domain of ankyrin, a regulatory domain which modulates the binding activity of both the 62 kD spectrin-binding and 89 kD membrane-binding domains (Davis et al., 1992). The smaller ankyrin protein derived by deleting part of the C-terminal region results in three times higher binding affinity for spectrin (Hall and Bennett, 1987; Lambert et al., 1990). This property offers a good reason for using a reduced ankyrin

fragment in constructing chimaeric channel ShanX as it might maximize the binding affinities. Moreover, a shorter linker between the channel and spectrin may provide a reasonable chance of forming a rigid linkage with fewer degrees of freedom. This was deemed desirable because it might allow the mechanical energy to be delivered to the channel more directly; a long flexible linker might serve as a shock absorber and prevent mechanical force delivery (see rationale below).

Multiple isoforms of ankyrin are present in human erythrocytes, brain and other tissues (Kordeli et al., 1990). Up to now, four human ankyrin genes, isoform I-IV, for erythrocyte ankyrin, brain ankyrin, "general" ankyrin, and node of Ranvier ankyrin, have been identified based on the distribution properties (Chan et al., 1993; Kordeli et al., 1995). Sequence analysis revealed that the 62 kD spectrin-binding domain was highly conserved among those ankyrin isoforms with a 90% amino acid identity.

Since the spectrin family of cytoskeletal proteins also has multiple isoforms which differ in cellular expression and localization in various cell types (Winkelmann and Forget, 1993), and each ankyrin isoform binds preferentially to a specific isoform of spectrin, we constructed a fusion protein with a specific ankyrin isoform designed to match (i.e. bind well) the specific spectrin isoform in the expression system. To achieve this optimization, Dr. Peter Juranka in our laboratory isolated an isoform of ankyrin cDNA from *Xenopus* oocyte. We expected that the chimaeric ShanX containing the spectrin-binding domain of *Xenopus* oocyte ankyrin would bind to *Xenopus* oocyte spectrin with a binding affinity comparable to that of the native linkage.

IV. Shaker-IR: the channel

The voltage-dependent Na^+, Ca^{2+}, and K^+ channels control the permeability of cells to specific

ions by their opening or closing activities in response to changes of the membrane potential. To test the hypothesis that any arbitrary channel would be susceptible to changes in P_{open} during mechanical stimulation when tethered rigidly to the membrane skeleton, Shaker-IR, a modified Shaker channel with its "inactivation-ball" removed from its N-terminal, was used for constructing our fusion protein ShanX. Reasons for using Shaker-IR were covered in **Chapter 3**.

RATIONALE

Channels may exhibit mechanosensitivity when directly and rigidly linked to a spectrin network. This hypothesis is based on the finding that, in an isolated spectrin network, mechanical tension can make the spectrin twist as the network extends (**Fig. A-2**). Because channels are confined to the plane of membrane bilayer, any rotating spectrin filaments with a channel bound to it could convey mechanical torque to channels. The channel constructs were expected to exhibit an altered gating in responses to mechanical perturbation for the following reasons.

I. A possible rigid and high affinity linkage

As mentioned above, native ankyrin / spectrin transporter linkages are of high enough affinity to withstand extremes of shear in circulatory erythrocytes. Ideally, we would expect to create a high affinity rigid linkage between the fusion protein and the spectrin network. The ankyrin biochemistry (reviewed above) did not indicate that the absence of the C- and N-terminal regions would lower the affinity. Moreover, with the channel tethered to spectrin, mechanical tension conveyed directly from "mechanically-loaded" spectrin should not be dissipated before being felt by the channel.

II. Contributions of adjacent transmembrane segments to the S4 gating

To reduce the energetic cost of placing charges in a low dielectric lipid bilayer, it has been proposed that positively charged residues in S4 are stabilized by forming ion pairs with negatively charged residues at the adjacent transmembrane segments (Catterall, 1986; Durrell and Guy, 1992). These positively charged residues in S4 interact electrostatically with only three negatively charged residues, two in S2 and one in S3, indicating that these charged residues may detect changes in membrane potential and may play a role as a voltage sensor (Papazian et al., 1995). During membrane depolarization, the S4 segment of the voltage-dependent channel, moves outward prior to channel opening (Yang and Horn, 1995 and Larsson et al., 1996). The channel conducting pore, S5 and S6 transmembrane loop and S4-S5 cytoplasmic loop, are located in the centre of the Shaker-IR channel (Liu et al., 1997).

With one of the Shaker-IR transmembrane segments (S6) tethered directly to the underlying cytoskeleton network through a covalently linked ankyrin (**Fig. A-3**), we hypothesize that if mechanical stimulation could displace or destabilize S6, the mechanical stimulation may disturb the interactions between S4 and its adjacent transmembrane segments. Since hydrophobic interactions are also important in S4 stability, mechanical stimulation causing a movement of any region of the channel protein relative to the immediate environment might affect the conformational stability of S4.

Figure A-3. Model of channel / ankyrin linkage via ankyrin-spectrin network

(a) Ankyrin's N-terminal domain (N) binds to the channel, its spectrin binding domain (S) binds to the β subunit of the spectrin. It also has a regulatory C-terminal (C) domain. The native Na^+ channel /spectrin tethering is depicted here. **(b)** Chimeric Shaker / ankyrin model: a direct linkage between a Shaker-IR subunit and spectrin is depicted. As Shaker-IR forms homotetrameric channels, each subunit would carry one ankyrin fragment, but for simplicity, only one ankyrin fragment is shown fused to one Shaker-IR subunit.

a Native situation

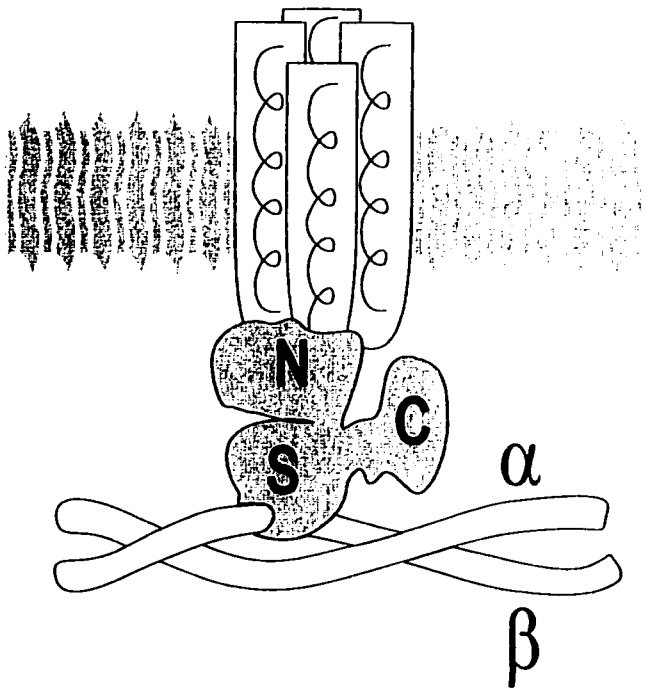

b Fusion channels

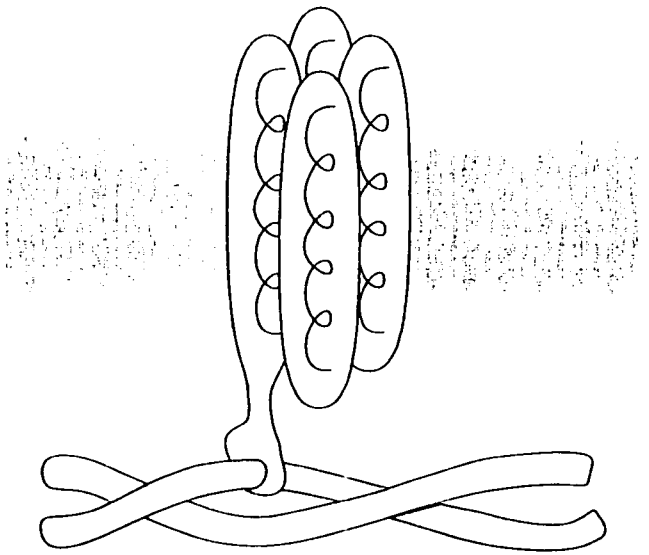

HYPOTHESIS

Channels bound directly to the spectrin cytoskeleton may exhibit a mechanosensitive P_{open}.

METHODS

I. Preparation of Shaker-IR and ShanX cRNA

Molecular biology preparations including the chimaeric construct and subcloning of Shaker-IR and ShanX into different vectors were carried out by Dr. Juranka in our laboratory. A detailed procedure of Shaker-IR cRNA preparation is included in **Chapter 2**.

Chimeric channel ShanX contains *Shaker*-IR plus the entire 62 kD spectrin binding domain of *Xenopus* oocyte ankyrin (**Fig. A-1**). Briefly, the adjacent AatII and SphI restriction enzyme sites at the C-terminus of Shaker-IR (*, see **Fig. A-1**) were used to ligate the entire spectrin binding fragment of *Xenopus* oocyte ankyrin. The *Xenopus* ankyrin fragment was cloned by screening a cDNA library kindly provided by Dr. Melton from Harvard University. Since the forward and reverse PCR primers for the *Xenopus* oocyte ankyrin have the AatII and SphI sites, the PCR products of ankyrin were cut and ligated into the AatII/SphI-cut Shaker-IR cDNA, which was then subcloned into "the Melton expression vector", a modified pSP64TM (**Chapter 2**). This vector totally replaced the *Drosophila* 5'UTR of Shaker-IR and ShanX with *Xenopus* ß-globin 5'UTR and also added *Xenopus* β-globin 3'UTR sequences, thus generating cRNA that is *Xenopus* oocyte friendly. The successful creation of the chimaeric construct was confirmed by restriction mapping and by dideoxy

sequencing across the splicing sites. Finally, these vectors were linearized and *in vitro* transcription was performed.

II. Heterologous expression in *Xenopus* oocyte (Chapter 2)

III. Two-electrode voltage clamp and cell-attached patch-clamp (Chapter 2)

RESULTS

I. Functional expression of Shaker-IR and ShanX in *Xenopus* oocytes

Two to six days after injection, the voltage-dependent and mechanosensitive gating properties of the ShanX chimaera were tested and compared with those of Shaker-IR. With the pSP64TM expression vector, a nearly 100% success of channel expression in *Xenopus* oocytes was obtained via cytoplasm cRNA microinjection. Both Shaker-IR (**Fig. A-4a and 4c**) and the chimeric channel ShanX (**Fig. A-4b and 4d**) expressed well in *Xenopus* oocytes, as recorded by either two-electrode voltage clamp (**Fig. A-4a and 4b**) or cell-attached patch clamp recordings (**Fig. A-4c and 4d**). As shown, cRNA encoding ShanX gave rise to voltage-dependent channel currents at a similar current level as with Shaker-IR. As early as one day after cRNA injection, two-electrode voltage clamp started to show adequate currents in both Shaker-IR and ShanX-injected oocytes (**Fig. A-4a and 4b**). The currents of both channel types were still evident at day seven. However, based on the currents measured with cell-attached macropatch recordings, Shaker-IR current was observed one day post-

Figure A-4. Expression of Shaker-IR and ShanX in *Xenopus* oocytes

Families of voltage-dependent outward currents were recorded from Shaker-IR- (left panels) or ShanX-injected oocytes (right panels) using two voltage clamp configurations: TEVC (**a, b**) and cell-attached patch-clamp recordings (**c, d**). For TEVC, the holding potential (V_h) was -100 mV and steps were 10 mV apart. For cell-attached patch clamp, the V_h was ~-80 mV and steps were 5 mV apart.

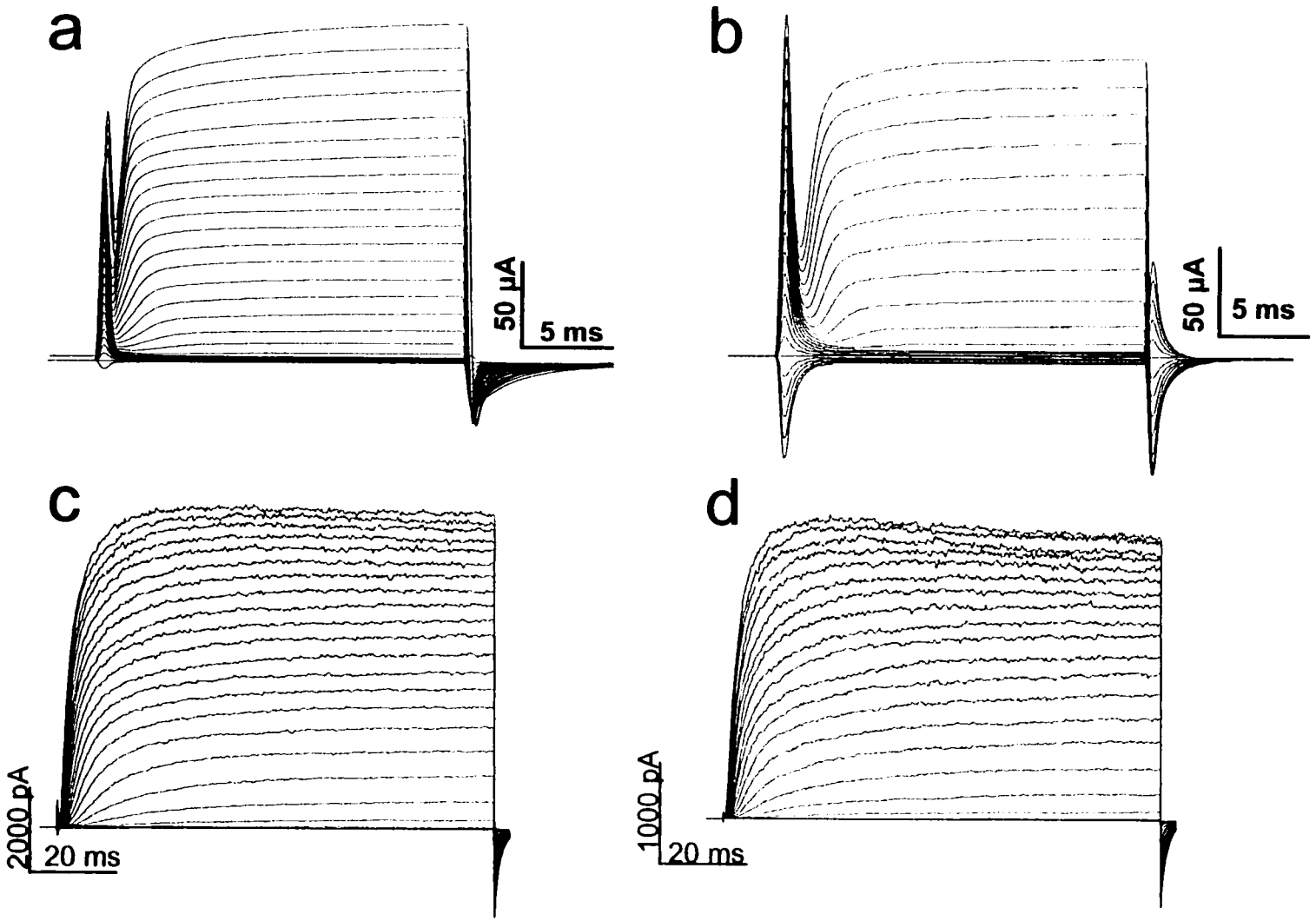
a
50 µA
5 ms
b
50 µA
5 ms
c
2000 pA
20 ms
d
1000 pA
20 ms

injection whereas ShanX was more variable and usually took two days to reach a similar current level, indicating an earlier expression and higher channel density with Shaker-IR than with ShanX. Higher variability of current amplitude between patches after ShanX than after Shaker-IR injection suggest that the chimaeric protein was more inhomogeneously distributed in a given oocyte.

Since Shaker-IR and, presumably, ShanX, is a homotetramer, one chimeric subunit with one ankyrin fragment would consequently give rise to a channel-ankyrin in stoichiometry of 1:4. The successful expression of ShanX as shown above suggests that 4 x 62 kD of cytoplasmic globular protein does not prevent assembly of the channel, and, as shown below, does not disable its fundamental gating properties. Evidently, the "ankyrin loading" of the channel did not affect the proper folding and insertion of the transmembrane segments of the channel.

II. Confirmation of expression by analysis of biophysical properties

The successful expression of Shaker-IR and ShanX can be confirmed by analysis of the characteristic voltage-dependent gating properties, as shown in the following.

A. Voltage-dependent activation

To determine if ShanX was a voltage-dependent channel comparable to Shaker-IR, voltage clamp was performed as described for Shaker-IR (**Chapter 3**) and the steady-state conductance was calculated and plotted as a function of voltage. Like any other voltage-dependent channels, both constructs yielded G-V curves which fits well to the Boltzmann function (see **Chapter 3** for equation). A typical example is shown in **Fig. A-5a**, indicating that the ShanX protein behaved as a typical voltage-dependent channel. **Fig. A-5b** shows these curves superimposed along with data from a water injected control oocyte.

Figure A-5. G-V curves of Shaker-IR, ShanX and control

Sample G-V curves for **(a)** Shaker-IR, **(b)** ShanX and their fits (solid line) to a Boltzmann function. To emphasize the similarities and the differences, two comparable plots plus water-injected controls are superimposed in **(c)**.

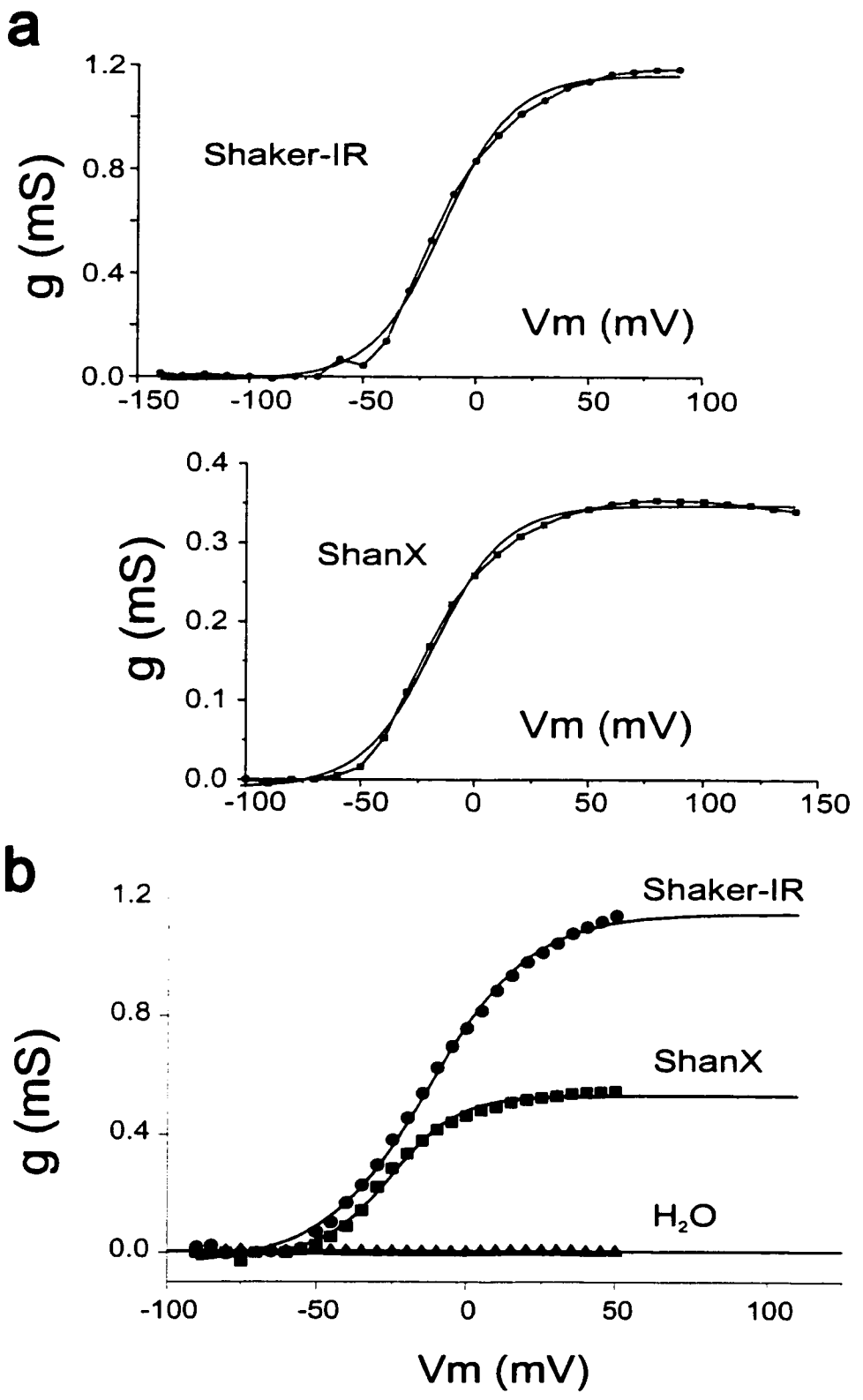
a
1.2
0.8
0.4
0.0
g (mS)
Shaker-IR
Vm (mV)
-150
-100
-50
0
50
100
0.4
0.3
0.2
0.1
0.0
g (mS)
ShanX
Vm (mV)
-100
-50
0
50
100
150
b
1.2
0.8
0.4
0.0
g (mS)
Shaker-IR
ShanX
H2O
-100
-50
0
50
100
Vm (mV)

To quantitatively compare the voltage-dependent gating properties of ShanX with Shaker-IR, data like that in **Fig. A-5** were obtained from many oocytes over 2-6 days post-injection. From fitting the Boltzmann function to the G-V data, three parameters: G_{max}, V_{50} and slope factor were extracted and compared (see **Chapter 3**) between ShanX and Shaker-IR. G_{max} of ShanX (0.4 ± 0.04 mS, n = 41) was significantly smaller ($p<0.01$) than that of Shaker-IR (1.1 ± 0.07 mS, n = 24), indicating that less than one half as much functional chimaeric protein was present in ShanX-injected oocytes plasma membrane compared with Shaker-IR over the entire 2-6 days expression time. Although the same amount of both cRNAs (same concentration and same volume) was injected, the smaller G_{max} indicates that less ShanX than Shaker-IR was expressed or perhaps that ShanX was more rapidly degraded than Shaker-IR or did not traffic to the surface as well.

The slope factor relates to the channel's gating charge or sensitivity of the voltage-dependent channels (Papazian et al., 1991). A slope factor was also found to be significantly different ($p<0.01$, paired and unpaired t-test), 12 ± 0.4 mV for Shaker-IR (n =24) and 17 ± 0.5 mV for ShanX (n =41), indicating a slightly lower voltage sensitivity for ShanX over Shaker-IR.

The third parameter, mid-point (V_{50}), provides an estimate of the stability of the open and/or closed states of the channels as a function of voltage. A positive shift (toward more depolarized potential), for some reference voltage, indicates that channels are stabilized at the closed state whereas a negative shift indicates a stabilization of the open state. In other words, change in V_{50} indicates an alteration of the equilibrium distribution between the open/closed channel states and hence a shift in the channel's voltage-dependence (Papazian et al., 1991). In contrast to differences seen with G_{max} and the slope factor, V_{50} showed no significant difference between ShanX (-21 ± 0.5 mV) and Shaker-IR (-21 ± 1.4 mV).

B. Ion-selectivity

As discussed in **Chapter 3**, Shaker-IR has many functional properties, a voltage sensor, a gate and an ion permeation pore, all thought to involve discrete protein domains. These domains may not, however, be mutually exclusive. Mutations of the pore-region residues in Shaker-IR result in shifting of the voltage-dependence of activation as well as in changes of ion selectivity (Zheng and Sigworth, 1997). As ShanX is composed of Shaker-IR and the spectrin-binding fragment of ankyrin, it should share the same conducting property and ion selectivity as that of Shaker-IR, but this needed confirmation.

To determine whether the outward currents recorded from ShanX-injected oocytes was K^+ selective as expected for a voltage-dependent channel, V_{rev} for chimaeric ShanX was determined and compared with that of the wild-type channel Shaker-IR using a tail current protocol (**Chapter 3**). If the outward currents of ShanX were carried by K^+, then the V_{rev} should be at the equilibrium potential for K^+ with the signature exponential decay, a shared gating property of all K^+ channels (Heginbotham and MacKinnon, 1993).

Using a tail-current protocol, currents by two-electrode voltage clamp were generated after an initial depolarizing pulse to +20 mV (for instance), then currents relaxed gradually towards the steady-state at given test potentials in a characteristic time course. **Fig. A-6** is a representative tail current from Shaker-IR (**Fig. A-6a**) or ShanX (**Fig. A-6b**) cRNA-injected oocytes. From the measurement of the steady-state tail currents, the V_{rev} values for Shaker-IR and ShanX were defined either from the tail current I-V relations (**Fig. A-6**, right panels) as the point at which straight lines between the measured values crossing the abscissa or simply from the current traces (**Fig. A-6**, left panels) at which the tail current starts reversing. Oocytes injected with ShanX cRNA had a V_{rev} of

Figure A-6. ShanX has the same V_{rev} as that of Shaker-IR

Examples of TEVC tail currents (left), and their I-V relations (right). **(a)** Shaker-IR and **(b)** ShanX. V_m was first stepped from a holding potential of -100 mV to +20 mV, then returned to various test potentials between +20 and -100 mV. No linear current subtraction was done. The V_{rev} was assessed both from the current traces (horizontal arrows) and from steady-state tail currents I-V curve. Currents used to generate the I-V relations were measured 40 ms after the second step (arrowheads). expressed Shaker-IR and chimaeric ShanX are K^+ selective.

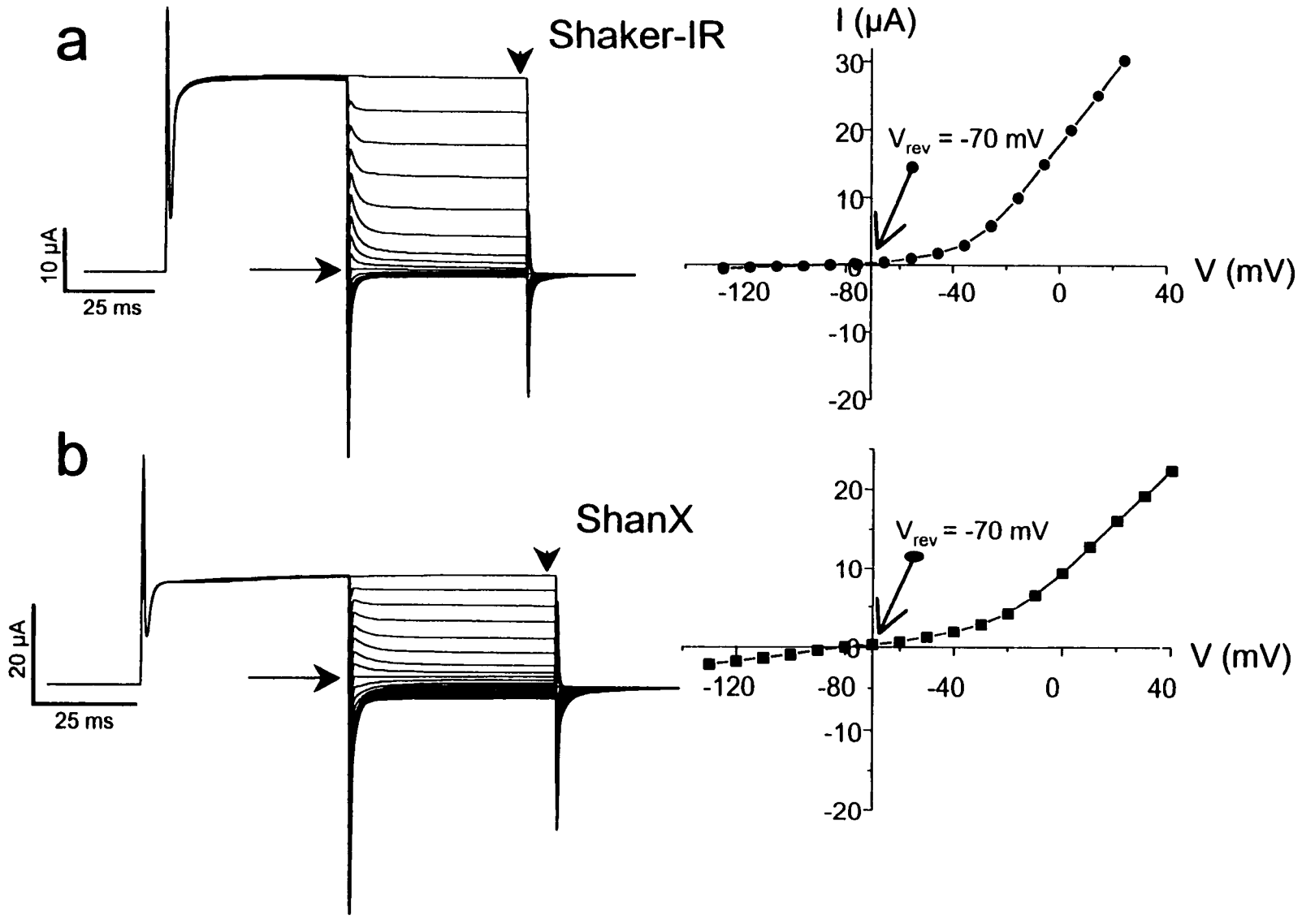
a
Shaker-IR
10 µA
25 ms
I (µA)
30
20
10
-10
-20
V_{rev} = -70 mV
-120
-80
-40
0
40
V (mV)
b
ShanX
20 µA
25 ms
20
10
-10
-20
V_{rev} = -70 mV
-120
-80
-40
0
40
V (mV)

-72 ± 1.2 (n = 41) mV whereas Shaker-IR cRNA injected oocytes had a V_{rev} of -70 ± 1.4 mV (n = 24). Thus, the observed V_{rev} for Shaker-IR and chimaeric protein ShanX were not significantly different ($p > 0.05$) from each other and were comparable to the value for Shaker-IR expressed in *Xenopus* oocytes (Hoshi et al., 1990, **Chapter 3**). In conclusion, these results demonstrate that the

III. Mechanical stimulation on Shaker-IR and ShanX currents

Having established that ShanX was a voltage-dependent K^+ channel, various protocols for testing the effects of mechanical stimulation on ShanX were attempted using Shaker-IR as a control. Results presented in **Chapter 4 and 5** demonstrated that the control, Shaker-IR, exhibited mechanosensitivity. Results shown in this **Appendix** were actually from experiments done prior to much of the work presented in previous chapters. At that time, it was not yet clear that the control was mechanosusceptible and emphasis was put on the chimaeric channel ShanX. To test the susceptibility of the channels to mechanical perturbation of their voltage-dependence, current amplitude was measured from oocytes before, during and after mechanical stimulation. Shaker-IR-injected or non-injected oocytes were used as controls. Cell-attached patch clamp was used rather than TEVC since this configuration would allow us to apply mechanical stimulation by stretching the membrane through the recording pipette. To exclude any effects from the endogenous MS channels in oocytes, 100 μM gadolinium (Gd^{3+}), an MS channel blocker, was applied in the pipette solution. To further ensure the elimination of these endogenous MS currents, membrane potential was stepped to the assumed V_{rev} of the MS channel, ~ 0 mV. Under these conditions, the currents were measured with or without mechanical stimulation.

As predicted, non-injected oocytes showed only capacitative and very small leak currents

with no evidence of voltage-dependent or MS channel activity. A typical example is shown in **Fig. A-7a**. In response to mechanical stimulation, no endogenous MS currents were recorded in the presence of 100 μm Gd^{3+} and suctions near membrane rupture did not induce any responses from the non-injected oocytes ($n > 30$), excluding the possibility of contamination by these endogenous MS channels to the detection of mechanical effects. In comparison with the non-injected oocytes, with the same recording protocol, voltage-dependent outward currents were detected from both Shaker-IR and ShanX-injected oocytes. Although not consistent from patch to patch, these currents nevertheless seemed to respond to mechanical stimulation, that is, suction either increased or decreased current amplitudes, in a pressure-dependent manner. **Fig. A-7** illustrates, for Shaker-IR **(7b)** and ShanX (**7c**), examples of apparent stretch-activation, where increasing suction from 0 to -20 mmHg suction (in 10 mmHg increments with 2-5 s of rest between mechanical stimuli) increased current amplitudes. Upon releasing suction, the currents returned partially to the original level.

To compare the mechanical effects on Shaker-IR and ShanX, the ratio of steady-state current amplitudes were calculated (the current amplitudes at different suction steps minus the current amplitude without suction) from all patches and plotted as a function of applied suction (negative pressures). For these "dose-response" curves, expected mechanical effects can be described as: 1) no mechanical effect, the current difference were the same at all suction steps, hence a flat line at 0 pA; 2) stretch-activation, suction increases the current amplitudes in a pressure-dependent manner, positive slope and 3) stretch-inactivation, suction decreased current amplitude, negative slope. As shown in **Fig. A-8**, both Shaker-IR and ShanX were inconsistent in their response from patch to patch, but consistent within any given patch to mechanical stimulation, with some patches showing no response, some patches showing stretch-activation whereas some patches showing -inactivation.

Figure A-7. Macropatch currents of Shaker-IR and ShanX with mechanical stimulation

Current traces from three different oocytes (**a:** uninjected; **b:** Shaker-IR; **c: ShanX**) under cell-attached patch clamp are illustrated Patches were stepped to V_m = 0 mV with or without suction following sequences of 0 mm Hg (control), -10 mmHg, -20 mmHg and 0 mmHg (release). Normal frog ringer solution was used in both pipette and bath solution except that 100 μM Gd^{3+} was added in the pipette.

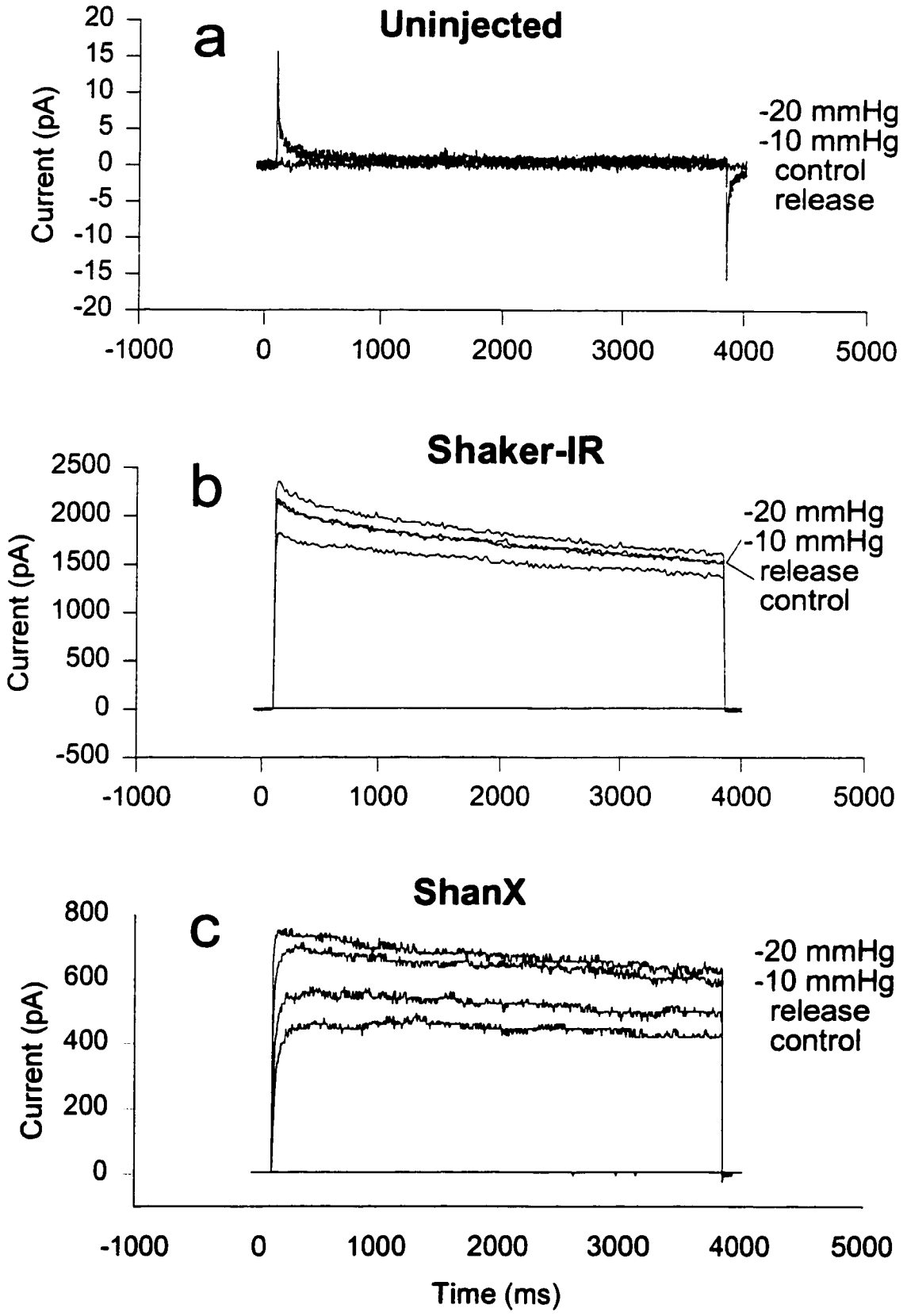
a
Uninjected
Current (pA)
20
15
10
5
0
-5
-10
-15
-20
-1000
0
1000
2000
3000
4000
5000
-20 mmHg
-10 mmHg
control
release
b
Shaker-IR
Current (pA)
2500
2000
1500
1000
500
0
-500
-1000
0
1000
2000
3000
4000
5000
-20 mmHg
-10 mmHg
release
control
c
ShanX
Current (pA)
800
600
400
200
0
-1000
0
1000
2000
3000
4000
5000
Time (ms)
-20 mmHg
-10 mmHg
release
control

Figure A-8. Susceptibility to mechanical interference of Shaker-IR and ShanX

Current differences (relative to control) were obtained with cell-attached patch clamp recordings for **(a)** Shaker-IR and **(b)** ShanX as a function of the applied negative pressures from 0 to -50 mmHg. Pressures beyond the depicted points indicate that leak had suddenly increased and/or the seal had ruptured. Each plot represents the mechanical response from a single patch, all patches were at a membrane potential range from ~ -20 to +20 mV. The zero level indicates no mechanical effects, positive values represent stretch-activation whereas negative value represents stretch-inactivation. Steeper slopes indicate higher mechanosensitivity. 100 μM Gd^{3+} in the pipettes.

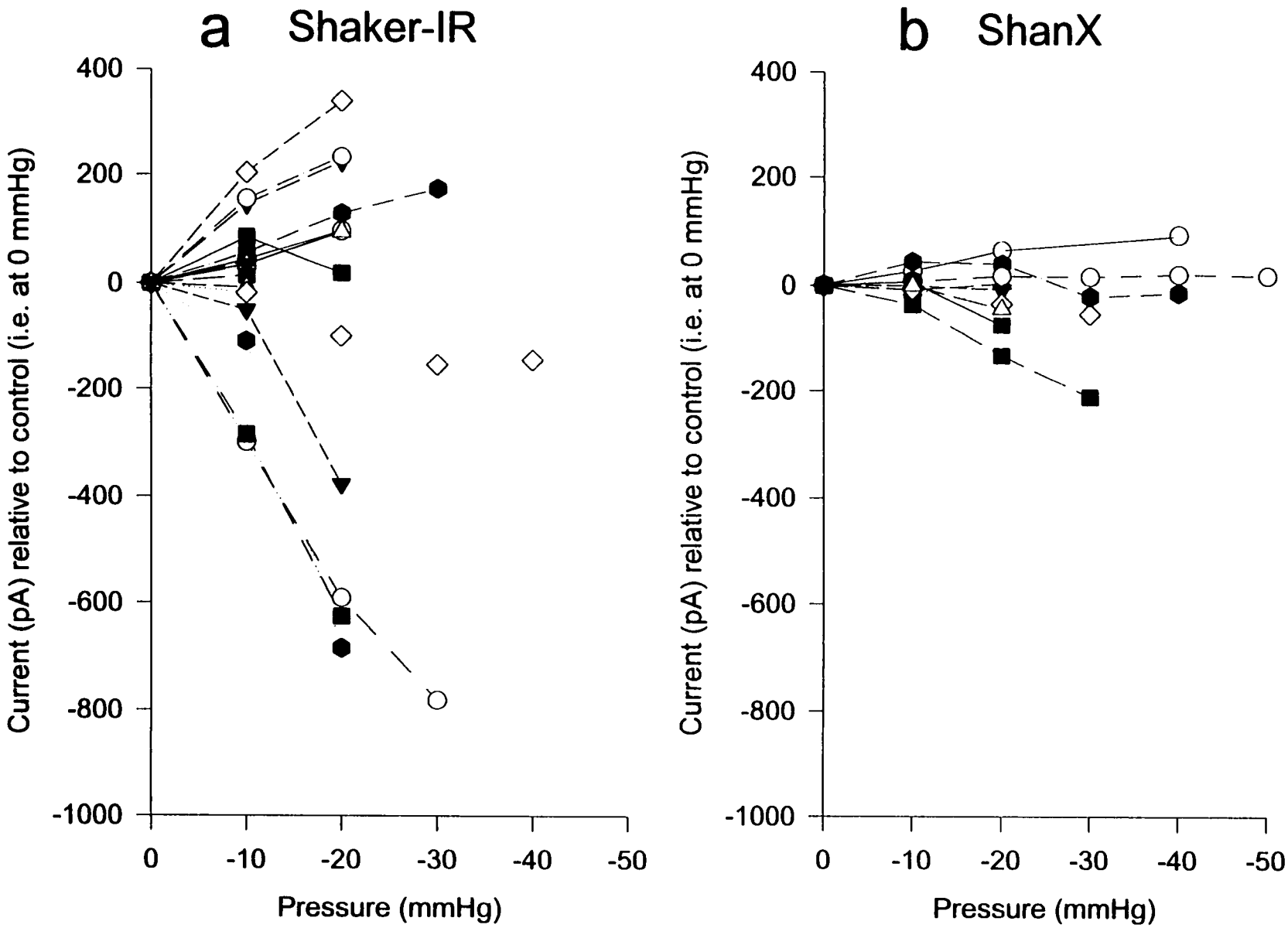
a Shaker-IR
b ShanX
Current (pA) relative to control (i.e. at 0 mmHg)
400
200
0
-200
-400
-600
-800
-1000
0
-10
-20
-30
-40
-50
Pressure (mmHg)

The slope of the plots represents the mechanosensitivity, since the steeper the slope, the bigger the mechanical effects. By this criterion, and contrary to prediction, Shaker-IR was more susceptible to mechanical stimulation than ShanX. For a total of 12 Shaker-IR-injected oocytes, 6 patches showed stretch-activation, 5 showed stretch-inactivation and 1 showed no consistent effect. Whereas for a total of 9 ShanX-injected oocytes, 2 showed stretch-activation, 4 showed stretch-inactivation and 3 patches showed either no or has inconsistent effects.

Although there were no specific predictions about how membrane stretch would impact on ShanX's voltage-dependent gating, the general expectation held was that Shaker-IR, the control model, should exhibit no mechanosensitivity since no stretch sensitivity was reported for Shaker in its native membrane under conditions that activated native membrane SA K^+, the TREK type channels (**Chapter 1, Table 1-1**, Zagotta et al., 1990; Gorczyca and Wu., 1991). This preliminary data was therefore both confusing and surprising, and necessitated the shifting of our focus to Shaker-IR.

IV. Mechanical effects on Shaker-IR and ShanX co-injected oocytes

Since "wild-type" Shaker-IR seemed to be more susceptible to mechanical perturbation than ShanX, we wondered if ShanX channels might interfere with each other, resulting in a failure of any linkage to the spectrin skeleton. We therefore co-expressed Shaker-IR and ShanX in *Xenopus* oocytes. Because Shaker-IR expressed better than ShanX, ratios of Shaker:ShanX 1:2 and 1:1 were used. Twenty-eight cell-attached patches (one or two per oocyte) were studied (1:1, n =12, 1:2, n =16). The membrane potential was held near the reversal potential of endogenous MS cation channels while steps of suction were applied.

As illustrated in **Fig. A-9**, both stretch-activation and - inactivation were observed, similar to previous findings. Most patches (70%) exhibited stretch-activation whereas others showed stretch-inactivation, regardless of the coinjection ratio. **Fig. A-9** illustrates mechanical effects on two sample oocytes, one (**9a**) shows the largest stretch-inactivation and the other (**9b**) shows the largest stretch-activation, among all 28 patches tested under the above experimental condition.

Shaker-IR alone produced similar effects. While continuing to search for appropriate conditions for testing mechanical effects, Shaker-IR currents were elicited at different voltages then stretched was applied. It was noted that the stretch-activation became consistent at voltages near the foot of the G-V curve. **Fig. A-9c** shows the mechanical effects on the steady-state Shaker-IR currents at 0, -10 and -20mV. Though suction increased current amplitudes at all three voltages, the effects were proportionally larger when membrane potential was stepped to -20 mV, the relatively more hyperpolarized potential at which Shaker-IR P_{open} was lowest. The follow-up of these findings are dealt with in **Chapter 4 and 5**.

V. Mechanical stimulation during voltage-dependent gating of Shaker-IR

Voltage-dependent channels have S-shaped G-V curves (see **Chapter 3**). If a voltage-dependent channel can be interfered by mechanical stimulations, changes in the channel activity might be detected by the standard voltage-dependent parameters: V_{50}, G_{max} and the slope factor.

A family of Shaker-IR currents were obtained using excised patches before, during and after mechanical stimulation (~ 20 mmHg). The G-V curves were plotted and fitted to the Boltzmann function and the above three voltage-dependent gating parameters were extracted. The mechnaical effects on these parameters are summarized (n = 23) in **Table A-1**. Suction significantly decreased

Figure A-9. Mechanical effects on steady-state voltage-dependent currents

Cell-attached patch clamp recordings were obtained from co-injected oocytes with Shaker:ShanX at a ratio of **(a)** 1:2, **(b)** 1:1 or with **(c)** Shaker-IR alone. Current traces were recorded during a 10 s voltage pulses as indicated. Mechanical stimulation (bars) was ~ -18 mmHg. 100 μM Gd^{3+} was used in the pipettes.

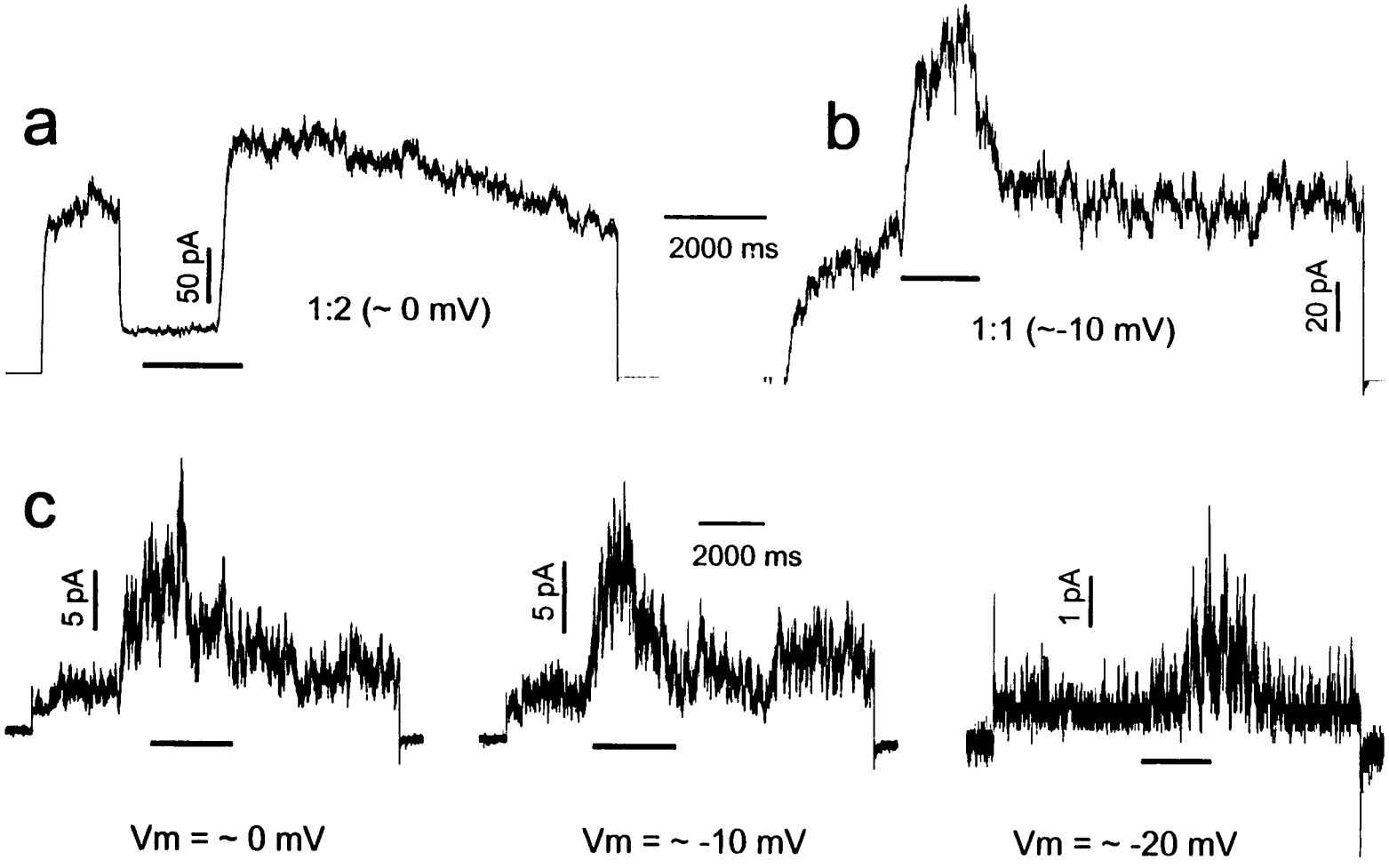
a
50 pA
1:2 (~ 0 mV)
2000 ms
b
1:1 (~-10 mV)
20 pA
c
5 pA
Vm = ~ 0 mV
5 pA
2000 ms
Vm = ~ -10 mV
1 pA
Vm = ~ -20 mV

Table A-1 Voltage-dependent gating parameters with & without suction

V-gating parameter (mean ± SE, n =23)	Before	Suction	Release
V_{50} (mV)	19 ± 3	20 ± 2	28 ± 2
Slope factor (mV per e-fold change)	12 ± 2	13 ± 0.5	12 ± 0.6
G_{max} (nS)	40 ± 10	47 ± 11	46 ± 13

within patch comparisons: between before and during suction

V-gating parameter	Paired t-test	Change	*Unpaired*
V_{50}	P < 0.01*	1.4 ±1.7 mV rightward shift	*P > 0.05*
Slope factor	P < 0.01	0.5 ± 0.5 mV decrease per e-fold change	*P > 0.05*
G_{max}	P> 0.05	—	*not applicable*

* Statistically significant

the slope factor [from 12 to 13 (mean of change is 0.5 ± 0.5 mV, mean ± SE)] and caused a rightward shift of V_{50} [from 19 to 20 mV (mean of change is 1.4 ± 1.7 mV/e-fold, mean ± SE) ($P < 0.01$, paired t-test). As shown, the variations of changes for both parameters are large, therefore only paired t-test within patch revealed the significance of these changes. In contrast, G_{max} was not changed significantly by suction ($P > 0.05$, paired t-test).

Since the averaged value from all patches showed an increased G_{max}, two examples are shown in **Fig. A-10.** For clarity, only current traces without and with suction were shown. The first example shows that suction increased the current amplitude by about two-fold at the most depolarized voltage steps, the largest effect under the same experimental conditions **(Fig. A-10a)**. To directly compare the mechanical effects on the voltage-dependent current, a superimposed G-V curve (using the same data as in **10a)** was plotted without and with mechanical stimulation, which shows that suction not only increased G_{max} but also changed the slope of the conductance of Shaker-IR (**Fig. A-10a, right**). Similarly, with the same protocol, the second example also demonstrates that suction augmented Shaker-IR conductance, especially at the more positive membrane potentials (**Fig. A-10b**).

DISCUSSION

Both the TEVC and the cell-attached patch clamp techniques indicated successful expression though chimaeric ShanX as well as the "wild-type" (Shaker-IR) in *Xenopus* oocytes. ShanX retained standard voltage-dependent gating properties though significant differences in G_{max} and slope were found between the two channel types.

Originally, the project was designed to test the hypothesis that a rigid channel/cytoskeleton

Figure A-10. Mechanical effects on Shaker-IR current (I_{Sh}) and G-V curves

Two excised patch examples are shown. The membrane was clamped at a series of potentials between -100 mV and +80 mV from a holding potential of -100 mV. Currents were recorded with or without mechanical stimulations. In the resulting G-V curves on the right, squares and circles represent before and during suction, respectively.

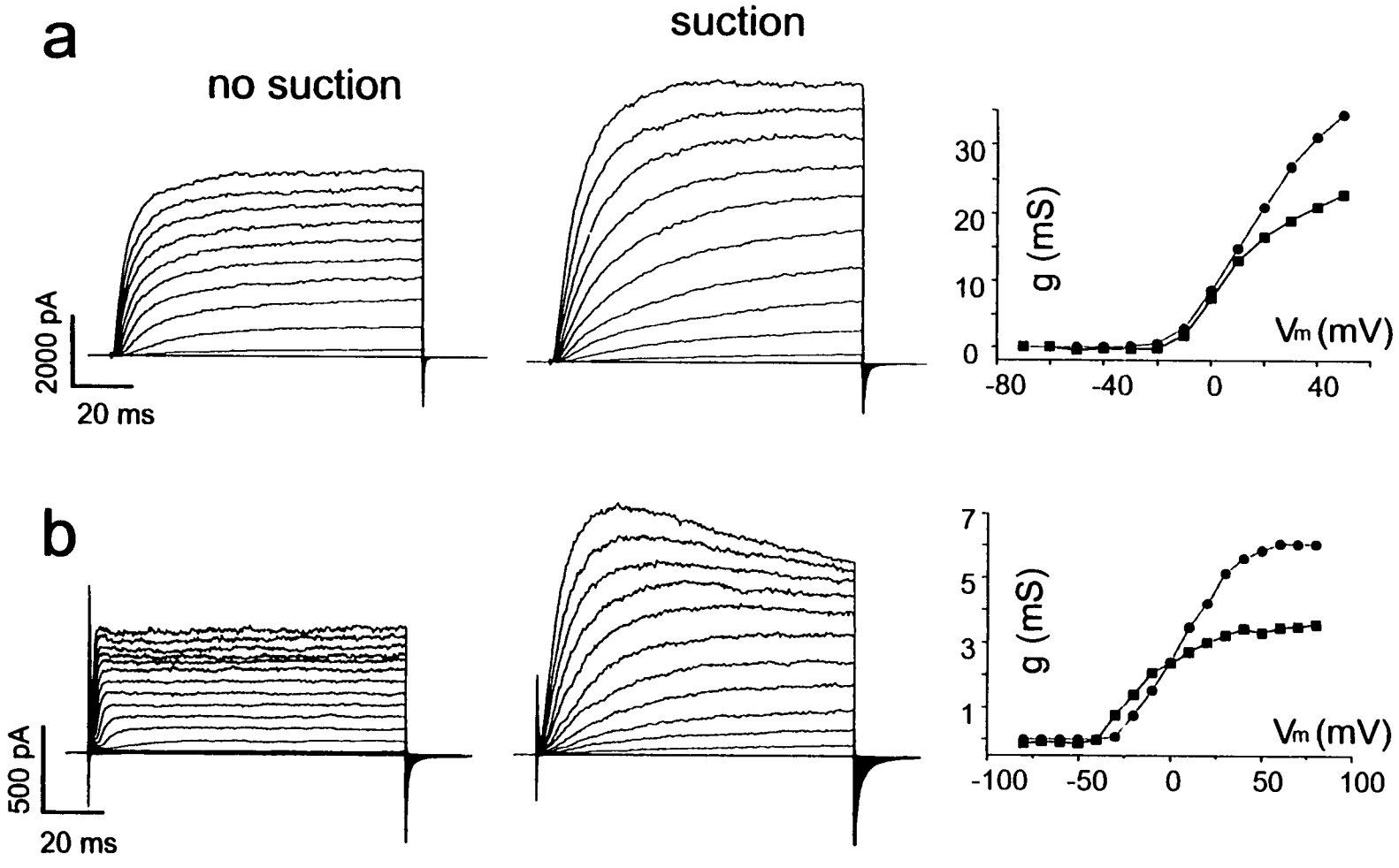
a
no suction
suction
2000 pA
20 ms
g (mS)
30
20
10
0
-80
-40
0
40
Vm (mV)
b
500 pA
20 ms
g (mS)
7
5
3
1
-100
-50
0
50
100
Vm (mV)

linkage could cause mechanical interference with voltage-dependent gating. To our surprise, the control model, a typical voltage-dependent channel, Shaker-IR, seemed susceptible to mechanical stimulation. Moreover, when the effects of mechanical stimulation between Shaker-IR and ShanX were compared, the preliminary data suggested that Shaker-IR had bigger mechanical responses than ShanX. Two possible explanations for this observation: (1) ShanX with the spectrin-binding domain of ankyrin binds to the oocyte spectrin network as expected, but this linkage might provide a mechanical load buffer and protect rather than destabilize the channel from mechanical interference; (2) recent studies have shown that Shaker-like K^+ channels contain a PDZ binding domain at their C-terminus which binds to cytoplasm proteins, that are enriched at post-synaptic density (Kim et al., 1995). Thus it is possible that Shaker-IR might bind to PSD homology proteins in *Xenopus* oocytes (Jing et al., 1997) and produce a direct linkage between the channel and the membrane cytoskeleton.

Using the exploratory stimulation protocols that we developed at the earlier stage of my work, there were no consistent effects for the channels in response to mechanical stimulation. In light of subsequent work (**Chapter 4** and **5**), it is seems that the between patches inconsistency was largely because we were testing near the steep part of the G-V curve, where its mechanosusceptibility proved to be least evident. Our rationale was the usual one: by working on the steep part of the Boltzmann, we would be able to detect either current decreases or increases produced by mechanical stimulation. The hypothesis that linked to the spectrin network would induce a mechanical component in voltage-dependent channel has not been adequately tested. To begin with, we did not establish if there was indeed binding between ShanX and *Xenopus* oocytes spectrin. The future experiment for studying the mechanical effects on ShanX was described in **Chapter 6**, emphasis was put on the foot of the activation curve where changes in P_{open} are easiest to detect.

REFERENCES

Ackerman, M.J., Wickman, K.D. and Clapham, D.E. (1994) Hypotonicity activates a native chloride current in *Xenopus* oocytes. *J. Gen. Physiol.* **103**:153-179.

Aggarwal, S.K. and MacKinnon, R. (1996) Contribution of the S4 segment to gating charge in the Shaker K^+ channel. *Neuron* **16**:1169-77.

Arahata, K., Ishiura, S., Ishiguro, T., Tsukahara, T., Suhara, Y., Eguchi, C., Ishihara, T., Nonaka, I., Ozawa, E. and Sugita, H. (1988) Immunostaining of skeletal and cardiac muscle surface membrane with antibody against Duchenne muscular dystrophy peptide. *Nature* **333**:861-863.

Armstrong, C.M. and Cota, G. (1990) Modification of sodium channel gating by lanthanum. Some effects that cannot be explained by surface charge theory. *J. Gen. Physiol.* **96**:1129-1140.

Armstrong, C.M. and Miller, C. (1990) Do voltage-dependent K^+ channels require Ca^{2+}? A critical test employing a heterologous expression system. *Proc. Natl. Acad. Sci. U SA* **87**:7579-7582.

Armstrong, C.M. and Hille, B. (1998) Voltage-gated ion channels and electrical excitability. *Neuron* **20**:371-380.

Armstrong, C.M. (1999) Distinguishing surface effects of calcium ion from pore-occupancy effects in Na^+ channels. *Proc. Natl. Acad. Sci. USA* **96**:4158-4163.

Assad, J.A., Shepherd, G.M. and Corey, D.P. (1991) Tip-link integrity and mechanical transduction in vertebrate hair cells. *Neuron*Armstrong, C.M. and Bezanilla, F. (1973) Currents related to movement of the gating particles of the sodium channels. *Nature* **242**:459-461.

Auld, V.J., Goldin, A.L., Krafte, D.S., Catterall, W.A., Lester, H.A., Davidson, N. and Dunn, R.J. (1990) A neutral amino acid change in segment II S4 dramatically alters the gating properties of the voltage-dependent sodium channel. *Proc. Natl. Acad. Sci. USA* **87**:323-327.

Baker, O.S., Larsson, H.P., Mannuzzu, L.M. and Isacoff, E.Y. (1998) Three transmembrane conformations and sequence-dependent displacement of the S4 domain in shaker K^+ channel gating. *Neuron* **20**:1283-1294.

Bargmann, C.I. (1994) Molecular mechanisms of mechanosensation? *Cell* **78**:729-731.

Baukrowitz, T. and Yellen, G. (1995) Modulation of K^+ current by frequency and external $[K^+]$: a tale of two inactivation mechanisms. *Neuron* **15**:951-960.

Bedard, E. and Morris, C.E. (1992) Channels activated by stretch in neurons of a helix snail. *Can. J. Physiol. Pharmacol.* **70**:207-213.

Bell, J.E. and Miller, C. (1984) Effects of phospholipid surface charge on ion conduction in the K^+ channel of sarcoplasmic reticulum. *Biophys. J.* **45**:279-287.

Ben-Tabou, S., Keller, E. and Nussinovitch, I. (1994) Mechanosensitivity of voltage-gated calcium currents in rat anterior pituitary cells. *J. Physiol.* **476**:29-39.

Benke, D., Wenzel, A., Scheuer, L., Fritschy, J.M and Mohler, H (1995) Immunobiochemical characterization of the NMDA-receptor subunit NR1 in the developing and adult rat brain. *J. Recept. Signal. Transduct. Res.* **15**:393-411.

Bennett, V. (1990) Spectrin-based membrane skeleton: a multipotential adaptor between plasma membrane and cytoplasm. *Physiol. Rev.* **70**:1029-1065.

Bennett, V. (1992) Ankyrins: adaptors between diverse plasma membrane proteins and the cytoplasm. *J. Biol. Chem.* **267**:8703-8706.

Bertrand, D., Cooper, E., Valera, S., Rungger, D. and Ballivet, M. (1991). Electrophysiology of neuronal nicotinic acetylcholine receptors expressed in *Xenopus* oocyte following nuclear injection of genes or cDNAs. In: *Methods in neurosciences* (Ed. Conn, P.M.) **4**:174-193. Academic Press, San Diego, CA.

Bezanilla, F., Perozo, E., Papazian, D. M. and Stefani, E. (1991) Molecular basis of gating charge immobilization in Shaker potassium channels. *Science.* **254**: 679-683.

Bezanilla, F., Perozo, E. and Stefani, E. (1994) Gating of Shaker K^+ channels: II. The components of gating currents and a model of channel activation. *Biophys. J.* **66**:1011-1021.

Blount, P., Sukharev, S.I., Moe, P.C., Schroeder, M.J., Guy, H.R. and Kung, C. (1996a) Membrane topology and multimeric structure of a mechanosensitive channel protein of *Escherichia coli*. *EMBO J.* **15**:4798-4805.

Blount, P., Sukharev, S.I., Schroeder, M.J., Nagle, S.K. and Kung, C. (1996b) Single residue substitutions that change the gating properties of mechanosensitive channel in *Escherichia coli*. *Proc. Natl. Acad. Sci. USA* **93**:11652-11657.

Boland, L.M., Brown, T.A. and Dingledine, R. (1991) Gadolinium block of calcium channels: influence of bicarbonate. *Brain Res.* **563**:142-150.

Bourque, C.W. (1996) Ionotropic mechanoreceptors: The mechanosensitive channels. In: *Cellular and Molecular Neurobiology* (Ed. Hammond, C.) p290-303. Adademic Press, London, U.K.

Bourque, C.W. and Oliet, S.H. (1997) Osmoreceptors in the central nervous system. *Annu. Rev. Physiol.* **59**:601-619.

Bowman, C.L., Ding, J.P., Sachs, F. and Sokabe, M. (1992) Mechanotransducing ion channels in astrocytes. *Brain Res.* **584**:272-286.

Boyle, M.B., Azhderian, E.M., MacLusky, N.J., Naftolin, F. and Kaczmarek, L.K. (1987) *Xenopus* oocytes injected with rat uterine RNA express very slowly activating potassium currents. *Science* **235**:1221-1224.

Brezden, B.L. and Gardner, D.R. (1986) A potassium-selective channel in isolated *Lymnaea stagnalis* heart muscle cells. *J. Exp. Biol.* **123**:175-189.

Caldwell, R.A., Clemo, H.F. and Baumgarten, C.M. (1998) Using gadolinium to identify stretch-activated channels: technical considerations. *Am. J. Physiol.* **275**:C619-621.

Campbell, K.P. and Kahl, S.D. (1989) Association of dystrophin and an integral membrane glycoprotein. *Nature* **338**:259-262.

Canessa, C.M., Schild, L., Buell, G., Thorens, B., Gautschi, I., Horisberrger, J.D. and Rossier, B.C. (1994) Amiloride-sensitive epithelial Na^+ channel is made of three homologous subunits. *Nature* **367**:463-477.

Casado, M. and Ascher, P. (1998) Opposite modulation of NMDA receptors by lysophospholipids and arachidonic acid: common features with mechanosensitivity. *J. Physiol.* **513**:317-330.

Casey, P.J. (1995) Protein lipidation in cell signaling. *Science* **268**:221-225.

Catterall, W.A. (1986) Molecular properties of voltage-sensitive sodium channels. *Annu. Rev. Biochem.* **55**:953-985.

Catterall, W.A. (1988) Structure and function of voltage-sensitive ion channels. *Science* **242**:50-61.

Catterall, W.A. (1993) Structure and function of voltage-gated ion channels. *Trends. Neurosci.* **16**:500-506.

Chan, W., Kordeli, E. and Bennett, V. (1993) 440-kD ankyrinB: structure of the major developmentally regulated and selective localization in unmyelinated axons. *J. Cell Biol.* **123**:1463-1473.

Chang, G., Spencer, R.H., Lee, A.T., Barclay, M.T. and Rees, D.C. (1998) Structure of the MscL homolog from *Mycobacterium tuberculosis*: a gated mechanosensitive ion channel. *Science* **282**:2220-2226.

Chapman, M.L., VanDongen, H.M. and VanDongen, A.M. (1997) Activation-dependent subconductance levels in the drk1 K channel suggest a subunit basis for ion permeation and gating. *Biophys. J.* **72**:708-719.

Chazot, P.L. and Stephenson, F.A. (1997) Biochemical evidence for the existence of a pool of unassembled C2 exon-containing NR1 subunits of the mammalian forebrain NMDA receptor. *J. Neurochem.* **68**:507-516.

Cho, K.O., Hunt, C.A. and Kennedy, M.B. (1992) The rat brain postsynaptic density fraction contains a homolog of the *Drosophila* discs-large tumor suppressor protein. *Neuron* **9**:929-942.

Chua, K., Tytgat, J., Liman, E. and Hess, P. (1992) Membrane topology of RCK1 K-channels. *Biophysiol. J.* **61**:A289.

Clapham, D.E. and Neer, E.J. (1997) G protein beta gamma subunits. *Annu. Rev. Pharmacol. Toxicol.* **37**:167-203.

Corey, D.P. and Hudspeth, A.J. (1979) Ionic basis of the receptor potential in a vertebrate hair cell. *Nature* **281**:675-77.

Corey, D.P. and Hudspeth, A.J. (1983) Kinetics of the receptor current in bullfrog saccular hair cells. *J Neurosci.* **3**:962-976.

Corey, D.P. and Garcìa-Añoveros, J. (1996) Mechanosensation and the DEG/ENaC ion channels. *Science* **273**:323-324.

Crawford, A.C., Evans, M.G. and Fettiplace, R. (1989) Activation and adaptation of transducer currents in turtle hair cells. *J. Physiol. (Lond)* **419**:405-434.

Cukierman, S., Zinkand, W.C., French, R.J. and Krueger, B.K. (1988) Effects of membrane surface charge and calcium on the gating of rat brain sodium channels in planar bilayers. *J. Gen. Physiol.* **92**:431-447.

Dai, J., Sheetz, M.P., Wan, X. and Morris, C.E. (1998) Membrane tension in swelling and shrinking molluscan neurons. *J. Neurosci.* **18**:6681-6692.

Davies, K.A. and Lux, S.E. (1989) Hereditary disorders of the red cell membrane skeleton. *Trends Genet.* **5**:222-227.

Davis, LH., Davis, J.Q. and Bennett, V. (1992) Ankyrin regulation: an alternatively spliced segment of the regulatory domain functions as an intramolecular modulator. *J. Biol. Chem.* **267**:18966-18972.

Denk, W., Holt, J.R., Shepherd, G.M.G. and Corey, D.P. (1995) Calcium imaging of single stereocillia in hair cells: localization of transduction channels at both ends of tip links. *Neuron* **16**:1311-1321.

Ding, J.P., Pickard, B.G. (1993) Mechanosensory calcium-selective cation channels in epidermal cells. *Plant J.* **3**:83-110.

Dolly, J.O. and Parcej, D.N. (1996) Molecular properties of voltage-gated K^+ channels. *J. Bioenerg. Biomembr.* **28**:231-253.

Dopico, A.M., Kirber, M.T., Singer, J.J. and Walsh, Jr. J.V. (1994) Membrane stretch directly activates large conductance Ca^{2+}- activated K^+ channels in mesenteric artery smooth muscle cells. *Am. J. Hyperten.* **7**:82-89.

Doyle, D.A., Morais Cabral, J., Pfuetzner, R.A., Kuo, A., Gulbis, J.M., Cohen, S.L., Chait, B.T. and MacKinnon, R. (1998) The structure of the potassium channel: molecular basis of K^+ conduction and selectivity. *Science* **280**:69-77.

Drain, P., Dubin, A.E. and Aldrich, R.W. (1994) Regulation of Shaker K^+ channel inactivation gating by the cAMP-dependent protein kinase. *Neuron* **12**:1097-1109.

Du, H., Gu, G., William, C. and Chalfie, M. (1996) Extracellular proteins needed for *C. elegans* mechanosensation *Neuron* **16**:183-194.

Dumont, J.N. (1972) Oogenesis in *Xenopus laevis* (Daudin). I. Stages of oocyte development in laboratory maintained animals. *J. Morphol.* **136**:153-180.

Durell, S.R. and Guy, H.R. (1992) Atomic scale structure and functional models of voltage-dependent potassium channels. *Boiphys. J.* **62**:238-247.

Durell, S.R., Hao, Y. and Guy, H.R. (1998) Structural models of the transmembrane region of voltage-gated and other K^+ channels in open, closed, and inactivated conformations. *J. Struct. Biol.* **121**:263-284.

Elinder, F. and Århem, P. (1994a) Effects of gadolinium on ion channels in the myelinated axon of *Xenopus laevis*: four sites of action. *Biophys. J.* **67**:71-83.

Elinder, F. and Århem, P. (1994b) The modulatory site for the action of gadolinium on surface charges and channel gating. *Biophys. J.* **67**:84-90.

Ellis, S.B., Williams, M.E., Ways, N.R., Brenner, R., Sharp, A.H., Leung, A.T., Campbell, K.P., McKenna, E., Koch, W.J. and Hui, A. (1988) Sequence and expression of mRNAs encoding the alpha 1 and alpha 2 subunits of a DHP-sensitive calcium channel. *Science* **241**:1661-1664.

Erxleben, C. (1989) Stretch-activated current through single ion channels in the abdominal stretch receptor organ of the crayfish. *J. Gen. Physiol.* **94**:1071-1083.

Evans, E.A., Waugh, R. and Melnik L. (1976) Elastic area compressibility modules of red cell membrane. *Biophys. J.* **16**:585-95.

Fink, M., Duprat, F., Lesage, F., Reyes, R., Romey, G., Heurteaux, C. and Lazdunski, M. (1996) Cloning, functional expression and brain localization of a novel unconventional outward rectifier K^+ channel. *EMBO J.* **15**:6854-6862.

Franco, A., Jr. and Lansman, J.B. (1990) Calcium entry through stretch-inactivated ion channels in *mdx* myotubes. *Nature* **344**:670-673.

Franco, A., Jr., Winegar, B.D. and Lansman, J.B. (1991) Open channel block by gadolinium ion of the stretch-inactivated ion channel in mdx myotubes. *Biophys. J.* **59**:1164-1170.

Franco-Obregón, A., Jr. and Lansman, J.B. (1994) Mechanosensitive ion channels in skeletal muscle from normal and dystrophic mice. *J. Physiol.(London)* **481**:299-309.

Frankenhaeuser, B and Hodgkin, A.L. (1957) The action of calcium on the electrical properties of squid axons. *J. Physiol.* **137**:218-244.

Furukawa ,Y, Kim, H.N. and Kubo, T. (1995) Up- and down-modulation of a cloned *Aplysia* K^+ channel (AKv1.1a) by the activators of protein kinase C. *Zoolog. Sci.* **12**:35-44.

Gandhi, C.S., Mannuzzu, L.M., Baker, O.S. and Isacoff, E.Y. (1998) Possible lateral movement of S4-bound rhodamines in a voltage-gated K^+ channel. *Biophy. J.* **76**:A266.

Garcia-Añoveros, J. and Corey, D.P. (1997) The molecules of mechanosensation. *Annu. Rev. Neurosci.* **20**:567-594.

Giebelhaus, D.H., Zelus, B.D., Henchman, S.K. and Moon, R.T. (1987) Changes in the expression of α-fodrin during embryonic development of *Xenopus* laevis. *J. Cell. Biol.* **105**:843-853.

Gilbert, D.L. and Ehrenstein, G. (1969) Effect of divalent cations on potassium conductance of squid axons: determination of surface charge. *Biophys. J.* **9**:447-463.

Gillespie, P.G. and Corey, D.P. (1997) Myosin and adaptation by hair cells. *Neuron* **19**: 955-958.

Glogauer, M., Arora, P., Chou, D., Janmey, P.A., Downey, G.P. and McCulloch, C.A.G. (1998) The role of actin-binding protein 280 in integrin-dependent mechanoprotection. *J. Biol. Chem.* **273**:1689-1698.

Goldin, A.L. (1991) Expression of ion channels by injection of mRNA into *Xenopus* oocytes. In: *Methods in Cell Biology* (Eds. Kay, B.K. and Peng, H.B.) p487-509. Academic Press. San Diego, CA.

Goldstein, S.A. and Miller, C. (1992) A point mutation in a Shaker K^+ channel changes its charybdotoxin binding site from low to high affinity. *Biophy. J.* **62**:5-7.

Goldstein, S.A. and Miller, C. (1993) Mechanism of charybdotoxin block of a voltage-gated K^+ channel. *Biophys. J.* **65**:1613-1619.

Gorczyca, M.G. and Wu, C.F. (1991) Single-channel K^+ currents in *Drosophila* muscle and their pharmacological block. *J. Membr. Biol.* **121**:237-248.

Gu, L., Liu, W. and Martinac, B. (1998) Electromechanical coupling model of gating the large mechanosensitive ion channel (MscL) of Escherichia coli by mechanical force. *Biophys. J.* **74**:2889-2902.

Guharay, F. and Sachs, F. (1984) Stretch-activated single ion channel in tissue-cultured embryonic chick skeletal muscle. *J. Physiol.* **352**:685-701.

Gustin, M.C., Zhou, X.L., Martinac, B. and Kung, C. (1988) A mechanosensitive ion channel in the yeast plasma membrane. *Science* **242**:762-765.

Gustin, M.C. (1991) Single-channel mechanosensitive currents. *Science* **253**:800.

Gustin, M.C. (1992) Mechanosensitive ion channels in yeast. Mechanisms of activation and adaptation. In: *Advances in Comparative and Environmental Physiology*. Vol. 10. Springer-Verkag. Berlin.

Hall, T.G. and Bennett, V. (1987) Regulatory domains of erythrocyte ankyrin. *J. Biol. Chem.* **262**:10537-10545.

Hall, Z.W. (1992) Ion channels. In: *An Introduction to Molecular Neurobiology*. (Eds. Hall, Z.W. and 11 contributors) p108-113. Sinauer Associates: Sunderland, MA.

Hamill, O.P. and McBride, D.W. (1992) Rapid adaptation of single mechanosensitive channels in *Xenopus* oocyte. *Proc. Natl. Acad. Sci. USA* **89**:7462-7466.

Hamill, O.P. and McBride, D.W. (1994). The cloning of a mechano-membrane channel. *Trends Neurosci.* **17**:439-443.

Hamill, O.P. and McBride, D.W. (1996) The Pharmacology of mechanogated membrane ion channels. *Pharmacol. Rev.* **48**:231-252.

Hamill, O.P. and McBride, D.W. Jr. (1997) Induced membrane hypo/hyper-mechanosensitivity: a limitation of patch-clamp recording. *Annu. Rev. Physiol.* **59**:621-631.

Harder, T., Scheiffele, P., Verkade, P. and Simons, K. (1998) Lipid domain structure of the plasma membrane revealed by patching of membrane components. *J. Cell Biol.* **141**:929-942.

Hase, C.C., Le Dain, A.C. and Martinac, B. (1995) Purification and functional reconstitution of the recombinant large mechanosensitive ion channel (MscL) of *Escherichia coli*. *J. Bio. Chem.* **270**:18329-18334.

Heginbotham, L. and. MacKinnon, R. (1992) The aromatic binding site for tetraethylammonium ion on potassium channels. *Neuron*. **8**:483-491.

Heginbotham, L. and MacKinnon, R. (1993) Conduction properties of the cloned Shaker K^+ channel. *Biophys. J.* **65**:2089-2096.

Heginbotham, L., Lu, Z., Abramson, T. and MacKinnon, R. (1994) Mutations in the K^+ channel signature sequence. *Biophys J.* **66**:1061-1067.

Heginbotham, L., Odessey, E. and Miller, C. (1997) Tetrameric stoichiometry of a prokaryotic K^+ channel. *Biochemistry* **36**:10335-10342.

Hevers, W. and Hardie, R.C. (1995) Serotonin modulates the voltage dependence of delayed rectifier and Shaker potassium channels in *Drosophila* photoreceptors. *Neuron* **14**:845-856.

Hille, B. (1992) Modifiers of gating. In: *Ionic Channels of Excitable Membranes.* 2nd ed. P. 457-461. Sinauer Associates, Sunderland, MA.

Hisada, T., Ordway, R.W., Kirber, M.T., Singer, J.J. and Walsh, J.V. Jr (1991) Hyperpolarization-activated cationic channels in smooth muscle cells are stretch sensitive. *Pflugers Arch.* **417**:493-499.

Hodgkin, A.L. and Huxley, A.F. (1952) A quantitative description of membrane current and its application to conduction and excitation in nerve. *J. Physiol.* **117**:500-544.

Hong, K. and Driscoll, M. (1994) A transmembrane domain of the putative channel subunit MEC-4 influences mechanotransduction and neurodegeneration in *C. elegans*. *Nature* **367**:470-473.

Horber, J.K., Mosbacher, J., Haberle, W., Ruppersberg, J.P. and Sakmann, B. (1995) A look at membrane patches with a scanning force microscope. *Biophys. J.* **68**:1687-1693.

Hoshi, T., Zagotta, W.N. and Addrich, R.W. (1990) Biophysical and molecular mechanisms of Shaker potassium channel inactivation. *Science* **250**:533-538.

Hoshi, T., Zagotta, W.N. and Addrich, R.W. (1991) Two types of inactivation in Shaker K^+ channels: effects of alternation in the carboxyl-terminal region. *Neuron* **7**:547-556.

Hoshi, T., Zagotta, W. N. and Aldrich, R. W. (1994) Shaker potassium channel gating. I: Transitions near the open state. *J. Gen. Physiol.* **103**: 249-278.

Huang, M. and Chalfie, M. (1994) Gene interactions affecting mechanosensory transduction in Caenorhabditis elegans. *Nature* **367**:467-470.

Huang, M., Gu, G., Ferguson, E.L. and Chalfie, M. (1995) A stomatin-like protein necessary for mechanosensation in *C. elegans*. *Nature* **378**:292-295.

Hudspeth, A.J. (1982) Extracellular current flow and the site of transduction by vertebrate hair cells. *J. Neurosci.* **2**:1-10.

Hudspeth, A.J. (1989) How the ear's works work. *Nature* **341**:397-404.

Isacoff, E.Y., Jan, Y.N. and Jan, L.Y. (1991) Putative receptor for the cytoplasmic inactivation gate in the Shaker K^+ channel. *Nature* **353**:86-90.

Iwasa, K.H., Li, M.X., Jia, M. and Kachar, B. (1991) Stretch sensitivity of the lateral wall of the auditory outer hair cell from the guinea pig. *Neurosci. Lett.* **133**:171-174.

Jan, L.Y. and Jan, Y.N. (1989) Voltage-sensitive ion channels. *Cell* **56**:13-25.

Jaramillo, F. and Hudspeth, A.J. (1991) Localization of the hair cell's transduction channels at the hair bundle's top by iontophoretic application of a channel blocker. *Neuron* **7**:409-420.

Ji, S., John, S.A., Lu, Y. and Weiss, J.N. (1998) Mechanosensitivity of the cardiac muscarinic potassium channel. *J. Bio. Chem.* **273**:1324-1328.

Jing, J., Peretz, T., Singer-Lahat, D., Chikvashvili, D., Thornhill, W.B. and Lotan, I. (1997) Inactivation of a voltage-dependent K^+ channel by beta subunit. Modulation by a phosphorylation-dependent interaction between the distal C terminus of alpha subunit and cytoskeleton. *J. Biol. Chem.* **272**:14021-14024.

Kell, A and Glaser R.W (1993) On the mechanical and dynamic properties of plant cell membranes: their role in growth, direct gene transfer and protoplast fusion. *J. Theor. Biol.* **160**:41-62.

Kim, D. (1992) A mechanosensitive K^+ channel in heart cells. Activation by arachidonic acid. *J. Gen. Physiol.* **100**:1021-1040.

Kim, E., Niethammer, M., Rothschild, A., Jan, Y.N. and Sheng, M. (1995) Clustering of Shaker-type K^+ channels by interaction with a family of membrane-associated guanylate kinases. *Nature* **378**:85-88.

Kim, K.S., Neu, J. and Oster, G. (1998) Curvature-mediated interactions between membrane proteins. *Biophys. J.* **75**:2274-2291.

Kordeli, E., Davis, J., Trapp, B. and Bennett, V. (1990) An isoform of ankyrin is localized at nodes of Ranvier in myelinated axons of central and peripheral nerves. *J. Cell. Biol.* **110**:1341-1352.

Kordeli, E., Lambert, S. and Bennett, V. (1995) AnkyrinG. A new ankyrin gene with neural-specific isoforms localized at the axonal initial segment and node of Ranvier. *J. Biol. Chem.* **270**:2352-2359.

Kornau, H.C., Schenker, L.T., Kennedy, M.B. and Seeburg, P.H. (1995) Domain interaction between NMDA receptor subunits and the postsynaptic density protein PSD-95. *Science* **269**:1737-1740.

Kornau, H.-C., Seeburg, P.H. and Kennedy M.B. (1997) Interaction of ion channels and receptors with PDZ domain protein. *Curr. Opin. Neurobiol.* 7:368-373.

Kozak, M. (1987) An analysis of 5'-noncoding sequences from 699 vertebrate messenger RNAs. *Nucleic Acids Research* **15**: 8125-8132.

Krapivinsky, G., Gordon, E.A., Wickman, K., Velimirovic, B., Krapivinsky, L. and Clapham, D.E. (1995) The G-protein-gated atrial K^+ channel I_{KACh} is a heteromultimer of two inwardly rectifying K^+-channel proteins. *Nature* **374**:135-141.

Kressmann, A., Clarkson, S.G., Telford, K.L. and Birnstiel, M.L. (1978) Transcription of *Xenopus* tDNAmet1 and sea urchin histone DNA injected into the *Xenopus* oocyte nucleus. *Cold Spring Harb. Symp. Quant. Biol.* **42**:1077-1082.

Kreusch, A., Pfaffinger, P.J., Stevens, C.F. and Choe, F (1998) Crystal structure of the tetramerization domain of the Shaker potassium channel. *Nature* **392**:945-948

Krieg, P.A. and Melton, D.A. (1984) Functional messenger RNAs are produced by SP6 *in vitro* transcription of cloned cDNAs. *Nuc. Acids Res.* **12**:7057-7070.

Kushner, L., Lerma, J., Bennett, M.V.L. and Zukin, R.S. (1989) Using the *Xenopus* Oocyte system for expression and cloning of neuroreceptors and channels. In: *Methods in Neurosciences* (Ed. Conn, P.M.) **1**:3-30. Academic Press, San Diego, CA.

Kwok, R. and Evans, E. (1981) Thermoelasticity of large lecithin bilayer vesicles. *Biophys. J.* **35**:637-652.

Lacampagne, A., Gannier, F., Argibay, J., Garnier, D. and Le Guennec, J.Y. (1994) The stretch-activated ion channel blocker gadolinium also blocks L-type calcium channels in isolated ventricular myocytes of the guinea-pig. *Biochim. Biophys. Acta.* **1191**:205-208.

Laemmli, U.K. (1970) Cleavage of structural proteins during the assembly of the head of bacteriophage T4. *Nature* **227**:680-685.

Lambert, S., Yu, H., Prchal, J.T., Lawlerm J., Ruff, P., Speicher, D., Cheung, M.C., Kan, Y.W. and Palek, J. (1990) cDNA sequence for human erythrocyte ankyrin. *Proc. Natl. Acad. Sci. USA* **87**:1730-1734.

Lambert, S. and Bennett, V. (1993). From anemia to cerebellar dysfunction- a review of the ankyrin gene family. *Eur. J. Biochem.* **211**:1-6.

Langton, P.D. (1993) Calcium channel currents recorded from isolated myocytes of rat basilar artery are stretch sensitive. *J. Physiol.* **471**:1-11.

Larsson, H.P., Baker, O.S., Dhillon, D.S. and Isacoff, E.Y. (1996) Transmembrane movement of the Shaker K^+ channel S4. *Neuron.* **16**:387-397.

Le Dain, A.C., Saint, N., Kloda, A., Ghazi, A. and Martinac, B. (1998) Mechanosensitive ion channels of the archaeon Haloferax volcanii. *J. Biol .Chem.* **273**:12116 -12119.

Levina, N., Totemeyer, S., Stokes, N.R., Louis, P., Jones, M.A. and Booth, I.R. (1999) Protection of Escherichia coli cells against extreme turgor by activation of MscS and MscL mechanosensitive channels: identification of genes required for MscS activity. *EMBO J.* **18**:1730-1737.

Li, M., Jan, Y. N. and Jan, L. Y. (1992) Specification of subunit assembly by the hydrophilic amino-terminal domain of the Shaker potassium channel. *Science* **257**:1225-1230.

Li, Z.P., Burket, E.P., Frank, J.S., Bennett, V. and Philipson K.D. (1993) The cardiac Na^+-Ca^{2+} exchanger binds to the cytoskeletal protein ankyrin. *J. Biol. Chem.* **268**:11489-11491.

Liu, Y., Jurman, M. E. and Yellen, G. (1996) Dynamic rearrangement of the outer mouth of a K^+ channel during gating. *Neuron* **16**:859-867.

Liu, Y., Holmgren, M., Jurman, M. E. and Yellen, G. (1997) Gated access to the pore of a voltage-dependent K^+ channel. *Neuron* **19**:175-184.

Logothetis, D.E., Movahedi, S., Satler, C., Lindpaintner, K. and Nadal-Ginard, B. (1992) Incremental reductions of positive charge within the S4 region of a voltage-gated K^+ channel result in corresponding decreases in gating charge. *Neuron* **8**:531-540.

Loots, E. and Isacoff, E.Y. (1998) Protein rearrangements underlying slow inactivation of the Shaker K^+ channel. *J. Gen. Physiol.* **112**:377-389.

Lopez, G.A., Jan, Y.N. and Jan, L.Y. (1991) Hydrophobic substitution mutations in the S4 sequence alter voltage-dependent gating in Shaker K^+ channels. *Neuron* **7**:327-336.

Lopez-Barneo, J., Hoshi, T., Heinemann, S.H. and Aldrich, R.W. (1993) Effects of external cations and mutations in the pore region on C-type inactivation of Shaker potassium channels. *Receptors Channels* **1**:61-71.

Lumpkin, E.A. and Hudspeth, A.J. (1995) Detection of Ca^{2+} entry through mechanosensitive channels localizes the site of mechanoelectrical transduction in hair cells. *Proc. Natl. Acad. Sci. USA* **92**:10297-10301.

Luna, E.J. and Hitt, A.L. (1992) Cytoskeleton-plasma membrane interactions. *Science* **258**:955-964.

Lux, S.E., Pease, B., Tomaselli, M,B,, John, K.M. and Bernstein, S.E. (1979) Hemolytic anemias associated with deficient or dysfunctional spectrin. *Prog. Clin. Biol. Res.* **30**:463-469.

MacKinnon, R., Reinhart, P. H. and White, M. M. (1988) Charybdotoxin block of Shaker K^+ channels suggests that different types of K^+ channels share common structural features. *Neuron* **1**:997-1001.

MacKinnon, R. (1991) Determination of the subunit stoichiometry of a voltage-activated potassium channel. *Nature* **350**:232-235.

Mannsfeldt, A.G., Carroll, P., Stucky, C.L. and Lewin, G.R. (1999) Stomatin, a MEC-2 like protein, is expressed by mammalian sensory neurons. *Mol. Cell Neurosci.* **13**:391-404.

Mannuzzu, L.M., Moronne, M.M. and Isacoff, E.Y. (1996) Direct physical measure of conformational rearrangement underlying potassium channel gating. *Science* **271**:213-216.

Marchenko, S.M. and Sage, S.O. (1997) A novel mechanosensitive cation channel from the endothelium of rat aorta. *J. Physiol. (Lond)* **498**:419-425.

Marcus, D.C. (1998) Acoustic transduction. In: *Cell Physiology Source Book*, 2nd Edition. (Ed. Sperelakis, N.) p688-703. Academic Press. San Diego, CA.

Martinac, B., Buechner, M., Delcour, A.H., Adler, J. and Kung, C. (1987) Pressure-sensitive ion channel in *Escherichia coli. Proc. Natn. Acad. Sci. USA* **84**:2297-2301.

Martinac, B., Adler, J. and Kung, C. (1990) Mechanosensitive ion channels of *E. coli* activated by amphipaths. *Nature* **348**:261-263.

Martinac, B. (1993) In: Thermodynamics of Membrane Receptors and Channels (Ed. Jackson, M.B.) p327-352. CRC, Boca Raton.

McBain, C.J. and Mayer, M.L. (1994) N-methyl-D-aspartic acid receptor structure and function. *Physiol. Rev.* **74**:723-760.

McBride, D.W. and Hamill, O.P. (1993) Pressure-clamp technique for measurement of the relaxation kinetics of mechanosensitive channels. *TINS* **16**:341-345.

McCormack, K., Tanouye, M.A., Iverson, L.E., Lin, J.W., Ramaswami, M., McCormack, T., Campanelli, J.T., Mathew, M.K. and Rudy, B. (1991) A role for hydrophobic residues in the voltage-dependent gating of Shaker K^+ channels. *Proc. Natl. Acad. Sci. USA* **88**:2931-2935.

Methfessel, C., Witzemann, V., Takahashi, T., Mishina, M., Numa, S. and Sakmann, B. (1986) Patch clamp measurements on *Xenopus* laevis oocytes: currents through endogenous channels and implanted acetylcholine receptor and sodium channels. *Pflugers. Arc.* **407**:577-588.

Moczydlowski, E., Alvarez, O., Vergara, C. and Latorre, R. (1985) Effect of phospholipid surface charge on the conductance and gating of a Ca^{2+}-activated K^+ channel in planar lipid bilayers. *J. Membr. Biol.* **83**:273-282.

Moody, W.J. and Bosma, M.M. (1989) A nonselective cation channel activated by membrane deformation in oocytes of the ascidian Boltenia villosa. *J. Membr. Biol.* **107**:179-188.

Morris, C.E. and Sigurdson, W.J. (1989) Stretch-inactivated ion channels coexist with stretch-activated ion channels. *Science* **243**:807-809.

Morris, C.E. (1990) Mechanosensitive ion channels. *J. Membr. Biol.* **113**:93-107.

Morris, C.E. and Horn, R. (1991) Failure to elicit neuronal macroscopic mechanosensitive currents anticipated by single-channel studies. *Science* **251**:1246-1249.

Morris, C.E. (1992) Are stretch-sensitive channels in molluscan cells and elsewhere physiological mechanotransducers? *Experientia* **48**:852-858.

Morris, C.E. (1995) Stretch-sensitive ion channels. In: *Principles of Cell Physiology and Biophysics.* (Ed. Sperelakis, N.) p483. Academis Press, New York, NY.

Morris, C.E. (1997) Mechanosensitive ion channels in eukaryotic cells. In: *Cell Physiology Source Book* 2nd Edition. (Ed. Sperelakis, N.) p668-681. Academic Press, San Diego, CA.

Morrow, J.S., Cianci, C.D., Ardito, T., Mann, A.S. and Kashgarian, M. (1989) Ankyrin links fodrin to the alpha subunit of Na, K-ATPase in Madin-Darby Canine kidney cells and in intact renal tubule cells. *J. Cell. Biol.* **108**:455-465.

Naruse, K. and Sokabe. M. (1993) Involvement of stretch-activated ion channels in Ca^{2+} mobilization to mechanical stretch in endothelial cells. *Am. J. Physiol.* **264**:C1037-1044.

Neher, E. and Sakmann, B. (1976) Single-channel currents recorded from membrane of denervated frog muscle fibres. *Nature* **260**:799-802.

Nichol, J.A. and Hutter, O.F. (1996) Tensile strength and dilatational elasticity of giant sarcolemmal vesicles shed from rabbit muscle. *J Physiol (Lond)* **493**:187-198.

Nielsen, C., Goulian. M. and Andersen, O.S. (1998) Energetics of inclusion-induced bilayer deformations. *Biophys J* **74**:1966-1983.

Nilius, B. (1998) Ion channels in non-excitable cells. In: *Cell Physiological Source Book* 2nd Edition. (Ed. Sperelakis N.) p436-455. Academic Press, San Diego, CA.

Noda, M., Shimizu, S. , Tanabe, T., Takai, T., Kayano, T., Ikeda, T., Takahashi, H., Nakayama, H., Kanaoka, Y. and Minamino, N. (1984) Primary structure of Electrophorus electricus sodium channel deduced from cDNA sequence. *Nature* **312**:121-127.

Olcese, R., Latorre, R., Toro, L., Bezanilla, F. and Stefani, E. (1997) Correlation between charge movement and ionic current during slow inactivation in Shaker K^+ channels. *J. Gen. Physiol.* **110**:579-589.

Oliet, S.H. and Bourque, C.W. (1993) Mechanosensitive channels transduce osmosensitivity in supraoptic neurons. *Nature* **364**:341-343.

Oliet, S.H. and Bourque, C.W. (1996) Gadolinium uncouples mechanical detection and osmoreceptor potential in supraoptic neurons. *Neuron* **16**:175-181.

Opsahl, L. and Webb, W.W. (1994) Transduction of membrane tension by the ion channel alamethicin. *Biophys. J.* **66**:71-74.

Paoletti, P. and Ascher, P. (1994) Mechanosensitivity of NMDA receptors in cultured mouse central nuerons. *Neuron* **13**:645-655.

Papazian, D.M., Schwarz, T.L., Tempel, B.L., Jan, Y.N. and Jan, L.Y. (1987) Cloning of genomic and complementary DNA from Shaker, a putative potassium channel gene from *Drosophila*. *Science* **237**:749-753.

Papazian, D.M., Timpe, L.C., Jan, Y.N. and Jan, L.Y. (1991) Alteration of voltage-dependence of Shaker potassium channel by mutations in the S4 sequence. *Nature* **349**:305-310.

Papazian, D.M., Shao, X.M., Seoh, S.A., Mock, A.F., Huang, Y. and Wainstock, D.H. (1995) Electrostatic interactions of S4 voltage sensor in Shaker K^+ channel. *Neuron* **14**:1293-1301.

Patel, A.J., Honore, E., Maingret, F., Lesage, F., Fink, M., Duprat, F. and Lazdunski, M. (1998) A mammalian two pore domain mechano-gated S-like K^+ channel. *EMBO J.* **17**:4283-4390.

Peled-Zehavi, H., Arkin, I.T., Engelman, D.M. and Shai, Y. (1996) Coassembly of synthetic segments of Shaker K^+ channel within phospholipid membranes. *Biochemistry* **35**:6828-6838.

Perozo, E., Papazian, D.M., Stefani, E. and Bezanilla, F. (1992) Gating currents in Shaker K^+ channels. Implications for activation and inactivation models. *Biophys. J.* **62**:160-168.

Perozo, E., MacKinnon, R., Bezanilla, F. and Stefani, E. (1993) Gating currents from a nonconducting mutant reveal open-closed conformations in Shaker K^+ channels. *Neuron* **11**:353-358.

Perozo, E., Santacruz-Toloza, L., Stefani, E., Bezanilla, F. and Papazian, D.M. (1994) S4 mutations alter gating currents of Shaker K channels. *Biophys. J.* **66**:345-354.

Pickles, J.O., Comis, S.D. and Osborne, M.P. (1984) Cross-links between stereocilia in the guinea pig organ of Corti, and their possible relation to sensory transduction. *Hear Res.* **15**:103-112.

Pickles, J.O. (1993) An analysis of actin isoforms expressed in hair-cell enriched fractions of the chick basilar papilla by the polymerase chain reaction technique. *Hear Res.* **71**:225-229.

Planells-Cases, R., Sun, W., Ferrer-Montiel, A.V. and Montal, M. (1993) Molecular cloning, functional expression, and pharmacological characterization of an N-methyl-D-aspartate receptor subunit from human brain. *Proc. Natl. Acad. Sci. USA.* **90**:5057-5061.

Platt, O.S., Lux, S.E. and Falcone, J.F. (1993) A highly conserved region of human erythrocyte ankyrin contains the capacity to bind spectrin. *J. Bio. Chem.* **268**:24421-24426.

Pleumsamran, A and Kim, D. (1995) Membrane stretch augments the cardiac muscarinic K^+ channel activity. *J. Membr. Biol.* **148**:287-297.

Purves, D., Augustine, G.J., Fitzpatrick, D., Katz, L.C., LaMantia A-S. and McNamara, J.O. (1997) Channels and pumps. In: *Neuroscience.* p69-84. Sinauer Associates, Sunderland, MA.

Ross P.E., Garber, S.S. and Cahalan, M.D. (1994) Membrane chloride conductance and capacitance in Jurkat T lymphocytes during osmotic swelling. *Biophys. J.* **66**:169-178.

Rotin, D., Bar-Sagi, D., Brodovich, H.O., Merilainen, J., Lehto, V.P., Canessa, C.M., Rossier, B.C. and Downey, G.P. (1994) An SH3 binding region in the epithelial Na^+ channel (αrENaC) mediates its localization at the apical membrane. *EMBO J.* **13**:4440-4450.

Ruknudin, A., Song, M.J. and Sachs, F. (1991) The ultrastructure of patch-clamped membranes: a study using high voltage electron microscopy. *J. Cell. Biol.* **112**:125-134.

Ruknudin, A., Sachs, F. and Bustamante, J.O. (1993) Stretch-activated ion channels in tissue-cultured chick heart. *Am. J. Physiol.* **264**:H960-972.

Sachs, F (1987) Baroreceptor mechanisms at the cellular level. *Fed. Proc.* **46**:12-16.

Sachs, F. (1988) Mechanical transduction in biological systems. *Crit. Rev. Biomed. Eng.* **16**:141-169.

Sachs, F. (1990) Stretch-sensitive ion channels. *Semin. Neurosci.* **2**:49-57.

Sachs, F. and Sokabe, M. (1990) Stretch-activated ion channels and membrane mechanics. *Neurosci. Res. (Suppl.)* **12**:S1-S4.

Sachs, F. (1997) Mechanical transduction by ion channels: how forces reach the channel. *Soc. Gen. Physiol. Ser.* **52**:209-218.

Sachs, F. and Morris, C.E. (1998) Mechanosensitive ion channels in non-specialized cells. *Rev. Physiol. Biochem. Pharmacol.* **132**:1-78.

Sackin, H. (1995) Stretch-activated ion channels. *Kidney Int.* **48**:1134-1147.

Saint, N., Lacapere, J.J., Gu, L.Q., Ghazi, A., Martinac, B. and Rigaud, J.L. (1998) A hexameric transmembrane pore revealed by two-dimensional crystallization of the large mechanosensitive ion channel (MscL) of *Escherichia coli. J. Biol. Chem.***273**:14667-14670.

Santacruz-Toloza, L., Huang, Y., John, S.A. and Papazian, D.M. (1994) Glycosylation of Shaker potassium channel protein in insect cell culture and in *Xenopus* oocytes. *Biochemistry* **33**:5607-5613.

Schoppa, N.E., McCormack, K., Tanouye, M.A. and Sigworth, F.J. (1992) The size of gating charge in wild-type and mutant Shaker potassium channels. *Science* **255**:1712-1715.

Schoppa, N.E. and Sigworth, F.J. (1998) Activation of Shaker potassium channels. I. Characterization of voltage-dependent transitions. *J.Gen. Physiol.* **111**:271-294.

Schroeder, F., Wood, W.G. and Kier A.B. (1998) The biological membrane and lipid domains. In: *Cell Physiological Source Book* 2nd Edition. (Ed. Sperelakis N.) p61-74. Academic Press, San Diego, CA.

Schulteis, C.T., John, S.A., Huang, Y., Tang, C.Y. and Papazian, D.M. (1995) Conserved cysteine residues in the Shaker K^+ channel are not linked by a disulfide bond. *Biochemistry* **34**:1725-1733.

Schwarz, T.L., Tempel, B.L., Papazian, D.M., Jan, Y.N. and Jan, L.Y. (1988) Multiple potassium-channel components are produced by alternative splicing at the Shaker locus in Drosophila. *Nature* **331**:137-142.

Sentenac, H., Bonneaud, N., Minet, M., Lacroute, F., Salmon, J.N., Gayard, F. and Grignon, C. (1992) Cloning and expression in yeast of a plant potassium ion transport system. *Science* **256**:663-665.

Seoh, S.A., Sigg, D., Papazian, D.M. and Bezanilla, F. (1996) Voltage-sensing residues in the S2 and S4 segments of the Shaker K^+ channel. *Neuron* **16**:1159-1167.

Shao, X.M. and Papazian, D.M. (1993) S4 mutations alter the single-channel gating kinetics of Shaker K^+ channels. *Neuron* **11**:343-352.

Sheetz, M.P. and Singer, S.J. (1974) Biological membranes as bilayer couples. A molecular mechanism of drug-erythrocyte interactions. *Proc. Natl. Acad. Sci. USA* **71**:4457-4461.

Sheetz, M.P. and Dai, J.(1996) Modulation of membrane dynamics and cell motility by membrane tension. *Trends. Cell Biol.* **6**:85-89.

Shen, N.V., Chen, X., Boyer, M.M. and Pfaffinger, P.J. (1993) Deletion analysis of K^+ channel assembly. *Neuron* **11**:67-76.

Shepherd, G.M.G. and Corey, D.P. (1994) The extent of adaptation in bullfrog saccular hair cells. *J. Neurosci.* **14**:6217-6229.

Shih, T.M. and Goldin, A.L. (1997) Topology of the Shaker potassium channel probed with hydrophilic epitope insertions. *J. Cell Biol.* **136**:1037-1045.

Sive, H.L., Grainger, R.M. and Harland R.M. (1996) Early development of *Xenopus Laevis*. A course manual, 4th Edition. Cold Spring Harbor Lab, New York.

Small, D.L., and Morris, C.E. (1994) Delayed activation of single mechanosensitive channels in Lymnaea neurons. *Am. J. Physiol.* **267**:C598-C606.

Small, D.L. and Morris, C.E. (1995) Pharmacology of stretch-activated K^+ channels in *Lymnaea* neurones. *Br. J. Pharmacol.* **114**:180-186.

Smith, L.D., Xu, W.L. and Varnold R.L. (1991) Oogenesis and oocyte isolation. In: *Methods in Ceil Biology*. (Ed. Kay, B.K. and Peng, H.B.) **36**:45-60. Academic Press, San Diego, CA.

Sokabe, M. and Sachs, F. (1990) The structure and dynamics of patch-clamped membranes: a study by differential interference microscopy. *J. Cell Bio.* **111**:599-606.

Sokabe, M., Sachs, F. and Jing, Z. (1991). Quantitative video microscopy of patch-clamped membranes: stress, strain, capacitance and stretch activation. *Biophys. J.* **59**:722-728.

Sokabe, M., Nunogaki, K., Naruse, K. and Soga, H. (1993) Mechanics of patch clamped and intact cell-membranes in relation to SA channel activation. *Jap. J. Physiol.* **43**:71-78.

Srinivasan, Y., Elmer, L., Davis, J., Bennett, V. and Angelides, K.J. (1988) Ankyrin and spectrin associate with voltage-dependent sodium channels in brain. *Nature* **333**:177-180.

Srinivasan, Y., Lewallen, M. and Angelides, K.J. (1992) Mapping the binding site on ankyrin for the voltage-dependent sodium channel from brain. *J. Biol. Chem.* **267**:7483-7489.

Stefani, E., Toro, L., Perozo, E. and Bezanilla, F. (1994) Gating of Shaker K+ channels: I. Ionic and gating currents. *Biophys J.* **66**:996-1010.

Steffensen, I., Bates, W.R. and Morris, C.E. (1991) Embryogenesis in the presence of blockers of mechanosensitive ion channels. *Dev. Growth Differ.* **5**:437-442.

Stewart, G.W., Argent, A.C. and Dash, B.C. (1993) Stomatin: a putative cation transport regulator in the red cell membrane. *Biochem. Biophys. Acta.* **1225**:15-25.

Stühmer, W., Conti, F., Suzuki, H., Wang, X.D., Noda, M., Yahagi, N., Kubo, H. and Numa, S. (1989) Structural parts involved in activation and inactivation of the sodium channel. *Nature* **339**:597-603.

Stühmer, W. and Parekh, A.B. (1995) Electrophysiological recordings from *Xenopus* oocytes. In: *Single-Channel Recording.* 2nd Edition. (Eds. Sakmann, B. and Neher, E.) p341-356. Plenum Press, New York, NY.

Sukharev, S.I., Blount, P., Martinac, B., Blattner, F.R. and Kung, C. (1994) A large-conductance mechanosensitive channel in *E. coli* endoded by mscL alone. *Nature* **368**:265-268.

Sukharev, S.I., Blount, P., Martinac, B. and Kung, C. (1997) Mechanosensitive channels of *Escherichia coli*: the MscL gene, protein, and activities. *Ann. Rev. Physiol.* **59**:633-657.

Taniguchi, J. and Guggino, W.B. (1989) Membrane stretch: a physiological stimulator of Ca^{2+} activated K^+ channels in thick ascending limb. *Am. J. Physiol.* **257**:F347-352.

Tavernarakis, N. and Driscoll, M. (1997) Molecular modeling of mechanotransduction in the nematode *Caenorhabditis elegans*. *Annu. Rev. Physiol.* **59**:659-689.

Tempel, B.L., Papazian, D.M., Schwarz, T.L., Jan, Y.N. and Jan, L.Y. (1987) Sequence of a probable potassium channel component encoded at Shaker locus of *Drosophila*. *Science* **237**:770-775.

Terakawa, S. and Nakayama T. (1985) Are axoplasmic microtubules necessary for membrane excitation? *J. Mem. Bio.* **85**:65-77.

Tiwari-Woodruff, S.K., Schulteis, C.T., Mock, A.F. and Papazian, D.M. (1997) Electrostatic interactions between transmembrane segments mediate folding of Shaker K^+ channel subunits. *Biophys. J.* **72**:1489-1500.

Turner, A.J. (1994) PIG-tailed membrane proteins. *Essays Biochem.* **28**:113-127.

Tytgat, J. and Daenens, P. (1997) Effect of lanthanum on voltage-dependent gating of a cloned mammalian neuronal potassium channel. *Brain Res.* **749**:232-237.

Ursitti, J.A. and Wade, J.B. (1993) Ultrastructure and immunocytochemistry of the isolated human erythrocyte membrane skeleton. *Cell Motil. Cytoskeleton* **25**:30-42.

Van Wagoner, D.R. (1993) Mechanosensitive gating of atrial ATP-sensitive potassium channels. *Circ. Res.* **72**:973-983.

Vandorpe, D.H., Small, D., Dabrowski, A. and Morris, C.E. (1994) FMRFamide and membrane stretch as activators of the *Aplysia* S-channel. *Biophys. J.* **66**:46-58.

Vandorpe, D.H. and Morris, C.E. (1992) Stretch-activation of the Aplysia S-channel. *J. Memb. Biol.* **127**:204-214.

Wan, X., Juranka, P. and Morris, C.E. (1999) Activation of mechanosensitive currents in traumatized membrane. *Am. J. Physiol.* **276**:C318-327.

Wilkinson, N.C., Gao, F. and Hamill, O.P. (1998) Effects of mechano-gated cation channel blockers on *Xenopus* oocyte growth and development. *J. Membr. Biol.* **165**:161-174.

Winkelmann, J.C. and Forget, B.G. (1993) Erythroid and nonerythroid spectrins. *Blood* **81**:3173-3185.

Yang, X.C. and Sachs, F (1987) Stretch-activated channels in several tissues. *Biophys. J.* **51**:252a.

Yang, X.C. and Sachs, F. (1989) Block of stretch-activated ion channels in *Xenopus* oocytes by gadolinium and calcium ions. *Science* **243**:1068-1071.

Yang, X.C. and Sachs, F. (1990) Characterization of stretch-activated ion channels in *Xenopus* oocyte. *J. Physiol* .**431**:103-122.

Yang, N. and Horn, R. (1995) Evidence for voltage-dependent S4 movement in sodium channels. *Neuron* **15**:213-218.

Yang, N., George, A.L. Jr and Horn, R. (1996) Molecular basis of charge movement in voltage-gated sodium channels. *Neuron* **16**:113-122.

Yang, Y., Yan, Y. and Sigworth, F.J. (1997) How does the W434F mutation block current in Shaker potassium channels? *J. Gen. Physiol.* **109**:779-789.

Zagotta, W.N., Brainard, M.S. and Aldrich, R.W. (1988) Single channel analysis of four distinct classes of potassium channels in *Drosophila* muscle. *J. Neurosci.* **8**:4765-4779.

Zagotta, W.N., Hoshi, T. and Aldrich, R.W (1989) Gating of single Shaker potassium channels in *Drosophila* muscle and in *Xenopus* oocytes injected with Shaker mRNA. *Proc. Natl. Acad. Sci. USA* **86**:7243-7247.

Zagotta, W.N. and Aldrich, R.W. (1990) Voltage-dependent gating of Shaker A-type potassium channels in *Drosophila* muscle. *J. Gen. Physiol.* **95**:29-60.

Zagotta, W.N., Hoshi, T. and Aldrich, R.W. (1990) Restoration of inactivation in mutants of Shaker potassium channels by a peptide derived from ShB. *Science*. **250**:568-571.

Zagotta, W.N., Hoshi, T., Dittman, J. and Aldrich, R.W. (1994a) Shaker potassium channel gating. II: Transitions in the activation pathway. *J. Gen. Physiol.* **103**:279-319.

Zagotta, W.N., Hoshi, T. and Aldrich, R.W. (1994b) Shaker potassium channel gating III: Evaluation of kinetic models for activation. *J. Gen. Physiol.* **103**:321-362.

Zheng, J. and Sigworth, F.J. (1997) Selectivity channels during activation of mutant Shaker potassium channels. *J. Gen. Physiol.* **110**:101-107.